Lecture Notes in Civil Engineering

Chandrashekhar Bhuiyan
Wolfgang-Albert Flügel
Sharad Kumar Jain *Editors*

Water Security and Sustainability

Proceedings of Down To Earth 2019

Springer

Lecture Notes in Civil Engineering

Volume 115

Lecture Notes in Civil Engineering (LNCE) publishes the latest developments in Civil Engineering - quickly, informally and in top quality. Though original research reported in proceedings and post-proceedings represents the core of LNCE, edited volumes of exceptionally high quality and interest may also be considered for publication. Volumes published in LNCE embrace all aspects and subfields of, as well as new challenges in, Civil Engineering. Topics in the series include:

- Construction and Structural Mechanics
- Building Materials
- Concrete, Steel and Timber Structures
- Geotechnical Engineering
- Earthquake Engineering
- Coastal Engineering
- Ocean and Offshore Engineering; Ships and Floating Structures
- Hydraulics, Hydrology and Water Resources Engineering
- Environmental Engineering and Sustainability
- Structural Health and Monitoring
- Surveying and Geographical Information Systems
- Indoor Environments
- Transportation and Traffic
- Risk Analysis
- Safety and Security

To submit a proposal or request further information, please contact the appropriate Springer Editor:

– Pierpaolo Riva at pierpaolo.riva@springer.com (Europe and Americas);
– Swati Meherishi at swati.meherishi@springer.com (Asia - except China, and Australia, New Zealand);
– Wayne Hu at wayne.hu@springer.com (China).

All books in the series now indexed by Scopus and EI Compendex database!

More information about this series at http://www.springer.com/series/15087

Chandrashekhar Bhuiyan ·
Wolfgang-Albert Flügel ·
Sharad Kumar Jain
Editors

Water Security and Sustainability

Proceedings of Down To Earth 2019

Springer

Editors
Chandrashekhar Bhuiyan
Sikkim Manipal Institute of Technology
Sikkim, India

Wolfgang-Albert Flügel
Friedrich Schiller University, Jena
Jena, Thüringen, Germany

Sharad Kumar Jain
Department of Civil Engineering
Indian Institute of Technology Roorkee
Roorkee, India

ISSN 2366-2557 ISSN 2366-2565 (electronic)
Lecture Notes in Civil Engineering
ISBN 978-981-15-9804-3 ISBN 978-981-15-9805-0 (eBook)
https://doi.org/10.1007/978-981-15-9805-0

This Springer imprint is published by the registered company Springer Nature Singapore Pte Ltd.
The registered company address is: 152 Beach Road, #21-01/04 Gateway East, Singapore 189721, Singapore

Committees

Steering Committee

Dr. M. D. Venkatesh, Hon'ble Vice Chancellor, Sikkim Manipal University, Sikkim, India
Dr. Karma Sonam Sherpa, Registrar, Sikkim Manipal University, Sikkim, India
Dr. Ashis Sharma, Director, Sikkim Manipal Institute of Technology, Sikkim, India
Dr. Ajeya Jha, Associate Director (Research & Development), Sikkim Manipal Institute of Technology, Sikkim, India
Dr. Chandrashekhar Bhuiyan, Sikkim Manipal Institute of Technology, Sikkim, India
Dr. Somenath Chatterjee, Sikkim Manipal Institute of Technology, Sikkim, India
Dr. H. K. D. Sharma, Sikkim Manipal Institute of Technology, Sikkim, India
Mr. Kiran Sriram, Sikkim Manipal Institute of Technology, Sikkim, India
Mr. Tamal Ghosh, Sikkim Manipal Institute of Technology, Sikkim, India
Ms. Upama Bomzon, Sikkim Manipal Institute of Technology, Sikkim, India
Mr. Kiran Kumar G. R., Sikkim Manipal Institute of Technology, Sikkim, India
Mr. Abhranil Adak, Sikkim Manipal Institute of Technology, Sikkim, India
Mr. Sajal Sarkar, Sikkim Manipal Institute of Technology, Sikkim, India
Mr. Guru Prasad Sharma, Sikkim Manipal Institute of Technology, Sikkim, India
Mr. Himangshu Pal, Sikkim Manipal Institute of Technology, Sikkim, India
Mr. Chinmoy Kar, Sikkim Manipal Institute of Technology, Sikkim, India
Dr. David Raj Micheal, Sikkim Manipal Institute of Technology, Sikkim, India
Ms. Uden K. Sherpa, Sikkim Manipal Institute of Technology, Sikkim, India
Mrs. Reena Pradhan, Sikkim Manipal Institute of Technology, Sikkim, India
Mr. Sourav Gupta, Sikkim Manipal Institute of Technology, Sikkim, India
Mr. Soumyadip Chowdhury, Sikkim Manipal Institute of Technology, Sikkim, India
Mr. Supradeep Singh, Sikkim Manipal Institute of Technology, Sikkim, India
Mr. Rajdeep Roy, Sikkim Manipal Institute of Technology, Sikkim, India

Program Committee

Dr. Wolfgang-Albert Flügel, (Retired Prof.) Friedrich Schiller University, Jena, Germany
Dr. Sharad Kumar Jain, National Institute of Hydrology, Roorkee, India
Dr. P. K. Champati Ray, Indian Institute of Remote Sensing, Dehradun, India
Dr. Dhrubajyoti Sen, Indian Institute of Technology, Kharagpur, India
Dr. Suresh Chand Rai, University of Delhi, India
Dr. Siddhartha Kumar Lahiri, University of Dibrugarh, India
Dr. Sudipta Sarkar, NASA, USA
Dr. Biswa Bhattacharya, UN-IHE Delft, Netherlands
Dr. Bhola Nath Sharma Ghimire, Tribhuvan University, Nepal
Dr. Sadhana Pradhanang Kayastha, Tribhuvan University, Nepal
Dr. Shivam Tripathy, Indian Institute of Technology, Kanpur, India
Dr. Venu Chandra, Indian Institute of Technology, Madras, India
Dr. Briti Sundar Sil, National Institute of Technology, Silchar, India
Dr. Ashis Kumar Saha, University of Delhi, India
Prof. Anil Dutt Vyas, Manipal University, Jaipur, India
Dr. Nairwita Bandyopadhyay, University of Kalyani, India
Dr. Ratika Pradhan, Sikkim Manipal Institute of Technology, Sikkim, India

Preface

Water is the elixir of life, and life cannot thrive without the sustainability of water resources. Due to the galloping rise in population and proliferation of agriculture and industry, demand for water has increased drastically. Pollution of the land and water bodies has caused health hazards and has put life under threat. Ongoing climate change also has a significant impact on the hydrosphere resulting in frequent occurrence of extreme events such as flood and drought causing negative impacts on socio-economic, agricultural, and environmental spheres. High water demand and low water supply due to intense, frequent, or prolonged droughts have resulted in acute water scarcity in many parts of the world leading to mass migration and famine. In the Himalayan basins too, changing climate has increased the threat of flash flood, glacial lake outburst flood (GLOF), and low spring discharge. Thus, the security and sustainability of water resources are under acute risk. Thorough research, proper planning, and effective management of water resources are the need of the hour to ensure its safety, security, and sustainability, to overcome the risks and threats of extreme hydrological events, and to avoid hydrological disasters.

This publication is the outcome of *Down to Earth–2019: Water Security and Sustainability*, the first International Conference organised by the Department of Civil Engineering of Sikkim Manipal Institute of Technology located in Sikkim, India. The conference involved academicians, researchers, eminent scientists, and students in brain-storming sessions. Majority of the participants were young researchers, who presented their research overviews, as well as discussed and debated on water-related problems and solutions.

Selected peer-reviewed manuscripts presented in this conference have been shortlisted for this publication. The shortlisted manuscripts cover a wide range of general topics such as error estimation in rainfall, rainfall–run-off modelling, water quality assessment, arsenic contamination in groundwater, flood characterisation, flood hazard mapping as well as innovative and not so conventional topics like IOT-based water management for smart cities, quantification and characterisation of micro-plastics in freshwater, applications of nanotechnology for degradation of textile effluents in water, removal of organic matters from water using bio-balls,

river bed filtration for pollution removal, GIS-based water pipeline routing, etc. These manuscripts with diverse topics and titles have been categorised into four themes, viz. *Water Resources Assessment*, *Hydro informatics and Geospatial Modelling*, *Extreme Hydrology*, and *Innovative Techniques and Technologies*. We hope that students, academicians, and researchers will enjoy reading these articles and will explore further the innovative ideas and technologies presented in this volume.

Sikkim, India — Chandrashekhar Bhuiyan
Jena, Germany — Wolfgang-Albert Flügel
Roorkee, India — Sharad Kumar Jain

Acknowledgements

Down to Earth–2019: Water Security and Sustainability was supported by the Ministry of Environment, Forest and Climate Change (MoEFCC), Government of India, as an associate and mentor. In this regard, we extend our sincere thanks to Mr. Jigmet Takpa, Joint Secretary, MoEFCC, for his cordial help in initiating this association. We are thankful to organising committee, technical committee, and advisory committee members of the conference for their technical contribution and valuable suggestions. In this regard, the name of Mr. Kiran Sriram deserves special mentioning for his dedicated and tireless efforts to make the conference a great success. We express our genuine thanks to our colleagues from various parts of the world for extending their helping hands whenever sought or needed.

Reviewing of manuscripts is a tedious and so-called thankless job. However, without rigorous review, it is just impossible to identify and rectify errors and mistakes in the research and in the manuscript. A critical appraisal in the form of review report immensely helps authors in improving the standard of their manuscripts. Therefore, we are taking this opportunity to express our genuine thanks to all the reviewers who have offered their valuable time in critical appraisal of the manuscripts and rendered suggestions to the authors.

Finally, this is an opportunity to acknowledge the help we received from Mr. Aninda Bose, Senior Editor of Springer, for introducing and coordinating our proposal with Springer.

Chandrashekhar Bhuiyan
Wolfgang-Albert Flügel
Sharad Kumar Jain

Conference Logo

Sponsor Logo

Abstracts of Invited Talk

Sustainable Water Resources Management in India—Some Thoughts

Dr. Sharad Kumar Jain
Director, National Institute of Hydrology
Roorkee, India

Management of water resources in India has become a challenging task, and the magnitude of the task is rising in recent times due to a number of reasons. Major reasons are the growing population and economy, leading to rising demands; high irrigation water demands; impacts due to climate change; and growing environmental degradation. Broadly, most of the challenges in water management in India can be categorised in the following groups:

(a) Water availability, variability, and increasing withdrawals,
(b) Environment and water quality,
(c) Project construction and maintenance,
(d) Water sharing disputes,
(e) Water governance and institutions, and
(f) Challenges due to climate and land-use/cover changes.

The present talk will discuss these challenges in greater details and will suggest some possible remedies to address the challenges.

Sustainable Groundwater Resource Management in Changing Climate Scenario: Satellite Sensing and Geophysics-based Approach

Dr. P. K. Champati Ray
Group Head, Geosciences and Disaster Management Studies
Indian Institute of Remote Sensing (ISRO)
Dehradun, India

Groundwater resource management in mountainous region has emerged as a challenge particularly in the vast stretches of Himalaya mainly due to high demand and changing climate scenario. Monitoring of groundwater fluctuation using the conventional methodology and space-based observations using GRACE satellites data brings new paradigm to groundwater resource assessment and drought monitoring. Improvements in proven geophysical techniques like earth resistivity tomography (ERT) aided by remote sensing (RS) and GIS can significantly contribute in augmenting precious water resources of the mountainous region. In the present paper, mutually exclusive but complementary techniques are discussed in the light of efficient groundwater resource estimation and management.

The GRACE twin satellites, launched on 17 March 2002, have made detailed measurements of Earth's gravity field and improved understanding of Earth's water reservoirs by providing some of the path-breaking observations on terrestrial water storage changes, ice-mass variations, ocean bottom pressure changes, and sea-level variations. Several studies have been taken up at IIRS which used observations derived from GRACE satellite mission and land surface model outputs from the Global Land Data Assimilation System (GLDAS) to show tremendous variations and decline of the precious groundwater resource, thus making space-based observation very critical for large-scale monitoring of the groundwater.

Many hill towns like Mussoorie in Himalaya starve for water in peak tourist season. The springs which had provided water for ages are in a precarious condition, and there is an urgent need to improve recharge of such precious drinking water sources in hilly areas. Using electrical resistivity tomography (ERT), potential recharge conduits were identified in some watersheds of Mussoorie, and other potential spring sheds were identified for augmenting water resources for Mussoorie based on RS and GIS. Secondly in Mussoorie hilltop/ridge area, it is popularly

believed that the water table is very deep, and it may not be feasible to tap such resources for drinking water purposes. However, based on lineament analysis on high-resolution satellite images and geophysical survey (2-D ERT and single point resistivity survey), it was proved that at a selected place, groundwater resources can be locally tapped. Therefore, it is imperative that such new technological approaches must be integrated in regular monitoring, assessment, and resource augmentation to address the challenges of overall groundwater management in different geological set-up in changing climate scenario.

Vulnerability and Conservation of Himalayan Wetlands with Special Reference to Sikkim

Prof. Suresh C. Rai
Department of Geography
Delhi School of Economics
University of Delhi
New Delhi, India

Wetlands are very important and productive ecosystems that support a wide range of plants and animals and provide livelihood opportunities to local communities. However, they are increasingly being threatened by rapid urbanisation, developmental interventions, unsustainable management practices, and encroachment. The Himalayas, with its unique topography and climatic regimes, support diverse wetland habitats across a range of altitudes. Himalayan high-altitude wetlands (HAWs) include lakes, ponds, and rivers located at altitudes higher than 3000 masl and are often fed by glaciers or snow from the surrounding mountains. Sikkim, a small state in the Eastern Himalaya, has only natural inland wetlands belonging to the category lakes/ponds. By using data of high resolution, we obtain 1104 glacial and high-altitude lakes with total area 30.498 km^2, of which 472 have an area >0.01 km^2. Most of it are fed by glaciers and considered sacred.

The hydrology and ecological linkages between Khecheopalri Lake and its surrounding watershed in Sikkim were investigated to assess the long-term impacts of land-use/cover change on the hydrology of the lake ecosystem and bog formation around the glaciated lake. Significant land-use/cover change occurred in the past 4 decades. The bog areas expand by 67%, while the area under agriculture land in the lake watershed grew by 63% between 1988 and 1997. These changes accelerate the annual soil loss from the lake watershed which was 502 Mg km^{-2} and a net sediment deposition in the lake was 141 Mg yr^{-1}. To conserve the lake, it is necessary to minimise agricultural practices in the upper part of the watershed, and agroforestry practices should be encouraged to maintain the health and longevity of the lake.

Contents

About the Editors

Dr. Chandrashekhar Bhuiyan is a researcher in the field of Applied Geoscience. He obtained his Bachelor's in Geology from the University of Burdwan followed by his M.Tech. in Applied Geology from the University of Roorkee (presently, Indian Institute of Technology Roorkee), and his Ph.D from Indian Institute of Technology Kanpur. He is a DAAD Fellow, and carried out a part of his doctoral research at the Friedrich Schiller University, Jena, Germany through DAAD "Sandwich-model PhD" programme. He has post-PhD research experience at several national and international institutes including School of Environmental Sciences, Jawaharlal Nehru University and School of Environmental Studies, University of Delhi. Dr. Bhuiyan was a recipient of DAAD 'Reinvitation Fellowship' to visit the University of Cologne, Germany in 2009 as a Visiting Scientist. He has authored more than 25 research articles in reputed international journals and conferences, and also published several book chapters. His research interests include hydrogeology, extreme hydrology, water resources, aquifer vulnerability modelling, artificial groundwater recharge, and natural hazards. He has carried out extensive research on hydrogeological modelling, drought dynamics, water resources assessment, and water scarcity problems of Rajasthan and Gujarat. He along with his associates is also engaged in research on anthropogenic and climate change impacts on Himalayan springs, particularly in Sikkim. He has worked also in international projects (funded by World Bank) on seismic micro-zoning through trench survey and active fault mapping in Kachchh, Gujarat. Currently, Dr. Bhuiyan is affiliated to Sikkim Manipal Institute of Technology, as Professor and Head of the Civil Engineering Department.

Prof. Wolfgang-Albert Flügel is retired Chair for Geoinformatics and former Head of the Department of Geoinformatics, Hydrology and Modelling (DGHM) at the University of Jena, Germany. Earlier he was an Assistant Professor at the University of Heidelberg, Germany (1978–1984), Senior Specialist Scientist at the Hydrological Research Institute (HRI), Department of Water Affairs in South Africa (1985–1990), Professor for Geohydrology at the University of Bonn, Germany, (1990–1994), and Principal Researcher at the International Water

Management Institute (IWMI), Colombo, Sri Lanka (2002–2003). His research expertise is about hydrological system analysis, process based rainfall-runoff modelling, climate change impact assessment and analysis in large river basins, e.g. the Brahmaputra River basin, and integrated land and water resources management (ILWRM). He acquired and fund raised 93 interdisciplinary research projects in Southern Africa, Brazil, Europe and South Asia funded e.g. by the European Commission (EC), the German Research Association (DFG), and the Federal Ministry of Education and Research (BMBF). He supervised 96 MSc theses, and 24 PhD projects, has authorship in more than 120 publications, and was editor of a Springer booklet on the Brahmaputra River basin. He established the Integrated Land Management System (ILMS) at the Jena University, in 2006 and coordinated the INNO-Asia project in the North-Eastern Region (NER) of India. In 2000, he was awarded with the Biennial Medal of Natural Systems of the Modelling and Simulation Society of Australia and New Zealand (MSSANZ), and in 2012 and 2014 he was appointed by the former Chief Minister of Assam, India, as international member of the "Advisory group of experts on flood and erosion and water management" for the Brahmaputra River. Since his retirement in 2014, he is an internationally active consultant for applied Geoinformatics in Integrated Land and Water Resources Management (ILWRM) and hydrological climate change analysis in river basins.

Dr. Sharad Kumar Jain is an eminent hydrologist and researcher. He recently superannuated from the post of the Director of National Institute of Hydrology (NIH), Roorkee, India and is currently serving as Visiting Professor, Civil Engineering Department, IIT Roorkee. He received his B.E (Civil) from University of Roorkee, (1980) and M. Tech (Hydraulics & Water Resources) from Indian Institute of Technology Kanpur (1982). He received his PhD from University of Roorkee (1990). He has a vast experience in research and teaching for more than 38 years. His research interests include Surface Water Hydrology, Water Resources Planning and Management, and Application of Advanced Tools such as Artificial Neural Networks, Remote Sensing, GIS and Decision Support Systems etc.

Dr. Jain has authored 5 books, and contributed to over 250 technical papers in various international and national journals. He has also edited 5 books, and written 8 chapters in handbooks/ encyclopedia, 20 book chapters and over 80 technical reports at NIH. He has also worked on more than 40 research and consultancy projects. Dr. Jain has worked as visiting faculty at the Department of Civil and Environmental Engineering in Louisiana State University, Baton Rouge, USA. He is a member of many national/international committees in his field of work and is a member of editorial boards of three journals.

Water Resources Assessment

Numerical Analysis of Water Movement in Agricultural Fields with Heterogeneous Unsaturated Soils

Ephrem Yetbarek and Richa Ojha

Abstract The natural variability exhibited by soil hydraulic properties poses severe challenges to model water movement through porous formations in agricultural fields. In this study, a 3D numerical approach coupled with the turning bands method to generate realizations of soil formation properties with different heterogeneity levels to solve the governing partial differential equation in variably saturated soils was used to simulate field scale water flow to investigate the impact of soil heterogeneity and root water uptake on subsurface flow dynamics in cropped fields. Soil moisture, suction head and hydraulic conductivity were observed to be significantly affected by heterogeneity of the media and root water uptake. Soil heterogeneity was found to increase soil water content while root water uptake was decreasing it. The effect of root water uptake on soil moisture distribution was more pronounced under homogenous soils than in heterogeneous soils. Soil suction head decreases with increasing soil heterogeneity whether root water uptake was considered or not. Hydraulic conductivity increases with increasing soil heterogeneity when root water uptake was ignored, and it depends on the heterogeneity level when root water uptake was accounted.

Keywords Soil heterogeneity · Cropped fields · Numerical simulation · Richards equation

1 Introduction

The natural variability exhibited by soil hydraulic properties poses severe challenges to modeling of water movement through the porous formation in cropped fields [1–3]. The relationship between soil physical and hydraulic properties at different scales has been investigated [4], and one- or two-order degree of spatial variability in soil hydraulic conductivity has been observed [2, 5–8].

E. Yetbarek (✉) · R. Ojha
Department of Civil Engineering, Indian Institute of Technology Kanpur, Kanpur 208016, India
e-mail: ephrem@iitk.ac.in

C. Bhuiyan et al. (eds.), *Water Security and Sustainability*,
Lecture Notes in Civil Engineering 115,
https://doi.org/10.1007/978-981-15-9805-0_1

In real-world conditions, where water flow around the surface of the unsaturated zone is affected by time-dependent, non-monotonic processes such as irrigation, rainfall, root water uptake, and evaporation, a more realistic predictions can be obtained from a numerical approach that combines a turning band method to generate realizations of soil formation with different heterogeneity levels to solve the governing partial differential equations [9, 10]. Furthermore, a numerical approach can overcome most of the limitations of deterministic and stochastic models. It should be emphasized that extreme difficulties may arise while solving the numerical problem when dealing with steep head gradients due to the nonlinearity and complexity of unsaturated flows. Further, a numerical grid size much smaller than the heterogeneity scale should be used to preserve a given statistics of the formation properties [9]. However, a 3D numerical formulation allows the fluid particles to evade zones of low conductivity in lateral flows and may describe locally the actual flow in spatially variable soils for cropped fields.

In this study, a nonlinear root water uptake model developed by Ojha and Rai [11] coupled with 3D Richards equation was used to investigate the impact of soil heterogeneity and root water uptake on subsurface flow dynamics in cropped fields. A 3D numerical approach coupled with the turning bands method to generate realizations of soil formation properties with different heterogeneity levels to solve the governing partial differential equation in variably saturated soils was used to simulate field scale water flow to investigate the impact of soil heterogeneity and root water uptake on subsurface flow dynamics in cropped fields. The governing partial differential equation was solved by a block-centered, finite-difference method with a variable time step and uniform grid. To linearize the nonlinear terms of the governing equation, the modified Picard iteration schemes were used. The spatial heterogeneity of the soil hydraulic properties, evaporation, irrigation, and root water uptake was incorporated into the simulation model to account the real-world scenarios. The results of this work may help modelers and experimentalists to observe the significance of spatial heterogeneity in cropped lands and consider it for irrigation scheduling and water resources management at large.

2 Methodology

The governing equation for flow through unsaturated soils is the Richards equation. The 3D mixed form of it can be written as follows:

$$\frac{\partial \theta(\psi)}{\partial t} = \frac{\partial}{\partial x}\left[K_x(\psi)\frac{\partial \psi}{\partial x}\right] + \frac{\partial}{\partial y}\left[K_y(\psi)\frac{\partial \psi}{\partial y}\right] + \frac{\partial}{\partial z}\left[K_z(\psi)\left[\frac{\partial \psi}{\partial z} + 1\right]\right] - S_{\mathrm{w}} \tag{1}$$

where $\theta(\psi)$ is the moisture content ($\mathrm{L}^3\mathrm{L}^{-3}$), $K_x(\psi)$, $K_y(\psi)$ and $K_z(\psi)$ is unsaturated hydraulic conductivities (LT^{-1}) in the x-, y-, and z-directions, respectively; ψ is the soil water pressure head (L); S_{w} is the root water uptake term ($L^3L^{-3}T^{-1}$).

2.1 Soil Hydraulic Property Models

Since Richards equation is an open form equation, constitutive equations are required to solve it. In the present study, the model proposed by van Genuchten and Nielsen [12], which relates the independent parameter suction head with soil moisture and hydraulic conductivity, was used.

2.2 Initial and Boundary Conditions

A hydrostatic condition with a suction pressure head of −2 m was assumed as the initial condition. The upper boundary condition switches between prescribed flux and constant head boundary conditions depending on the availability of water on the surface. It is also assumed that any water beyond the maximum ponding depth will be runoff and will not be considered in the analysis. No flow and free gravity drainage boundary conditions were assumed at the walls and bottom boundary, respectively.

2.3 Generation of Flow Parameters and Choice of Domain Size

Saturated hydraulic conductivity, K_s, and van Genuchten pore size distribution parameter, α, were treated as a continuous stochastic functions with multivariant lognormal probability density function with mean values of 1.06 (cm/day) and −1.48 (cm^{-1}), respectively. Three different sandy clay soil formations: a spatially homogeneous media ($\sigma_Y^2 = 0$) and two heterogeneous formations with two variances ($\sigma_Y^2 = 0.3$ and $\sigma_Y^2 = 0.6$), where $Y = \ln K_s$ or $\ln \alpha$, were considered in the simulations. The correlation length scales of the van Genuchten model parameters were assumed to be equal to those of Y, which is taken from [13], i.e. $I_{px} = I_{py} = 0.8$ m and $I_{pz} = 0.2$ m. All the formations will have similar geometric mean of K_s and α, and the only parameter which will vary is the variance. Considering ergodic assumption and single realization approach to be economical, the flow domain size was fixed to be 10, 20, and 5 m along the x-, y-, and z-directions, respectively. Saturated moisture content, θ_s, was taken to be 0.4 (cm^3/cm^3). Residual moisture content, θ_r, and van Genuchten pore size shape parameter, n, were considered to be 0.01 (cm^3/cm^3) and 1.4, respectively.

3 Results and Discussion

3.1 *Effect of Root Water Uptake and Soil Heterogeneity on Soil Moisture Dynamics*

Mean soil moisture increases with increasing soil heterogeneity, and root water uptake significantly reduced soil moisture content. When root water uptake was not considered, as shown in Fig. 1a, c, and e, soil moisture dynamics was mainly active in the top 1.5 m depth only, the minimum soil water content on the profile was observed at 0.5 m depth from the surface, and the moisture pattern was almost similar under all soil conditions. Root water uptake effect on soil moisture distribution was more pronounced under homogenous soils than in heterogeneous soils. The depth range where root water uptake effect on soil moisture pattern was observed

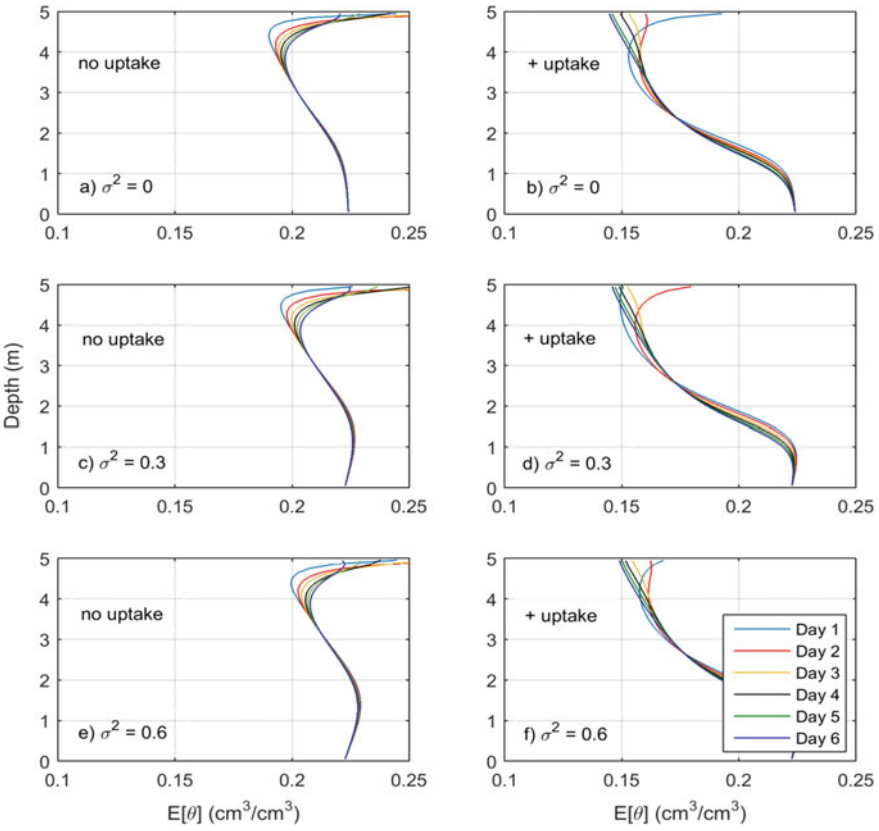

Fig. 1 Mean soil moisture profile for six successive days after irrigation (64th day of the simulation) in homogeneous ($\sigma^2 = 0$) and heterogeneous sandy clay soil ($\sigma^2 = 0.3$ and $\sigma^2 = 0.6$) with (**a**, **c**, **e**) and without (**b**, **d**, **f**) root water uptake

significantly varies with soil type. It shrinks from around 2.5 m from the surface in homogeneous medium (Fig. 1b) to around 2 m in the highly heterogeneous media (Fig. 1f). The soil moisture variability range also depends on the media type, and it decreases with increasing soil heterogeneity. Near to the surface, for example, it varies between 14–19% and 15–17% on homogenous and highly heterogeneous soils, respectively. Unlike in the cases where water uptake was ignored, the minimum mean soil moisture was observed near to the surface when root water uptake was accounted. Under homogeneous and highly heterogeneous soils, the response of soil moisture change was fast for the applied water (Fig. 1b, f). But, it was delayed for the moderately heterogeneous soil (Fig. 1d). When there was no root water uptake, the maximum soil moisture content was observed on the second day after irrigation for all soil types, and the peak value was observed on the moderately heterogeneous soil (Fig. 1c).

3.2 Effect of Root Water Uptake and Soil Heterogeneity on Suction Head

Mean suction head distribution when there was no crop cover exhibits small range of negative head. As shown in Fig. 2a, c, and e, the matric head profile shows decrement in head (became less negative) with increasing soil heterogeneity simulated under the same initial conditions. A significant change in suction head was observed when root water uptake was considered. Under homogeneous soil condition, the minimum head range dropped from −4.5 to −27 m (Fig. 2a, b). From Fig. 2, it is possible to see a shift in the location where the minimum suction head took place as root water uptake was accounted. When it was ignored, the minimum head was observed at 0.5 m depth from the surface irrespective of heterogeneity. But, it was shifted to around the surface when root water uptake was considered. In addition, a smooth shift in head profile was exhibited from day 1 to day 6 in no uptake scenarios. A sudden rise and maximum value in head was observed on the day of irrigation in cropped surfaces. The maximum head achieved under irrigation condition varies with soil heterogeneity. For example, for homogeneous case, the maximum head recorded was −4 m, and it was −6 and −9 m on moderately heterogeneous and highly heterogeneous cases, respectively, when root water uptake was considered. The range where root water uptake effect was observed depends on soil heterogeneity.

3.3 Effect of Root Water Uptake and Soil Heterogeneity on Hydraulic Conductivity

Hydraulic conductivity increases with increasing heterogeneity of soil when root water uptake was not considered, and its maximum value was observed near to

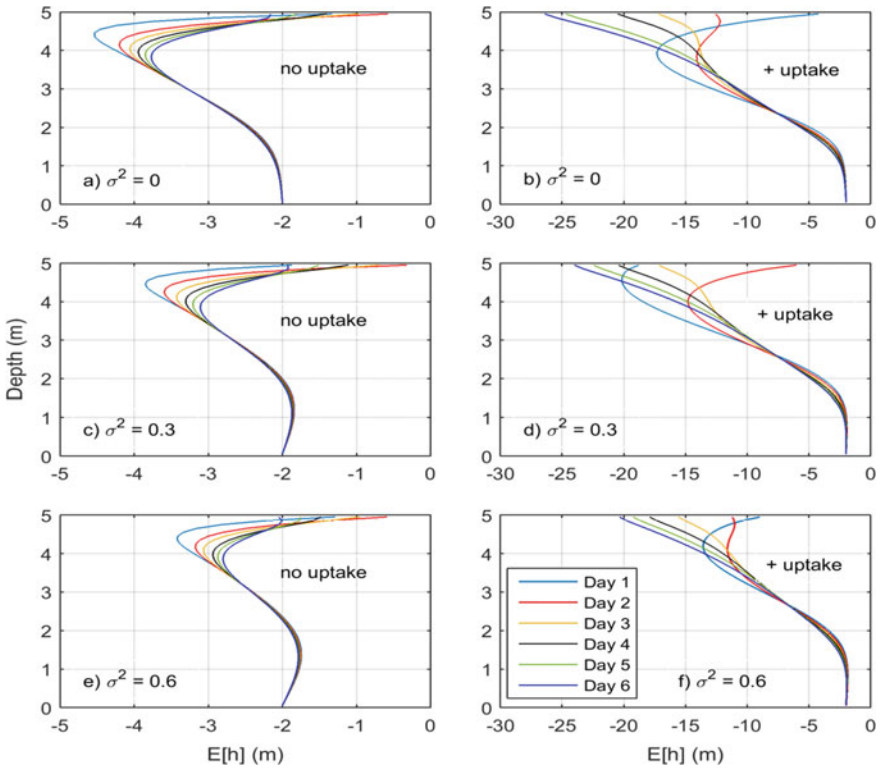

Fig. 2 Mean soil matric head profile for six successive days after irrigation (64th day of the simulation) in homogeneous ($\sigma^2 = 0$) and heterogeneous sandy clay soil ($\sigma^2 = 0.3$ and $\sigma^2 = 0.6$) with (**a**, **c**, **e**) and without (**b**, **d**, **f**) root water uptake

the surface. As shown in Fig. 3, root water uptake significantly reduced hydraulic conductivity. There was a slight reduction in hydraulic conductivity for less heterogeneous soil (Fig. 3d) as compared to the homogeneous case (Fig. 3b), and it again increases for a highly heterogeneous soil (Fig. 3f). For no root water uptake conditions, the maximum hydraulic conductivity was observed on the second day after irrigation for homogeneous and highly heterogeneous soils (Fig. 3a, e), and on the third day for moderately heterogeneous soils (Fig. 3c). When root water uptake was considered, the maximum hydraulic conductivity observed on the second day after irrigation irrespective of heterogeneity. The depth range where the effect of root water uptake on hydraulic conductivity observed depends on the type of medium. As shown in Fig. 3b, d, and f, it decreases with increasing soil heterogeneity. One visible difference in hydraulic conductivity distribution near to the surface related to consideration of root water uptake was how it approaches the surface. When uptake was considered, it approaches the surface asymptotically in all the days considered. However, it approaches the surface perpendicularly, except the first two days after irrigation, when uptake was accounted.

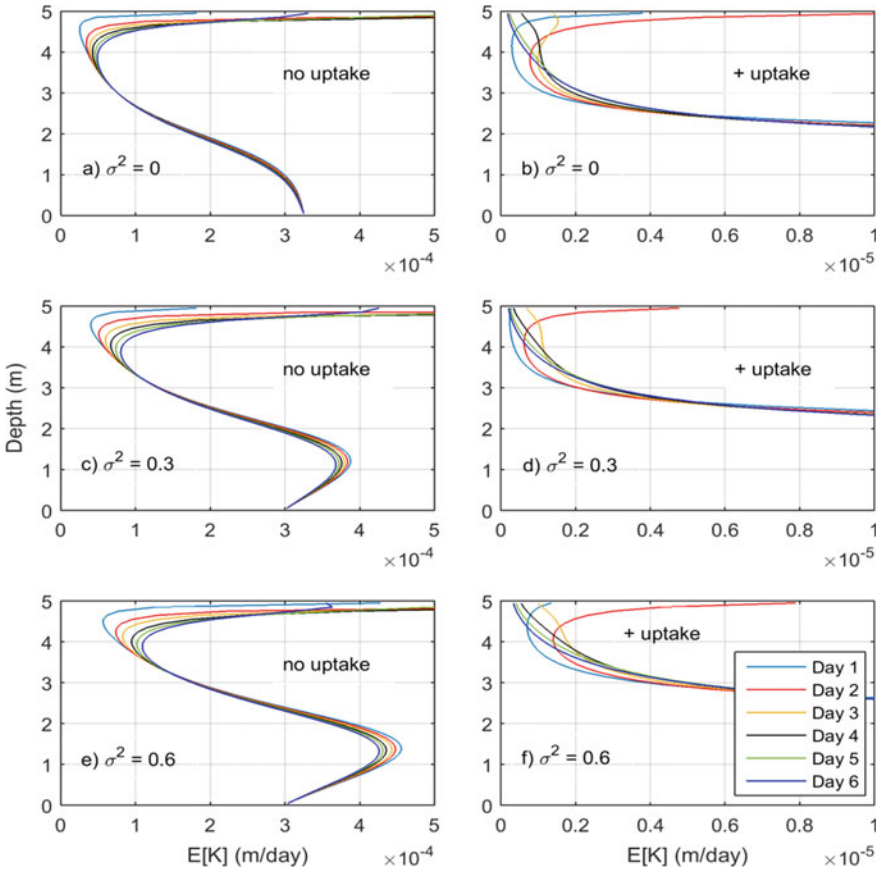

Fig. 3 Mean hydraulic conductivity profile for six successive days after irrigation (64th day of the simulation) in homogeneous ($\sigma^2 = 0$) and heterogeneous sandy clay soil ($\sigma^2 = 0.3$ and $\sigma^2 = 0.6$) with (**a**, **c**, **e**) and without (**b**, **d**, **f**) root water uptake

4 Conclusion

In this study, the effect of soil heterogeneity and root water uptake on subsurface water flow in agricultural fields was investigated. A 3D numerical approach coupled with the turning bands method to generate soil formation properties realizations with different heterogeneity levels to solve the governing partial differential equation in heterogeneous and variably saturated soils was used to simulate field scale water flow to investigate the impact of soil heterogeneity and root water uptake on subsurface flow dynamics in cropped fields. Soil hydraulic properties spatial heterogeneity, evaporation, irrigation, and root water uptake were coupled into the simulation model to mimic the real-world scenarios. Soil moisture dynamics was observed to be significantly affected by soil heterogeneity and root water uptake.

Soil heterogeneity was observed to increase soil moisture while root water uptake was decreasing it. Root water uptake effect on soil moisture distribution was more pronounced under homogenous soils than in heterogeneous soils. The soil moisture variability range depends on the media type, and it decreases with increasing soil heterogeneity. Soil suction head decreases with increasing soil heterogeneity whether root water uptake was considered or not. Its response for the applied water depends on heterogeneity and consideration of root water uptake. Hydraulic conductivity increases with increasing soil heterogeneity when root water uptake was ignored, and it depends on the heterogeneity level when root water uptake was accounted. The depth range where the effects of root water uptake on suction head and hydraulic conductivity observed depends on the type of medium.

Acknowledgements The research was funded by Science and Engineering Research Board, Department of Science and Technology, India, under Grant No. ECR/2016/000378.

References

1. Bresler E, Dagan G (1988) Variability of yield of an irrigated crop and its causes 1. Statement of the problem and methodology. Water Resour Res. 24(3):381–387
2. Green TR, Dunn GH, Erskine RH, Salas JD, Ahuja LR (2009) Fractal analyses of steady infiltration and terrain on an undulating agricultural field. Vadose Zone J 8(2):310–320
3. Usowicz B, Lipiec J (2017) Spatial variability of soil properties and cereal yield in a cultivated field on sandy soil. Soil Tillage Res 174:241–250
4. Bevington J, Piragnolo D, Teatini P, Vellidis G, Morari F (2016) On the spatial variability of soil hydraulic properties in a Holocene coastal farmland. Geoderma 262:294–305. https://doi.org/10.1016/j.geoderma.2015.08.025
5. Nielsen DR, Biggar W, Erh KT (1973) Spatial variability of field-measured soil-water properties. Hilgardia 42(7):215–260
6. Sharma ML, Gander GA, Hunt CG (1980) Spatial variability of infiltration in a watershed. J Hydrol 45:101–122
7. Warrick AW, Nielsen DR (1980) Spatial variability of soil physical properties in the field. In: Applications of soil physics. Academic Press, Inc., pp 319–344
8. Herbst M, Diekkrüger B, Vereecken H (2006) Geostatistical co-regionalization of soil hydraulic properties in a micro-scale catchment using terrain attributes. Geoderma 132:206–221
9. Russo D, Zaidel J, Laufer A (1998) Dimensional partially saturated heterogeneous soil. Water Resour Res 34(6):1451–1468
10. Chen P-Y, Chen C-H, Hsu N-S, Wu C-M, Wen J-C (2012) Influence of heterogeneity on unsaturated hydraulic properties: (1) local heterogeneity and scale effect Hydrol Process 26(23):3593–3603
11. Ojha CSP, Rai AK (1996) Nonlinear root-water uptake model. J Irrig Drain Eng 122(4):198–202
12. van Genuchten MT, Nielsen DR (1985) On describing and predicting the hydraulic properties of unsaturated soils. Ann Geophys 3(5):615–628
13. Fiori A, Russo D (2007) Numerical analyses of subsurface flow in a steep hillslope under rainfall: the role of the spatial heterogeneity of the formation hydraulic properties. Water Resour Res 43(7):1–14

Three-Dimensional Numerical Simulation of Pressure-Flow Scour

Sofi Aamir Majid and Shivam Tripathi

Abstract An estimate of scour depth is required in the design of bridges. Much of the research on scour estimation has focussed on the local scouring, i.e. scouring near abutments or around piers. In comparison, contraction scouring has received less attention. Contraction scouring occurs when the waterway is contracted either laterally or vertically. During extreme flood events, the water level may rise above the bottom chord of the bridge, creating a pressure-flow situation in the passage below the bridge. The pressure scour thus induced is not clearly understood in terms of its location, geometry and time evolution. Some recent experimental studies have tried to establish empirical relations between scour parameters and various properties of flow, fluid and bed material. However, numerical approach has not been employed to study the pressure scour. The present study is an attempt to numerically simulate the pressure scour caused due to vertical contraction. International River Interface Cooperative (iRIC) solver NAYSCube is used to simulate the flow over mobile bed. NAYSCube, an open source 3D flow solver, employs finite volume method to solve Navier–Stokes equations and couples turbulence and bed-load models. Due to the limitations of the computational capacity, the simulations are performed to generate the flow and bed data for a period of one hour. The approaching flow velocity, channel slope and the sediment size of the bed are kept constant. The results show that bed shear has the maximum value inside the contraction section. The scour hole is observed to develop within the contraction towards the upstream face of the contraction. The magnitude of maximum scour is found to increase with increase in degree of contraction or length of contraction or both. The study establishes the need to conduct more numerical simulations to investigate pressure-flow scouring.

Keywords Bed scour · Pressure flow · Sediment transport · Numerical simulation

S. A. Majid (✉) · S. Tripathi
Department of Civil Engineering, Indian Institute of Technology Kanpur, Kanpur 208016, India
e-mail: aamirm@iitk.ac.in

C. Bhuiyan et al. (eds.), *Water Security and Sustainability*,
Lecture Notes in Civil Engineering 115,
https://doi.org/10.1007/978-981-15-9805-0_2

1 Introduction

Scouring is a very complex process that occurs due to the interaction of the flow with the bed material. Different theories have been proposed to explain the inception of sediment motion. The most widely accepted theory is the Shield's theory [4]. It states that the motion of sediment is initiated only when the bed shear stress exceeds the critical shear stress. The numerical modelling for scouring by Shield's theory would thus require a good understanding of flow as well as bed properties. An extensive literature exists on fluid mechanics as well as sediment transport and scouring [1, 5].

Scouring can occur due to a localised obstruction to the flow or due to contraction in the flow passage. The contraction can be either vertical or horizontal. During flood events, a pressure flow situation may be developed in the passage under the bridge. The pressure flow is associated with increased bed stresses increasing the chances of scouring in the passage [5]. The local scouring has been studied extensively from both numerical and experimental perspectives. In comparison, the pressure flow scouring due to the vertical contraction has received less attention. A few experimental studies have reported the magnitude of vertical contraction scouring to be a function of flow velocity, degree and length of contraction together with the bed properties. A proper physical understanding of the contraction scouring is lacking due to the absence of velocity field data. Further, no numerical approach has been reported to study the pressure flow scouring due to vertical contraction.

2 Numerical Model

In the present study, clear-water pressure-flow scouring is simulated by solving the Navier–Stokes equations coupled with k-ε closure turbulence model and Meyer-Peter and Müller bed load transport model [3]. Clear-water scouring is achieved by setting the average approach flow velocity below the critical velocity for sediment motion inception. The critical velocity is calculated by Neil's formula:

$$V_c = 1.52\sqrt{g(s-1)D_{50}}\left(\frac{y}{D_{50}}\right)^{\frac{1}{6}} \tag{1}$$

where 'y' is the depth of flow, 's' is the specific gravity and 'd_{50}' is the median diameter of the bed material. This numerical model solves the time-dependent Reynolds-averaged Navier–Stokes equations:

$$\frac{\partial U_i}{\partial t} + U_j\frac{\partial U_i}{\partial x_j} = \frac{1}{\rho}\frac{\partial}{\partial x_j}\left(-P\delta_{ij} - u_i u_j\right) \tag{2}$$

where 'U_i' is the time-averaged velocity field, 'ρ' is the density of the fluid, 'P' is the piezometric pressure field, 'δ_{ij}' is the Dirac-delta operator and '$-\rho u_i u_j$' is the Reynolds stress tensor. The first term on the left side of Eq. 2 is the transient term

followed by the advection term. The eddy viscosity model is used to evaluate the Reynolds stress term as

$$-u_i u_j = \nu_t \frac{\partial U_i}{\partial x_j} - \frac{2}{3}\alpha\delta_{ij} \tag{3}$$

where 'ν_t' is the eddy viscosity and 'α' is the turbulent pressure. The k–ε model is used to calculate the eddy viscosity:

$$\nu_t = c_\mu \frac{k^2}{\varepsilon} \tag{4}$$

where 'k' is the turbulent kinetic energy modelled as:

$$\frac{\partial k}{\partial t} + U_j \frac{\partial k}{\partial x_j} = \frac{\partial}{\partial x_j}\left(\frac{\nu_t}{\sigma_k}\frac{\partial k}{\partial x_j}\right) + P_k - \varepsilon. \tag{5}$$

P_k is given by:

$$P_k = \nu_t \frac{\partial U_i}{\partial x_j}\left(\frac{\partial U_j}{\partial x_i} + \frac{\partial U_i}{\partial x_j}\right). \tag{6}$$

'ε' is the energy dissipation in turbulent flows modelled as:

$$\frac{\partial \varepsilon}{\partial t} + U_j \frac{\partial \varepsilon}{\partial x_j} = \frac{\partial}{\partial x_j}\left(\frac{\nu_t}{\sigma_\varepsilon}\frac{\partial \varepsilon}{\partial x_j}\right) + C_{\varepsilon_1}\frac{\varepsilon}{\beta}P_k - C_{\varepsilon_2}\frac{\varepsilon^2}{\beta} \tag{7}$$

where c_μ, σ_k, σ_ε, C_{ε_1}, C_{ε_2} and 'β' are model constants having values of 0.09, 1.00, 1.30, 1.92, 1.44 and 0.43, respectively. The above equations are supplemented by the continuity equation to numerically close the model.

$$\frac{\partial U_i}{\partial x_i} = 0 \tag{8}$$

For the modelling of bed load, Meyer-Peter and Müller model is used:

$$\frac{q_{\mathrm{Bs}}}{\sqrt{(s-1)g d_{50}^3}} = 8\left(\tau^* - \tau_{\mathrm{c}}^*\right)^{1.5} \tag{9}$$

where 'q_{Bs}' is the bed load per unit width of channel in m^2/s, 'τ^*' is the non-dimensional bed shear stress and 'τ_{c}^*' is the critical bed shear stress.

In the present study, International River Interface Cooperative (iRIC) solver NAYSCube is used to solve the flow field. The flow domain is discretised to form a grid of finite number of control volumes. The velocity flux is calculated at the face of each control volume, and the pressure field is calculated at the centre of each control

volume. Further, the surface changes and the bed deviations are incorporated into the flow domain using the interface tracking method (ITM) to increase computational efficiency [2]. The bed deviations are calculated explicitly after the flow field has been calculated for each time step. The advection terms are discretised using TVD-MUSCL scheme (TVD: Taylor–Green vortex flow; MUSCL: monotone upstream-centred scheme for conservation laws) which is a third-order accurate discretisation scheme. The coefficient for *Courant–Friedrichs–Lewy (*CFL) condition to determine the time step between two successive computations is set to 0.2. Six problems of pressure scouring are simulated, and the details are given in Table 1.

A typical computational grid is shown in Fig. 1. The coordinate 'x' is measured from the upstream face of the contraction.

The particle mean diameter, d_{50}, bed slope, S_0, length, L, and breadth, W, of the channel are kept constant for every simulation having values of 0.0003 m, 0.0002, 3.0 m and 0.3 m, respectively. A constant discharge of 0.006 m^3/s is set for each simulation, and the outlet water level is set by assuming the flow in the channel to be uniform. A uniform depth of 0.0085 m is obtained for each simulation.

Table 1 Geometry of the simulated cases

S. No.	Designation	Length of contraction (m)	Width of contraction (m)
1	L15W6	0.15	0.06
2	L15W7	0.15	0.07
3	L15W8	0.15	0.08
4	L20W6	0.20	0.06
5	L20W7	0.20	0.07
6	L20W8	0.20	0.08

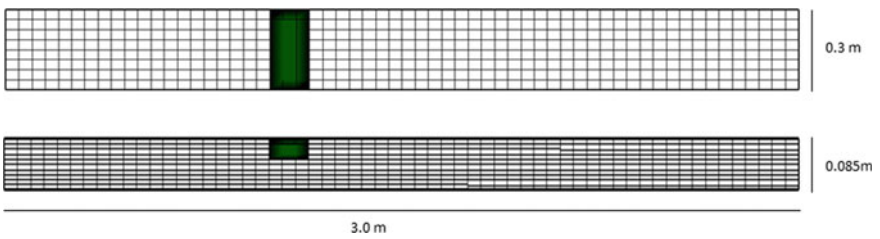

Fig. 1 Computational grids for L15W6 numerical experiment. The top panel shoes the plan view and the bottom panel shows the side view of the channel

3 Results and Discussions

For the erosion to take place at some point in the flow domain, bed shear stress at that point has to exceed the critical shear stress. The critical stress, which is a function of the particle diameter as well as the flow depth, is calculated from the classical shield's diagram. For the present study, the particle diameter and flow depth are 0.0003 m and 0.085 m, respectively, and the critical shear stress comes out to be 0.185 N/m^2. The bed shear is calculated using the rough logarithmic law. The three parameters of interest include the time evolution of scour hole, magnitude and location of maximum scouring. The magnitude of scouring is measured as the bed deviation from the original bed level at the start of the simulation. It is observed that the magnitude of scouring inside the contraction is very fast in the initial phases of the simulation (Fig. 2), and with time, the bed attains an equilibrium level when the flow passage increases to a value such that bed shear becomes equal to critical shear stress. However, the rate of bed deviation for L15W6 is smaller than L20W6 (Fig. 2a) because of the bed stress concentration which increases with the increase in length. Similarly, the rate of deviation increases as the contraction is reduced due to increase in bed shear (Fig. 2b).

The maximum pressure flow scour is a function of both the length of contraction and degree of contraction. It is observed that the magnitude of maximum scour increases with the increase in the length of contraction (Fig. 3a). The location of maximum scour is at the upstream face of the contraction for both L15W7 and L20W7. A possible explanation to this phenomenon are the vortices developed due to obstruction of flow. Further, it is observed that the magnitude of maximum scouring increases with an increase in the degree of contraction (Fig. 3b). The increase in the degree of contraction increases the bed shear in the contraction which increases the scouring potential of flow. However, the degree of contraction has no effect on the location of the scour hole.

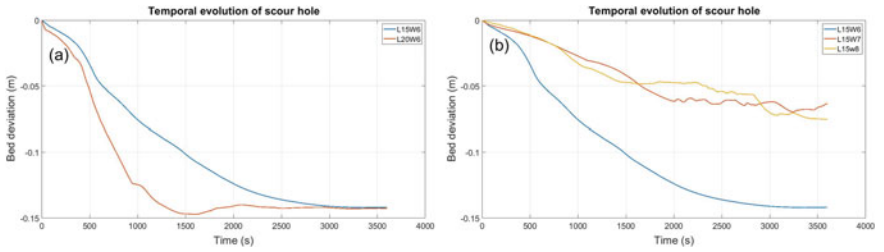

Fig. 2 Temporal deviation of bed for **a** different lengths of contraction with same degree of contraction and **b** different degrees of contraction with same length of contraction

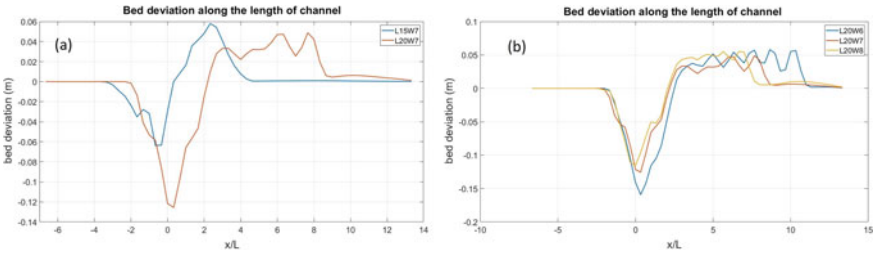

Fig. 3 Scour hole geometry along the length of channel for **a** different lengths and **b** different degrees of contraction

4 Conclusions

The present study is based on the numerical simulations of the pressure flow scouring due to vertical contraction in a flow passage. The scouring thus induced is a function of the flow geometry and bed characteristics. However, the present study is restricted to the flow geometry only. Other parameters like bed slope, flow depth, particle diameter and the flow velocity are kept constant. It is observed that the bed shear has the maximum value inside the contraction. For all the simulations, the scour hole is observed to develop within the contraction towards the upstream face of the contraction. The magnitude of maximum scour is a function of both the length of the contraction and the degree of the contraction. The magnitude of maximum scour increases with increase in degree of contraction or length of contraction or both. A complete understanding of the pressure flow scour would require the inclusion of the other flow and bed properties in the simulations and the validation of numerical results with experimental observations.

References

1. Arneson LA, Abt SR (1998) Vertical contraction scour at bridges with water flowing under pressure conditions. Transportation Research Record 1647 Paper No. 98-0443
2. Kimura I, Hosoda T, Onoda S (2002) Numerical simulator on full staggered boundary fitted coordinate system for the analysis of 3D turbulent flows in open channels. Yokkaichi Univ J Environ Inf 5(combined issue for no. 1 and 2):145–170 (in Japanese)
3. Meyer-Peter E, Müller R (1948) Formulas for bed-load transport. In: Proceedings of 2nd meeting, IAHR, Stockholm Sweden, pp 39–64
4. Shields A (1936) Application of similarity principles and turbulence research to bed-load movement. Report (trans: Ott WP, van Uchelen JC, California). Institute of Technology, Pasadena
5. Umbrell ER, Young GK, Stein SM, Jones JS (1998) Clear-water contraction scour under bridges in pressure flow. J Hydraul Eng 124(2):236–240

Contamination of Arsenic in Groundwater of Bara District, Nepal

Sadhana Pradhanang Kayastha and Kailash Pradhanang

Abstract Groundwater is the major source of water for drinking and household purposes in Nepal's Tarai districts. This study was conducted to evaluate the concentration of arsenic (As) in deep and shallow groundwater and its association with iron, manganese, depth and age of the tube wells/dug wells in Bara District. Groundwater samples (36) were collected from randomly chosen wells (dug wells and tube wells) of Bara District, in 2017. As concentrations of water were measured by hydride generation atomic absorption spectrometry (AAS). About 50% of tube wells/dug wells exceeded permissible value 10 ppb of WHO drinking water guideline, but 16% tube wells/dug wells exceeded permissible values of Nepal Interim Standard of arsenic (50 ppb). As concentrations were highly correlated with iron and manganese. The higher concentrations of As in some of the sites of the study area were attributed to the groundwater geochemistry in the study area. As contamination was found high at the depth range of tube wells <20 m, which was constructed in last 10–15 years. The risk of As contamination to the people living in and around study area is high because the contaminated water has been used daily for household purposes such as cooking, drinking and other purposes.

Keywords Groundwater · Tarai · Arsenic · Bara District · Permissible

1 Introduction

Nepal is famous for its surface and groundwater resources. Due to rapid growth of urban population, the demand for water is always increasing. Groundwater has always been the major source of water for drinking in Tarai District [14]. About 90% of people are using groundwater for drinking purpose since ancient period,

S. P. Kayastha (✉)
Central Department of Environmental Science, Tribhuvan University, Kirtipur, Kathmandu, Nepal
e-mail: sadhana.pradhanang@gmail.com

K. Pradhanang
Ratna Rajya Laxmi Campus, Tribhuvan University, Kirtipur, Kathmandu, Nepal

C. Bhuiyan et al. (eds.), *Water Security and Sustainability*,
Lecture Notes in Civil Engineering 115,
https://doi.org/10.1007/978-981-15-9805-0_3

withdrawal of groundwater has been done with the use of dug wells and tube wells [14].

Arsenic (As) in groundwater is considered as one of the most toxic elements. Arsenic (As) contamination is a severe issue not just in Nepal but throughout the world. Excessive concentration of arsenic in drinking water has been observed from different parts of the world [1, 2]. Distribution of arsenic in shallow groundwater has been observed highly irregular both vertically and horizontally on local or regional scales [10]. The natural source of As in the natural environment is the release from As-enriched minerals. Weathering processes, particularly the rocks and minerals, are the major sources of arsenic in soils [28].

The sources of As comprise natural arsenic and anthropogenic. Natural arsenic contamination occurs through dissolution of compounds (pyrite ores) in water. With the increase in population, there has been corresponding increase in agricultural waste, rich in phosphate fertilizers, insecticides, herbicides, end products of mining processes, coal combustion and timber preservatives [6]. These are the anthropogenic sources which can affect the purity of surface water [19]. Similarly, mining wastes disposal has caused As contamination of groundwater in several places [9].

As occurs naturally in groundwater in concentrations which can pose serious health effects after continuous consumption [23]. Long-term human and excessive intake of inorganic arsenic with food and water cause arsenicosis, skin cancer gastrointestinal, neurological pulmonary, respiratory problems and reproductive system [3, 28, 30]. Many studies have been carried out to determine the toxicity of As and its impacts on human health in various As-contaminated areas [19]. In soils and groundwater, As is a significant contaminant and pollutant across the many regions of the globe.

The concentration of As in groundwater is a function of solubility, which is governed predominantly by pH, redox conditions, temperature, salinity, presence of complex ions and others metals ions, not merely related to the abundance of minerals in aquifers [12, 26]. In poorly ventilated place where As-rich coal or cow dung is used as a fuel, inhaled amounts of As may be high [18].

In Nepal, As contamination is mainly observed in the Tarai region. Out of 24 districts that have been reported with arsenic contamination, 20 districts are from the Tarai region and four are from the hilly region [7]. Highest arsenic-affected districts are Nawalparasi, Rautahat, Bara and Parsa [24]. In drinking water, the concentration of arsenic permissible has been set at 0.01 mg/L by the World Health Organization (WHO) guidelines [30]. In Nepal, the maximum permissible limit of As in water used for drinking purposes is 0.05 mg/L [8]. Groundwater is the major drinking water source in the Tarai. Drinking water quality in Nepal has been an issue of prevalent concern. The aim of this study was toexaminethe distribution of groundwater As and also to identify the relationship between arsenic concentration and tube well/dug well depths.

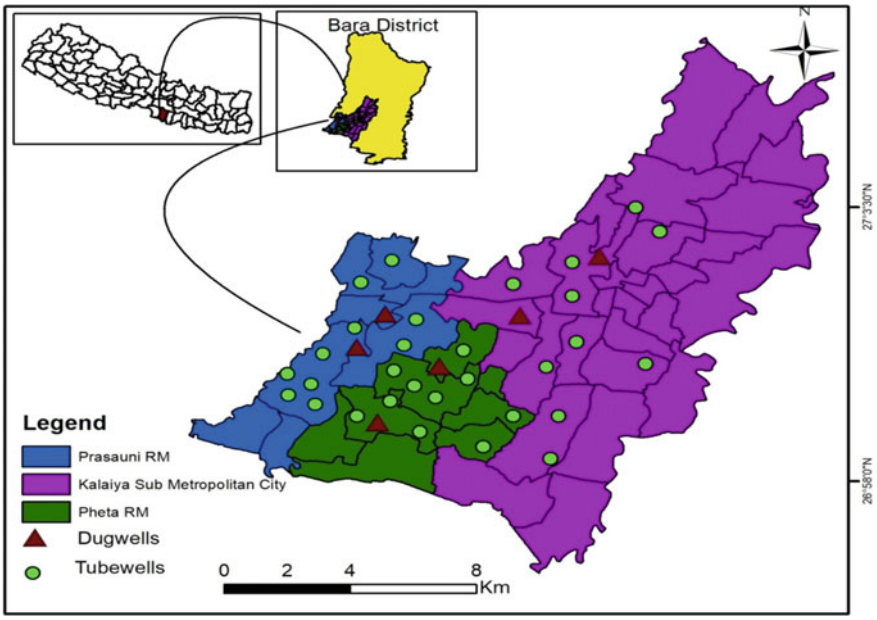

Fig. 1 Location of the study area and the sampling sites

2 Materials and Methods

2.1 Study Area

Study area lies in Bara District of Province No. 2, which is among one of the seventy-seven districts of Nepal. Kalaiya is the district headquarter and covers an area of 1,190 km^2 and had a population of 687, 708 as of 2011. Bara District is surrounded by Rautahat, Makawanpur, Parsa and India in east, north, west and south, respectively (Fig. 1).

2.2 Water Sampling

In overall, thirty-six water samples were sampled from three different locations of Bara District (Kalaiya Sub-metropolitan, Pheta Rural Municipality and Prasauni Rural Municipality) in the month of June 2017 (Fig. 1). Collected samples for analysis were from six dug wells and 30 tube wells. Depending on availability and the level of groundwater at different locations, the tube wells are in place but constituting various depths. For this study, water samples were collected from ten tube wells and two dug wells water samples from each municipality.

Water samples from tube wells were collected after few minutes of pumping and collected in 500 mL bottles of polyethylene [14]. The water sample from each site was taken in a high-density polypropylene, pre-cleaned bottle and then closed with a cap. Before sampling, sample bottles were prepared by soaking with 10% nitric acid for 24 h and then thoroughly cleaned with double distilled water. After then, all the bottles were dried in an oven at 120 °C for 6 h. All the water samples were filtered through 0.45 μm cellulose acetate membrane (Millipore Corporation) and water sample was acidified with ultra-purified nitric acid to pH < 2, immediately after collection. Water samples were collected then kept at 4 °C and brought to the laboratory for chemical analysis. The samples were digested with high purity HNO_3 (Merck) within a week of sample collection for the analysis of arsenic, iron and manganese [2]. Milli-Q water having a resistivity of 18.2 MΩ/cm was used for preparing all reagent solutions. Arsenic was analyzed by hydride generation atomic absorption spectrometry (A Perkin-Elmer Model 300, UK). For accuracy, three replications of each analysis were carried, and mean values were used for comparisons. For each batch of the digestion set, analytical reagent blanks were prepared and then analyzed for the same elements of the samples.

2.3 Statistical Analysis

Pearson correlation analysis was used to test the relationship between arsenic, iron and manganese concentrations. Statistical tests were performed using significant at p-value < 0.05. All the statistical analysis were conducted using the SAS/PC 9.3 (SAS Institute Inc., USA).

3 Results and Discussion

3.1 Distribution of Arsenic in Tube Wells

As concentration in the tube wells/well waters ranged from 0.127 μg/L to 75.7 μg/L. The mean iron concentration in tube wells/wells was found to range from 0.34 to 8.5 mg/L, with the maximum concentration (8.5 mg/L) at Kalaiya Sub-metropolitan. Concentration of Manganese varied from 0.20 to 1.72 mg/L. The WHO has set a drinking water guideline concentration for arsenic of 10 μg/L, and Nepal Interim Standard has adopted the limit of 50 μg/L. Out of total thirty-six tube wells/wells, about 50% exceeded permissible values of WHO guideline (10 ppb) but 16.6% tube wells/wells (Table 1) exceeded permissible concentrations of Nepal Standards of arsenic (50 ppb). The higher values of As in some of the sites of the study area are attributed to the groundwater with several geochemical processes, such as reductions of Fe oxyhydroxides and dissolution of carbonate [5].

Table 1 Arsenic concentration of tube well/dug well

Arsenic concentration (ppb)	No. of tube well	Percent
0–10	12	33.33
> 10	18	50.00
> 50	6	16.66
Total	36	100.00

Table 2 Arsenic concentration in Bara tube wells/wells ($n = 36$)

	1–10 (ppb)	11–50 (ppb)	Above50 (ppb)
Kalaiya Sub-metropolitan	8	9.0	5.0
Pheta Rural municipality	1.0	5.0	1.0
Parsauni Rural municipality	2.0	4.0	1.0

3.2 Concentrations of Arsenic

The pattern of arsenic concentration revealed that Kalaiya Sub-metropolitan has higher % of tube wells/dug wells above 50 ppb, which is Nepal Interim Standard (NIS) with 14% followed by Pheta (2.8%) and Parsauni (2.8%). However, the distribution showed that Kalaiya Sub-metropolitan has higher percentage of tube wells above 10 ppb (WHO guideline) with 25% (Kalaiya Sub-metropolitan), Pheta (14%) and Parsauni (11%) as shown in Table 2. Composition of recharging water, the mineral composition, reactivity of the geological formations in aquifers and anthropogenic activities are the factors affecting As concentration [15].

3.3 Variations of as with Depth of Tube Wells/Well

The variations with depth of tube wells/dug wells and concentrations of As are shown in Table 3. As concentration was usually observed to decrease with increasing tube well/well depth; however, only 9% of tube wells were deeper than 60 m, which is often considered to be a safe depth. As for the depth of the tube well, 55.56% have depths of 10–20 m out of which, 36.11% had As levels higher than 10 ppb and 13.9% above 50 ppb. Similarly, deep tube wells were observed to have a depth higher than 50 m, out of which 8.34% has As level less than 10 ppb (Table 3). Not a single tube well that had depth above 20 meters had As concentration greater than 50 ppb [14, 25]. As concentration is highly dependent on depth of the groundwater [13, 14]. Over pumping water from aquifers oxidizes sulfide minerals and releases co-precipitated As into groundwater [11].

In Tarai region, As concentration was higher in shallow tube well (<20 m) in comparison with deep wells [25]. The distribution of As described above is with

Table 3 Distribution of tube wells/dug wells by depth and levels of As concentration

Depth of tube wells (meter)	≤ 10 ppb		>10 ppb		> 50 ppb		Total	
	No	%	No	%	No	%	No	%
0–10	2	5.55	2	5.55	2	5.55	6	16.65
10–20	2	5.55	13	36.11	5	13.9	20	55.56
20–30	2	5.55	1	2.78			3	8.33
30–40	1	2.78	1	2.78			2	5.56
40–50	1	2.78	1	2.78			2	5.56
50–70	3	8.34	0	0.0			3	8.33
Total	11	30.55	18	50.0	7	19.45	36	100

respect to depth of the well. Moreover, As concentration relates to the age of the sediments, aquifer properties and flow characteristics also influence the distribution of As [21].

4 Relation of Arsenic Concentration with Age of Tube Wells/Wells

The tube wells and dug wells water have been used by the households in the Tarai date back to ancient time. Groundwater is a combination of various aged water because recharge generally has several underground flow paths to release stations [16, 27].

Table 4 shows that tube wells/wells of 5-10 years share the largest proportion with 38.9%, of which 25% and 8.35% cover greater than, respectively, for 10 ppb and 50 ppb, which is followed by 2–5 years (Table 4). The age of wells alone cannot be considered as an indicator of high As concentration [7, 14]. The relation between age and As concentrations likely indicates that geochemical circumstances, driven

Table 4 Years of use of tube wells/dug wells by levels of arsenic concentration

Year of tube wells	Tube wells by arsenic concentration (ppb)							
	0–10		>10		>50		Total	
	No	%	No	%	No	%	No	%
< 1	2	5.55	1	2.78	–	0	3	8.34
1–2	2	5.55	2	5.55	–	0	4	11.11
2–5	2	5.55	1	2.78	1	2.78	4	11.11
5–10	2	5.55	9	25.0	3	8.35	14	38.90
11–20	2	5.55	2	5.55	2	5.55	6	16.66
≥ 20	2	5.55	2	5.55	1	2.78	5	13.88
Total	12	33.33	17	47.21	7	19.46	36	100

Table 5 Correlation between iron, manganese and arsenic ($n = 36$)

Parameters	Fe	Mn	As
Fe	1.000		
Mn	0.423**	1.000	
As	0.621**	0.510**	1.000

**significant value at $p < 0.01$

by alterations in depth to water or pumping rate, are determining factors in arsenic variability [14, 17].

4.1 Correlation Between Iron, Manganese and Arsenic

The relationship between of Fe, Mn and As in tube wells/wells was analyzed by Pearson's correlation (Table 5). Strong positive correlations of As were observed with iron and manganese ($r = 0.621$, $p < 0.01$; $r = 0.423$, $p < 0.01$), which is attributed to common geographic origin of these metals. A similar study reported that arsenic and iron have positive correlation [22]. Naturally occurring As that is absorbed to iron oxyhydroxides is released when the iron oxyhydroxide is reduced as anoxic conditions developed during burial of the sediments [4].

5 Conclusion

Groundwater is the major source for drinking, household and irrigation purposes in the Tarai areas of Nepal. The demand for groundwater is accelerating due to fast population growth and industrial activities. From this study, out of total tube wells/well, about 50% of tube wells exceeded permissible guideline value of WHO (10 ppb), whereas 16.6% tube wells exceeded permissible value (50 ppb) of Nepal Interim Standard. In addition to that, dug wells provide arsenic-safer drinking water compared to tube wells. Since contaminated water is regularly used for drinking, cooking and other household purposes, it can be said that risk of As poisoning is high in the study areas. The conditions of As poisoning are related to minerals solubility in aquifer (iron and manganese), pH, redox conditions, etc.

Acknowledgements This work was supported by REACH, Nepal. We would also like to acknowledge Mr. Chandra Nath Kayastha for his valuable time helping to find out dug wells/tube wells and also to collect the water samples.

References

1. Agusa T, Kunito T, Kubota R, Monirith I, Tanabe S, Tana TS (2002) Arsenic pollution in Cambodia. Biomed Res Trace Elem 13:254–255
2. APHA-AWWA-WEF (2005) Standard Methods for the Examination of Water and Wastewater. 21st edn, American Public Health Association, American Water Works Association, Water Environment Federation, Washington DC
3. ATSDR (2000) Toxicological profile for arsenic. U.S. Department of Health & Human Services, Public Health Service Agency for Toxic Substances and Disease Registry
4. Bhattacharya P, Chang CL, Santra SC (2012) Arsenic induced health crisis in peri-urban Moyna and Ardebok villages, West Bengal, India: an exposure assessment study. Environ Geochem Health 34:563–574
5. Brikowski TH, Neku A, Shrestha SD, Smith LS (2014) Hydrologic control of temporal variability in groundwater arsenic on the Ganges floodplain of Nepal. J Hydrol 518(C):342–353
6. Bundschuh J, Bhattacharya P, Sracek O, Mellano MF, Ramírez AE, Storniolo AR, Martín RA, Cortés J, Litter, MI, Jean JS (2011) Arsenic removal from groundwater of the Chaco-Pampean plain (Argentina) using natural geological materials as adsorbents. Sci Health 46:1297–1310
7. FAO (2004) Arsenic threat and irrigation management in Nepal. Rome
8. Fendorf S, Michael HA, van Geen A (2010) Spatial and temporal variations of groundwater arsenic in South and Southeast Asia. Science 328(5982):1123–1127
9. GoN/MPP (2006) National drinking water quality standards. In: Nepal Gazette (B.S. 2063/03/12), Kathmandu, Ministry of Physical Planning, Government of Nepal
10. Gunduz O, Simsek C, Hasozbek A (2010) Arsenic pollution in the groundwater of Simav plain, Turkey: its impact on water quality and human health. Water Air Soil Pollut 205:43–62
11. Guo HM, Wang YX (2004) Hydro-geochemical processes in shallow quaternary aquifers from the northern part of the Datong Basin. China Appl Geochem 19:19–27
12. Hoang TH, Bang S, Kim KW, Nguyen MH, Dang DM (2010) Arsenic in groundwater and sediment in the Mekong River delta. Vietnam Environ Pollut 158:2648–58
13. Hug SJ, Leupin O (2003) Iron-catalyzed oxidation of arsenic (III) by oxygen and by hydrogen peroxide: pH-dependent formation of oxidants in the Fenton reaction. Environ Sci Technol 37(12):2734–2742
14. Karim M, Komori Y, Alam M (1997) Arsenic occurrence and depth of contamination in Bangladesh. J Environ Chem 7:783–792
15. Kayastha SP (2015) Arsenic contamination in the deep and shallow groundwater of Bara District, Nepal. Cross Border: Int J Interdisc Stud 3(1):65–69
16. Kouras A, Katsoyiannis I, Voutsa D (2007) Distribution of arsenic in groundwater in the area of Chalkidiki. Northern Greece J Hazard Mater 147(3):890–899
17. Landsey BD, Ayotte JD, Jurgens BC, Desimone LA (2017) Using groundwater age distributions to understand changes in methyl tert-butyl ether (MtBE) concentrations in ambient groundwater, northeastern United States. Sci Total Environ 579:579–587
18. Levitt PJ, Degnan RJ, Flanagan MS, Bryant C, Jurgen CB (2019) Arsenic variability and groundwater age in three water supply wells in southeast new hampshire. Geosci Front 10:1669–1683
19. Lin GF, Meng H, Du H, Lu HC, Zhou YS, Chen JG, Golka K, Lu JC, Shen JH (2010) Factors impacting on the excess arseniasis prevalence due to indoor combustion of high arsenic coal in a hyperendemic village. Int Arch Occ Env Health 83:433–440
20. Maity JP, Nath B, Kar S, Chen CY, Banerjee S, Jean JS, Liu MY, Centeno JA, Bhattacharya P, Chang CL, Santra SC (2012) Arsenic-induced health crisis in peri-urban Moyna and Ardebok villages, West Bengal, India: an exposure assessment study. Environ Geochem Health 34(5):563–57
21. Martin AJ, Pedersen TF (2002) The seasonal and inter-annual mobility of arsenic in a mine-impacted lake. Environ Sci Technol 36:1516–1523

22. Meharg AA, Scrimgeour C, Hossain SA, Fuller K, Cruickshank K, Williams PN, Kinniburgh DG (2006) Codeposition of organic carbon and arsenic in Bengal delta aquifers. Environ Sci Technol 40:4928–4935
23. Nakano A, Kurosawa K, Shamim UM, Tani M (2014) Geochemical assessment of arsenic contamination in well water and sediments from several communities in the Nawalparasi District of Nepal. Environ Earth Sci 72(9):3269–3280
24. Naujokas MF, Anderson B, Ahsan H, Aposhian HV, Graziano JH, Thompson C, Suk WA (2013) The broad scope of health effects from chronic arsenic exposure: update on a worldwide public health problem. Environ Health Perspect 121(3):295–302
25. Neku A, Tandukar N (2003) An overview of arsenic contamination in groundwater of Nepal and its removal at household level. J. Phys. IV France 107:941–944
26. Pradhan B (2006) Arsenic contaminated drinking water and nutrition status of the rural communities in Bagahi village, Rautahat district. Nepal JIOM 28(2):47–51
27. Smedley PL, Kinniburgh DG (2002) A review of the source, behaviour and distribution of arsenic in natural waters. J Appl Geochem 17:517–568
28. Suckow A (2014) The age of groundwater e definitions, models and why we do not need this term. J Appl Geochem 50:222–230
29. Thambidurai P, Chandrashekhar AK, Chandrasekharam D (2013) Geochemical signature of arsenic-contaminated groundwater in Barak Valley (Assam) and surrounding areas, northeastern India. Procedia Earth Planet 7:834–837
30. United States Environmental Protection Agency (U.S. EPA) (1986) Health and Environmental. Washington, DC: U.S. EPA; 1987. The risk assessment guidelines of 1986. EPA/600/8-87/045
31. WHO (2011) Guidelines for drinking-water quality. World Health Organ Geneva 4:315–318

Runoff Prediction Using Artificial Neural Network and SCS-CN Method: A Case Study of Mayurakshi River Catchment, India

Subhadeep Mandal and Sujata Biswas

Abstract Runoff estimation, as well as forecasting, is a challenging hydro-climatological topic since governing physical processes is complex, and in reality, it is hardly represented by a system of the equations. Due to the complex nature and extreme spatial-temporal variability of the processes which control runoff, it is difficult to set up a reliable framework for runoff prediction and forecasting based on available observations only. In this research, two kinds of methods have been approached. The first one is a conceptual method, Soil Conservation Service Curve Number (SCS-CN) method, which combines the climatic factors and watershed parameters in one unit called the Curve Number (CN). The other method is the Artificial Neural Network (ANN) modeling, where two different kinds of models, Feed Forward Back Propagation (FFBP) and Cascade Forward Back Propagation (CFBP) model have been applied. The runoff-rainfall coefficient has been chosen as the standard parameter of the study result. Among 16 years, the year 2000 has the highest annual, seasonal monthly total runoff (monsoon season, July to Sept.). In artificial neural network models, generated coefficient correlation (R) values varied from 0.96 to 0.99 range, which indicated a good correlation between the rainfall-runoff data set. The models developed for the present study can be utilized for further basin hydrologic analysis.

Keywords Curve number · GIS · Mayurakshi catchment · Neural network · Rainfall-runoff

S. Mandal
School of Water Resources Engineering, IIT Kharagpur, Kharagpur, India

S. Biswas (✉)
Department of Civil Engineering, IIEST Shibpur, Howrah, India
e-mail: sujata@civil.iiests.ac.in

C. Bhuiyan et al. (eds.), *Water Security and Sustainability*,
Lecture Notes in Civil Engineering 115,
https://doi.org/10.1007/978-981-15-9805-0_4

1 Introduction

Rainfall-runoff (RR) models are of paramount importance for the strategic planning of water resources and its development. This issue becomes more crucial and challenging as the population grows in a particular area and makes the basin more heterogeneous from the landcover perspective. The difficulty in the analysis exists mainly due to the complex nonlinear relationships in the transformation of rainfall into runoff. Inconsistent watershed characteristics and overland, as well as inland flow generation processes, make this transformation more complex in modeling. Nonuniform precipitation patterns, along with the uneven distribution of soil moisture, influence the infiltration rates and affect the runoff generation process [1]. The analyzed outcomes are essential in the design and operation of works in water resources management sectors.

In the recent scenario, the role of climate change also imparts importance in the design of RR modeling [2]. Intensification of the global hydrologic cycle due to changed climatic factors [3] such as rainfall distribution, increased temperature makes it necessary for preparing an accurate RR modeling for predicting future scenarios toward the utilization of the available resources in an optimized way. Anthropogenic activities such as groundwater exploitation, inefficient, excessive irrigation alter the river characteristics, which also affect the basin hydrology and related ecosystem. In this context, understanding the interdependent processes and analyzing the cause and effect study, an RR modeling with minimum uncertainty is significant.

Since the last few decades, various methods with different prediction models have been developed to increase the efficiency of RR models for forecasting the accurate runoff in scarce data situation. Among them, statistical methods [4] combined with a GIS-based approach, an analytical approach based on dynamic stochastic models with different algorithms [5] is popular. However, the uses of those models require a range of different data sets, which is also a rigorous and time-consuming operation. Recently, the evolution of machine learning and artificial intelligence [6] makes that scenario different and exciting due to their variety of broad approaches with optimized nonlinear algorithms. Among the machine learning techniques, artificial neural network is a relatively new concept used in hydrologic and water resources systems modeling [7]. Artificial neural networks can be considered as black-box models. ANN is a nonlinear mathematical structure, competent in analyzing the complexity in nonlinear relationships between raw and processed data of a system [8]. ANN models are particularly helpful as well as most useful to use as pattern-recognition tools for generalization of input–output relationships. Thus, it is mostly used as a quite common approach in hydrologic problems such as streamflow prediction [9], flood forecasting [10], prediction of water quality parameters [11], and runoff forecasting [12–14] which is the main concerned area of focus.

Runoff is affected by various factors such as the area of the catchment, land use pattern, soil characteristics, slope distribution of the area, and initial abstraction rate of that catchment. To construct a hydrologic model, predicting runoff is one of the essential hydrologic variables in water resources applications. For the prediction of

discharge, various models are used which require various types of data sets like land use pattern, soil property, slope distribution, temperature variation, amount of rainfall precipitated, and change of river stage in various times. Sometimes, all types of required data may not be available at that catchment. Building a hydrologic model in an ungauged area is sometimes difficult for the sake of expensive data and its collection procedure. The soil conservation service–curve number (SCS-CN) method is popular in RR modeling [15]. In 1969, the US Department of Agriculture developed this lumped model for the prediction of hydrologic flow components. This stable conceptual method correlates the catchment characteristics and climatic factors through one entity called the curve number (CN). Soil infiltration capacity and the amount of land cover in a watershed are the two essential parameters for CN value determination. So, in this method, the model structure is simplified to avoid the complexity, the model calibration can also be easily realized, and the runoff can be reflected well [16]. A GIS helps to utilize spatially varied data of soil and land use for generating curve numbers [17]. In this context, an attempt has been made in the present research to compute the runoff using the SCS-CN method and also forecast the runoff using ANN in a part of the Mayurakshi catchment.

2 Study Area

Mayurakshi river basin is chosen as the present study area. Mayurakshi river is a significant river in Jharkhand and West Bengal. The origin of this river is Trikut hill, about 16 km from Deoghar in Jharkhand. It flows from northwest direction to southeast direction and meets with Hoogly river. The upper catchment of the river experiences a hilly slope terrain. While traveling down to the mouth, it flows over alluvial plains of Ganga.

The areal extent of the catchment is 5292 Km^2. It lies between 86°50′13.2″ and 88°09′39.6″E longitude and 23°37′58.8″ and 24°37′48″N from its origin to the Narayanpur located in Jamtara district of Jharkhand state and some extent including Tilpara barrage. Figure 1 represents the study area in India and its enlarged view. In the year 1956, the Massanjore Dam was constructed across Mayurakshi river at the Dumka district in Jharkhand state. Tilpara barrage was constructed across the river in the Birbhum District of West Bengal. The annual rainfall of the catchment varies between 957 to 1455 mm, as analyzed from the data collected for the study with the exception of more than 2400 mm for the year 2000.

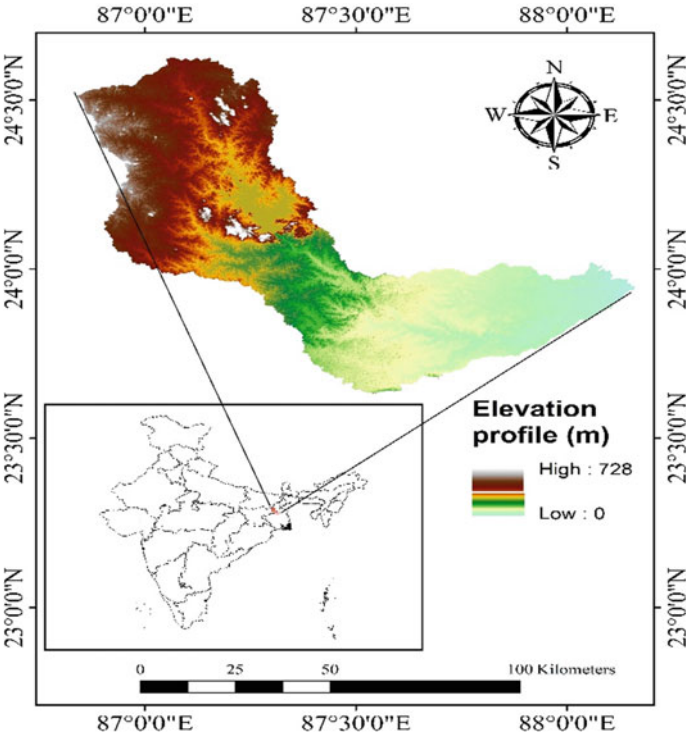

Fig. 1 Mayurakshi river basin with an elevation profile

3 Materials and Methods

3.1 Datasets

For the present study, the following data sets are collected: Advanced Space-borne Thermal Emission and Reflection Radiometer (ASTER) Digital Elevation Model (DEM) data of 30 meter spatial resolution of Terra satellite collected from http://reverb.echo.nasa.gov. Satellite Image have four spectral bands, procured from National Remote Sensing Center, Hyderabad, and date of pass of that images is 07th Feb, 2011, of Resourcesat-1: LISS-III. Soil map is from the National Bureau of Soil Survey and Land Use Planning (ICAR) Nagpur-44010. Daily rainfall data of 16 years (2000–2015) in a 0.25-degree gridded format from India Meteorological Department, Pune, have been utilized for the study.

3.2 Methods

3.2.1 SCS-CN Method

The SCS-CN method, based on the water balance equation of the total precipitation (P), is divided into three components (I) initial abstraction (I_a), (ii) cumulative infiltration excluding I_a (F) and (iii) direct surface runoff (Q), which is given in Eq. 1 (all units are in volume occurring in Δt time interval)

$$P = I_a + F + Q \tag{1}$$

$$I_a = \lambda S \tag{2}$$

For use in Indian conditions, $\lambda = 0.1$ and 0.3 subject to certain constraints of soil type and AMC conditions. In this study, $\lambda = 0.3$ value has been used. To compute the basin runoff (Q), Eq. 3

$$Q = \frac{(P - I_a)^2}{P + (1 - \lambda)S} \tag{3}$$

$$CN_I = \frac{CN_{II}}{2.281 - 0.01281CN_{II}} \tag{4}$$

$$CN_{III} = \frac{CN_{II}}{0.427 + 0.00573CN_{II}} \tag{5}$$

has been used, which combines two basic hypotheses, expressed in Eqs. 1 and 2. The potential maximum retention (S) has been computed using Eq. 6 with the help of a unique parameter, Curve number (CN) integrates the soil types, landcover, and antecedent moisture conditions (AMC). Here, CN_{II} indicates the curve number corresponding to AMC-II condition. Equations 4 and 5 represent the curve number corresponding to AMC-I and AMC-III condition.

$$S = 254\left(\frac{100}{CN_{II}} - 1\right) \tag{6}$$

This method considers four different hydrologic soil groups based on their runoff potential. A, B, C, and D stand for low, moderately low, moderately high, and high runoff potential. Details can be found in the literature [18].

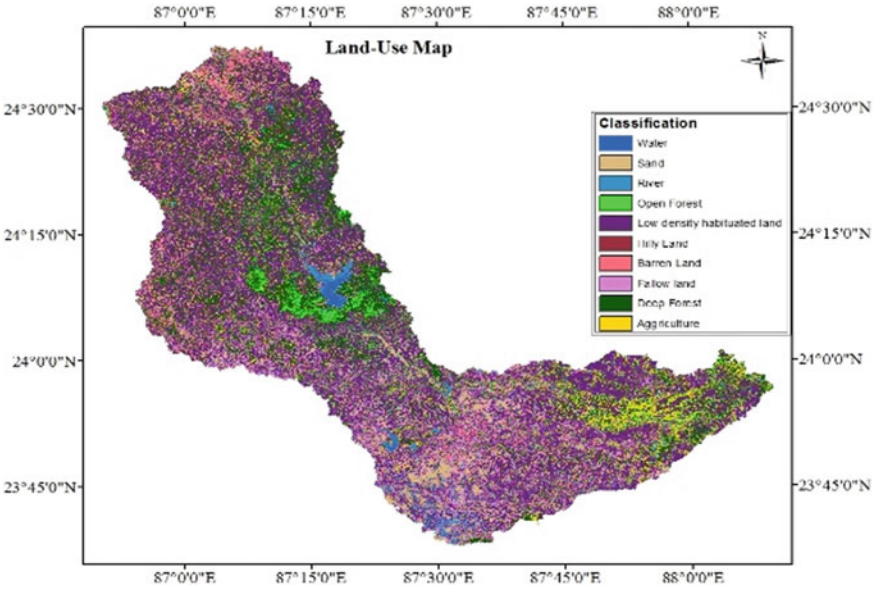

Fig. 2 Classified land use map of the basin

Preparation of Land Use Map

Land use pattern influences surface runoff to a great extent. For this purpose, satellite images (source: IRS-P6 LISS III) have been utilized, and the maximum likelihood technique of supervised classification has been used to derive the land use map. In classification, eight types of classes are established deepwater, river-body, sand, dense forest, open forest, agricultural land, wasteland, and non-agricultural land. The detailed land use map is represented in Fig. 2.

Preparation of Soil Map

The present study area is comprised of sixteen types of soils. Figure 3 represents the different types of soil present in the study area.

Hydrologic Soil Group (HSG)

HSG classification is adopted in the determination of curve number. Based on infiltration characteristics, soils are classified into four classes A, B, C, and D, which is also dependent on their effective depth of soil, average clay content, and permeability. Groups A, B, C, and D signify low, moderate, moderately high, and high runoff potential. In this study, the soil map has been classified into these groups to

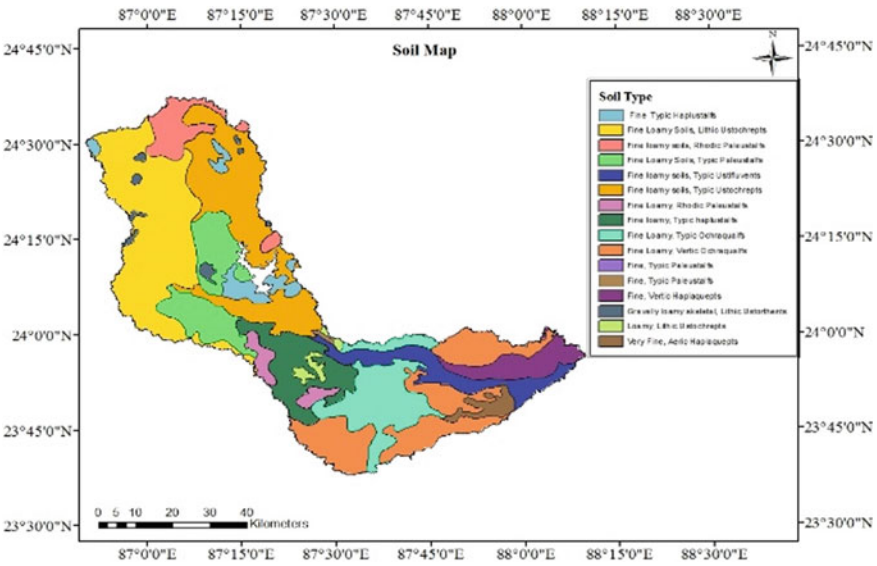

Fig. 3 Soil map of the present study area

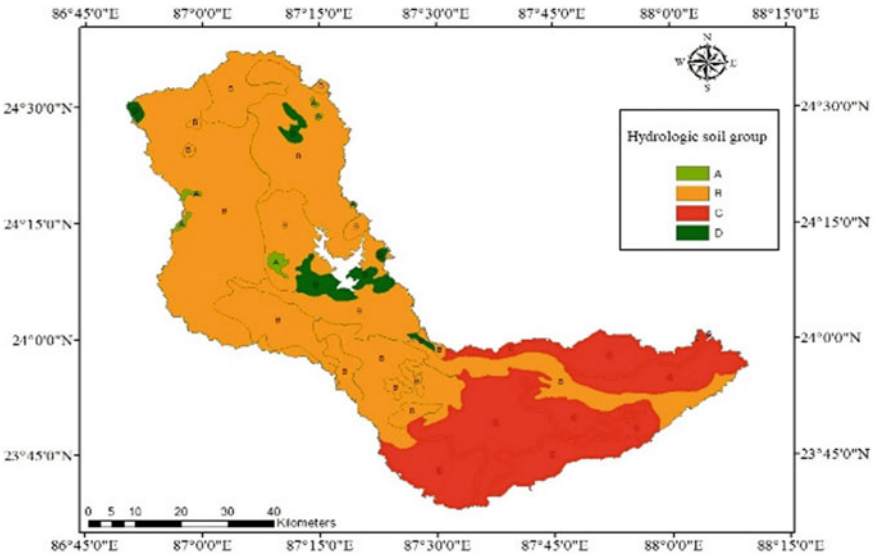

Fig. 4 Hydrologic soil group map of the basin

derive the hydrologic soil group map. Figure 4 represents the hydrologic soil group map.

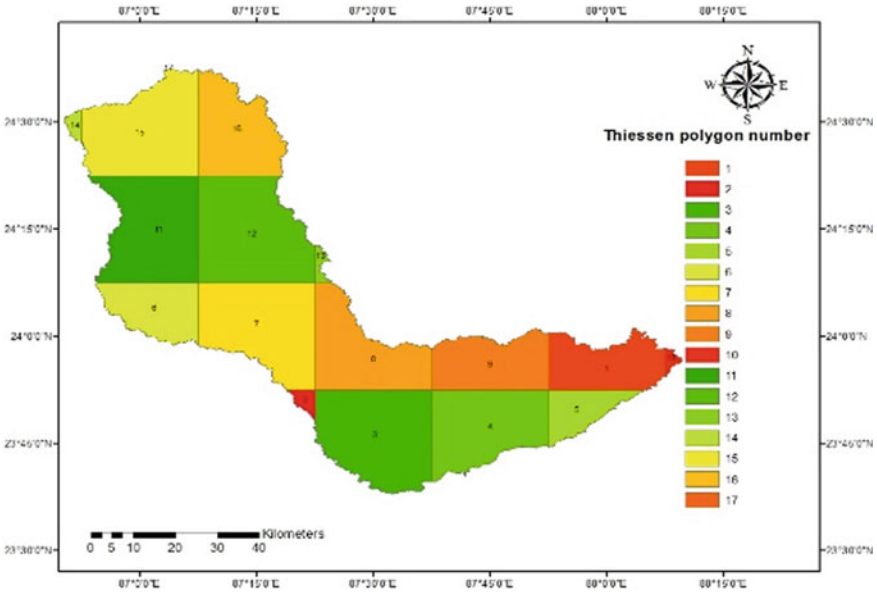

Fig. 5 Thiessen polygons of the present area of study

Preparation of Rainfall Distribution Map

In the present study, seventeen stations, which are located in and around the catchment area, are selected. The rainfall distribution map is prepared using the Thiessen polygon method, which is shown in Fig. 5.

3.2.2 Artificial Neural Network Method

Different distributed mathematical models, combined with a class of functions, are known as ANN models. Deep learning and machine learning methods are the other two parts of Artificial Intelligence (AI). As information in the human brain transferred through neurons from one region to another region, in AI, raw and processed information are transferred into the networks through linear and nonlinear mathematical functions called neurons, conceptually the same as neurons in the human brain. Different patterns, the orientation of information flow structures, and specific uses type make the ANN models unique within them.

Feed-Forward Back Propagation (FFBP) Network

This model is a well-known artificial neural network model where processed information is getting feed in the forward direction, shown in Fig. 6. In this case, the back

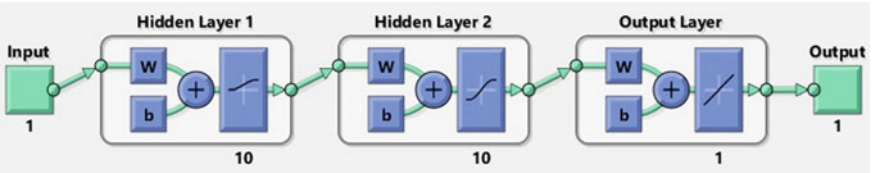

Fig. 6 Feed-forward back propagation network diagram

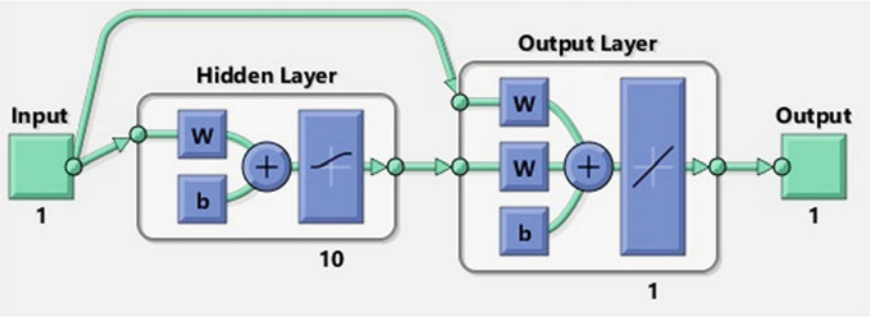

Fig. 7 Diagram of cascade-forward back propagation network

propagation Lavenberg–Marquardt training algorithm ("trainlm") was applied for network learning. In the training phase, simultaneous calculations were carried out in the forward direction, and then to adjacent layers, error values were propagated. This network has two hidden layers with log-sigmoid and tan-sigmoid nonlinear transfer functions, and a purelin linear function in the output layer.

Cascade-Forward Back Propagation (CFBP) Networks

This model, presented in Fig. 7, is almost identical to feed-forward networks. Distribution of weights with each successive layer along with the individual input connections makes a difference from the previous one. A single hidden layer using a log-sigmoid transfer function with a combination of an output layer of purelin function has been used in this study.

4 Results and Discussions

4.1 SCS-CN Method Outcome

4.1.1 Computation of Weighted Curve Number

Hydrologic soil group map and land use map have been integrated to account for spatial variability of a soil group and land use type. A General curve number (CN-II) is assigned for each hydrologic soil group under the AMC-II conditions, which correspond to each land use area. The soil-land use layer is then overlaid with the previously created Thiessen polygon layer of the catchment, where each Thiessen polygon represents the influence area of each rain gauge station. The curve number for the whole catchment has been computed as 76. The weighted curve number has been calculated for each Thiessen cell, which varies from 54 to 85.

4.1.2 Computation of Runoff

Daily rainfall values for 16 years (2000–2015), as mentioned in Sect. 2, have been utilized for runoff estimation for the catchment. Daily runoff values have been converted into monthly and annual runoff values. Figures 8 and 9 highlight the representation of seasonal and annual runoff against rainfall. The highest runoff-rainfall ratio has been observed in the year 2000.

According to research documents [19], there were flooding situations that occurred in the year 2000 in the Mayurakshi catchment. The minimum annual runoff is 44.99 mm, corresponding to rainfall 957.81 mm, which is less than 5% of total catchment precipitation in the year 2011. In monsoonal seasons (June, July, August, September), monthly total runoff values are very predominant. The highest monthly total runoff has been computed as 793.88 mm, corresponding to rainfall 1169.54 mm in September month of the year 2000. Runoff volume computed is 43% and 48%

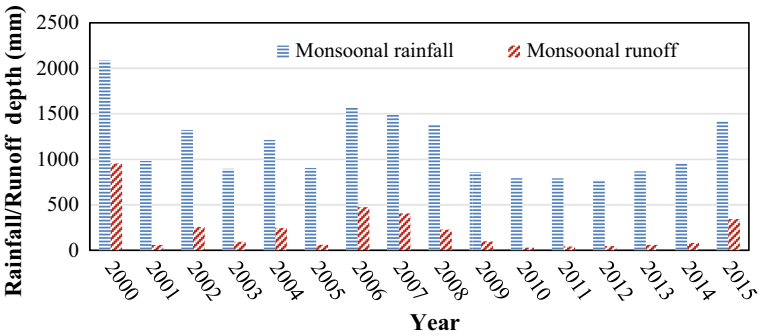

Fig. 8 Graphical representation of monsoonal (June–September) rainfall-runoff depth

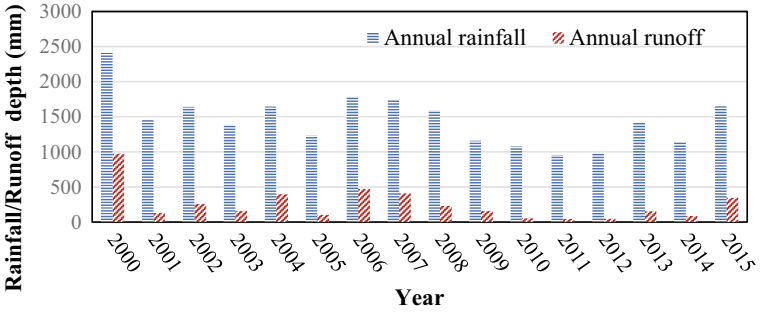

Fig. 9 Graphical representation of annual rainfall-runoff depth

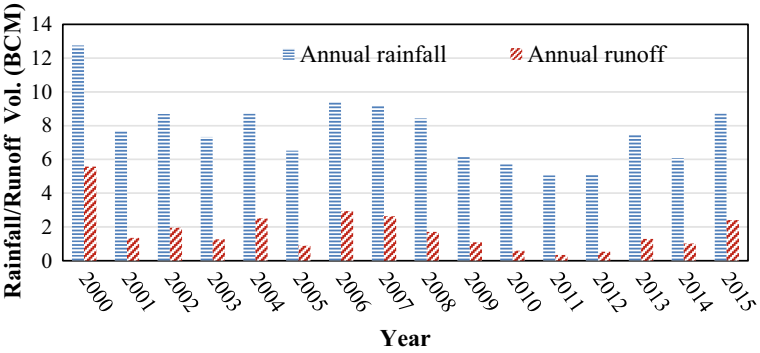

Fig. 10 Graphical representation of annual rainfall-runoff volume

of rainfall volume for annual and seasonal basis when computed Thiessen cellwise, which are around 40% and 45% when computed with a single curve number for the whole catchment. In these 16 years, the highest monsoonal runoff has been found as 5.39 BCM (billion cubic meter) corresponding to rainfall 11.06 BCM when computed based on Thiessen cell. Figures 10 and 11 represent the annual and seasonal runoff volume against rainfall when computed Thiessen cellwise.

The study highlights a good potential of estimation of runoff using the curve number method, which can be utilized for different purposes. In the present study, due to the scarcity of data in the gauging site, this data has been utilized further for computing runoff using the ANN technique.

4.2 Artificial Neural Network Outcome

Chosen models have been simulated for the same set of rainfall-runoff data produced by the SCS-CN method but with different training periods and simulation periods.

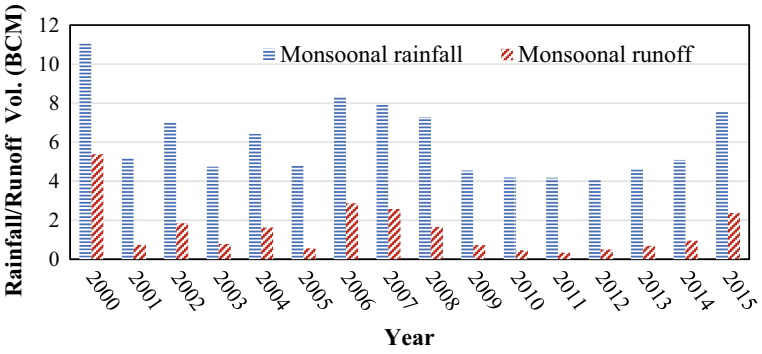

Fig. 11 Graphical representation of monsoonal (June–September) rainfall-runoff volume

The coefficient of correlation values of those two models (FFBP and CFBP) is represented in Figs. 12 and 13.

In almost both cases, the correlation coefficient (R) value ranges between 0.96 to 0.99, which indicates a good correlation among precipitation and runoff data sets. FFBP and CFBP model have been run for two types of data sets. (15 + 1) Years monsoonal data sets for the whole catchment and (12 + 4) years monthly total rainfall-runoff values for the whole catchment have been utilized. Here, 15 and 12 years of data have been used for training and validation purposes, and the rest one and four years of data were used for simulation purpose. For (12 + 4) years dataset, R values are 0.993 and 0.996, respectively, in the CFBP and FFBP model, which are

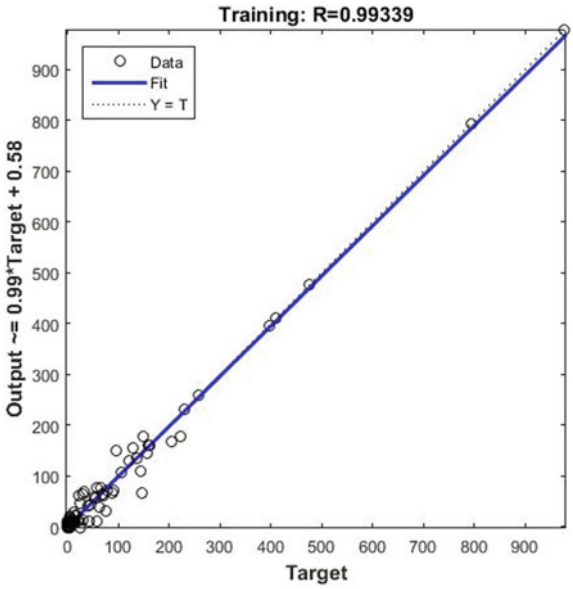

Fig. 12 Correlation in CFBP model for (12 + 4) years

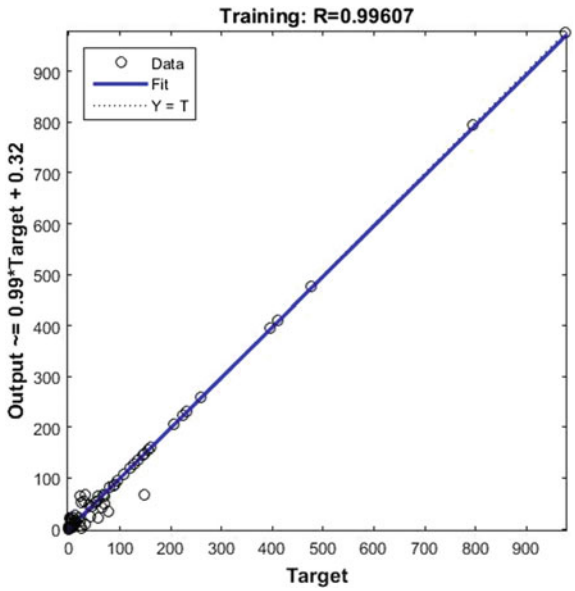

Fig. 13 Correlation in FFBP model for (12 + 4) years

shown in Figs. 12 and 13. For (15 + 1) years dataset, R values were 0.998 and 0.997, respectively, in the FFBP and CFBP model, which are shown in Figs. 14 and 15.

All the simulated values of the models are represented in Fig. 16. Both simulated model values have not perfectly matched with SCS-CN values. Predicted values

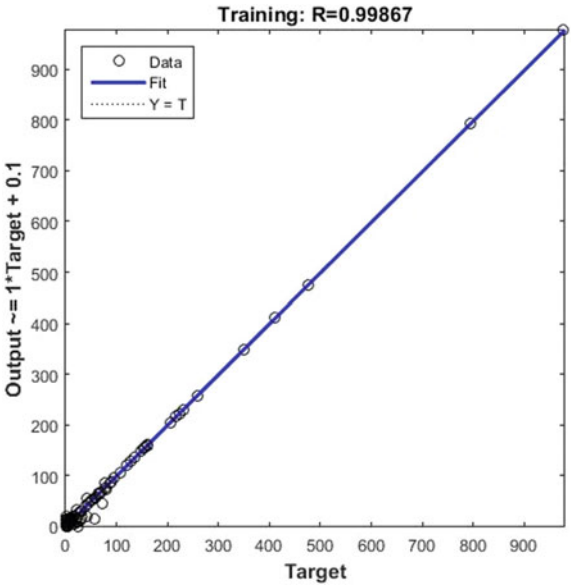

Fig. 14 Correlation in FFBP model for (15 + 1) years

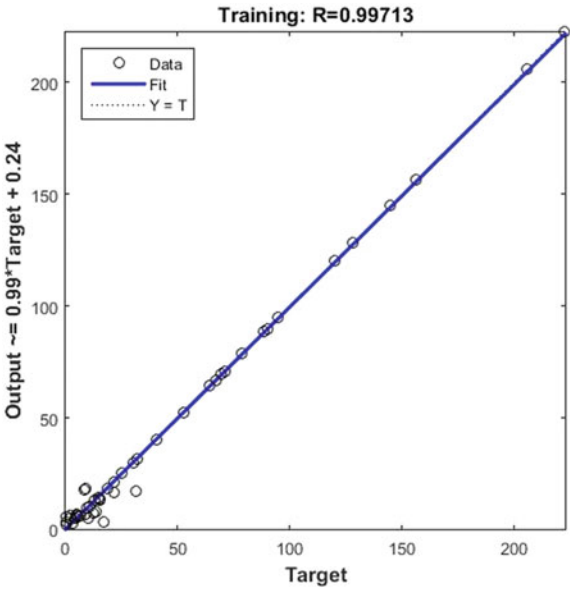

Fig. 15 Correlation in CFBP model for (15 + 1) years

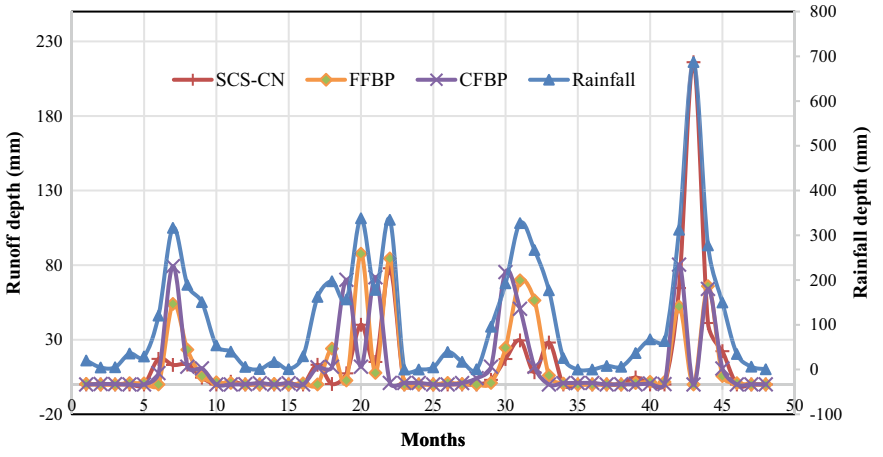

Fig. 16 Simulated runoff data of SCS-CN, FFBP, and CFBP model for 48 months

from these models are very close to the peak values only. Medium range values were too distributed in both cases. Correlation coefficient (R) value had shown a good correlation between runoff and precipitation data set though data sets which were not checked with the observed field data. Models are very responsive to peak values for all the years. As they were mathematical models, runoff values have been shown in (−ve) range for minimal rainfall values or no rainfall cases. Practically, those values should be considered zero.

5 Conclusions

Rainfall-runoff modeling has been carried out using the conceptual and practical method, the SCS-CN method accounting the spatial variation of land use, soil texture throughout the region, and heterogeneous rainfall distribution in the GIS environment. The computed runoff for the year 2000 is highest, which is also found from the available literature discussed in the result section. The summed runoff of individual runoff depth for each Thiessen cell shows a higher magnitude compared to the weighted curve number approach applied on all the Thiessen cells. This insight needs further more study in terms of applicability of curve number with observed data in a distributed scenario rather than applying as a cumulative approach.

The results from the SCS-CN method have been used in modeling the ANN as there is no observed data in the gauging site. In the ANN method, both the FFBP and CFBP model reflect a good correlation between the rainfall-runoff data set.

Among all three models (SCS-CN model, FFBP model, and CFBP model), CFBP model shows a very satisfying performance in terms of rainfall pattern in its peaks. Though with the help of a smaller number of variables, the ANN model can predict runoff in a shorter time, and it is not always the right decision to say the ANN is better than an existing conceptual model in the field of hydrology.

Comparison of the present results with the other popular models viz HEC-HMS model, SWAT model, and VIC model will lead the study more pronounced and significant in this field of research.

References

1. Duan Q, Gupta V (1992) Effective and efficient global optimization. Water Resour 28:1015–1031
2. Bronstert A (2004) Rainfall-runoff modelling for assessing impacts of climate and land-use change. Hydrol Process 18:567–570
3. Arnell NW, Gosling SN (2013) The impacts of climate change on river flow regimes at the global scale. J Hydrol 486:351–364
4. Pisarenko VF, Lyubushin AA, Bolgov MV, Rukavishnikova TA, Kanyu S, Kanevskii MF, Savel'eva EA, Dem'yanov VV, Zalyapin IV (2005) Statistical methods for river runoff prediction. Water Resour 32:115–26
5. Patil S, Patil S, Valunjkar S (2012) Study of different rainfall-runoff forecasting algorithms for better water consumption, vol 051
6. Adamowski J, Prasher SO (2012) Comparison of machine learning methods for runoff forecasting in mountainous watersheds with limited data. J Water L Dev 17:89–97
7. Kişi Ö (2007) Streamflow forecasting using different artificial neural network algorithms. J Hydrol Eng 12:532–539
8. Phukoetphim P, Shamseldin AY, Melville BW (2014) Knowledge extraction from artificial neural networks for rainfall-runoff model combination systems. J Hydrol Eng 19:1422–1429
9. Noori N, Kalin L (2016) Coupling SWAT and ANN models for enhanced daily streamflow prediction. J Hydrol 533:141–151
10. Elsafi SH (2014) Artificial neural networks (ANNs) for flood forecasting at Dongola Station in the River Nile. Sudan Alexandria Eng. J 53:655–662

11. Asce 2000 Artificial Neural networks in hydrology. By the ASCE task committee on application of artificial neural networks in hydrology 1. J Hydrol Eng 5:124–137
12. Ghumman AR, Ghazaw YM, Sohail AR, Watanabe K 2011 Runoff forecasting by artificial neural network and conventional model. Alexandria Eng J 50:345–350
13. Wang Y, Guo S, Xiong L, Liu P, Liu D (2015) Daily runoff forecasting model based on ANN and data preprocessing techniques. Water (Switzerland) 7:4144–4160
14. Mishra S, Gupta P, Pandey SK, Shukla JP (2014) An efficient approach of artificial neural network in runoff forecasting. Int J Comput Appl 92:9–15
15. Chung WH, Wang IT, Wang RY (2010) Theory-based SCS-CN method and its applications. J Hydrol Eng 15:1045–1058
16. Shadeed S, Almasri M (2010) Application of GIS-based SCS-CN method in West Bank catchments, Palestine. Water Sci Eng 3:1–13
17. Bhaskar J, Suribabu CR (2014) Estimation of surface runoff for urban area using integrated remote sensing and GIS approach. Jordan J Civ Eng 8:70–80
18. Subramanya K (2008) Engineering hydrology, 3rd edn. Tata McGraw-Hill Publishing Company Limited, New Delhi
19. Anon 2000 a Study of Catastrophe Flood in 197–204

Water Quality and Designated Best Use (DBU) Determination of Bhim Taal Lake of Panchkula, Haryana

Prachi Vasistha and Rajiv Ganguly

Abstract There are large number of water sources available on earth such as oceans, springs, lakes, and ponds but not all the water sources can be considered as usable. Only 2.5% out of the available sources of water are freshwater and only 1% out of them can be considered as an accessible source; considering this fact ***lakes*** can be considered as a reliable source of water comprising of about 0.3% of freshwater resources available to humans for use, they have been used for years as a source of water for drinking, bathing, washing, swimming, and other recreational activities. Since there is an availability of limited amount of freshwater resources, the optimum utilization of the available resources should be the major area to focus upon. The sustainability concept needs to be implemented for the water resources because discovering the new water sources for fulfilling the ever-increasing demands of humans is not possible. The anthropogenic activities around the lakes have deteriorated the quality of lakes; therefore, there is a need for maintenance of these water resources based on the determination of degraded water quality characteristics and utilizing the water according to the designated best use based on the measured values of the parameters. In this study, we focus on the utilization of a lake as a source for drinking, bathing, propagation of wildlife and fisheries and industrial and irrigational use based on the parameters measured and in comparison with the guidelines issued by Central Pollution Control Board (CPCB). The site has been utilized for years by local communities for their personal use but no study has been made for the determination of the parameters and putting the water body to use according to the DBU neither the developmental activities has been seen and reported for the site to be used as a source of water for human and animal consumption. The samples were collected for the site and tested in the laboratory for determination of values of various parameters. The values were then compared with the values of DBU table issued by Central Pollution Control Board (CPCB) for various parameters to determine the designated uses of the water body. The project is at an initial stage and a

P. Vasistha (✉) · R. Ganguly
Department of Civil Engineering, Jaypee University of Information Technology, Waknaghat, Solan, Himachal Pradesh, India
e-mail: pihu20.vasistha@gmail.com

C. Bhuiyan et al. (eds.), *Water Security and Sustainability*,
Lecture Notes in Civil Engineering 115,
https://doi.org/10.1007/978-981-15-9805-0_5

single sampling program has been carried till now as a first step toward optimum utilization of the water source.

Keywords Designated best use (DBU) · Central Pollution Control Board (CPCB) · Lakes · Anthropogenic activities

1 Introduction

Water is an elixir of life. It contains many vital nutrient and minerals necessary for the human beings [1]. Rivers, lakes, and springs are a few important water bodies [2]. The water body' quality is dependent upon the geology of the earth as well as the human activities surrounding it, namely construction, dumping of waste, and agricultural activities [3–5] which affect the quality of water [6]. As the water gets absorbed through the soil layer, it adds into it a large amount of suspended and dissolved impurities making it unfit for usage and in some cases non-potable [7]; therefore, the physico-chemical properties vary both spatially and temporally [8]. The lakes being an important water source are generally divided into either man-made or natural [9]. Water scarcity is considered to be an alarming environmental issue; therefore, the focus lies on characterization of the lakes for improvement and restoration [10]. The determination of physical, chemical, and biological parameters can be defined as the basis of water quality analysis [11]. These values determine the present status as well as forecast the future hydrological modifications in a water body [12]. The purpose of using the water body is based on the requirements of humans, animal, and plants around the place; in this context, the designated best use (DBU) is the best approach which classifies the characteristic uses of the water body based on the measured physico-chemical & biological parameters and comparing them with the DBU table given by CPCB [13].

2 Study Area

The Tikkar Taal or Bhim Taal is a lake located in the Morni hills of Panchkula district of Haryana. It has a height of 1,267 m and is a well-known tourist spot used for recreational activities. The area has twin lake, larger one is popularly known as Tikkar Taal and is about 550 m in length and 460 m wide with a depth of about 5–6 m at the lake center. The lake depth has been considerably reduced as per the local sources due to constant influx of silt and sediment loads from the waterfall which is a lake water source. The lake is managed by Haryana Tourism Department and is used for boating. The geographical location of the place is 30° 42′N 77°5′E. Figure 1 gives a view of the lake. The place is located at a distance of 45 km from Chandigarh and 35 km from Panchkula into the hills. The population of the place is near about 1200 persons with a variable tourist influx around the year. The water

Fig. 1 3D view of the lake located at Morni hills in Panchkula

from the lakes is used by locals for light irrigation purpose and for boating activities but the suitability of water for irrigation and boating is still an issue since no testing procedures have been carried on the lake water.

The site is a regular tourist spot which has reported to have a degrading effect on the quality of water. The lake being a natural freshwater source is shrinking in size with the water quality being degraded every year as per the site survey carried out and confirmation by the locals. The lake has a sacred background and is pious to the locals.

3 Methodology

The lake site was sampled in the month of August for the determination of physical, chemical, and biological parameters. Four sampling points were selected for collecting the water samples so that a complete water quality determination could be carried out (Fig. 2). The points were selected in such a manner that the whole lake area could be covered. The sampling point 1 was located near the forest farms

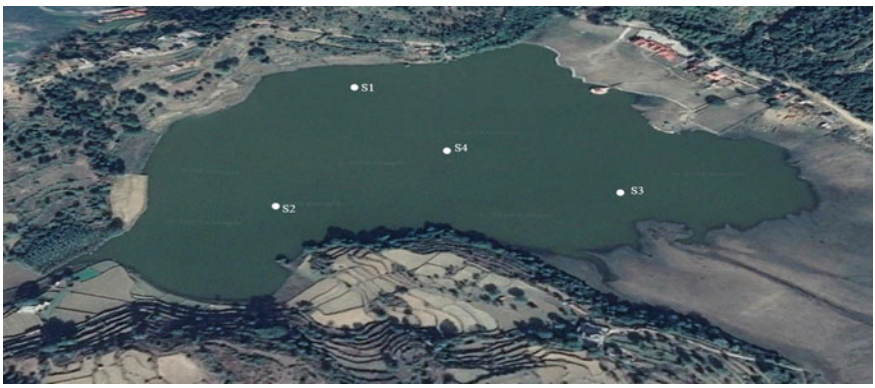

Fig. 2 Sampling points for water sampling

used by forest department for the plantation of medicinal plants, sampling point 2 was near the local farms used for rice, wheat, maize, and barley cultivation, sampling point 3 was near the marshy area of the lake, and sampling point 4 was the center of the lake.

The samples were collected using the boats available at the site. The sampling was done at about half meter below the surface of the lake, and the samples were stored in PVC bottles filled up to the brim then tested for various physical, chemical, and biological parameters, namely pH, temperature, BOD, DO, total coliform, ammonia, nitrate, nitrite, conductivity of water and total dissolved solids (TDS). The values for electrical conductivity (EC), pH, dissolved oxygen (DO), total dissolved solids (TDS), and temperature were determined on site using portable meters and rest of the parameters were measured according to the standard procedures by [14] and [15] after the samples are transferred to the laboratory.

Table 1 describes the designated best use, water quality class, and the criteria for water quality for the characterization of a water body, so that the water body can be utilized to its finest use.

Table 2 shows the values of various physical, chemical, and biological parameters that were measured at all the four sampling points and averaged for getting the single

Table 1 Designated best use criteria for water

DBU	Class of water quality	Criteria for quality of water
Potable water resource with chlorination but lacking any conventional treatment	A	1. Total coliform group count (MPN/100 ml)—50 or less 2. pH 6.5 to 8.5 3. D.O. $\geq$ 6 mg/l 4. BOD < 2 mg/l
Bathing outdoors (organized)	B	1. Total coliform group count (MPN/100 ml) organism shall be $\leq$ 500 2. pH = between 6.5 and 8.5 3. D.O. $\geq$ 5 mg/l 4. B.OD. < 3 mg/l
Potable water source with treatment	C	1. Total coliform group count (MPN/100 ml) organism $\leq$ 5000 2. pH = 6.5 to 9 3. D.O. $\geq$ 4 mg/l 4. B.OD. $\leq$ 3 mg/l
Development of wildlife and fisheries	D	1. pH between 6.5 and 9 2. D.O. $\geq$ 4 mg/l 3. NH_3 (in form of Nitrogen) $\leq$ 1.2 mg
Irrigation, controlled disposal and cooling in industries	E	1. ph between 6.0 and 8.5 2. E. C. < 2250 micromhos/cm 3. SAR < 26 4. Boron (B) quantity < 2 mg/l

Source [13]) (N.P.—not present)

Table 2 Values of physico-chemical and biological parameters of the lake water

Parameters	Sampling point 1 (S1)	Sampling point 2 (S2)	Sampling point 3 (S3)	Sampling point 4 (S4)	Average value
pH	8.1	7.2	7.5	7.3	7.5
Temperature (°C)	30.7	30.4	29.1	29.7	29.97
DO (mg/l)	7.33	3.18	2.76	3.06	4.08
BOD (mg/l)	0.2	0.3	1.0	0.1	0.4
TDS (ppm)	112	127	130	126	123.75
E.C. (μmhos/cm)	262	255	260	248	256.25
Total Coliform	0	0	0	0	0
Boron	–	–	–	–	–
NO_3	–	–	–	–	–
NO_2	–	–	–	–	–
NH_4	–	–	–	–	–

value. The values in Table 2 were then compared with Table 1 which gives the criteria for determination of DBU for the water body.

4 Results and Discussions

The experiments were performed for the determination of total coliform in the laboratory for all the four samples to confirm the presence of coliform group; the results confirmed that no coliform group was present in four of the water samples after checking for growth at 2nd, 3rd, and 4th day. The value confirmed the water is fit for usage in all three categories, namely A, B, and C (Table 3).

Portable pH meter after calibration with buffers of pH 4 and pH 7 was used for determination of the value of ph. The value for the pH was averaged to be 7.5. The pH value confirms that the water is fit for usage in all five categories, namely A, B, C, D, and E.

The value of DO was calculated with the help of portable DO meter, and the value averaged out to be 4.08 which confirms its fitness in three categories, namely C, D, and E.

The BOD value was calculated with standard procedure by APHA and the value averaged out to be 0.4 which confirms fitness in all three categories, namely A, B, and C.

The NH_3 (as N) was determined using standard APHA procedure of calorimetry came out to be nill or negligible for all the samples; therefore, the water could be considered to be fit for use in category D.

Table 3 Comparison of physical, biological, and chemical parameters of the lake to determine DBU

DBU	Class	Average parameter value	Criteria for quality of water	Status
Drinking water source with chlorination but without treatment	A	1. Total coliform—0 2. pH—7.5 3. DO—4.08 4. BOD—0.4	1. Total coliform group count (most probable number/100 ml) $\geq$ 50 2. pH between 6.5 and 8.5 3. D.O. $\geq$ 6 mg/l 4. BOD < 2 mg/l	Ok Ok Not ok Ok
Bathing outdoors (organized)	B	1. Total coliform—0 2. pH—7.5 3. DO—4.08 4. BOD—0.4	1. Total coliform group count (MPN/100 ml) organism shall be $\leq$ 500 2. pH between 6.5 and 8.5 3. Dissolved Oxygen (D.O.)—5 mg/l or more 4. B.OD. < 3 mg/l	Ok Ok Not ok Ok
Potable water source with treatment	C	1. Total coliform—0 2. pH—7.5 3. DO—4.08 4. BOD—0.4	. Total coliform group count (MPN/100 ml) organism $\leq$ 5000 2. pH between 6.5 and 9 3. D.O. $\geq$ 4 mg/l 4. Biological oxygen demand (BOD) $\leq$ 3 mg/l	Ok Ok Ok Ok
Development of wildlife and fisheries	D	1. pH—7.5 2. DO—4.08 3. NH_3 (as N)—nill	1. pH between 6.5 and 9 2. D.O. $\geq$ 4 mg/l 3. NH_3 (in form of nitrogen) $\leq$ 1.2 mg	Ok Ok Ok
Irrigation, controlled disposal, and industrial cooling	E	1.pH—7.5 2. E.C.—256.25 3. SAR-NA 4. Boron-NILL	1. pH between 6.0 and 8.5 2. Electrical conductivity < 2250 micromhos/cm 3. SAR < 26 4. Boron (B) < 2 mg/l	Ok Ok Ok Ok

The value of electrical conductivity was a criteria in category E only and the value was averaged to be 256.25 which was well below the permissible value.

The boron was calculated following standard procedure by APHA using UV absorption at 540 nm and 670 nm. The boron was found to be negligible, and therefore, the water could be considered fit to be used under category E.

The SAR value is not available for the samples.

5 Conclusion

The values of total coliform, DO, pH, BOD, EC, NH_3, SAR, and boron were determined, and the values clearly show that in the category A (potable source with chlorination but without conventional treatment) the value of DO was much less than limits, and therefore, the water cannot be used under the category A.

The value of parameters for category B (outdoor bathing) showed that the value of DO was much less than the prescribed limit so the water cannot be used under this category.

The value of parameters for C class (potable water source with treatment) was within limits, and therefore, the water can be used under this category.

The value of parameters for category D (propagation of wildlife and fisheries) was within limits, and therefore, water can be used under this category.

The value of parameters for category E (irrigation, industrial cooling, and controlled disposal) is within limits, and therefore, the water can be used under this category. Therefore, it can be concluded that the water is fit to be used for following categories.

Class C (Potable source of water with treatment).
Class D (fisheries development and wildlife propagation).
Class E (irrigation, industrial cooling, and controlled disposal).

Acknowledgements I would like to thank the local people of the lake site for extending a helping hand for sample collection and for providing useful information about the site. I would also like to thank the Laboratory of Central Pollution Control Board (CPCB) at Parwanoo, Himachal Pradesh for providing facilities for sample testing.

References

1. Versari A, Parpinello GP, Galassi S (2002) Chemometric survey of Italian bottled mineral waters by means of their labelled physico-chemical and chemical composition. J Food Compos Anal 15:51–64. https://doi.org/10.1006/jfca.2002.1058
2. Bhateria R, Jain D (2016) Water quality assessment of lake: a review. Sustain Water Resour Manag 2:161–173. https://doi.org/10.1007/s40899-015-0014-7
3. Tamiru A (2004) Assessment of pollution status and groundwater vulnerability mapping of the Addis Ababa Water Supply Aquifers. Ethopia. https://doi.org/10.1007/s12665-009-0134-1
4. Mahananda MR, Mohanty BP, Behera NR (2010) Physico-chemical analysis of surface and ground water of bargarh district, Orissa, India. Int J Res Rev Appl Sci 2(3):284–295
5. Mehari M, Mulu B (2013) Distribution of trace metals in two commercially important fish species, Tilapia Zilli and Oreochromis Niloticus, Sediment and Water from Lake
6. Tank SK, Chippa RC (2013) Analysis of water quality of Halena Block in Bharatpur Area. Int J Sci Res Publ **3**(3). ISSN 2250–3153
7. Hartman J, Berna Z, Stuben D, Henze N (2005) A statistical procedure for the analysis of seismo tectonically induced hydro chemical signals: a case study from the Eastern Carpathians, Romania. Tectonophysics 405:77–98

8. Wang JL, Yang YS (2008) An approach to catchment-scale groundwater nitrate risk assessment from diffuse agricultural sources: a case study in the Upper Bann, Northern Ireland. Hydrol Proces 22:4274–4286. https://doi.org/10.1002/hyp.7036
9. Yogendra K, Puttaiah ET (2008) Determination of water quality index and suitability of an Urban Waterbody in Shimoga Town, Karnataka. In: Sengupta M, Dalwani (eds) The 12th world lake conference, proceedings of Taal 2007, pp 342–346
10. Cosgrove WJ, Loucks DP (2015) Water management: current and future challenges and research directions. Water Resour Res 51:4823–4839. https://doi.org/10.1002/2014WR016869
11. Diersing N (2009) Water quality: frequently asked questions. Florida Brook Keyss National Marine Sanctuary, Key West, FL. Gudbahri, Eastern Tigray of Northen Ethiopia. Int J Sci Res Publ 3:2250–3153. ISSN 2250-3153
12. Thitame SN, Pondhe GM (2010) Assessment of seasonal variations in physico chemical characteristics and quality of Pravara river water for irrigation use in Sangamner dist. Ahmednagar Maharashtra. J Chem Pharm Res 2(2):316–320. ISSN 0975-7384
13. CPCB Ministry of environment and forest 2008. Guidelines of water quality monitoring. CPCB Guidelines, 2007–2008, pp 1-35
14. APHA, AWWA, WPCF (1985) Standard Methods for the Examination of Water and Waste Water, 16th edn, Washington
15. Trivedi RK, Goel PK (1984) Chemical and biological method for water pollution studies. Enviromedia Publication, Karad

Hydrochemical Analysis of Six Sacred Lakes of Sikkim

Roshni Chettri, Dipankar Tuladhar, and Chandrashekhar Bhuiyan

Abstract Sikkim, the north-eastern state of India has more than 200 lakes, whose serene beauty attracts tourists from all over the world. Some of the lakes act as the sources for drinking water while some are considered sacred and are used for religious purpose. Chemical analysis of lake water may provide vital information about the possible reasons of anomaly, level of pollution, if any as well as effect of anthropogenic activities. In the present study, water chemistry of six important and sacred lakes of Sikkim, namely Gurudongmar, Lamapokhari, Kheheopalri, Karthok, Menmecho and Kupup, has been analysed and critically examined. Water samples were collected from these lakes and their chemical analysis has been carried out. General water quality parameters of these water samples were tested and compared with the standards laid by the Bureau of Indian Standards (BIS) and the World Health Organization (WHO) to find whether the lakes are suitable for domestic and agricultural uses. Results have revealed difference in the lake water quality of these lakes with respect to different chemical parameters. Anomalous concentrations of dissolved oxygen (DO), calcium (Ca) and total dissolved solids (TDS) obtained in water samples of certain lakes have been examined and correlated with natural and anthropogenic factors. This paper has discussed the possible reasons of anomalous chemistry of these sacred lakes and has advocated for their environmental protection.

Keywords Lakes · Water chemistry · Sikkim · Himalaya

1 Introduction

Limnology is the study of the biological, chemical, physical, geological and other attributes of all inland waters including lakes. Sikkim, the least populous and second smallest state of India, is located in the north-eastern part of the country between 27° 05′N to 28° 09′N latitudes and 87° 59′E to 88° 56′E longitudes covering 7096 km

R. Chettri · D. Tuladhar · C. Bhuiyan (✉)
Department of Civil Engineering, Sikkim Manipal Institute of Technology, Sikkim Manipal University, Sikkim 737136, India
e-mail: c.bhuiyan@smit.smu.edu.in

C. Bhuiyan et al. (eds.), *Water Security and Sustainability*,
Lecture Notes in Civil Engineering 115,
https://doi.org/10.1007/978-981-15-9805-0_6

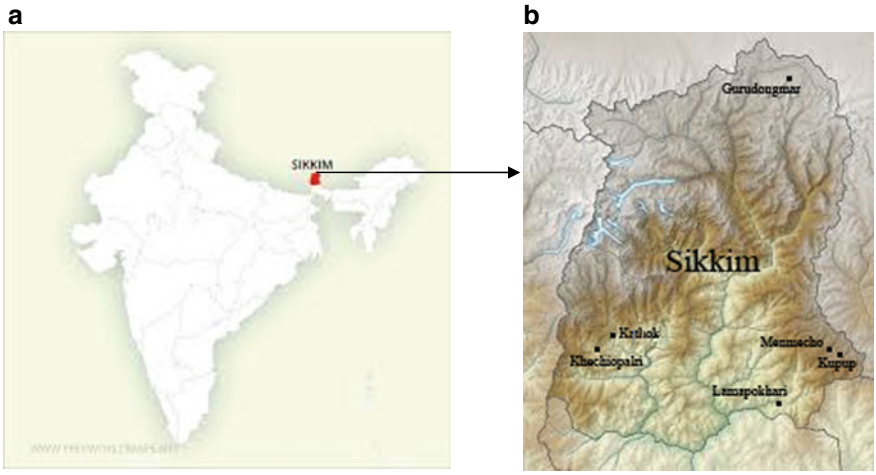

Fig. 1 **a** Location of Sikkim in India **b** Location of the six sacred lakes of Sikkim

(Fig. 1a). Sikkim is one of the few states in India known for its clean and green natural environment. The state hosts numerous lakes; many of them are the major tourist spots generating huge amount of revenue for the state. Lakes are more vulnerable to pollution as the water is stagnant or less dynamic [1]. Most of the lakes located in the northern part of Sikkim are fed by glaciers and are not easily accessible, and hence their natural water chemistry is protected. On the contrary, the lakes which are within the reach of the tourists or are used for socio-cultural-religious activities are vulnerable to pollution. Hence, routine test and hydrochemical analysis of water quality parameters are important to identify the level of pollution in such lakes. On this consideration, this study involved collection and chemical analysis of the water samples to assess water quality of six religiously sacred lakes of Sikkim. Chemical analysis of the water samples was carried out in the field and in the laboratory.

2 The Six Sacred Lakes

In the present study, water chemistry of six important lakes of Sikkim which have cultural, aesthetic and spiritual importance has been analysed. The six sacred lakes considered in this study, Gurudongmar, Lamapokhari, Kheheopalri, Karthok, Menmecho and Kupup, are located in different parts of Sikkim (Fig. 1b). Brief description of these lakes is given below.

***Gurudongmar Lake*:** Gurudongmar lake is one of the highest lakes in the world, located at an altitude of 5,430 m in the North District of Sikkim. The picturesque lake remains frozen during winter but displays various shades of blue in other seasons (Fig. 2). It is located at about 190 km away from Gangtok, the capital city of Sikkim.

Location: North Sikkim
Coordinates: 27°20′46″N - 88°49′06″
Maximum length: 5.34 km (3.32 miles)
Maximum width: 0.9km (0.56 miles)
Surface area: 118 hectares (290 acres)
Surface elevation: 5430 m (17, 800 ft)

Fig. 2 Gurudongmar lake. *Source* Google Images

Gurudongmar lake is a moraine-dammed lake fed by the of Gurudongmar glacier. Surface area of the lake expands and contracts following glacier dynamics as well as due to melting and freezing of ice and snow.

Several streams originate from the Gurudongmar lake and join the Tso Lahmu lake, which together act as the source of Teesta, the main river of Sikkim. This glacial lake remains completely frozen in the winter months during November to May. Although the lake is very big (118 hecters) with a peripheral length of 5.34 km, major part is not visible due to hilly topography. Due to high altitude, oxygen is very low resulting barren landscape with no vegetation. Gurudongmar lake is probably the most sacred lake in Sikkim regarded by the Buddhist and the larger Hindu community. Although the lake water appears very clean, it may contain impurities and pollutants.

Lamapokhari (Aritar) Lake: Lamapokhari lake or commonly known as Aritar lake is located in the East District of Sikkim. This boot-shaped natural lake is associated with Buddhist religious rituals since last 550 years, at least (Fig. 3). Located at an altitude of 1402 m, the lake is surrounded by lush green pine forest.

Although this lake is considered sacred, it is popular for social recreation including boating. The green colour of the lake water is mainly due to phytoplankton bloom.

Khecheopalri Lake: The Khecheopalri lake, originally *Kha-Chot-Palri*, is considered as one of the holy lakes in Sikkim by both Buddhists and Hindus [2]. This natural lake located in a village bearing the same name at an altitude of 1,700 m is also referred as 'wish-fulfilling lake'. Depth of the lake varies between 7.2 to 11.2 m below the ground surface, and age of the lake is estimated to be ~3500 years. The lake is associated with two perennial and five seasonal inlets and one outlet [3]. Although at present the source of water in the lake is rainfall and groundwater, it was formed by ancient glacial actions. Khecheopalri lake (Fig. 4) is mostly used by

Location: East Sikkim
Coordinates: 27°20′46″N - 88°49′06″
Maximum length: 0.35 km (0.217 miles)
Maximum width: 0.1 km (0.062 miles)
Surface area: 1.84 hectares (4.55 acres)
Surface elevation: 1553 m

Fig. 3 Aritar lake. *Source* Google Images

Location: West Sikkim
Coordinates: 27°20′57″N - 88°11′07″
Maximum length: 0.45 km (0.28 miles)
Maximum width: 0.28 km (0.174 miles)
Surface area: 8.28 hectares (20.46 acres)
Surface elevation: 1798 m (5899 ft)

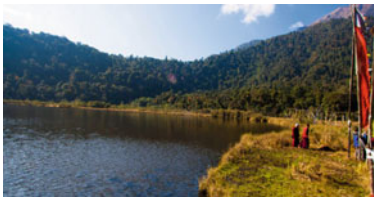

Fig. 4 Kheceopalri lake. *Source* Google Images

Location: West Sikkim
Coordinates: 27°22'17" N - 88°13'18" N
Maximum length: 0.13 km (0.08 miles)
Maximum width: 0.09 km (0.056 miles)
Surface area: 0.75 hectares (1.85 acres)
Surface elevation: 1735 m (5692 ft)

Fig. 5 Karthok lake. *Source* Google Images

local people, particularly Buddhists for religious activities. The lake is inhabited by phytoplankton, zooplankton and microbial organisms besides different varieties of fishes.

This sacred lake is also association with legends that birds and swans safeguard this celestial lake from intruders and even take away the fallen leaves from the lake surface.

***Karthok Lake*:** One among the sacred lakes of Sikkim, the Karthok lake (Fig. 5) is known to be the most appealing and serene lakes in the state.

The lake is located at Yuksom in the West District of Sikkim. It is elliptical in shape and is surrounded by green pastures and pine forest. The Buddhist community considers this a holy lake and use its water for religious purpose. This is said and believed that any wish made beside this lake with a pure heart never goes unheard by the Gods.

***Menmecho Lake*:** Menmecho lake is a natural mountain lake located in East District near the Jelepla Pass. The lake serves as the source of river Rangpo-chu, a tributary of Teesta River. The lake is fed by melting snow in the summer and by the south-west monsoon rainfall in the rainy season. Like most other lakes in Sikkim, Menmecho lake is also located in a valley surrounded by forested hills (Fig. 6).

The lake is located at an altitude of 3810 m above the mean sea level and remains snow covered in the winter. The lake is inhabited by different fish species including trout. In fact, tourists across the globe throng to this lake to enjoy the sport of fishing.

***Elephant Lake (Kupup lake)*:** The Elephant lake at Kupup (Fig. 7) rests at an altitude of 3983 m, on the way to Jelepla Pass bordering China. The lake got such a name as shape of the lake resembles an elephant trunk.

Location: East Sikkim
Coordinates: 27°19′49″N - 88°50′46″
Maximum length: ~ 350 m (1148 ft)
Maximum width: ~ 75m (246 ft)
Surface area:
Surface elevation: 3810 m (12,500 ft)

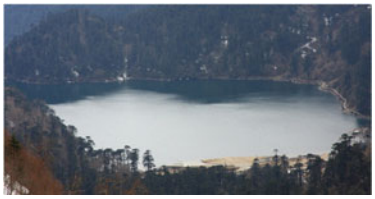

Fig. 6 Menmecho lake. *Source* Google Images

Location: East Sikkim
Coordinates: 27°19'49"N- 88°50'46"
Maximum length: 1 km (0.62 miles)
Maximum width: 0.385 km (0.239 miles)
Surface area: 28.05 hectares (69.31 acres)
Surface elevation: 4211 m (13816 ft)

Fig. 7 Elephant lake. *Source* Google Images

This is a closed lake with stagnant water. Unlike the other lakes (except Gurudongmar) studied and discussed here, the Kupup lake as it is commonly known is not surrounded by tall canopies of forest. The lake is located in a depression surrounded by hills, covered with pastures and shrubs unlike the Gurudongmar lake, which is surrounded by snow covered or barren hills.

3 Methodology

Water samples were collected from the aforesaid six lakes of Sikkim. The samples were collected in the winter and pre-monsoon periods during January 2017 to April 2017 in air-tight bottles to ensure no spillage would occur. Water quality parameters analysed in this study include: (i) pH, (ii) total dissolved solids (TDS), (iii) dissolved oxygen (DO), (iv) DO_5 content (i.e. DO after five days of sample collection), (v) total hardness, (vi) sodium, (vii) potassium, (viii) calcium, (ix) magnesium, (x) chloride, (xi) sulphate and (xii) phosphate. Out of these parameters, the pH was measured in situ using a microprocessor-based pH metre. The TDS was also measured in situ using a TDS probe and a temperature probe. Chemical analysis of other water quality parameters was carried out in the laboratory. Total hardness, calcium, magnesium and chloride concentration were determined using volumetric titration. The sulphate and phosphorous concentrations were determined using UV-spectrophotometer, whereas sodium and potassium concentrations were determined using flame photometer. The results were compared with the standard values recommended in the BIS (1991) [4] and WHO (2014) guidelines [5] for drinking water although water of these lakes

is hardly used for drinking purpose. Brief description of the water quality of these sacred lakes has been discussed in the following sections.

4 Results and Discussion

As already mentioned, water of these six sacred lakes is not used for drinking or irrigation purpose. However, in order to assess the state of purity or level of pollution, their water chemistry has been analysed and interpreted through comparison with the BIS (1991) and WHO (2014) standards for drinking water. Most of the hydrochemical parameters in these six sacred lakes are found to vary within the acceptable/permissible limits of BIS and WHO standards/guidelines for drinking water. However, variation could be found in the lake water chemistry. The pH of the water is found to vary between 6.4 and 7.2, which is more or less within the permissible limit. However, concentration of DO and DO_5 is found to be relatively low in two out of six lakes, particularly in the Khechiopalri and Lamapokhari lakes. While Khechiopalri is one of the most sacred lakes in Sikkim, Lamapokhari lake is used mostly for social and aesthetic purposes such as boating. Surprisingly, the DO and DO_5 values are found to be much higher in the water of Kupup lake and Gurudrongmar lake, in spite of their higher elevation (Kupup: 3983 m; Gurudrongmar: 5300 m). Among other parameters, only TDS is found to be high and comparatively higher in Khecheopalri lake and Kathok lake, both of which are extensively used for religious purpose. Comparatively higher concentrations of carbonate and bicarbonate are also found in samples from Khecheopalri lake (Table 1).

The Hill–Piper diagram (Piper 1944) [6] shows that water samples of all the six lakes have high concentrations (60 to 80%) of Ca, moderate concentration (30 to 50%) of Mg and lower concentrations (20 to 40%) of Na and K (Fig. 8). In most of the samples, chloride and sulphate are found to be low to moderate (20 to 40%), and concentrations of carbonate and bicarbonates are relatively much higher (60 to 80%). Combined water-chemistry statistics of the six lakes is presented further for better understanding (Table 2).

A statistical analysis (correlation) has further revealed strong or very strong (positive or negative) association between certain chemical parameters and weak or moderate association between other parameters (Table 3). For example, pH values are correlated inversely with K, Mg, SO_4 and PO_4 but positively with DO and DO_5 and their associations are strong. Dissolved oxygen is found to display inverse relationship with all other parameters, and the inverse relation is strongest with PO_4. On the contrary, TDS shows positive correlation with most of the parameters, which is significantly strong with Na, Ca, Cl, HCO_3 and PO_4. Among the ions, Na, Cl, HCO_3 and PO_4 are strongly correlated with each other and the correlation is positive. Mg is strongly correlated with K and SO_4. Correlation of Ca is positive with HCO_3 but negative with SO_4. Again, SO_4 shows strong positive correlation with PO_4 and strong negative correlation with HCO_3.

Table 1 Indian (BIS, 1991) and International (WHO, 2014) Standards for Drinking Water and concentration of various chemical parameters in the six lakes of Sikkim (unit: mg/l except for pH, hardness and TDS)

Parameters	BIS		WHO		Gurudrongmar (L1)	Lamapokhari (L2)	Khecheopalri (L3)	Karthok (L4)	Menmecho (L5)	Kupup (L6)
	Acceptable	Permissible	Acceptable	Permissible						
pH	6.5–8.5	No relaxation	7.0–8.5	6.5–9.2	7.1	6.4	6.9	6.7	7.0	6.8
DO	–	–	–	–	**9.3**	**4.3**	**4.1**	**6.8**	**8.3**	**13**
DO_5	–	–	–	–	8.9	3.5	3.1	5.4	6.1	10
Hardness	300	600	100	500	20	16	36	20	16	24
TDS	500	1500	500	1500	20	14	**610**	110	13	11
Na^+	–	–	–	–	0.2	0.8	2.1	1.5	1.5	0.7
K^+	–	–	–	–	6.6	7.6	7.3	7.9	6.3	7.3
Ca^{2+}	75	200	75	200	24	16	24	17	8	16
Mg^{2+}	30	100	<30	150	4.7	5.4	4.8	6	4.9	4.5
Cl^-	250	1000	200	600	7.9	11.9	25	5.0	9.9	8.0
HCO_3^-					24.4	19.5	43.9	24.4	19.5	29.3
SO_4^{2-}	200	400	200	400	0.37	0.63	0.43	0.66	0.56	0.41
PO_4^{3-}	–	–	–	–	0.01	0.03	0.03	0.02	0.02	0.01

Bold indicates Anomalous high value

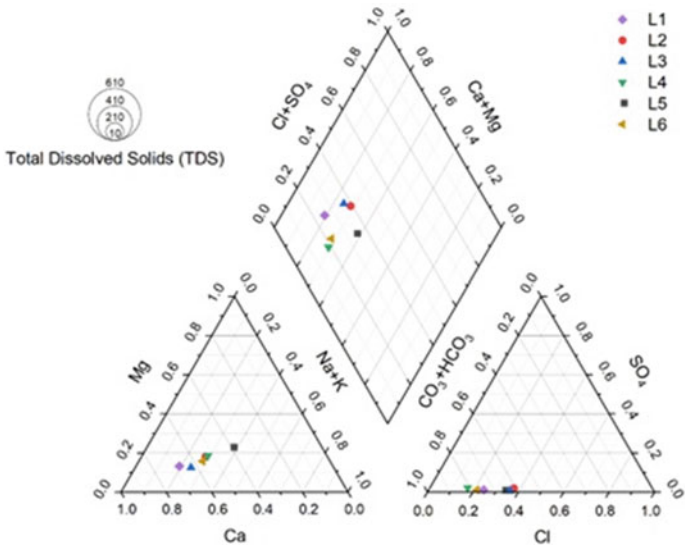

Fig. 8 Hill–Piper diagram reveals chemical nature of water in six sacred lakes of Sikkim

Sikkim is dominantly covered by evergreen and deciduous forests (Fig. 9). Nearly 25% of the state is covered by Khangchenzonga National Park and 5.70% by other wildlife sanctuaries. Altogether, 47.31% of the geographical area of the state covering 3357 km^2 comes under forest of which ~93.34% is reserved forest and 6.66% is protected forest. Other land-cover includes agricultural land (~8.52%), alpine pastures (~6.08%), glaciers (2.93%) and lakes (0.47%).

The Hill–Piper diagram when correlated with the lithological map of Sikkim (Fig. 10) has revealed moderate influence of lithology on the lake water chemistry. Gurudongmar lake is associated with schist whereas rocks at Kheceopalri lake are high-grade gneiss containing mica [7]. The other four lakes are associated with carbonates and bicarbonates (Fig. 8). Therefore, higher concentrations of Ca and Mg are associated with gneissic rocks, which are predominantly composed of silicates. On the contrary, these six lakes have higher Ca and lower Na and K contents, which are not solely due to natural factors such as lithology.

5 Discussion

Lakes play a very important role in the culture of Sikkim. They not only serve the key role for the ecosystem but also an important and integral component of the socio-religious-cultural life of the local community. This study involving hydrochemical analysis of six sacred lakes in Sikkim has revealed that although these lakes are not much polluted, concentration of some chemical and biochemical constituents is

Table 2 Statistical description of various chemical parameters tested

Statistics	pH	DO (ppm)	DO_5 (ppm)	TDS (ppm)	Na^+ (ppm)	K^+ (ppm)	Ca^{2+} (ppm)	Mg^{2+} (ppm)	Cl^- (ppm)	HCO_3^- (ppm)	SO_4^{2-}	PO_4^{3-} (ppm)
Minimum	6.4	4.1	3.1	11	0.2	6.3	8.0	4.5	5.0	19.5	0.37	0.01
Maximum	7.1	13.0	10.0	610	2.1	7.9	24.0	6.0	25.0	43.9	0.66	0.03
Mean	6.8	7.6	6.2	130	1.1	7.2	17.5	5.1	11.3	26.8	0.51	0.02
Median	6.9	7.6	5.8	17	1.2	7.3	16.5	4.9	9.0	24.4	0.50	0.02
Standard deviation	0.2	3.4	2.8	238	0.7	0.6	6.0	0.6	7.1	9.1	0.12	0.01

Table 3 Pearson's correlation matrix ($p < 0.05$) among various hydrochemical parameters tested

Parameters	pH	DO (ppm)	DO_5 (ppm)	TDS (ppm)	Na^+ (ppm)	K^+ (ppm)	Ca^{2+} (ppm)	Mg^{2+} (ppm)	Cl^- (ppm)	HCO_3^- (ppm)	SO_4^{2-} (ppm)	PO_4^{3-} (ppm)
pH	1.00											
DO (ppm)	0.41	1.00										
DO_5 (ppm)	0.47	**0.97**	1.00									
TDS (ppm)	0.14	**−0.55**	**−0.57**	1.00								
Na^+ (ppm)	−0.02	**−0.54**	**−0.68**	**0.74**	1.00							
K^+ (ppm)	**−0.77**	−0.33	−0.37	0.20	0.19	1.00						
Ca^{2+} (ppm)	0.18	−0.21	−0.03	**0.54**	−0.11	0.23	1.00					
Mg^{2+} (ppm)	**−0.57**	**−0.51**	**−0.51**	−0.09	0.26	**0.64**	−0.16	1.00				
Cl^- (ppm)	0.05	**−0.58**	**−0.61**	**0.89**	**0.61**	0.01	0.41	−0.30	1.00			
HCO_3^- (ppm)	0.24	−0.19	−0.22	**0.91**	**0.53**	0.19	**0.63**	−0.34	**0.79**	1.00		
SO_4^{2-} (ppm)	**−0.68**	−0.48	**−0.56**	−0.23	0.31	0.47	**−0.55**	**0.88**	−0.28	**−0.51**	1.00	
PO_4^{3-} (ppm)	**−0.54**	**−0.93**	**−0.98**	**0.56**	**0.65**	0.37	0.00	0.40	**0.66**	0.24	**0.51**	1.00

Bold indicates Anomalous high value

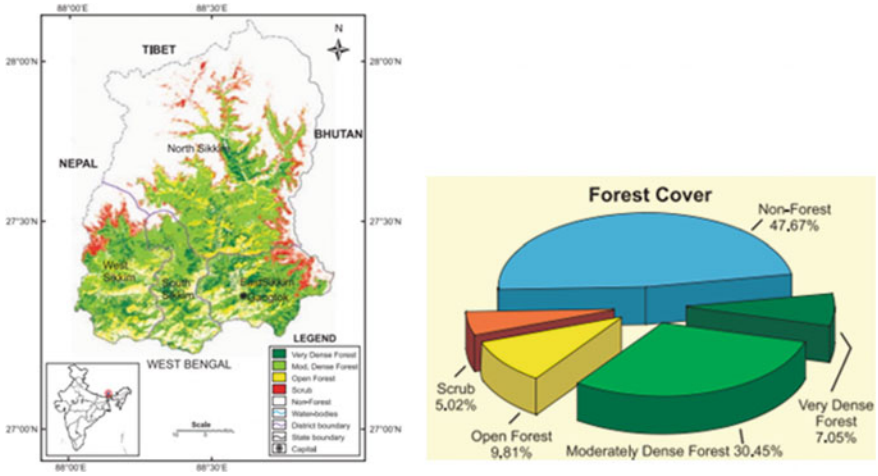

Fig. 9 Land-use/land-cover map and land-use/land-cover statistics of Sikkim

comparatively high. Both surface water and groundwater quality get significantly affected by land-use/land-cover [8]. Impact of land-use/land-cover is expected to be more prevalent in case of lakes since they are associated with stagnant water. The lake water chemistry is generally governed by soil and rocks of the lake sites. However, land-use/land-cover and socio-religious activities also have significant impact on their water quality. Slightly lower pH values (6.4 to 6.9) in Lamapokhari, Kheceopalri, Karthok and Kupup lakes are most likely due to organic acid formed due to decomposition of plant leaves [2, 3]. In fact total suspended solids (TSS) are also high in Karthok lake and very high in Khecheopalri lake. Relatively higher value of TSS in these lakes is due to coagulation of fodder, cow dung, muddy soil leached into the lake flowing from the surrounding hills and grazing field after rainfall.

A simple plot of TDS against the weight ratio of Na/(Na+Ca) as proposed by Gibbs provides information about dominant influence of major natural factors (precipitation, evaporation, rock weathering, fractional crystallization, etc.) on river water chemistry [9]. Similar plot has revealed that precipitation and leaching of soils have prevalent effect on the water chemistry of these six lakes over other natural controllers (Fig. 11). This is interesting to note that none of these six lakes are located in or associated with carbonate lithology, however the Hill–Piper diagram (the rhombus part) has revealed higher concentrations of Ca and Mg over those of Na and K (Fig. 8). Dominance of carbonate chemistry over silicates is further revealed when Ca+Mg is plotted against Na+K (Fig. 12). Since the lakes are not associated with carbonate rocks, possible reason for higher concentration of calcium and magnesium could be mineral-leaching from phyllite, schist and gneissic rocks. Besides, religious offerings in the lakes (flower, incandescent sticks, butter, etc.) and food for fishes and birds (puffed rice, bread, biscuits, etc.) may also have some bearing on high concentration of calcium, phosphorous and other minerals in the lake water.

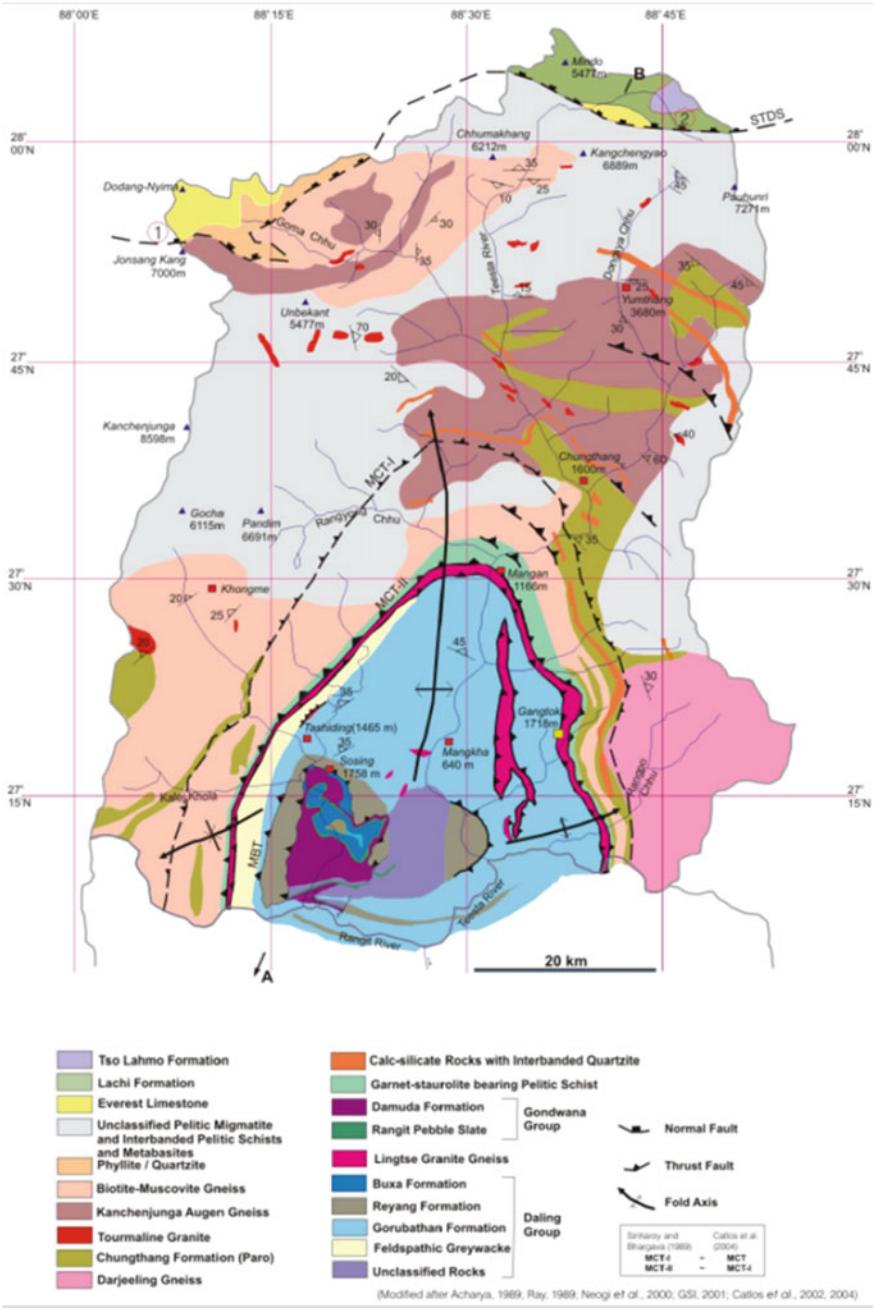

Fig. 10 Geological map of Sikkim [7]

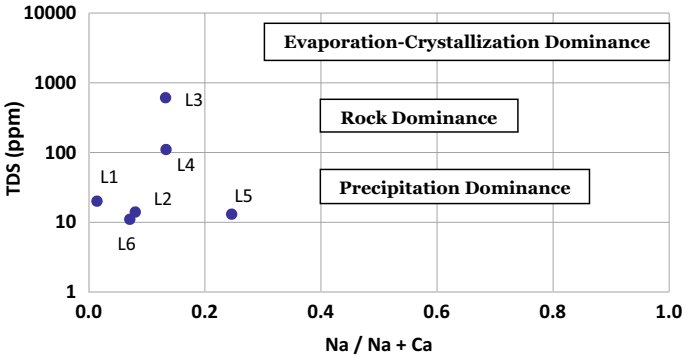

Fig. 11 Gibbs (1970) diagram revealing major dominance on the lake chemistry

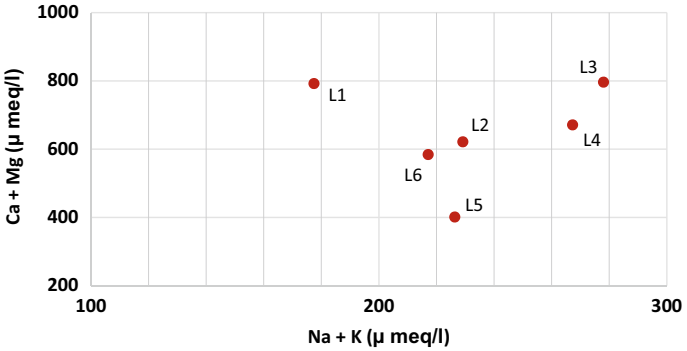

Fig. 12 Relation between alkali and alkaline earth elements in the six lakes studied

Chloride concentration is the most useful parameter for evaluating atmospheric input to the lakes as it shows little fractionation and common rocks do not have a significant amount of Cl [1, 10, 11]. Among the six lakes, lowest (5 mg/l) and highest (25 mg/l) chloride concentration is found, respectively, in Karthok lake and Kheceopalri lake. High concentration of chloride in all the six lakes is thus due to anthropogenic activities.

This is important to mention that algal bloom is prevalent in the Khecheopalri, Karthok and Lamapokhari lakes, due to social, cultural and religious activities. The situation is critical at Khecheoplari lake as it is surrounded by bogs, swamps and forest and is associated with various anthropogenic activities and has high sediment (soil and mud) influx [3]. Continuation of such activities will eventually lead to eutrophication or choking of the lakes as algae consume the oxygen present in the water. This is in fact already prevalent in Kheceopalri lake [2, 3].

6 Conclusion

Although the Government of Sikkim and its people are vigilant to protect and preserve the natural environment, due to unprecedented activities by a section of tourists, serene lakes of this state are getting polluted gradually. Apparently the pollution level is not very high. However, cumulative impact of gradual small-scale pollution might cause significant degradation of the aquatic ecosystem in the long run. Therefore, in order to protect the natural health of lakes and associated wetlands, the areas surrounding the lakes should be kept out of limits of people, and wetland ecosystem management practice needs to be taken up. More attention should be given to environmental sustainability, and ecological balance should be maintained by any cost.

References

1. Saini RK, Swain S, Patra A, Khanday GJ, Gupta H, Purushothaman P, Chakrapani GJ (2008) Water chemistry of three Himalayan Lakes: Dal (Jammu & Kashmir), Khajjar (Himachal Pradesh) and Nainital (Uttarakhand). Himalayan Geol 29(1):63–72
2. Wikipedia (2020). https://en.wikipedia.org/wiki/Khecheopalri_Lake. Accessed 12 Nov 2019
3. Jain A, Rai SC, Pal J, Sharma E (1999) Hydrology and nutrient dynamics of a sacred lake in Sikkim Himalaya. Hydrobiologia 416:13–22
4. Bureau of Indian Standards (1991) Indian standard specification for drinking water IS-10500. Indian Standard Institute, New Delhi
5. World Health Organisation (2014) Guidelines for drinking water quality, 4th edn. World Health Organization
6. Piper AM (1944) A graphic procedure in the geochemical interpretation of water analysis. Trans Am Geophys Union 25:914–928
7. CISMHE (2007) Carrying capacity study of Teesta basin in Sikkim, vol II: Land Environment – Geophysical Environment. Centre for Inter-disciplinary Studies of Mountain and Hill Environment, University of Delhi, Prepared for Ministry of Environment & Forests, Government of India
8. Bhuiyan C, Champati Ray PK (2016) Groundwater quality zoning in the perspective of health hazards. Water Resour Manag 31(1):251–267. https://doi.org/10.1007/s11269-016-1522-4
9. Gibbs RJ (1970) Mechanicsms controlling world water chemistry. Science 170:1088–1090
10. Zhang J, Huang WW, Letolle R, Jusserand C (1995) Major element chemistry of the Huanghe (Yellow river), China: weathering processes and chemical fluxes. J Hydrol 168: 173–203
11. Gaillardet J, Dupre B, Louvat P, Cj Allegre (1999) Global silicate weathering and CO_2 consumption rates deduced from the chemistry of large rivers. Chem Geol 159:3–30

Determination of Best-Fit Probability Distribution of Rainfall Data in Sikkim, India

S. Kiran and David Raj Micheal

Abstract Rainfall is an essential input in design of various hydraulic structures, urban planning, disaster management, and agriculture. In this study, an attempt is made to identify the probability distributions that best fits the rainfall data of Sikkim, India. Monthly rainfall data is collected in four rain gauge stations in Sikkim and the best-fit probability distributions of the rainfall data in each station in annual, dry, and wet seasons are identified. Goodness-of-fit tests such as χ^2, log-likelihood, Akaike information criterion (AIC), and Bayesian information criterion (BIC) are used to test the fit of probability distributions on the empirical data.

Keywords Sikkim · Rainfall · Probability distribution · Maximum likelihood estimation

1 Introduction

In India, the spatial and temporal distribution of rainfall has predominantly been dependent on the monsoons every year. This holds an adverse effect on irrigation scheduling and crop productivity, posing acute challenges on livelihood. It also triggers extreme events like acute water scarcity, drought, and flood which cause changes in land forms relating to the processes of mass movements. Knowledge of rainfall pattern, its distribution, and variability is thus important and useful to forecast rainfall which in turn helps in crop practice, irrigation scheduling, drought and flood management, and water supply.

The abrupt variation in the topography of Sikkim is a major factor that influences the distribution of rainfall throughout the state. The unique rainfall pattern is also influenced by the direction of wind, aspect of hill slopes, and complex orographic

S. Kiran (✉)
Department of Civil Engineering, Sikkim Manipal Institute of Technology, Sikkim, India
e-mail: kiran.sriram@smit.smu.edu.in

D. R. Micheal
Department of Mathematics, Sikkim Manipal Institute of Technology, Sikkim, India

C. Bhuiyan et al. (eds.), *Water Security and Sustainability*,
Lecture Notes in Civil Engineering 115,
https://doi.org/10.1007/978-981-15-9805-0_7

effects. Sikkim is divided into four quadrants based on the amount of rainfall it receives. Rainfall is more in the southeast and southwest quadrants when compared to the northeast and northwest quadrants. The narrow zone between the southeast and southwest quadrants also experiences lesser rainfall [1]. The high rainfall in Sikkim is controlled by the north–south oscillations of monsoon trough [2].

Variation in rainfall pattern, influenced by climate change, has cascading impacts on various sectors. The impact due to the variations in seasonal rainfall was elucidated through community observations in Sikkim. It also had a considerable influence on drying up of water sources and drastic reduction in the lean period discharge of springs bringing about crop yield instability [3]. The excess runoffs from high intensity rainfall have had a destabilizing impact on the sensitive topography leading to soil erosion and landslides especially in North Sikkim and inflicting damages on irrigation and urban infrastructure, shunting even their optimal utilization [4]. Hydropower generation in enhanced stream flows is susceptible to rockfalls, debris, and river bank erosion [5], knowing the distribution of rainfall assists in the interpretation of rainfall pattern and all associated hydrological parameters, particularly runoff. Identifying the best-fit probability distribution of seasonal and annual rainfall for stations in Sikkim will provide vital information required in planning, designing, managing water resource systems and mitigating the impact of extreme rainfall in hydrologically vulnerable regions.

Quantitative analyses involving rainfall or precipitation have predominantly focused on extreme event forecasting, frequency analysis, and trend analysis using time series. Frequency analysis of rainfall without adequate information about the probability distribution function that best fits the data leads to erroneous interpretation of recurrence interval which is an important input parameter in various hydrological designs. For example, rainfall data rarely follows normal distribution. However, it is a common practice to apply normal statistics rules for rainfall data analysis resulting in an inaccurate prediction. Therefore, precise knowledge about the probability distribution of rainfall at a station is important and crucial for rainfall data analysis, interpretation, anomaly identification, and events' prediction. Fitting probability distributions to sample hydrological data involves estimation of associated parameters representative of the population. This is accomplished using various methods of which the method of L-moments and the method of maximum likelihood estimation are widely used. The maximum likelihood method is consistent and theoretically generates the most efficient estimates of parameter in a probability distribution [6, 7]. L-moments are more robust, unbiased, and are less sensitive to the sample size and outliers [8, 9]. In this study, an effort is made to determine the best-fit probability distribution(s) of annual and seasonal rainfall from the monthly rainfall data recorded across four observation stations in Sikkim, India.

2 Data and Description

This study uses monthly rainfall data recorded in four meteorological stations in Sikkim from 1951 to 1999. The data is obtained from the study titled Carrying Capacity Study of Teesta Basin in Sikkim by Centre for Interdisciplinary Studies of Mountain and Hill Environment (CISMHE), University of Delhi under the supervision of Ministry of Environment and Forests, Government of India.

The stations in the study were selected based on the availability of data. The spatial distribution of the rain gauge stations is shown in Fig. 1 (Table 1).

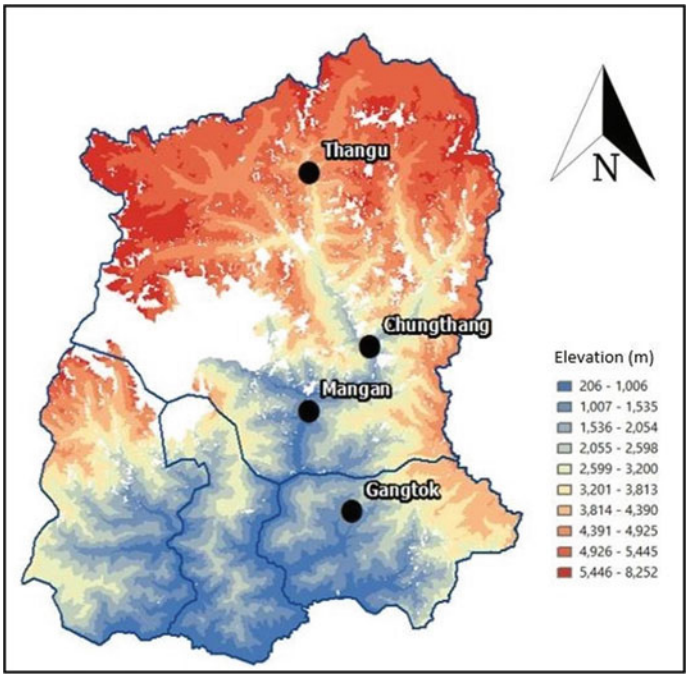

Fig. 1 Location of observation stations in Sikkim

Table 1 Information of rainfall observation stations

Observation station	Latitude (Degrees)	Longitude (Degrees)	Altitude (m)	Period of record
Thangu	27.53	88.31	3834	1951–1980
Chungthang	27.36	88.30	1631	1951–1980 & 1983–1984
Mangan	27.30	88.32	1310	1957–1980
Gangtok	27.30	88.37	1756	1957–1979 & 1990–1999

Sikkim experiences very high intensity rainfall during the monsoon which usually lasts from the end of May till the beginning of October signifying the wet season. The period between November and April receives scanty rainfall contributing to the dry season. The mean monthly rainfall illustrated in Fig. 2 and Table 2 reveals the occurrence of heavy rainfall in the mid and lower hills while at higher altitudes the rainfall is sparse. This is attributed to the variation in the altitude of hills over a short span. However, the descriptives of the data for the four meteorological stations considered in this study throw a puzzle, which is discussed in a later section.

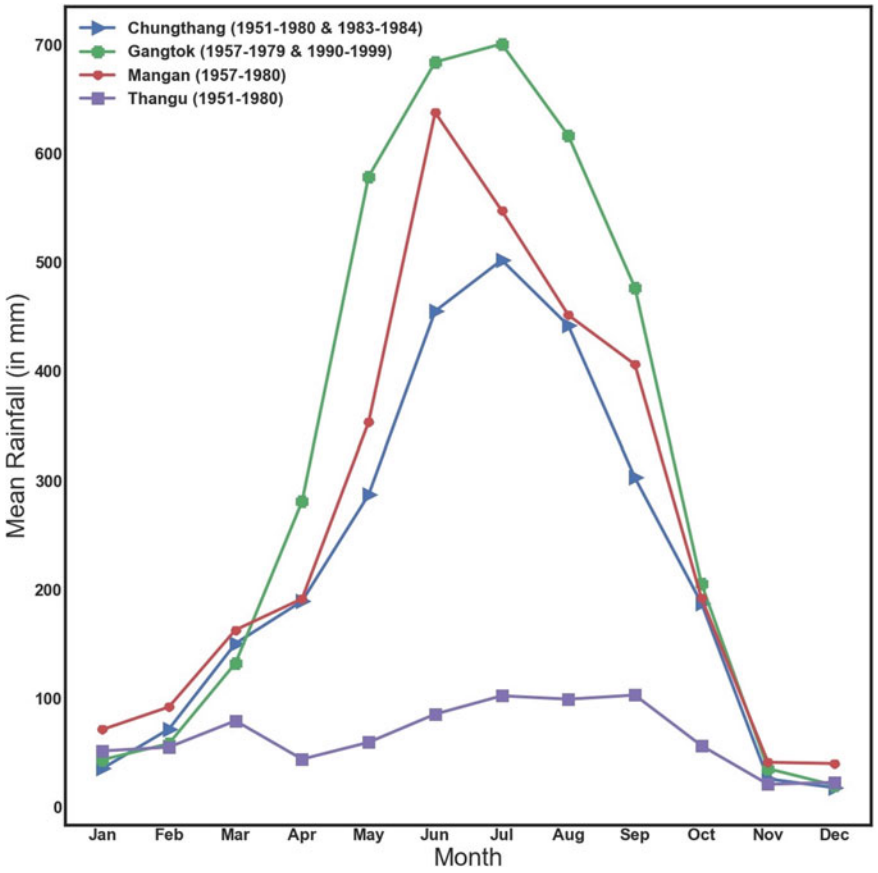

Fig. 2 Mean monthly rainfall of observation stations

Table 2 Descriptive of rainfall in observation stations (in mm)

Descriptive statistics	Season	Chungthang	Gangtok	Mangan	Thangu
First quartile	Annual	2306.8	3428.9	2801.3	596.5
	Wet	1886.3	2920.5	2224.3	395.4
	Dry	350.7	401.9	407.9	162.8
Median	Annual	2585	3641.6	3101.7	753.9
	Wet	2179.5	3092.2	2572.4	496.2
	Dry	446.7	516.5	551	226.1
Third quartile	Annual	2844.5	3928.6	3442.7	858.1
	Wet	2333.1	3292.5	2816.8	610.9
	Dry	560.5	623.7	666.9	288.1
Mean	Annual	2589.2	3726.3	3063.3	783
	Wet	2177.2	3185.8	2589.1	507.5
	Dry	480.1	540.5	582.1	275.6
Std. dev	Annual	918.1	978.8	1570.4	317.3
	Wet	708.1	776	1205.9	169.3
	Dry	200.0	265.7	331.5	206.7

3 Methodology

We have used maximum likelihood estimation to estimate the parameters of the probability distributions and used the number of goodness-of-fit tests, namely χ^2, log-likelihood, Akaike information criterion (AIC), and Bayesian information criteria (BIC) to find the best-fit model. In this section, we discuss in detail the methodology used in this study.

3.1 Maximum Likelihood Estimation (MLE) Method

The maximum likelihood estimation (MLE) method maximizes the function of the parameters in a distribution called the likelihood function. The estimates of distribution parameters are obtained by equating the likelihood function to the condition where it attains a maximum value. The extreme outliers from the samples were excluded. The MLE method was adopted in this study to fit the various probability distributions to the series of data. Samples $y_1, y_2, \ldots, y_N$ are drawn from a population having a continuous random variable Y and probability density function $f\left(y; \theta_1, \ldots, \theta_j\right)$ where $\theta_1, \ldots, \theta_j$ are distribution parameters. For every observed random sample $y_1, y_2, \ldots, y_N$ we define

$$f\left(y_1, \ldots, y_N; \theta_1, \theta_2, \ldots, \theta_j\right) = f\left(y_1; \theta_1, \ldots, \theta_j\right) \times \cdots \times f\left(y_N; \theta_1, \ldots, \theta_j\right).$$

Here $f\left(y;\theta_1,\ldots,\theta_j\right)$ is the probability density function and $f\left(y_1,\ldots,y_N;\theta_1,\ldots,\theta_j\right)$ is the joint density function of the random samples. The joint density function is also the likelihood function and is represented as $L(\theta)$. Likelihood function can be written as

$$L(\theta) = L\left(\theta_1,\ldots,\theta_j\right) = \prod_{i=1}^{N} f\left(y_i;\theta_1,\ldots,\theta_j\right).$$

For a discrete random variable, the likelihood function is the probability of the joint occurrence of $y_1, y_2, \ldots, y_N$. The values of θ that maximizes the likelihood function also maximize the probability density function $f\left(y;\theta_1,\theta_2,\ldots,\theta_j\right)$. The condition for maximum value of $L(\theta)$ is given by

$$\frac{\partial L(\theta)}{\partial \theta} = 0.$$

The solution to this system of equations $\hat{\theta}$ gives the maximum likelihood estimate of the parameter θ. In the maximum likelihood estimation method, the log-likelihood function $ln[L(\theta)]$ is maximized instead of $L(\theta)$. Maximizing the logarithm of a function is equivalent to maximizing the function itself as the logarithm is a continuous and monotonically increasing function. For further details, readers are referred to [10, 11].

3.2 Goodness of Fit Tests

Inferences on probability distribution of population are made based on parameter estimates calculated from small representative samples. The goodness-of-fit test provides a statistical hypothesis on the theoretical probability distribution functions fit to the observed sample points and whether there are any notable differences between theoretical and empirical data points. Nonparametric tests for goodness fit like χ^2, Kolmogorov–Smirnov (KS) and Anderson–Darling (AD) involve testing of hypotheses within confidence limits. χ^2 measures the departure of the observed value from the expected value. KS is based on the maximum difference between the empirical values and expected values of cumulative distributions. AD gives more weightage to the distribution tails where the maximum and minimum values of the sample data points impact the quality of curve fitting. In general, KS and AD check for the normality of data points. The log-likelihood ratio test compares the fit of two models using the maximum values of the likelihood function of the models. Higher the value, better is the fit. The Akaike information criterion (AIC), based on AIC score, is calculated by measuring the model performance of various probability distribution functions for the same samples. The Bayesian information criterion (BIC) is based on the likelihood function and resolves the problem of over-fitting by

introducing a penalty term for the number of parameters in a probability distribution function. The probability distribution with the minimum BIC and AIC score is considered the best fit. For further details, readers are referred to [10, 11]. Parameter estimations of various distributions and the goodness of fit tests mentioned in the article have been performed using the package 'fitdistrplus' in R software [12].

4 Results and Discussions

Mangan, located at the junction of the southeast and southwest quadrants, has a higher mean monthly rainfall than that of Gangtok in the dry season. This may be attributed to its location in the mid hills and the orographic effect on northern winds. Given its high altitude, Thangu experiences orographic precipitation more in the form of snow than rainfall. This can be validated with the observations of rainfall values that are consistently low in both wet and dry seasons (refer Fig. 2 and Table 2).

The two-parameter normal, log-normal, gamma, and Weibull distributions are considered based on the skewness and kurtosis of the sample data points. Figures 3, 4, 5 indicate the Q-Q plots of empirical and theoretical quantiles of the distributions for annual, wet, and dry seasons, respectively. Assessing the best-fit distribution of the data may not be decided based only on the Q-Q plots and hence performing the goodness of fit tests is mandatory.

Four goodness-of-fit tests, namely log-likelihood, AIC, BIC, and chi-square test, are performed on the empirical data, and the results are tabulated in Tables 3, 4, and 5 for annual, dry, and wet seasons, respectively, for each of the four stations. The best-fit probability distribution of the rainfall for annual, dry, and wet seasons in each of the stations can be identified from Tables 3, 4 and 5. The significant values of the goodness-of-fit tests are marked in bold in the table. For example, from the table wet, it is obvious that the best-fit probability distribution of rainfall in Gangtok in wet season is normal distribution with the chi-square p value 0.8886 at 5% significance level.

The same is validated from the value of log-likelihood and the scores of AIC and BIC. For Mangan in wet season, the rainfall may follow log-normal distribution according to the log-likelihood value, AIC and BIC scores, however, it may not follow any of the tested distributions as the Chi-square p values are not statistically significant at 5% significance level.

The best-fit distributions have been listed in Table 6. Rainfall in the wet season is five to six times higher than that in the dry season at Gangtok, Chungthang, and Mangan, and three times more in Thangu. The Weibull distribution seems to fit best for the dry season rainfall and the stations receiving less rainfall. However, the rainfall in Gangtok seems to follow the normal distribution during the dry season. It is also observed that the best-fit distribution of annual rainfall corresponding to each station is same as that of the wet season. For Mangan, the log-normal distribution is chosen as the best fit for annual rainfall over the gamma distribution since the χ^2 p value is

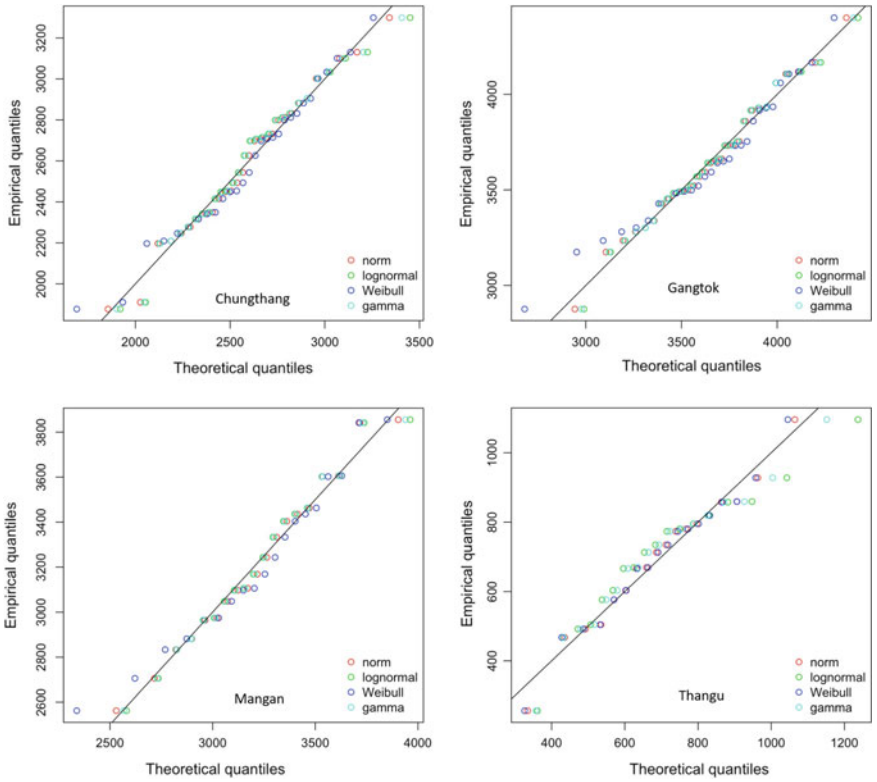

Fig. 3 Relationship between the theoretical and empirical quantiles for annual rainfall

higher and the other listed goodness-of-fit test values are close to that of log-normal distribution.

5 Conclusion

In this study, we have considered rainfall data recorded in four observation stations in Sikkim, three from North district, and one from East district. The influence of altitude on rainfall was observed with stations in the mid and lower hills (Chungthang, Gangtok, and Mangan) receiving more rainfall than the station at higher elevation (Thangu) where precipitation is predominantly in the form of snow. The annual rainfall follows either normal or log-normal distribution in stations located at the mid and lower ranges, and Weibull distribution in stations receiving less rainfall or at higher elevations. The present study has also revealed that probability distribution function is not only different across the various rain gauge stations within the

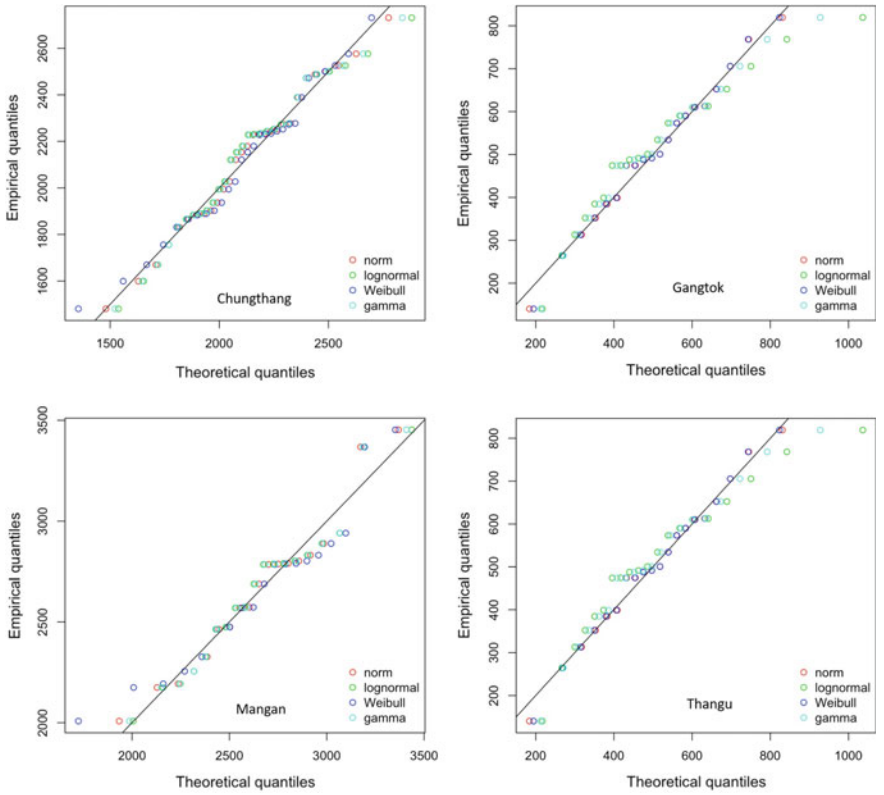

Fig. 4 Relationship between the theoretical and empirical quantiles for wet season rainfall

same basin but also at the same station in different seasons. For example, the rainfall at Mangan follows log-normal distribution during wet season whereas follows Weibull in the dry season. This shows that applying normal statistical rules without identifying the distribution of rainfall may result in misinterpretation and error in analysis. Knowledge of probability distribution will assist climatologists, meteorologists, hydrologists, and ecologists in understanding better the rainfall-dependent events and in subsequent decision making which then can be effectively employed in crop planning, irrigation scheduling, and mitigating the effects of extreme rainfall on the topography.

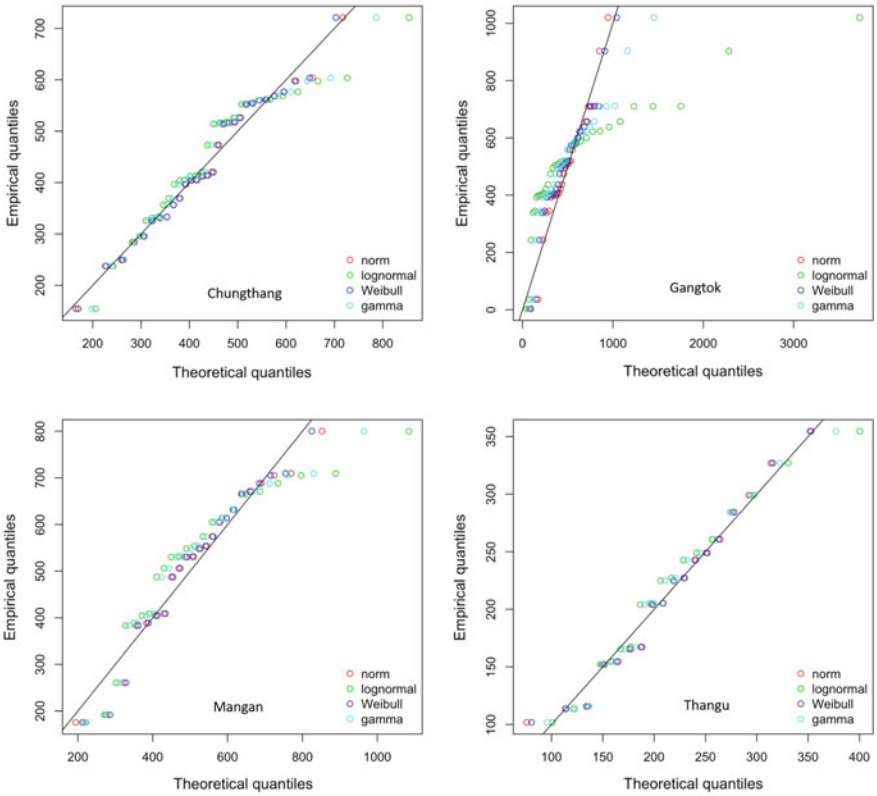

Fig. 5 Relationship between the theoretical and empirical quantiles for dry season rainfall

Table 3 Goodness-of-fit tests for annual rainfall (stationwise)

Station	Distribution	Log-likelihood	AIC	BIC	Chi-square *p* value
Chungthang	Gamma	−211.3631	426.7263	429.4609	0.4447
	Log-normal	−211.5875	427.1750	429.9096	0.4247
	Normal	**−211.1408**	**426.2817**	**429.0162**	**0.4620**
	Weibull	−211.3973	426.7945	429.5291	0.4065
Gangtok	Gamma	−209.8161	423.6321	426.3667	0.7279
	Log-normal	−209.8757	423.7514	426.4860	**0.7467**
	Normal	**−209.8145**	**423.6290**	**426.3636**	0.6796
	Weibull	−211.0884	426.1769	428.9115	0.3120
Mangan	Gamma	**−138.4389**	**280.8778**	**282.7667**	**0.7192**
	Log-normal	−138.4551	280.9102	282.7990	**0.7312**
	Normal	−138.4933	280.9865	282.8754	0.6832
	Weibull	−139.1217	282.2434	284.1323	0.4913
Thangu	Gamma	−121.1682	246.3364	248.1172	0.7062
	Log-normal	−122.2044	248.4088	250.1896	0.5632
	Normal	−120.0523	244.1045	245.8853	0.8621
	Weibull	**−119.9629**	**243.9258**	**245.7066**	**0.8935**

Table 4 Goodness-of-fit tests for dry season rainfall (stationwise)

Station	Distribution	Log-likelihood	AIC	BIC	Chi-square *p* value
Chungthang	Gamma	−189.6061	383.2122	386.0146	**0.0815**
	Log-normal	−190.8556	385.7111	388.5135	0.0704
	Normal	−188.5400	381.0800	383.8824	0.0730
	Weibull	**−188.2477**	**380.4954**	**383.2978**	0.0693
Gangtok	Gamma	−226.0649	456.1298	459.0613	0.0008
	Log-normal	−238.6465	481.2929	484.2244	0.0000
	Normal	**−215.3029**	**434.6059**	**437.5373**	**0.2901**
	Weibull	−220.8021	445.6041	448.5356	0.0644
Mangan	Gamma	−151.9315	307.8631	310.1341	0.3820
	Log-normal	−153.6466	311.2931	313.5641	0.1716
	Normal	−149.7748	303.5497	305.8207	0.8453
	Weibull	**−149.4195**	**302.8390**	**305.1100**	**0.9104**
Thangu	Gamma	−102.3295	208.659	210.4397	0.3933
	Log-normal	−102.5995	209.199	210.9798	0.2638
	Normal	−102.5562	209.1124	210.8932	0.6665
	Weibull	**−102.2912**	**208.5823**	**210.3631**	**0.6981**

Table 5 Goodness-of-fit tests for wet season rainfall (stationwise)

Station	Distribution	Log-likelihood	AIC	BIC	Chi-square *p* value
Chungthang	Gamma	−207.4741	418.9482	421.6828	0.0035
	Log-normal	−207.7508	419.5016	422.2361	0.0029
	Normal	**−207.1689**	**418.3378**	**421.0724**	0.0047
	Weibull	−207.2032	418.4064	421.1410	0.0054
Gangtok	Gamma	−203.2689	410.5379	413.2725	0.8629
	Log-normal	−203.5280	411.0559	413.7905	0.8433
	Normal	**−202.8809**	**409.7619**	**412.4965**	**0.8886**
	Weibull	−203.1738	410.3475	413.0821	0.7708
Mangan	Gamma	−139.0731	282.1461	284.0350	0.0377
	Log-normal	**−139.0313**	**282.0626**	**283.9515**	0.0318
	Normal	−139.3142	282.6285	284.5174	0.0495
	Weibull	−140.3603	284.7206	286.6095	0.0415
Thangu	Gamma	−131.8123	267.6246	269.6161	0.8196
	Log-normal	−133.2340	270.4679	272.4594	0.7179
	Normal	−130.5003	265.0006	266.9921	0.8646
	Weibull	**−130.4424**	**264.8848**	**266.8762**	**0.8718**

Table 6 Best-fit distribution for observation stations

Station	Annual	Dry season	Wet season
Chungthang	Normal	Weibull	Normal
Gangtok	Normal	Normal	Normal
Mangan	Log-normal	Weibull	Log-normal
Thangu	Weibull	Weibull	Weibull

References

1. Directorate of Census Operations, Sikkim: District census handbook, series 12, part XII-B, Census of India 2011
2. CISHME (2006) Carrying capacity study of Teesta basin in Sikkim: Volume IV Water Environment, Ministry of Environment & Forests, Government of India
3. Tambe S, Kharel G, Arrawatia ML, Kulkarni H, Mahamuni K, Ganeriwala AK (2012) Reviving dying springs: climate change adaptation experiments from the Sikkim Himalaya. Mt Res Dev 32(1):62–72. https://doi.org/10.1659/MRD-JOURNAL-D-11-00079.1
4. Mahendra. P (2001) Lama: Sikkim human development report. Technical report Government of Sikkim & Social Science Press, Delhi
5. Department of Science & Technology and Climate Change (2014) The Sikkim state action plan on climate change, Government of Sikkim
6. Markovic RD (1965) Probability functions of best fit to distributions of annual precipitation and runoff. Hydrology papers (Colorado State University), no 8
7. Chow VT, Maidment D, Mays L (2010) Applied hydrology. McGraw-Hill series in water resources and environmental engineering. Tata McGraw-Hill Education

8. Hosking JRM (1990) L-moments: analysis and estimation of distributions using linear combinations of order statistics. J R Stat Soc Ser B (Methodol) **52**(1):105–124
9. Yue S, Hashino M (2007) Probability distribution of annual, seasonal and monthly precipitation in Japan. Hydrol Sci J 52(5):863–877. https://doi.org/10.1623/hysj.52.5.863
10. Hosmer Jr DW, Lemeshow S, Sturdivant RX (2013) Applied logistic regression, vol 398. John Wiley & Sons
11. Naghettini M (2016) Fundamentals of statistical hydrology. Springer International Publishing
12. Delignette-Muller ML, Dutang C (2015) fitdistrplus: an R package for fitting distributions. J Stat Softw 64(4):1–34. http://www.jstatsoft.org/v64/i04/

Hydro-informatics and Geospatial Modelling

Suitable Locations of Ocean Renewable Energy in Coastal Indian State—Kerala

D. Ghose, S. Naskar, and Shabbiruddin

Abstract India, a diverse nation, is filled with variegate natural resources, most of which can be utilized for the production of energy, and in many cases, acting as an appropriate substitute to the pollution causing conventional power sources. Being largely a peninsula, India has a huge coastline facing the open ocean, representing a vast renewable energy source in the form of ocean currents, tidal energy, ocean winds, and wave energy, which can be utilized to account for an additional economical and eco-friendly energy reserve for the nation. This paper spatially explores Kerala, a state in India, having nearly 580 km of coastline in the Arabian Sea, using a Quantum Geographic Information System (Q-GIS)-based analysis, to gist out the areas available for generation of various forms of ocean renewable energy. Among the considered beaches, three beaches: Bekal, Kozhikode, and Cherai is found to be suitable for both wind and wave energy, while the other beaches adhere to either wind or wave energy. It is also concluded that ocean currents can be used as an energy source throughout the coastline of Kerala. Such an approach can also be applied to researches of similar nature, benefitting industries who are dealing with the same genre of development.

Keywords Q-GIS · Renewable energy · Ocean renewable energy · Tidal energy · Wind energy · Spatial analysis

D. Ghose (✉) · S. Naskar · Shabbiruddin
Department of Electrical and Electronics Engineering, Sikkim Manipal Institute of Technology, Sikkim Manipal University, Sikkim, India
e-mail: ghosedipanjan1998@gmail.com

S. Naskar
e-mail: sreejitanaskar1998@gmail.com

Shabbiruddin
e-mail: shabbiruddin85@yahoo.com

C. Bhuiyan et al. (eds.), *Water Security and Sustainability*,
Lecture Notes in Civil Engineering 115,
https://doi.org/10.1007/978-981-15-9805-0_8

1 Introduction

Kerala, having an area of over 38,863 km^2, is a state on the Malabar Coast in south-western India [1]. Kerala is land logged on its Northern, Southern, and North-eastern sides and has the Arabian Sea and the Lakshadweep Sea to its West [1]. The coastline of Kerala runs an approximate of 580 km in length along the seas. The long sea-facing coastline along the state provides opportunities for utilization of the energy of the ocean in various ways, particularly as a source of renewable energy. Oceans, covering vast areas of the Earth's surface, absorb most of the radiations from the sun and are established to be one of the largest reservoirs of energy [2]. They act as carbon-dioxide free, eco-friendly, vast renewable energy reserves [3]. Energy from the ocean can be in the form of wave energy, tidal energy, ocean currents, ocean winds, and ocean thermal energy. While tidal energy involves the conversion of the energy of tides by storing and controlling the release of water to pass through turbine generators producing electricity [4], wave energy is fundamentally the energy possessed by winds, created in the mid-latitude regions of the Earth under influence of heat from the Sun and Earth's rotation [5]. The capacity of the energy that can be generated from ocean resources is tremendous [6], as shown in Table 1. The units are in TWh, which refers to Tera-Watt hours per day.

According to the Ministry of New and Renewable Energy under the Government of India, the total tidal energy potential which has been recognized within the Indian peninsula is over 17,200 MW, while the total potential for energy generation from wave energy is preliminarily about 40,000 MW along the 6000 km long coastline of India [7]. Despite having given assurances to provide financial aids for 50% project costs in Feb 2011, the initiative that has been taken up by the ministry is largely questionable [7]. Though Ocean Thermal Energy Conversion (OTEC) has at present installed capacity of 180,000 MW in India [7], the other genres of utilizing ocean power as a renewable subject remains largely unexplored.

The total energy generation from conventional energy sources like coal, oil, and natural gas has been on the constant increase in India from 771.551 Billion Units (BU) in the year 2009–10 to 1160.141 BU in 2016–17 and 1206.306 BU in 2017–18 periods [8], despite there being rising concerns about carbon dioxide and global warming associated with the uncontrolled usage of fossil fuels [9]. The energy drawn from renewable energy sources (RES) here stands at only around 72,013 MW out of the total installed capacity of power at 346,048 MW [8]. Renewable energy sources, too, comprise only small hydro projects, biomass projects, industrial waste projects, and solar and wind projects in India [8]. Ocean renewable energy sources, despite

Table 1 Ocean energy world potential

S. No.	Energy type	Estimated global potential
1.	Energy from ocean currents	More than 800 TWh
2.	Energy from ocean waves	Around 8000–80,000 TWh
3.	Energy from ocean tides	More than 300 Wh

their immense capacity, remain unused within the country. Once this genre of energy is explored by the government, it would also fill up various deficits that the power distribution system in the country faces (a total power deficit of 8567 million units occurred during 2017–18 itself [8]). Thus, investments by the government in this renewable form of energy will act as an added benefit to the power distribution system of India.

A GIS-based approach to handle data involving spatial or land analysis has proven to be an efficient means in the field of research. From finding the location of solar photovoltaic and concentrated solar power plants near Murcia city, Spain [10, 11], identifying suitable solar sites in the Central Anatolia region of Turkey [12], to GIS-based analysis to search for the optimum sites for the location of electrical substation [13], or routing of transmission lines [14] and site location suitability for ocean renewable energy in Indonesia [15], the instances for the same are numerous.

In this study, the authors thoroughly examine the coastline of Kerala using a GIS-based approach, classifying the coasts based on the different forms of ocean's renewable energy, namely energy from ocean currents, wave energy, wind energy, and tidal energy, that can be extracted from them. The analysis is done by assessing the available physical data for the seashores and comparing them with predefined minimal values for extraction of that particular energy based on previous research in that genre and then concluding the optimal energy system that can be invested in for a particular beach of Kerala. This has further been explained under the '*Methodology*' section of the paper. The sample calculation for Kovalam beach within the state was taken up to show the real-time formulation of data values.

2 Methodology

As already explained, a GIS-based analysis is a proven mechanism to handle any case involving variations or calculations with spatial data. Open-source software, Q-GIS, has been used to sort out the collected geographical data into its computable forms. For the establishment of an ocean renewable energy plant, the following sources have been taken into consideration: ocean currents, the height of waves, ocean wind energy, and ocean tides. The data was collected over a year, and then it was filtered out to remove unreliable data values. Mean value and standard deviation methods were used to get the data used for calculation. Suitable assumptions were also made in cases where it could be pertained by checking previous or neighboring locational data.

For the calculation, ten major beaches were taken along the coastline of Kerala, namely the beaches of Bekal, Payyambalam, Kappad, Kozhikode, Beypore, Cherai, Alappuzha, Thirumullavaram, Varkala, and Kovalam. The collected data for the mentioned beaches were then implemented on a Q-GIS interface, to get to a conclusion. The beaches considered for calculation have been shown in Fig. 1.

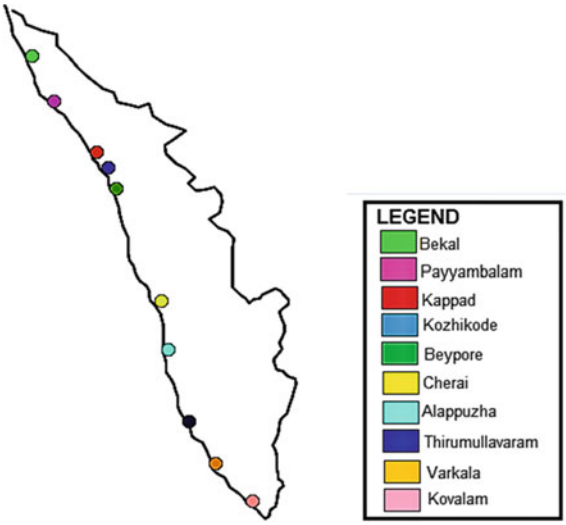

Fig. 1 Beaches of Kerala considered for calculation (plotted using Q-GIS)

2.1 Mechanism of Mapping

A GIS-based approach has been implemented to sort out the collected data accordingly. For each of the considered four parameters, certain minimum values were taken such that the parameter could be considered as a potential source of energy [15]. These minimum values have been taken after studying apposite literature for the same, especially Purba et al. on the coasts of Indonesia in 2015 [15]. The minimum factors are further enlisted in a tabular form for ease of observation as shown in Table 2.

Figure 2 illustrates the major ocean currents in the Arabian Sea around Kerala's coastline. The major currents are the Arabian Current with a speed of 7 knots and the Indian Equatorial current with a speed of 5 knots (Conversion: 1 knot = 0.514 ms^{-1}). Figure 3 shows the speed of winds along the considered ten beaches, while Fig. 4 is a map of the height of the waves of the ocean along the Kerala coastline. Figure 5 denotes the height of the tidal range in the considered beaches of Kerala. All the maps and figures have been extracted using Q-GIS.

Table 2 Minimum values for sources taken for ocean renewable energy

S. No.	Source of ocean energy used	Minimum value considered [15–19]
1.	Energy from ocean currents	0.5 ms^{-1}
2.	Speed of ocean winds	4.0 ms^{-1}
3.	Height of the waves	1.6 m
4.	Range of ocean tides	2.0 m

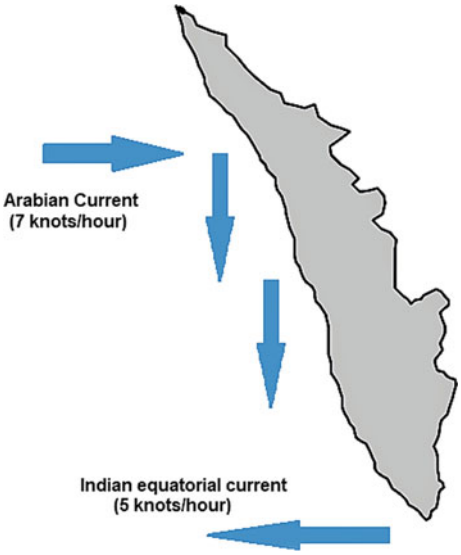

Fig. 2 Ocean currents in Kerala (plotted using Q-GIS)

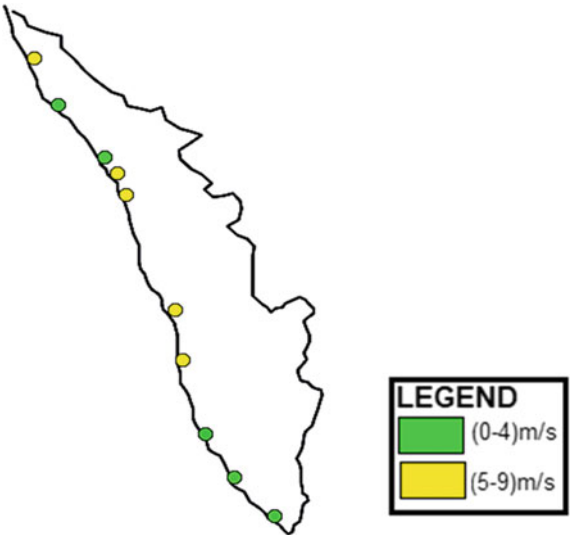

Fig. 3 Kerala wind speed (plotted using Q-GIS)

The data and information to obtain the maps using a Q-GIS-based interface were collected from ESSO—Indian National Center for Ocean Information Services, an Autonomous body under the Ministry of Earth Sciences, Government of India and the Tamil Nadu region of the Indian Ocean Forecast System (INDOFOS).

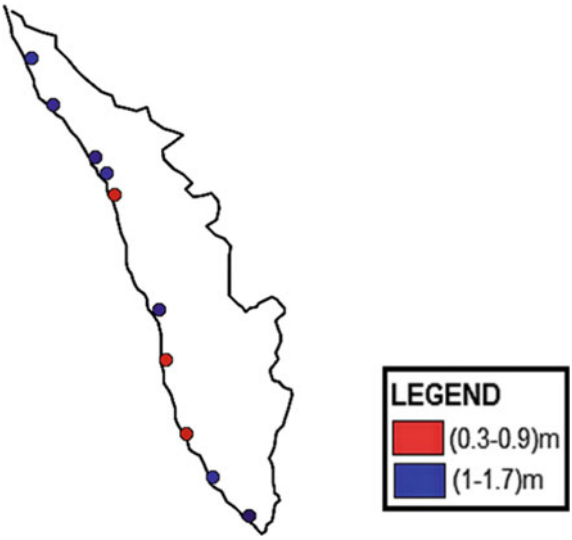

Fig. 4 Height of waves in Kerala (plotted using Q-GIS)

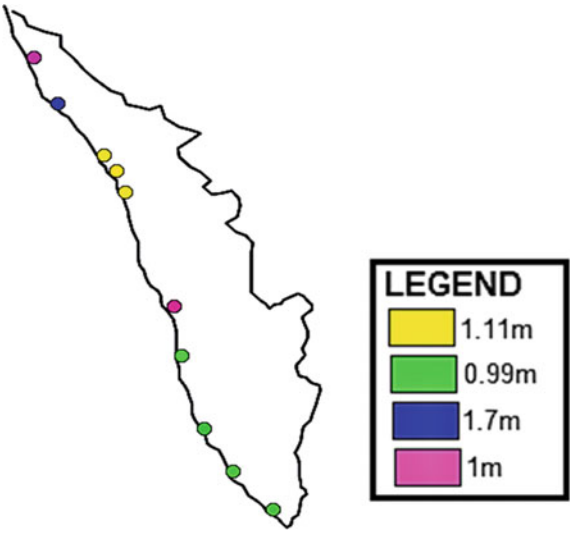

Fig. 5 Tidal height range in Kerala (plotted using Q-GIS

2.2 Assessment of the Expected Converted Energy

Common conversions of energy procedures in case of ocean renewable energy make use of certain formulae. Similar formulae were used to give an approximate estimation of the total energy which could be obtained from the considered sources. Each of the sources has different variables to get the energy from oceans and also

the dimensions of the turbines of the generators used for conversion of energy could also be largely varied.

Energy from Ocean Currents: Flow of ocean currents, adjudged to be in a relatively constant flow, comprises displacement of large amounts of ocean water, which generally pretty complexly get affected by wind flow, salinity of ocean water, temperature differences, and topography of the floor of the ocean among numerous other factors [20]. This energy is being targeted to be extracted and converted to useful power for consumption. This conversion can be estimated using the Fraenkel equation which can be shown as [15, 16]:

$$P = 0.5 \times D \times v^3 \times n \tag{1}$$

where P = net power that can be extracted, D = density of water, v = velocity of ocean current. n = coefficient (efficiency) of the generator. All the factors considered should be in Standard International (SI) units.

Energy from Ocean Winds: Wind is already a pretty established source of renewable energy and finds its sources in many places as a trusted power source [21]. Wind energy is highly dependent on factors like speed of the find, the density of the air at that point, the length of the blade used for wind energy conversion among many others [15]. The power estimation of obtained energy from wind power can be related using the following formula [17]:

$$P = 0.5 \times D \times R^2 \times \pi \times v^3 \tag{2}$$

where P = power which can be extracted from the winds, D = density of air, R = length of blade used for obtaining wind energy, v = velocity of the wind. All considered factors are in SI units.

Energy from Ocean Waves: Waves are known to be reservoirs of both kinetic as well as gravitational potential energy, and the total of the carried energy by the wave being dependent on its height (H) and its time-period (T) [15]. The average wave period was considered as 5 s. The obtained equation from the general equation of wave-train energy to facilitate the conversion of wave energy as potential power sources can be demonstrated as hereunder:

$$E(\text{kW/m}^2) = c \times H^2 \times T \tag{3}$$

where E = energy that can be extracted from ocean waves, c = a constant value given by $Dg^2/4\pi$ (where 'g' is the acceleration due to gravity, and the constant can be calculated as approximately 7.87 kW m^{-3} s^{-1}), H = height of the waves, T = time-period of the waves. All considered factors are in SI units.

Energy from Ocean Tides: Though tidal energy is not a widely used source of energy yet, ocean tides are known to have huge potential to be used as a power source. The tidal energy can be approximately calculated using the formula:

$$E = A'mgI \int (dH/T) \quad \text{the integration is performed using 0 as the lower limit and '}H\text{' as the upper limit.} \tag{4}$$

where E = energy obtained from the ocean tides, A' = surface area of the ocean basin in m^2, g = acceleration due to gravity, H = range of the tides, m = mass of seawater. All considered factors are in SI units.

Sample Calculation

Though this study is largely a derivative research, the methodology applied can be put into an account for superficial or theoretical analysis of the beaches in Kerala based on the energy that can be harnessed from them. For instance, a particular scenario can be taken into account as hereunder:

Beach considered: Kovalam Beach
Energy types which can be harvested: Ocean current energy, wind energy, wave energy

For calculating an estimate of the amount of energy which can be drawn from the ocean currents in the Kovalam beach, the following values were taken: Density of water as 1.025 kg m^{-3}, speed of the current (Arabian current) as 3.6011 m s^{-1}, and the general efficiency of the generator as 79.07%. Putting these values in the Fraenkel equation, denoted as Eq. (1), we obtain the power which can be drawn as:

$$P = 0.5 \times 1.025 \times (3.601)^3 \times 79.07 = 0.002 \text{ MW}$$

Quite similarly, the amount of energy which can be extracted in the form of wind energy at this beach can be calculated, taking the density of air as 1.225 kg m^{-3}, length of the blade of windmills as 15.6 m, based on Enercon E-33 and the velocity of winds as 4 m s^{-1}. Putting these values in Eq. (2), the estimated output from wind energy harvesting at the Kovalam beach will be:

$$P = 0.5 \times 1.225 \times (15.6)^2 \times \pi \times 4^3 = 0.029 \text{ MW}$$

An observable amount of increase can be noticed if the ocean renewable energy is extracted in the form of wind energy. This is because of higher and more optimized speeds of winds as compared to the speed of ocean currents. Again, considering the energy of waves as a source of renewable energy, we make the assumptions as, c = constant given as 7.87 kW m^{-3} s^{-1}, the height of waves as 1.7 m, and the average time-period of the waves as 5 s. Then, the extractable amount of energy from the waves after putting the values in Eq. (3) will be:

$$P = c \times 1.7^2 \times 5 = 0.114 \text{ MW}$$

The height of the ocean tides, however, is not appropriate enough for the extraction of tidal energy throughout the coastline of the state of Kerala, and hence, tidal energy

cannot be harvested in the Kovalam Beach area as well. If there is a similar data collection for all the beaches along the Kerala coastline, the estimated power which can be obtained can be calculated for each of the beaches for each source of ocean renewable energy.

However, extraction of data for each beach demands an exquisite and extensive study of the coastline areas, which is quite beyond the scope of this paper. As obtained from the results wave energy, if it can be harvested, then it will prove to be the most profitable among the ocean energy resources. This is basically due to favorable wave heights in the ocean along the beaches of Kerala, as opposed to the current energy, which is fairly lesser in amount because of the slower speeds of the Arabian and Equatorial currents along the Malabar Coast in India.

3 Results and Discussions

Currents in the ocean, ocean tides, wind energy, and energy in the form of wave energy are the main realms of ocean renewable energy. To utilize each of those energy realms, a different approach of energy production is used, unique to that form of energy, not only for Kerala but for any other part of the world as well. The areas which were found suitable for investment in ocean renewable energy sources have been demonstrated in Fig. 6. The figure has been extracted using Q-GIS. As evident from the resultant map, three beaches: Bekal, Kozhikode, and Cherai were found

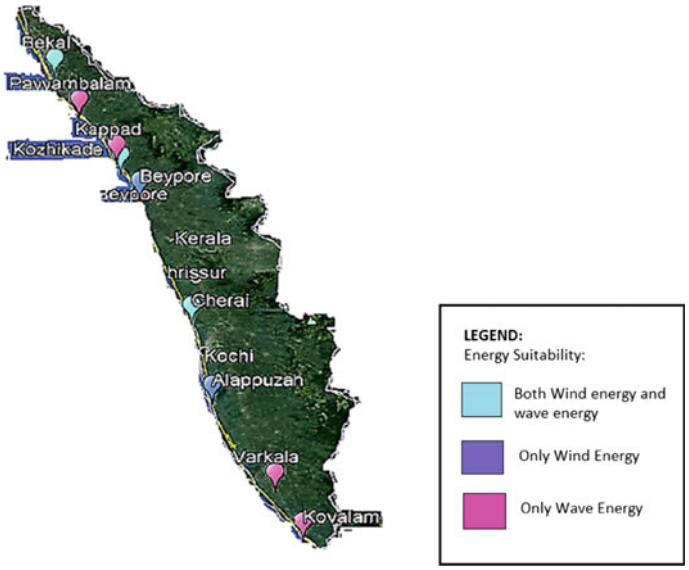

Fig. 6 Resultant map showing suitability for installation of ocean renewable energy plants in Kerala (plotted using Q-GIS)

suitable to harvest both wind energy as well as wave energy, while Payyambalam, Kappad, Varkala and Kovalam were found to be suited just for ocean wind energy. Beypore and Alappuzha beaches were found to be suitable sources of wave energy from the ocean.

Kerala is affected by two major ocean currents, the Arabian Current and the Indian Equatorial Current. While the Arabian Current has a speed of around 7 knots, the Equatorial Current has an average speed of above 3 knots; both of which are much greater than the minimum considered current value of around 0.5 ms^1. Hence, it brings us to an easy conclusion that the entire shoreline of Kerala which confronts the aforementioned currents can be considered to harness energy from ocean currents. The tidal range of all the Kerala beaches however was found to touch a maximum of 1.11 m, which is way below the prescribed and considered a minimum of 2 m. As a result of this, harnessing tidal energy along the Keralian shoreline could be considered a less profitable and less efficient investment, and if the other sources are catered properly, it can even be avoided.

Minimum current speeds of 0.5 m/s, minimum wind speeds of 4 m/s, a minimum wave height of 1.6 m, and a minimum tidal range of 2 m was considered; all the values having been obtained from previous works in this genre [15–19]. Equations (1), (2), (3) and (4) can be utilized after having obtained the required values prescribed in the mentioned equations to get a rough estimation of the total power that may be expectantly extracted from each of the respective ocean energy source being taken into consideration.

Strong winds of even speeds reaching as high as 9 m/s are not unusual in Kerala. Kerala is known to face a general trend of very high wind speeds, resulting due to which, energy from the ocean winds is an important aspect when considering the ocean renewable energy chapter. Though the second most likely genre to invest in the ocean energy sector in Kerala is seemingly wave energy, obtaining the energy of waves as a source of useful power is a difficult task. Lack of research and implementation in the real world adds up to the difficulties faced. Besides, the unpredictable nature of the oceans and the shortfall in very long-term data about the height of waves are also major hindrances faced while considering wave energy as a source of power. Even to date, there are limitations to the availability of data even from existing wave farms. Thus, in general, the harnessing of wave energy gains importance once we consider the prospects associated with ocean renewable energy. Ocean currents though are generally a more available and accessible energy form and can be put to utilization in an easier approach.

In general, oceans are known for their unpredictable nature. Collection and especially reliability and regular availability of data are big questions in this matter. However, the fact that oceans are tremendous sources of energy which, if once implemented in a manner beneficial to mankind could act as a solution to numerous issues faced today, is unquestionable. But the real implementation of the ocean as an energy resource and detailing of procedures as to how to harness this form of energy is beyond the scope of this study. This study simply projects the areas under consideration as prospected sources of the four main genres of ocean renewable energy: energy from ocean currents, energy from ocean winds, the energy of ocean tides, and energy of

ocean waves. Similar such an approach can also be implemented in any study of the same nature.

4 Conclusion

Out of most of the forms of energy, for example, solar energy, wind energy, biomass energy, and so on, the energy obtained from oceans is one of the least harnessed energy forms despite its enormous availability and reduced environmental impact. This study evaluates the state of Kerala in India as a vital source for ocean renewable energy, especially in its four genera forms: Current energy, wind energy, tidal energy, and wave energy. As has been often cited, many times a sheer lack of research in harnessing ocean resources as a form of energy bars it from entering the conventional renewable energy genre in our country. Usage of GIS-based interfaces to take into account geospatial data for such observational research further add up to the accuracy of the obtained solution for a particular scenario. The government of the country on many grounds has invested in the common renewable energy systems like solar, wind, and hydropower. However, many incentives by the authorities taken to introduce newer energy sources into the system stand as witness to their interest in exploring new varieties in this genre. Except for tidal energy, a form of energy that has yet to find a place in the Indian power market, the study proved Kerala to be a storehouse of all other variations of ocean energy, making it quite an energy goldmine when referring in terms of ocean's renewable energy. The study, despite many grounds being merely superficial and theoretical owing to the constrictions in its scope, hopes to provoke the concerned authorities to bring in applications of this diverse form of ocean energy for the state of Kerala and such coastline states alike into its ecosystem.

References

1. Article: Kerala. www.wikipedia.org/Kerala
2. Article: Ocean Energy. www.renewableenergyworld.com/ocean-energy/tech.html
3. Boehlert GW, Gill AB (2010) Environmental and ecological effects of ocean renewable energy development. Oceanography 23(2):68–81
4. Andre H (1978) Ten years of experience at the "La Rance" tidal power plant. Ocean Manage 4(2–4):165–178
5. Gill AE (1982) Atmosphere-ocean dynamics. Academic Press, London
6. Report: Implementing agreement on ocean energy systems (IEA-OES). Annual report 2007. International Energy Agency, Jochen Bard ISET, p 5
7. Ministry of New and Renewable Energy, Government of India web portal. www.mnre.gov.in/ocean-energy
8. Article: Power Sector at a glance ALL INDIA, Ministry of Power, Government of India. www.powermin.nic.in
9. Sharma RC, Sharma N (2013) Energy from the ocean and scope of its utilization in India. Int J Environ Eng Manage 4(13):397–404

10. Sanchez-Lozano JM, García-Cascales MS, Lamata MT (2015) Evaluation of suitable locations for the installation of solar thermoelectric power plants. Comput Ind Eng 87:343–355
11. Sanchez-Lozano JM, Teruel-Solano J, Soto-Elvira PL, García-Cascales M (2013) Geographical information systems (GIS) and multi-criteria decision making (MCDM) methods for the evaluation of solar farms locations: case study in south-eastern Spain. Renew Sustain Energy Rev 24:544–556
12. Uyan M (2013) GIS-based solar farms site selection using analytic hierarchy process (AHP) in Karapinar region, Konya/Turkey. Renew Sustain Energy Rev 28:11–17
13. Shabbiruddin, Ray A, Sherpa KS, Chakravorty S (2013) Evaluation of substation location using geographical information system: a case study. Elixir Int J Elixir Electr Eng 62:17464–17468
14. Shabbiruddin, Sherpa KS, Chakravorty S, Ray A (2017) Transmission line routing using open source software Q-GIS. Int J Open Source Softw Process 8(4):71–82, Article 4
15. Purba NP, Kelvin J, Sandro R, Gibran S, Permata RAI, Maulida F, Matrasuganda MK (2015) Suitable Locations of Ocean Renewable Energy (ORE) in Indonesia region—GIS approached. Energy Procedia 65:230–238
16. Yuningsih A, Sudjono EH, Rachmat B, Lubis S (2010) Prospek energi laut [Ocean current energy prospect]. ESDM, Report. Bahasa, Indonesia
17. Khaligh A, Onar OC (2009) Energy harvesting: solar, wind, and ocean energy conversion systems. Energy, power electronics, and machines series. CRC Press, Florida, pp 105–111
18. Cruz J (2008) Ocean wave energy: current status and future perspectives. Springer, Heidelberg, pp 220–241
19. Charlier RH, Finkl CW (2009) Ocean energy: tide and tidal power. Springer, Berlin, pp 38–39
20. Article: Ocean Current Energy, Bureau of Ocean Energy Management. www.boem.gov/Ocean-Current-Energy/
21. Blaabjerg F, Ma K (2017) Wind energy systems. Proc IEEE 105(11)

Study of Temporal Behaviour of Homogeneity Maps for Estimating Representative Area of a Ground Sample Using Remote Sensing

Prasad J. Deshpande, Anudeep Sure, Onkar Dikshit, and Shivam Tripathi

Abstract Modelling and prediction of hydro-meteorological variables over land and atmosphere involve ground sampling at selected locations over the study area. Optimally selecting the number and location of sampling points is important for making reliable predictions without escalating project costs. This study proposes an approach for selecting sampling locations by considering inter-dependency of predictor variables and the prediction variable using remote sensing data. A homogeneity map, i.e., a thematic map representing areas with the same expected value of the prediction variable, with a given level of uncertainty and spatial resolution, is generated. The homogeneity maps can be different at different times for the same location. Thus, along with the spatial variability of the prediction variable, its temporal variability is also obtained. Depending on the obtained variability, a decision on the number and location of sampling points can be taken prudently. In this paper, the proposed methodology is demonstrated by considering soil moisture over an experimental watershed as the prediction variable.

Keywords Hydro-meteorological variable · Regionalisation · Spatio-temporal clustering · Heterogeneity · Google Earth Engine

1 Introduction

Prediction of hydro-meteorological variables is the process of estimating the variable at unsampled locations by using observations at a few sampling locations. Hydro-meteorological variables change their value spatially and temporally, and hence, the selection of sampling locations is difficult. This paper proposes to use remotely sensed variables that are related to prediction variable (i.e., auxiliary variables) for selecting sampling locations. These auxiliary variables are used to find a representative area for each sample location. The representative area of a sample is the area surrounding the sample having similar value as the sample. The representative area

P. J. Deshpande (✉) · A. Sure · O. Dikshit · S. Tripathi
Department of Civil Engineering, Indian Institute of Technology Kanpur, Kanpur, India
e-mail: prasadj@iitk.ac.in

C. Bhuiyan et al. (eds.), *Water Security and Sustainability*,
Lecture Notes in Civil Engineering 115,
https://doi.org/10.1007/978-981-15-9805-0_9

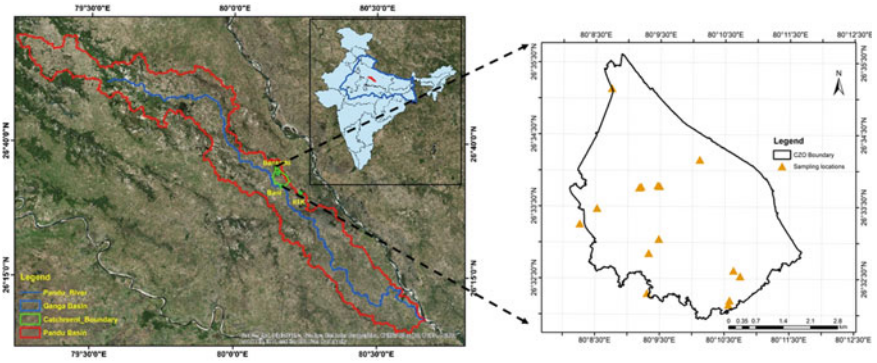

Fig. 1 Study area, HEART CZO, and the location of soil moisture senors in it [2]

may not have the exact same value as the sample, but it is within a certain pre-specified uncertainty level. The decision on the number of samples for a given study area is a challenging task, and the framework proposed in this paper helps to tackle this problem.

The objective of this work is to understand the temporal behaviour of soil moisture, using monthly homogeneity maps of soil moisture, for a Critical Zone Observatory (CZO), in the Ganga basin, India. These maps are compared with the temporally averaged homogeneity map [1]. This objective also includes the determination of the improved sampling locations and their representative area.

2 Study Area and Input Dataset

The proposed framework was applied on the bounding box enclosing the study area, Heterogeneous Ecosystem of an Agri-Rural Terrain (HEART)-CZO. The CZO is a small watershed (21 km^2; 80°8′0″E-80°11′0″E and 26°31′43.93″N 26°-36′14.85″N) of the basin of Pandu river, a tributary of the River Ganges, India (Fig. 1). This study area is selected, because it has a network of 15 in situ soil moisture measurement sites [2]. The in situ data are available from Aug 2017 to Oct 2018, i.e., for 15 months, and hence, the analysis is carried out for the same period. The remote sensing data for selected auxiliary variables [1] are described in Table 1.

3 Methodology

The methodology includes pre-processing followed by entropy-based discretization and clustering that leads to the formation of homogeneity maps [1]. The stepwise procedure is explained using a flow chart (Fig. 2).

Table 1 Details of remote sensing datasets used in the study

S. No.	Product	Spatial resolution	Temporal resolution	Min value in study area	Max value in study area	Unit
1.	SRTM DEM	30 m	Static	120	143	m
2.	LAI MODIS	500 m	4 day	0.0000	1.3118	m^2/m^2
3.	NDVI MODIS	250 m	16 day	0.2527	0.5515	
4.	Evapotranspiration	1000 m	8 day	0.0000	16.0167	kg/m^2
5.	Soil moisture SMAP	0.25 arc degrees	3 day	11.3784	11.3784	%
6.	Rainfall TRMM	0.25 arc degrees	1 Month	0.1040	0.1040	mm/hr

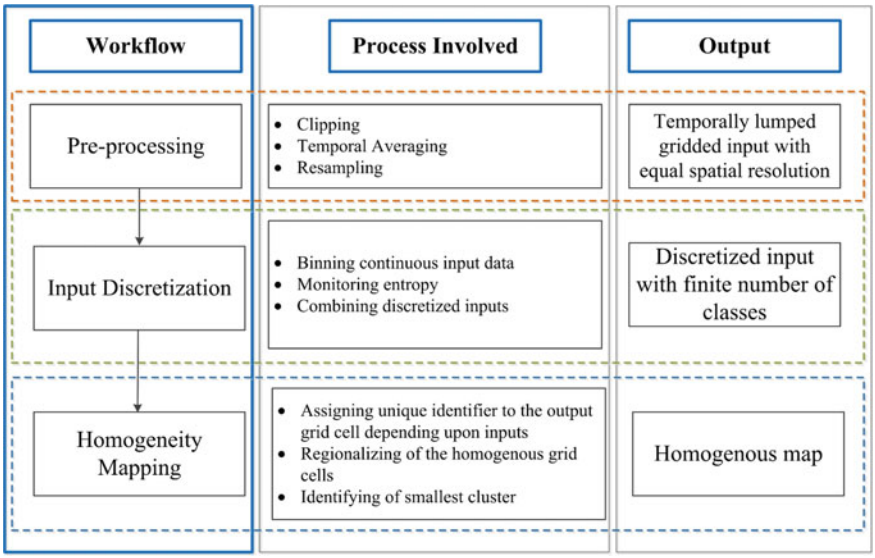

Fig. 2 A flow chart showing the proposed methodology for generating homogeneity maps

The proposed procedure is applied at a monthly time scale on the satellite data available for 15 months to generate monthly homogeneity maps. The homogeneity maps thus generated are further used for detection of suitable number of samples and sampling locations. The implementation of the framework is carried out in the Google Earth Engine [3] and Scikit-learn libraries [4] in Python3 language.

4 Results and Discussion

The monthly homogeneity maps are presented in the Fig. 3. A temporally averaged map for the study period is also provided at the end for comparison. The threshold value [1] is set as 10%.

The homogeneity maps for different months show homogeneous areas for different months. Same cluster ID belongs to same prediction variable, i.e., soil moisture. These clusters, i.e., homogeneous areas, are spread in different locations, i.e., the prediction variables may be same for different locations. Moreover, across the different months, it is observed that some of the clusters are changing while some are not changing for the same location. The clusters which are not changing across the months are the locations where we do not expect much temporal as well as spatial variablity. On the other hand, in the clusters which are changing across the months, a higher temporal variability is observed. The locations of less variability requires lesser samples as compared to the locations of higher variability. In the areas with higher variability, more samples (in terms of frequency and spatial distribution) are needed for a good representation. Finally, the temporally lumped map has more clusters as the accumulated variability over the time increases leading to generation of more clusters, i.e., homogeneous areas.

5 Conclusion

The homogeneity maps generated at a monthly scale can help to understand the variability of the prediction variable using auxiliary variables. Here, the number of clusters shows the minimum number of required sampling points. The pixels with same cluster ID are the locations with similar soil moisture. These maps show the representative area of different sampling locations at different times, thus helping in deciding the number and locations for samplings. Sampling in the same homogeneous area leads to redundancy, as the expected value of soil moisture is same. On the other hand, the sample can be taken in a different location. The proposed methodology avoids redundancy and thus presents a cost-effective way for sampling.

The framework can be applied in an online setting where any new input satellite data can be used to update the homogeneity maps. Also, the patchy nature of the homogeneity maps can be removed, i.e., the small partches of different cluster IDs can be merged together to make a single large cluster, by spatial aggregation.

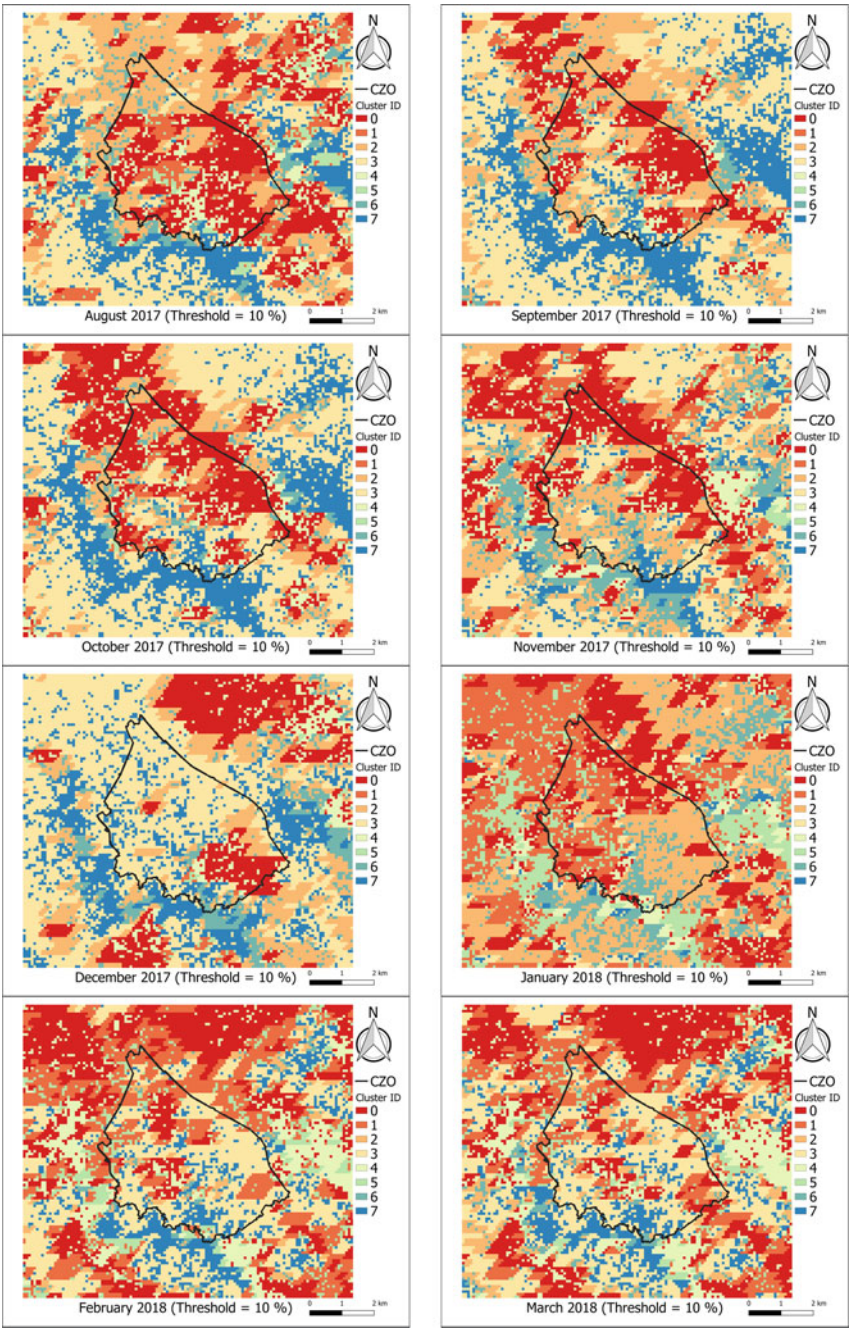

Fig. 3 Monthly homogeneity maps for the study area, HEART CZO

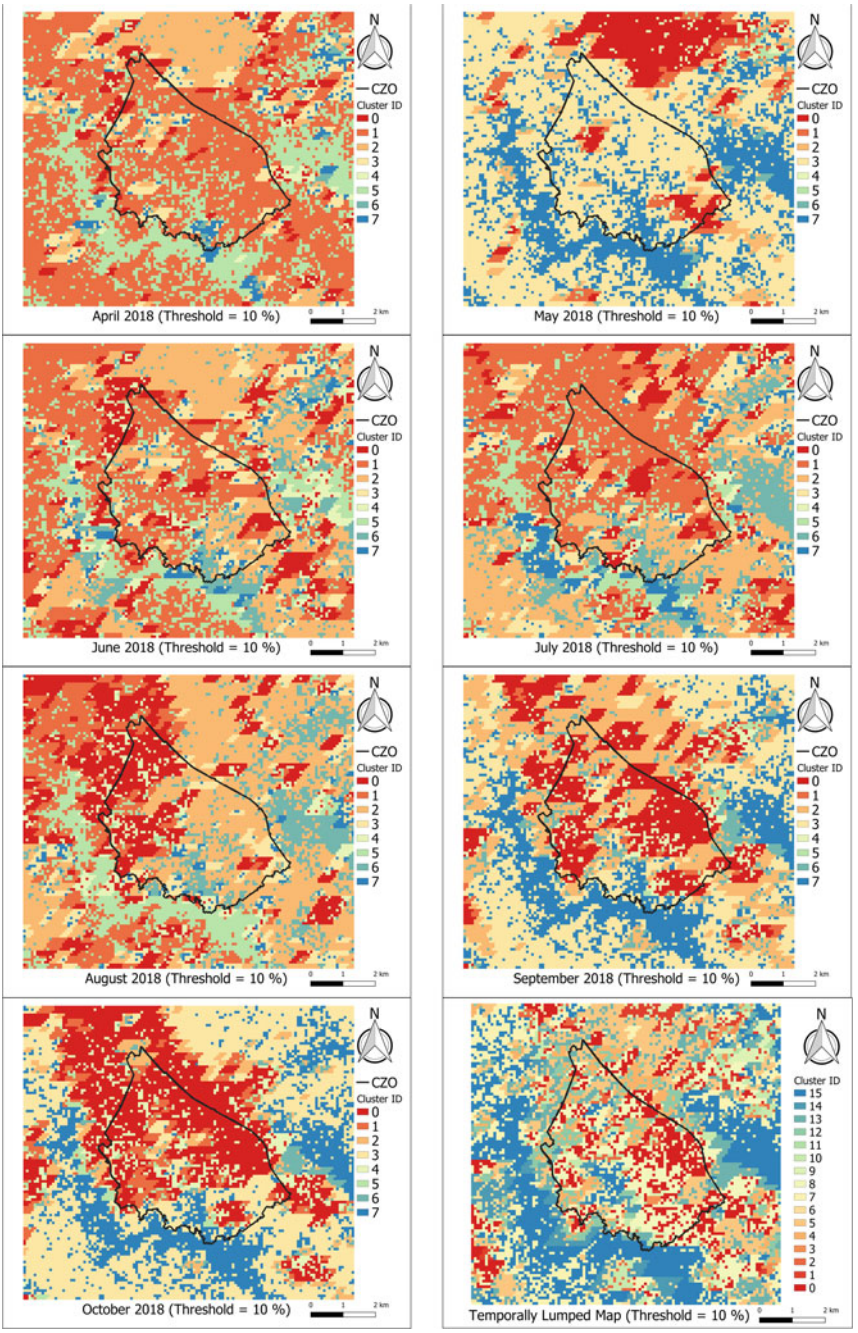

Fig. 3 (continued)

References

1. Deshpande PJ, Sure A, Dikshit O, Tripathi S (2019) A framework for estimating representative area of a ground sample using remote sensing. Int Arch Photogramm Remote Sens Spat Inf Sci XLII-2/W13:687–692. https://doi.org/10.5194/isprs-archives-XLII-2-W13-687-2019
2. Gupta S, Karumanchi SH, Dash SK, Adla S, Tripathi S, Sinha R, Paul D, Sen IS (2019) Monitoring ecosystem health in India's food basket. Eos 100. https://doi.org/10.1029/2019EO117683
3. Gorelick N, Hancher M, Dixon M, Ilyushchenko S, Thau D, Moore R (2017) Google earth engine: planetary-scale geospatial analysis for everyone. Remote Sens Environ 202:18–27. https://doi.org/10.1016/j.rse.2017.06.031
4. Pedregosa F, Varoquaux G, Gramfort A, Michel V, Thirion B, Grisel O, Blondel M, Prettenhofer P (2011) Scikit-learn: machine learning in Python. J Mach Learn Res 12:2825–2830

Water Pipeline Routing Using GIS

Varun Jain, Ramneek Singh Bhamra, Maitreya Mishra, and Rajiv Gupta

Abstract Pipeline route selection problem through an area is one of the oldest spatial challenges because of various influencing factors such as topography, geographic, geophysical, earth's surrounding and anthropological. It is a demanding issue which requires advanced scientific approaches to determine the shortest, most direct and cost-efficient route. This study identifies and evaluate various factors (elevation, slope, land use, rail and road network, water areas, etc.) influencing the pipeline route selection and develop a Geographical Information System (GIS)-based model to find the optimal pipeline route from Hanumangarh District to Jhunjhunu District using least cost approach. The proposed methodology involves calculation and unsupervised classification of the Euclidian distance for all factors. Classified rasters are then further reclassified and weights for different factors are provided using weighted overlay method to combine all the raster into a single raster image. Finally, the least cost path of the pipeline is determined using least cost tool of ArcGIS software. This research results provide a time-saving and efficient least cost path and proves the suitability of using ArcGIS in planning an optimal pipeline route.

Keywords Pipeline · ArcGIS · Route selection · Least cost path

1 Introduction

The water emergency in Rajasthan is one of the key issues that have impeded the growth of a state. The expansion and over-population have formed heavy stress on water assets in the country, especially in Rajasthan which is the worst affected state in terms of drought due to natural condition along with man-made calamities. Rajasthan's water crisis is so deep that if it is not dealt in comprehensive manner, it is very likely that government will not be able to meet day today's requirement of people. To, curb this menace, Indira Gandhi Canal Project was introduced in (IGCP) in the mid-1980s that traverses seven districts of Rajasthan: Barmer, Bikaner, Churu,

V. Jain · R. S. Bhamra · M. Mishra · R. Gupta (✉)
Department of Civil Engineering, Birla Institute of Civil Engineering, Pilani, Rajasthan, India
e-mail: rajiv@pilani.bits-pilani.ac.in

C. Bhuiyan et al. (eds.), *Water Security and Sustainability*,
Lecture Notes in Civil Engineering 115,
https://doi.org/10.1007/978-981-15-9805-0_10

Hanumangarh, Jaisalmer, Jodhpur and Sriganganagar. The IGCP has improved the situation in and around these districts to some extent but the issue of water scarcity still persists in other districts of Rajasthan. Water pipeline transport from Indira Gandhi Canal to other districts can be considered as a viable solution to improve the water paucity situation of the state.

This paper is an attempt to study the feasibility of water pipeline routing from the Indira Gandhi Canal in Hanumangarh District to Jhunjhunu District and determine the most optimal pipeline route (PR). Determination of the optimal route for pipeline placement using GIS is an area of research as connected technologies continues to change, data accessibility improves and the criteria are not same for such projects. Abudu and Williams used a GIS-based methodology for formative a best possible pipeline route that integrates multi-criteria evaluation and least cost path analysis [1]. Yildirim and Yomralioglu developed a decision support model to determine natural gas transmission line route using GIS and analytic hierarchy process (AHP) [2]. Another study conducted by Iqbal et al. involved planning a least cost gas pipeline route using an integrated approach comprising GIS and simple decision support system (SDSS) [3]. Delavar and Naghibi developed a model using GIS incorporating pipeline length, land use, wetland, road, stream, geography, terrain and a railroad crossing to identify a least cost pathway [4]. Malakahmad et al. investigated solid waste collection routes optimization using GIS in Ipoh City, Malaysia [5]. Balogun et al. employed the spatial analyst tool of ArcGIS for analysis and interpretation to determine an optimal oil pipeline route in Malaysia's oil-rich Baram Field [6]. Americo Gamarra developed a model to define the best route for a future pipeline in the south of Peru, which would start from Amazon forest, cross the Andes Mountains and arrive at Pacific coast [7]. Another study done by Bagli et al. developed an approach based on the integration of multi-criteria evaluation (MCE) and least cost path analysis using GIS to identify the most suitable route for a 132-kV power line [8]. Effat and Hassan carried out the evaluation of three highway routes using the analytic hierarchy process (AHP) and the least cost path analysis in Sinai Peninsula, Egypt [9]. Akbari et al. integrated multi-criteria evaluation (MCE-GIS) and fuzzy logic to evaluate land suitability for spatial planning in arid regions of eastern Iran [10]. All these studies used multi-criterion approach for defined paths, i.e. mostly in vector form. Different weightages were given for the different factors. These factors depend on the problem in hand. However, for unknown places, like new project, various barriers may come in and through the crow distance is minimum but the total cost be higher. In the present method, unsupervised classification is done to remove very high cost pixels. In our study, after removing the high cost pixels, we are using the weighted overlay method to find the cost surface and using least cost path tools of ArcGIS [11] the optimal pipeline route is determined.

2 Methodology

Long distance pipelines are complex arrangements in the specific GIS fields. For determining the more appropriate routing way, it is needed to find a geographic location closer to the study area. In this study, it was found to be in Hanumangarh district on Indira Gandhi Canal. The methodology followed to find the most cost effective path of the pipeline is as depicted in Fig. 1. The processes are as depicted in the following subsection.

2.1 Data Acquisition

Data depicting various factors such as land use pattern of study region, road and rail network, geological data, slope, water bodies in the region and various other factors is needed for pipeline routing. This data is generally obtained in the vector format. The data which is available in the form of maps is digitized into shape files. In present method, the vector data is rasterized for least cost path analysis. In case of slope, the DEM data of the region is first obtained. Using the slope spatial analyst tool, the slope of the region may be calculated. In this study, the factors considered are that of slope, land use pattern (built up area, crop area, waste land, fallow land and forest land), road and rail network and water bodies. The shape files of road and rail network and water bodies were downloaded from the DIVA-GIS Platform [12]. While the DEM and land use data were available in the raster form for the same, the coordinate system for all these datasets was WGS 1984.

2.2 Data Processing

The data gathered needs to be further processed to form the final cost surfaces. Firstly, all the data available needs to be rasterized for further use. Once rasterization is done, classification of the raster data is done followed by weight allocation. In this

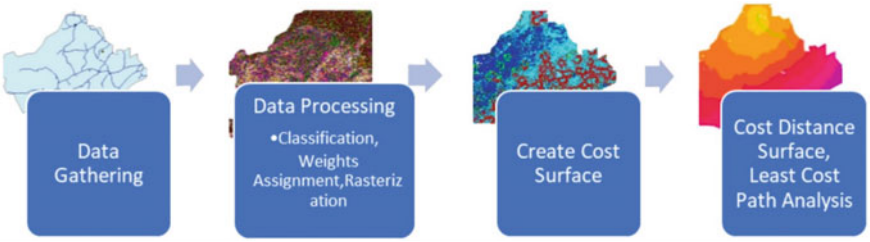

Fig. 1 Methodology to find least cost path

study, the feature data is rasterized using the Euclidean distance rule. It computes the Euclidean distance to the closest source for each cell, which serves as the preliminary raster set on which further operations are performed.

2.2.1 Classification

Each raster dataset requires some stage management to convert data into a format, whose values reflect the criteria for an optimum pipeline route analysis (PRA). Briefly, the process for each input dataset consists of assigning values (cost) to each pixel and converting vectors to raster for those cell values to which the weights are assigned. For this purpose, classification of data is done to subdivide each dataset into cells of various costs depending on their suitability for pipeline laying. In this study, we have done classification of preliminary dataset using the ISO cluster unsupervised classification tool

2.2.2 Cost Assignment

The classified data has some preliminary weights allocated by the system. These need to be further modified as per the need of the problem. This is done by reclassifying the datasets. Various factors such as the number of classes, break points and the costs given to these classes are here adjusted. High costs are given to classes where pipe laying will be difficult. For instance, in this study, very high costs are given to cells with rail, water bodies or built up areas in them.

2.3 Cost Surface

Once the various cost raster is prepared, these need to be combined into a single cost surface for further computations of least cost path. This is done by using the weighted overlay tool in ArcGIS. Herein, the various raster is summed up into a single raster. Every factor is given an importance value which acts as its weightage in the combined raster. The weights are given as per experts' opinions and references [1–4, 6, 7]. The cost given to the various factors and their subvalue in this study are as shown in Table 1.

2.4 Least Cost Path

Cost surface is the input to define the best pipeline route by calculating the least cost path (LCP). ArcGIS Spatial Analyst uses the following steps (a) use the cost distance tool to create two pre-requirements for LCP: (i) "cost distance (CD)" surface and

Table 1 Weightage given to the various factors and their subvalues

Factor	Influence value	Subvalues
Slope	10	1
		2
		3
		4
		5
		6
		7
		8
		9
		NODATA
Land use	30	1
		2
		9
		10
		100
		NODATA
Roads network	10	1
		5
		15
		NODATA
Water bodies	25	1
		2
		4
		5
		100
Rail network	25	1
		100
		NODATA

(ii) a "cost distance back link (CDBL)" surface. For CD and a source location, it denotes the "cost" to move to the origin for each cell pixel. CDBL surface signifies the direction for each pixel to travel to the origin ensuing the least cost path. Cost path provides a potential pipeline route.

3 Case Study

Indira Gandhi Canal, the longest canal of India. The canal enters from Haryana, moves through Punjab and comes into Rajasthan at Hanumangarh district as indicated in Fig. 2. The canal passes through seven districts of Rajasthan, namely Barmer, Bikaner, Churu, Hanumangarh, Jaisalmer, Jodhpur and Sriganganagar. With increased supplies, the total length of canal is nearby 9,245 km. Indira Gandhi Canal facilitates irrigation over a region of 6770 km^2 (1670000 acres) in Jaisalmer district and 37 km^2 (9100 acres) in Barmer district, respectively. Canal also provides water for agriculture, and drinking to millions of people in distant areas. This proposed pipeline project is from Indira Gandhi canal in Hanumangarh District to Jhunjhunu District. The study area is as shown in Fig. 2. The aim of this pipeline is to transfer surplus water of Indira Gandhi canal to water scarce region of Jhunjhunu District in North-Eastern Rajasthan for irrigation practices, drinking purpose, reducing ground water usage and dependence on rainfall. The climate is semiarid means hot summers and cold winters with low to medium rainfall. The annual potential evapotranspiration is about 1500 mm. Jhunjhunu is facing difficulties of groundwater depletion, groundwater pollution as the fluoride and nitrate concentration is increasing day by

Fig. 2 Map depicting water scarce Jhunjhunu District and Indira Gandhi Canal

day. This pipeline will fulfil many purposes along with improving living standards of people of Jhunjhunu.

The methodology adopted in our study can be seen in Fig. 3a, b, c and d. Figure 3a gives the general methodology, which is further explained in subsequent Figs. 3b, c and d, respectively.

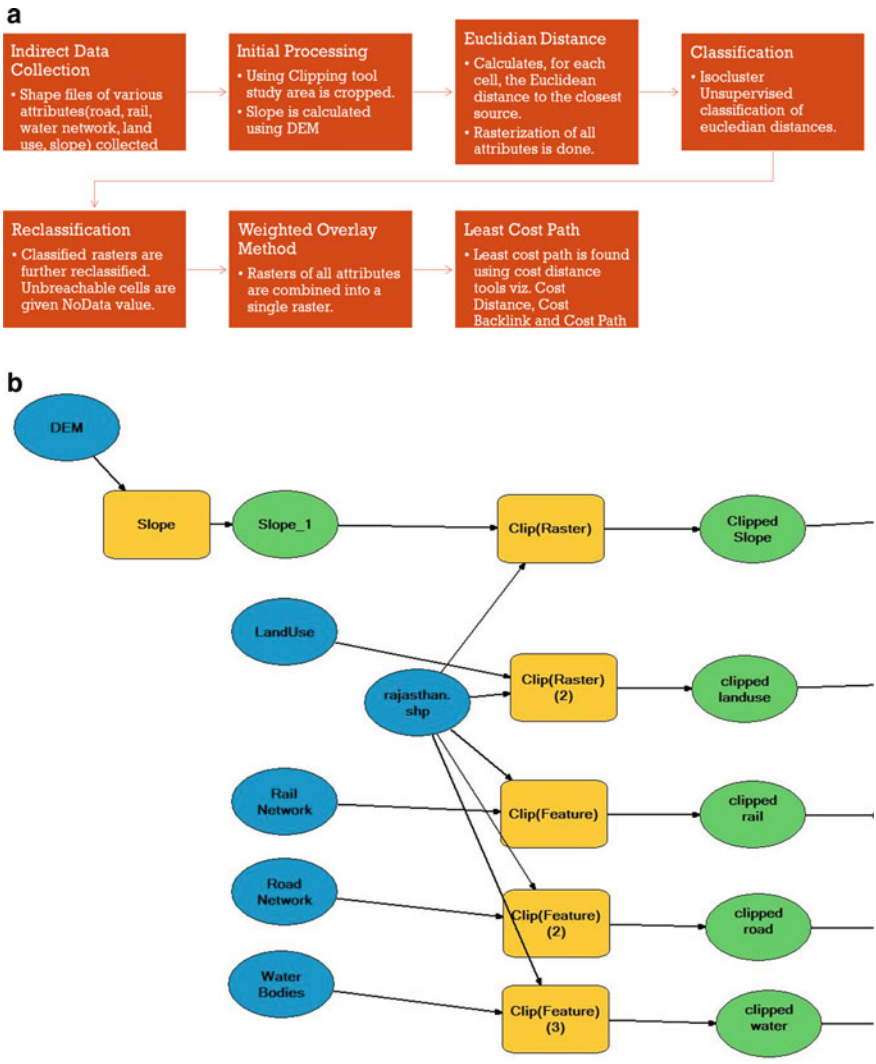

Fig. 3 Methodolgy

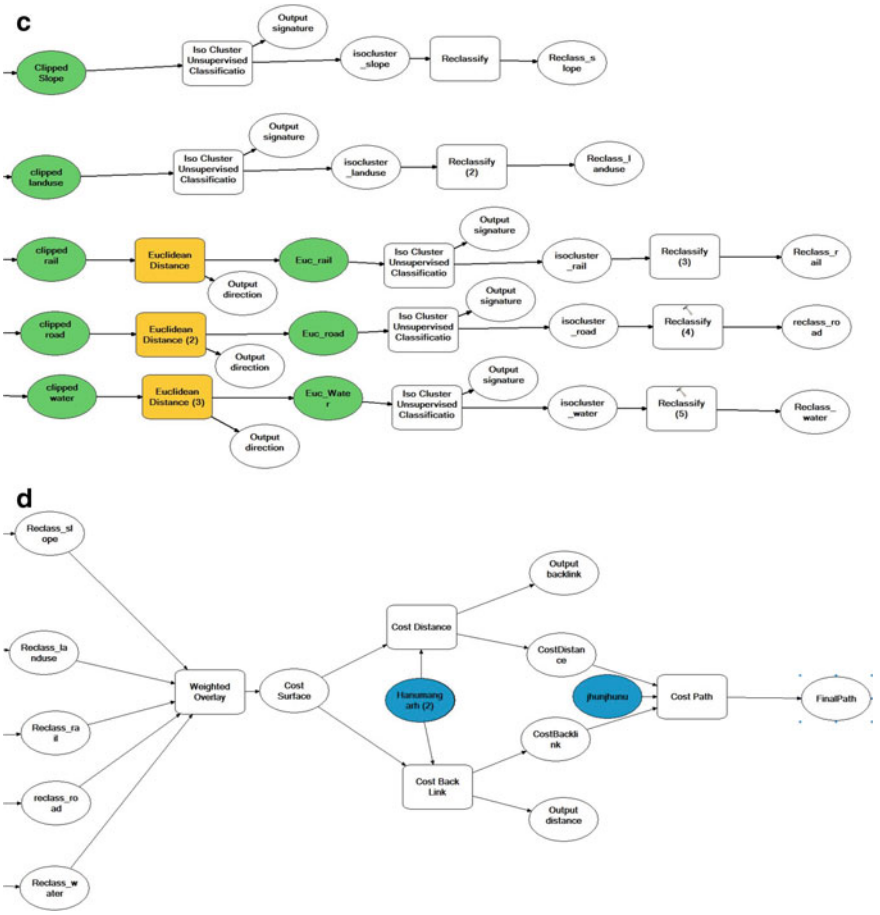

Fig. 3 (continued)

4 Results and Discussion

The outputs of the above mentioned methodology are shown in Figs. 4 and 5, which display the cost distance (Fig. 4) and the cost distance back link (Fig. 5).

Using the "CD" and "CDBL" surfaces, the cost path tool defines a passage(s) or vicinity right for a PR that connects the original and finishing locations. The identified "cost path" raster is shown in Fig. 6. The least cost path shown in green in Fig. 6 is the most effective PR by taking parameters (weights, importance factor) into consideration.

GIS provides a large number and a variety of analytical functions that are capable of replacing manual and traditional methods of route planning.

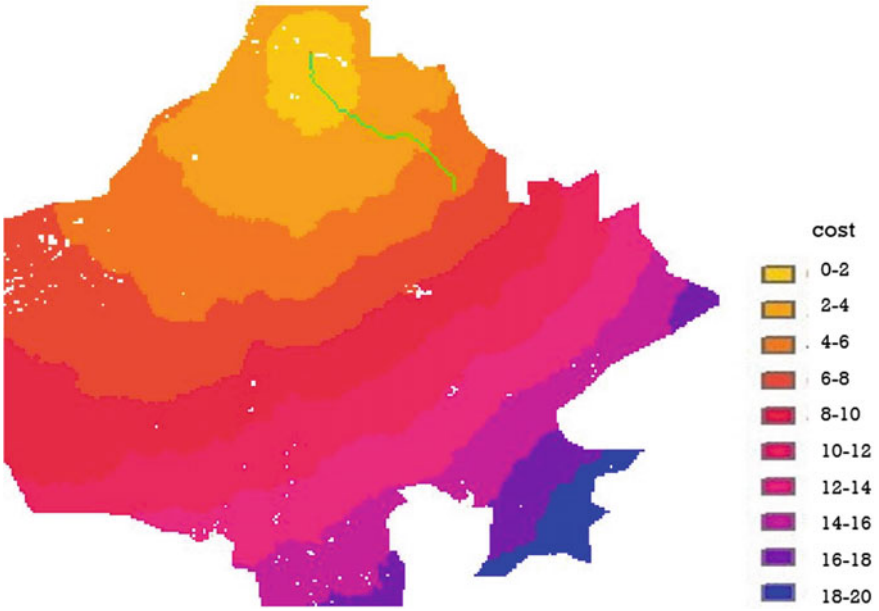

Fig. 4 Cost distance surface

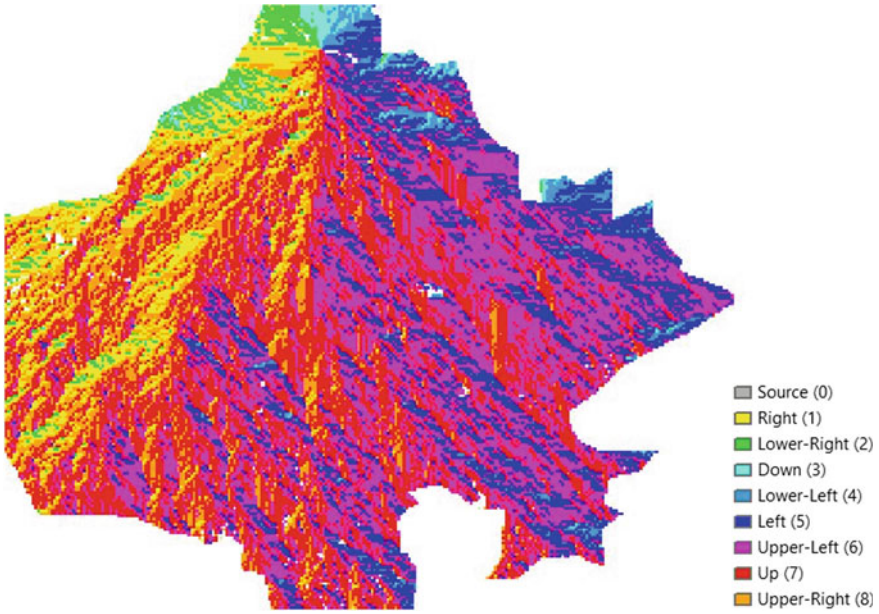

Fig. 5 Cost distance back link surface

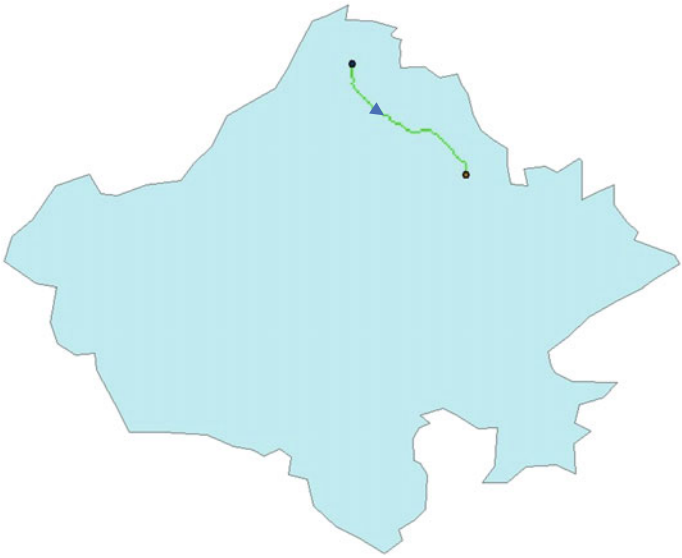

Fig. 6 Least cost path pipeline

One key limitation of this study is the criteria for weightage of different parameters that were used in the weighted overlay analysis because the weightage importance of different factors can vary with different decision makers. One other Key issue is community participation, which is a necessary module of any multifaceted project. Various other factors such as socio-political, socioeconomic and spiritual factors for which data are often unavailable and changeable are recommended to be included in future pipeline routing learning.

While the research had some boundaries with the amount of data accessible and its accuracy, the overall result was a viable LCP path that satisfied standards with routing for such type of infrastructure.

5 Conclusion

The present study develops an approach to determine the most optimal route for water pipeline from source to destination. Instead of developing the least cost path, where different paths are established, present approach works on optimization on pixel basis. Here, the path is not defined and through pixel cost (which may include, excavation, elevation, obstacles, soil type, length, etc.) is considered. This research, using similar studies as background and for reference, incorporated several key factors influencing the routing of a large-scale pipeline. The results clearly prove that least cost path in route planning is an inevitability preceding to the final decision-making. It is concluded that if least cost path analysis using ArcGIS is embedded in the early

planning system for determining a pipeline route, it proves to be spot on, economic and time-saving for a sustainable pipeline corridor location design. Due to pixel-based optimization, computation time is high but for green project this is the efficient methodology. The use of this type of cost and time effective, and efficient system in the planning is the need of the hour. A case study to identify the minimum length between Hanumangarh district to Jhunjhunu District by carrying out the least cost path analysis using ArcGIS is taken, and results are validated.

References

1. Abudu D, Williams M (2015) GIS-based optimal route selection for oil and gas pipelines in Uganda. ACSIJ Adv Comput Sci: Int J 4(4):16. ISSN 2322-5157
2. Yildirim V, Yomralioglu T (2007) GIS based pipeline route selection by ArcGIS in Turkey. In: ESRI international user conference, California, US
3. Iqbal M, Sattar F, Nawaz M (2006) Planning a least cost gas pipeline route a GIS & SDSS integration approach, October 2006. https://doi.org/10.1109/ICAST.2006.313812
4. Delavar MR, Naghibi F (2003) Pipeline routing using geospatial information system analysis. In: Conference: ScanGIS 2003—the 9th Scandinavian research conference on geographical information science, 4–6 June 2003, Espoo, Finland – proceedings
5. Malakahmad A, Bakri PM, Md Mokhtar MR, Khalil N (2014) Solid waste collection routes optimization via GIS techniques in Ipoh city, Malaysia. Procedia Eng 77:20–27
6. Balogun AL, Matori AN, Lawal DU, Chandio I (2012) Optimal oil pipeline route selection using GIS: community participation in weight derivation and disaster mitigation. In: 2012 international conference on future environment and energy IPCBEE, vol 28. IACSIT Press, Singapore
7. Gamarra A (2015) GIS suitability modelling to support a pipeline route selection. In: ESRI user conference in San Diego, CA, July 2015
8. Bagli S, Geneletti D, Orsi F (2011) Routeing of power lines through least-cost path analysis and multicriteria evaluation to minimise environmental impacts. Environ Impact Assess Rev 31(3):234–239
9. Effat HA, Hassan OA (2013) Designing and evaluation of three alternatives highway routes using the analytical hierarchy process and the least-cost path analysis, application in Sinai Peninsula, Egypt. Egypt J Remote Sens Space Sci 16(2):141–151
10. Akbari M, Neamatollahi E, Neamatollahi P (2019) Evaluating land suitability for spatial planning in arid regions of eastern Iran using fuzzy logic and multi-criteria analysis. Ecol Indic 98:587–598
11. http://webhelp.esri.com/arcgisdesktop/9.2/pdf/ArcMap_Tutorial.pdf
12. https://www.diva-gis.org/gdata

Predicting Meander Migration of the Barak River by Empirical and Time Sequence Methods

Wajahat Annayat and Briti Sundar Sil

Abstract Common phenomena associated with the alluvial river is its 'meandering'. Lateral migration of the Barak River creates geomorphic hazards in Assam, India. Predicting and preventing this migration are both difficult and necessary. In this article, we have tried to describe and evaluate the empirical approach and time sequence maps to predict meander migration. An empirical approach is based on correlations, while as, for a given meander, earlier observed movement is used in case of sequence method to predict the future migration. In this study, 12 meandering reaches of the Barak River are considered using multiperiod Landsat remote sensing images. In order to evaluate the accuracy of these methods, both predicted migrations, as well as measured migration, are compared. Results show that empirical methods are not precise and accurate, though some of the empirical methods are conservative, and some are unconservative. More accurate, precise information on the meandering movement is given by time sequence method to predict the radius of the best-fit circle of the future meander location.

Keywords Meandering channel · Barak River · Landsat images · Remote sensing · Empirical and time sequence method

1 Introduction

The river is a part of the hydrological cycle. On this globe, the main water source for life is a river which plays a significant role in the development of human civilization. The most significant geomorphic system which is considered to be active on the earth's surface is river and its processes [1]. In varying environmental conditions, morphology of river is changing over both spatial and temporal scales due to erosion and deposition of the river bank. Various processes that control the morphology of river includes channel dynamics, discharge, runoff, sediment supply and vegetation cover [2]. Successful and sustainable management of a river requires

W. Annayat (✉) · B. S. Sil
Department of Civil Engineering, National Institute of Technology Silchar, Silchar 788010, India
e-mail: Wajahatannayat123@gmail.com

C. Bhuiyan et al. (eds.), *Water Security and Sustainability*,
Lecture Notes in Civil Engineering 115,
https://doi.org/10.1007/978-981-15-9805-0_11

an understanding of which reaches are more susceptible to lateral migration. To predict meander migration, existing approaches make use of geometry, water and soil parameters in different ways [3]. Despite decades of research into bank migration prediction, knowledge of the subject is still imperfect, with much work remaining to be done. Exact mathematical representation of such prediction has yet to achieve, and the tools which are available produce results which possess lot of uncertainties [4]. The process of river migration does not occur simultaneously all through the river; rather, it occurs in some places separately at any period of time leading to the formation of the individual meander. Main source of sedimentation in the river is its own bank erosion although, some other parameters which are which are also responsible for sedimentation in the river are land use, soil composition of bank and bed materials, area of watershed, slope variability and discharge of river [5]. Also autogenic rivers have lost their dynamic equilibrium due to some human interference like irrigation, construction of dams and infrastructural developments which lead to the overexploitation of natural resources and changes in the variation of the streamflow [6].

The rate of river migration may be as high as several hundred metres at several locations and for which the habitats of the human are adversely affected. At large r_c/b (bend curvature) ratios, the radius (r_c) is large compared to the channel width (b), and for given flow velocity, the centrifugal force which is inversely proportional to the radius of curvature is small; this leads to a small erosion rate. At very small r_c/b ratios, the width of the channel b is large compared to the radius of curvature, the water can actually flow almost straight through the river, and its flow tends to straighten it. When the ratio r_c/b is between 2 and 3, the centrifugal force is significant, and the water is forced to follow the outer bank [7].

Ganguly [8, 9] found that the Barak River is structurally characterized by sequence of meridional to sub-meridional, curved, extended, doubly plunging, uneven folds arranged in an en-echelon pattern, trending N-S to NNE-SSW with slight convexity towards west. Geological and morphotectonic issues of the region can be found in the existing literature of as [10, 11, 12, 13, 14, 15, 16] during the assessment of hydrocarbons. Fold belt region of Barak River is tectonically surrounded on all four sides. Towards the north side, it is bounded by Dauki. Fault, and in the east side, it is bounded by Haflong-Disang Thrust, and on the south side, it is bounded by Arakan-Yoma Fold Belt, while as, on the west side, it is enclosed by Hail-Haka-Lulu Lineament and Chandpur-Barisal High [17]. In this article, we have tried to describe and evaluate the empirical approach and time sequence maps to predict the meander migration of the Barak River. 12 meandering reaches of the Barak River are considered using multiperiod Landsat remote sensing images. In order to evaluate the accuracy of these methods, both predicted migrations, as well as measured migration, are compared.

2 Study Area and Database

Barak River start offs from Japvo Mountain of Manipur hills at an elevation of 3015 m and follows the course south all the way through hilly terrain up to Tipaimukh close to the tri-junction of the three states: Assam, Manipur and Mizoram. At this point, the river takes a hairpin curve and enters into the plains of Cachar district of Assam and figures the border of states of Assam and Manipur up to Jirimat, slight upstream of Lakhimpur. The river then flows through westwards of the Barak valley of Assam. Finally, it enters into Bangladesh, where it is known as the Surma River and Kushiyara River which is later called as Magna River. Major parts covered by Barak River are north-eastern India, Bangladesh and Myanmar. The Barak basin lies between 89° 50′ E to 94° 0′ E and 22° 44′ N to 25° 58′ N. The basin has sub-tropical warm, and humid climate receives an annual rainfall of 2500–4000 mm. Digital Elevation Model (DEM), resolution 30 m (downloaded from http://earthexplorer.usgs.gov), was used to obtain the river network of Barak River, as shown in Fig. 1. Landsat images of the year 1984, 2002, 2012 and 2017 have been used to identify the meandering characteristics with the help of GIS and remote sensing technology. Details of the dataset utilized are shown in Table 1.

3 Methodology

3.1 Selected Empirical Methods

Empirical methods are commonly used methods. Main advantages of using these methods are that it is simple and is based on observed data. By this approach, the database of observed meander migration and associated parameters is assembled; out of which, most influential parameter is selected; a regression is performed; and an equation is proposed. Some of the commonly used empirical approaches described below.

3.1.1 Hooke [18]

Hooke collected a meander migration data in 1980, by using field measurement and historical maps for 11 streams in Devon, England. Hooke observed the catchment area A as the most influencing parameter and finally derived his equation based on these data.

$$M_{\mathrm{r}} = 0.0669A^{0.46} \tag{1}$$

where

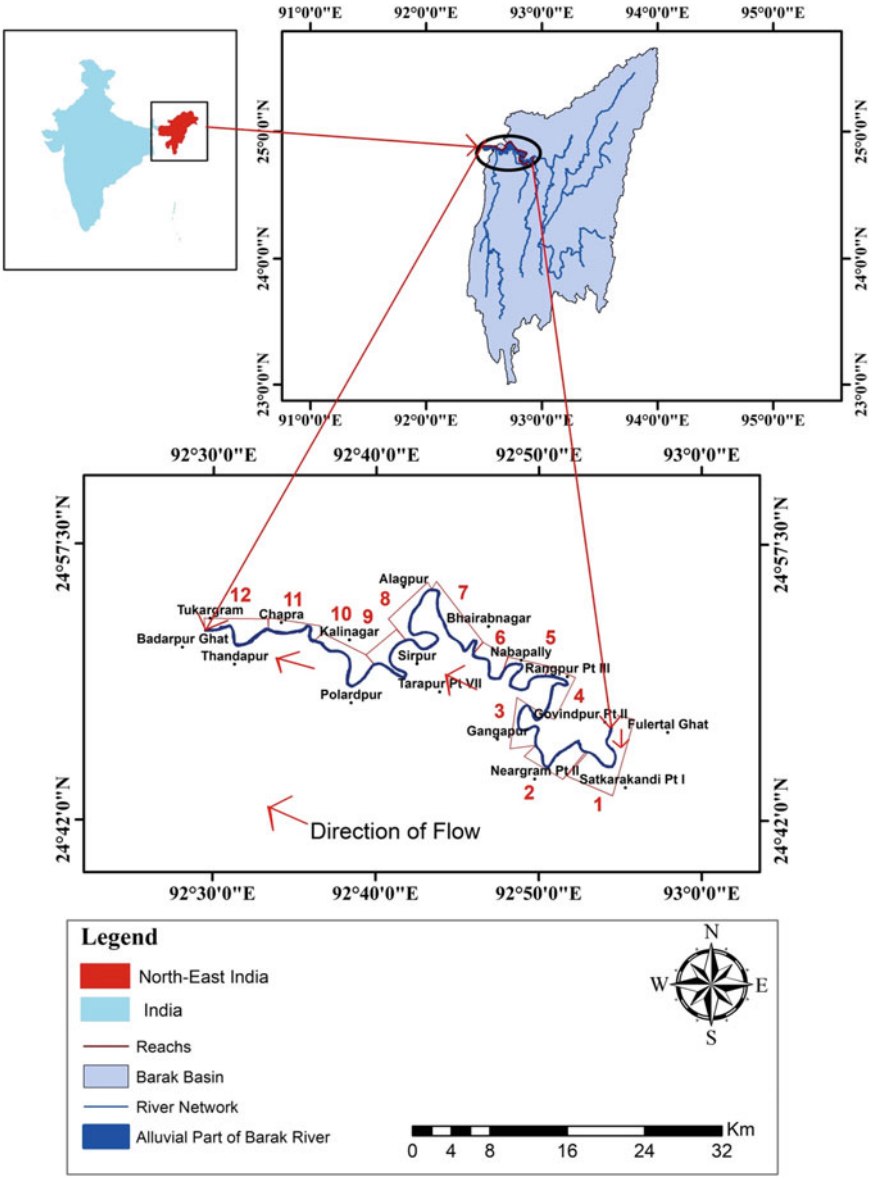

Fig. 1 The study area location and channel network

Table 1 Data used in the study area

Data	Path/Row	Resolution (m)	Year	Source
Landsat MSS	136/43	60	1984	USGS
Landsat MSS	136/43	30	1992	USGS
Landsat ETM$^+$	136/43	30	2002	USGS
Landsat TM	136/43	30	2012	USGS
Landsat TM	136/43	30	2017	USGS

M_r Meander migration rate (m/year)
A Catchment area (km^2).

3.1.2 Brice [19]

Brice collected a meander migration data of 43 meanders in four different types of rivers. Channel width b was observed as the main influencing parameter. Regression was performed against these data sets and finally derived the equation.

$$M_r = 0.01b \tag{2}$$

where

M_r Meander migration rate (m/year)
b Width of river channel (m).

3.1.3 Nanson and Hickin [7]

Nanson and Hickin collected a meander migration data in 1983 for 18 river channels in Western Canada. Bend curvature (r_c/b) was observed as the main influencing parameter. They plotted their data and found that when the ratio of r_c/b was between 2 and 3, the migration rate tends to be maximum.

$$\frac{M_r}{b} = 0.1\left[\left(\frac{r_c}{b}\right) - 1\right] \text{ When, } \frac{r_c}{b} < 2.3 \tag{3}$$

$$\frac{M_r}{b} = 0.3\left(\frac{r_c}{b}\right)^{-1} \text{ When, } \frac{r_c}{b} > 2.3 \tag{4}$$

where

M_r Meander migration rate (m/year)
b Width of river channel (m)
r_c Radius of curvature of the meander (m).

3.2 Time Sequence Maps

Scanning of Landsat images is done and then imported in Arc GIS format. For radiometric corrections, haze corrections and filtration of images ERDAS 9.1 were used. From the processed images, the area of interest was extracted. Eye interpretation and digital image processing techniques are used to delineate the bank lines, and then, the delineated bank lines are used to generate a channel centreline with the help of onscreen digitization in Arc Map.

In order to find the centre location and radius of an imaginary circle best fit to the data points representing the bend line, least square estimation is used. Equation of this circle with centre at $(x, y) = (a, b)$, and radius R is given by:

$$(X - a)^2 + (Y - b)^2 = R^2 \tag{5}$$

Assume (X_i, Y_i), $I = 1, 2, \ldots, n$, be a set of data points in the xy-plane. In order to find the values of a, b and R which provides the least square estimation of a circle according to data points; the equation is minimized:

$$\sum_{i=1}^{N}\left[(X_i - a)^2 + (Y_i - b)^2 - R^2\right] = F(a, b, R) \tag{6}$$

Further

For the outer bank during period A (year 1 to year 2), the rate of change of the radius of curvature is given by

$$\Delta R_{\mathrm{CA}} = (R_{\mathrm{C2}} - R_{\mathrm{C1}})/Y_{\mathrm{A}} \tag{7}$$

where

ΔR_{CA} Rate of change in radius of curvature during period A (m/year)
R_{C1} Radius of curvature of the outer bank in year 1 (m)
R_{C2} Radius of curvature of the outer bank in year 2 (m).

For the outer bank during period B (year 1 to year 2), the rate of change of the radius of curvature is given by

$$\Delta R_{\mathrm{CB}} = (R_{\mathrm{C3}} - R_{\mathrm{C2}})/Y_{\mathrm{B}} \tag{8}$$

where

ΔR_{CB} Rate of change in radius of curvature during period B (m/year)
R_{C2} Radius of curvature of the outer bank in year 2 (m)
R_{C3} Radius of curvature of the outer bank in year 3 (m).

Further, if the circles inscribed and channel positions on a particular bend are recorded in year 1, 2 and 3 with the corresponding period of A and B, then the predicted radius of curvature of the outer bank in the year 4 is given by Lagasse et al. [20]

$$R_{C4} = R_{C3} + \left[\left(\frac{R_{C3} - R_{C2}}{Y_B}\right)(Y_C)\right] \tag{9}$$

where

R_{C4} Predicted radius of curvature in year 4 (m)
R_{C3} Radius of curvature of the outer bank in year 3 (m)
R_{C2} Radius of curvature of the outer bank in year 2 (m)
Y_B Number of years in period B
Y_C Number of years in period C.

The amount of migration of the bend centroid for period A is D_A, and for period B is D_B. The rates of migration during period A are determined by dividing D_A and D_B by the number of years in the associated period. To predict the magnitude of centroid migration during period C, it is more accurate to use the most recent period B rate of centroid shift, which yields the following relationship

$$D_C = (D_B | Y_B) Y_C \tag{10}$$

where

D_C Magnitude of centroid migration for period C
D_B Magnitude of centroid migration for period B
Y_B Number of years in period B
Y_C Number of years in period C.

4 Results and Discussion

In this study, 12 meandering reaches of the Barak River are considered using multi-period Landsat remote sensing images to evaluate the accuracy of empirical approach and time sequence maps by comparing predicted and measured migration. In order to evaluate the accuracy and precision of the empirical methods, Eqs. 1 through 4 were used together with the data of Table 2 to obtain the predicted migration rates of Table 3. Also shown in Table 3 is the measured migration rates for the Barak River. Comparisons made from the empirical methods (Figs. 2, 3 and 4) indicate that Hooke and Brice's method is reasonably traditional. While as in the Nanson and Hickin method, the scatter is significant on the basis of data alone it appears to be a reasonably safe method.

Table 2 Summary of data of all the bends

Reach No.	Year	Channel width b (m)	Radius of curvature r_c (m)	Ratio r_c/b	Catchment area A (km^2)	Reach No.	Year	Channel width b (m)	Radius of curvature r_c (m)	Ratio r_c/b	Catchment area A (km^2)
Reach-1	1984	260	1019	3.9	24220	Reach-7	1984	300	532	1.7	17192
	1992	284	1093	3.8	24220		1992	496	558	1.1	17192
	2002	309	745	2.4	24220		2002	383	526	1.3	17192
	2012	396	719	1.8	24220		2012	437	553	1.2	17192
	2017	330	754	2.2	24220		2017	440	518	1.1	17192
Reach-2	1984	310	376	1.2	24206	Reach-8	1984	300	1180	3.9	17188
	1992	379	478	1.2	24206		1992	384	1237	3.2	17188
	2002	402	573	1.4	24206		2002	371	1188	3.2	17188
	2012	398	576	1.4	24206		2012	428	1085	2.5	17188
	2017	400	592	1.4	24206		2017	300	1150	3.8	17188
Reach-3	1984	240	1050	4.3	19389	Reach-9	1984	310	597	1.9	17108
	1992	608	1013	1.6	19389		1992	367	571	1.5	17108
	2002	327	1238	3.7	19389		2002	380	749	1.9	17108
	2012	318	1055	3.3	19389		2012	406	616	1.5	17108
	2017	390	1064	2.7	19389		2017	360	650	1.8	17108
Reach-4	1984	300	492	1.6	19288	Reach-10	1984	270	725	2.6	16734
	1992	309	524	1.6	19288		1992	361	738	2.0	16734
	2002	322	498	1.5	19288		2002	408	830	2.0	16734
	2012	339	474	1.3	19288		2012	414	734	1.7	16734
	2017	380	498	1.3	19288		2017	360	729	2.0	16734

(continued)

Table 2 (continued)

Reach No.	Year	Channel width b (m)	Radius of curvature r_c (m)	Ratio r_c/b	Catchment area A (km^2)	Reach No.	Year	Channel width b (m)	Radius of curvature r_c (m)	Ratio r_c/b	Catchment area A (km^2)
Reach-5	1984	340	565	1.6	19274	Reach-11	1984	260	826	3.1	16729
	1992	361	563	1.5	19274		1992	409	679	1.6	16729
	2002	405	556	1.3	19274		2002	418	625	1.4	16729
	2012	439	562	1.2	19274		2012	442	685	1.5	16729
	2017	400	557	1.3	19274		2017	420	602	1.4	16729
Reach-6	1984	360	550	1.5	18677	Reach-12	1984	370	826	2.2	16717
	1992	508	582	1.1	18677		1992	513	679	1.3	16717
	2002	490	565	1.1	18677		2002	407	625	1.5	16717
	2012	458	563	1.2	18677		2012	485	685	1.4	16717
	2017	450	529	1.1	18677		2017	390	602	1.5	16717

Table 3 Predicted and measured meander migration rates (empirical methods)

Reach No.	Period	Hooke [18] m/year	Brice [19] m/year	Nanson and Hickin [7] m/year	Measured m/year	Reach No.	Period	Hooke [18] m/year	Brice [19] m/year	Nanson and Hickin [7] m/year	Measured m/year
Reach-1	1984–1992	7	2.7	23.3	55.5	Reach-7	1984–1992	5.9	3.9	21	16.2
	1984–2002	7	2.9	26.1	36.8		1984–2002	5.9	4.3	4.9	4.2
	1984–2012	7	3.5	45.0	41.2		1984–2012	5.9	4.1	11.4	4.2
	1984–2017	7	3.6	31.6	22.7		1984–2017	5.9	4.3	8.7	4.7
Reach-2	1984–1992	6.9	3.4	6.2	58.3	Reach-8	1984–1992	5.9	3.4	26.9	8.6
	1984–2002	6.9	3.9	7.5	15.5		1984–2002	5.9	3.7	42	13.3
	1984–2012	6.9	4	16	19.2		1984–2012	5.9	3.9	40.5	2.8
	1984–2017	6.9	3.9	15.9	16.6		1984–2017	5.9	3.6	27.6	2.5
Reach-3	1984–1992	6.2	4.2	19.5	12.3	Reach-9	1984–1992	5.9	3.3	27.9	13.5
	1984–2002	6.2	4.6	36.4	15.2		1984–2002	5.9	3.7	18.3	1.7
	1984–2012	6.2	3.2	30.9	10.8		1984–2012	5.9	3.9	34.2	15.2
	1984–2017	6.2	3.5	33.7	10.4		1984–2017	5.9	3.8	28.8	12.0
Reach-4	1984–1992	6.2	3.0	18	20.3	Reach-10	1984–1992	5.8	3.1	36.4	29.8
	1984–2002	6.2	3.1	18.5	12.7		1984–2002	5.8	3.8	36.1	10.0

(continued)

Table 3 (continued)

Reach No.	Period	Hooke [18] m/year	Brice [19] m/year	Nanson and Hickin [7] m/year	Measured m/year	Reach No.	Period	Hooke [18] m/year	Brice [19] m/year	Nanson and Hickin [7] m/year	Measured m/year
	1984–2012	6.2	3.3	16.1	7.7		1984–2012	5.8	4.1	40.8	10.6
	1984–2017	6.2	3.5	10.1	4.8		1984–2017	5.8	3.8	28.9	10.4
Reach-5	1984–1992	6.2	3.5	20.4	13.6	Reach-11	1984–1992	5.8	3.3	29.3	16.0
	1984–2002	6.2	3.8	18	14.4		1984–2002	5.8	4.1	24.5	5.4
	1984–2012	6.2	4.2	12.1	6.1		1984–2012	5.8	4.3	16.7	5.7
	1984–2017	6.2	4.1	8.78	1.4		1984–2017	5.8	4.3	22.1	5.2
Reach-6	1984–1992	6.1	4.3	18	7.6	Reach-12	1984–1992	5.8	4.4	44.4	11.1
	1984–2002	6.1	4.9	5	3.3		1984–2002	5.8	4.6	15.3	3.5
	1984–2012	6.1	4.7	4.9	2.2		1984–2012	5.8	4.4	20.3	1.8
	1984–2017	6.1	4.5	9.16	5.2		1984–2017	5.8	4.3	19.5	1.7

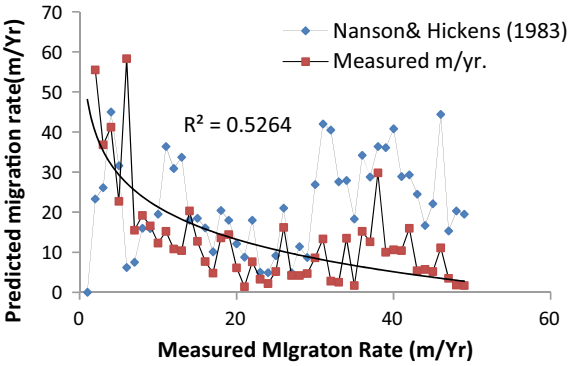

Fig. 2 Predicted versus measured migration rates

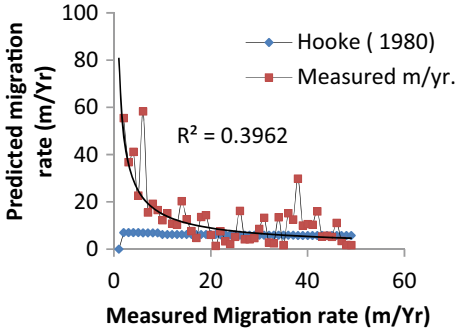

Fig. 3 Predicted versus measured migration rates

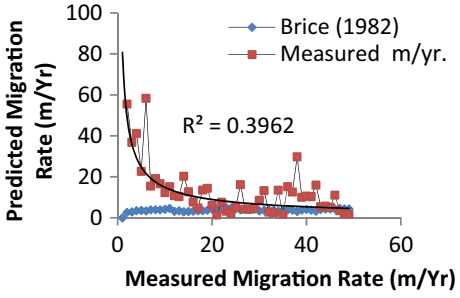

Fig. 4 Predicted versus measured migration rates

Predicted and measured rates of meander migration were found highly diverse. For example, Brice method gives 2.7 m/year (Bend-1, 1984–1992), measured value was 55.5 m/year. Brice methods focused on the width and correlation found was weak with $R^2 = 0.39$ which indicates that Brice's method are reasonably traditional, and it can be said that the width alone can't be the influencing parameters in the process river migration. Again, for another situation, if Nanson and Hickin method suggested meander migration rate as 40.5 m/year (Bend-8, 1984–2012), then measured value was just 2.8 m/year. As Nanson and Hickin method focus on bend curvature (r_c/b)

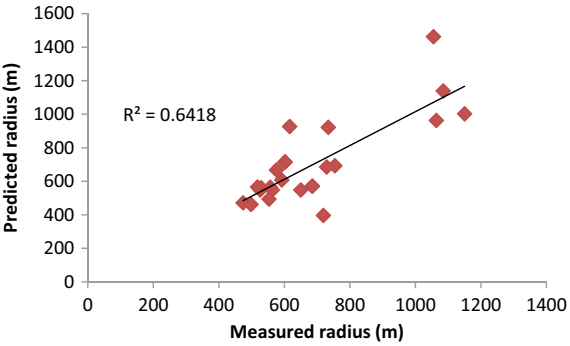

Fig. 5 Predicted radius versus measured radius for the time sequence maps

and method was analyzed by considering two active parameters radius of curvature and width of river even if this method gave a moderate correlation with $R^2 = 0.50$, the scatter is moderately significant on the basis of data alone. So this method appears to be a reasonably safe method, and it was found from the scatter plot that bend curvature (r_c/b) alone may be the main influencing parameter in the process river migration.

Based on the previous year records of bends, a prediction tool 'channel migration toolbox' was used for the prediction of bend radius and centroid for the year 2012 and 2017. Also the scatter between measured and predicted radius is significant (Fig. 5). Indeed, as the GIS approach is effective on the decadal scale, the predictions for 2012 and 2017 were based on the bend records of approximately 10 years. The comparisons are presented in Table 4. As can be seen the time sequence maps gives a reasonably satisfactory prediction of the radius of the meander. From 1984 to 2017, migration rates of the Barak River ranged from 1.4 to 58.3 m/year, with a mean and standard deviation value of 13.01 m/year and 12.46 m/year, respectively, (Fig. 6).

5 Conclusion

In this study, three empirical equations Hooke [18], Brice [19], Nanson and Hickin [7] and time sequence extrapolation are used to predict the meander migration rates. 12 meandering reaches of the Barak River are considered using multiperiod Landsat remote sensing images to evaluate the accuracy of these methods by comparing predicted and measured migration. Comparisons made from the empirical methods indicate that Hooke and Brice's method are reasonably traditional. On the basis of this data alone, Nanson and Hickin method provides significant scatters, so this method is reasonably safe. For the radius of meander, satisfactory predictions were given by time sequence extrapolation method. This method is superior to empirical methods because it gives a complete position of the meander. However, time sequence extrapolation method is more operator dependent than the empirical methods. The author believes that this study will help in conducting the better planning of flood protection

Table 4 Predicted and measured radius for the best-fit meander circle

Reach No.	Year	Radius measured (m)	Radius predicted (m)	Reach No.	Year	Radius measured (m)	Radius predicted (m)
Reach-1	1984	1019		Reach-7	1984	532	
	1992	1093			1992	558	
	2002	745			2002	526	
	2012	719	397		2012	553	494
	2017	754	693		2017	518	566.5
Reach-2	1984	376		Reach-8	1984	1180	
	1992	478			1992	1237	
	2002	573			2002	1188	
	2012	576	668		2012	1085	1139
	2017	592	608		2017	1150	1003.5
Reach-3	1984	1050		Reach-9	1984	597	
	1992	1013			1992	571	
	2002	1238			2002	749	
	2012	1055	1463		2012	616	927
	2017	1064	963.5		2017	650	549.5
Reach-4	1984	492		Reach-10	1984	725	
	1992	524			1992	738	
	2002	498			2002	830	
	2012	474	472		2012	734	922
	2017	498	462		2017	729	686
Reach-5	1984	565		Reach-11	1984	826	
	1992	563			1992	679	
	2002	556			2002	625	
	2012	562	549		2012	685	571
	2017	557	565		2017	602	715
Reach-6	1984	550		Reach-12	1984	826	
	1992	582			1992	679	
	2002	565			2002	625	
	2012	563	548		2012	685	571
	2017	529	562		2017	602	715

works as such river channel changes pose serious social, economic and hydro system challenges to the river users and communities and also help the government in decision making, management and implementation of future projects. These effects may be prevented by efficient and well planning of settlements and to adopt some bank protection measures.

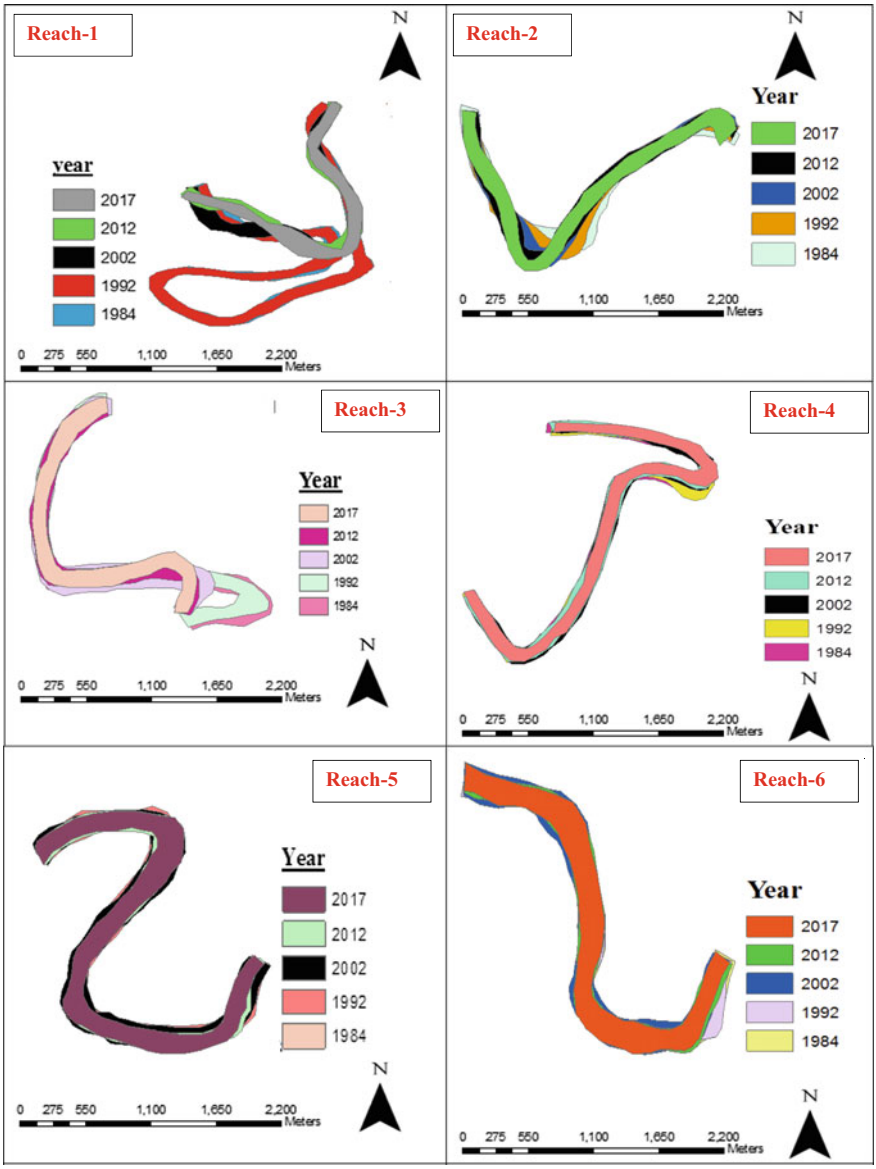

Fig. 6 Reach wise channel shifting of the Barak River for the period 1984–2017

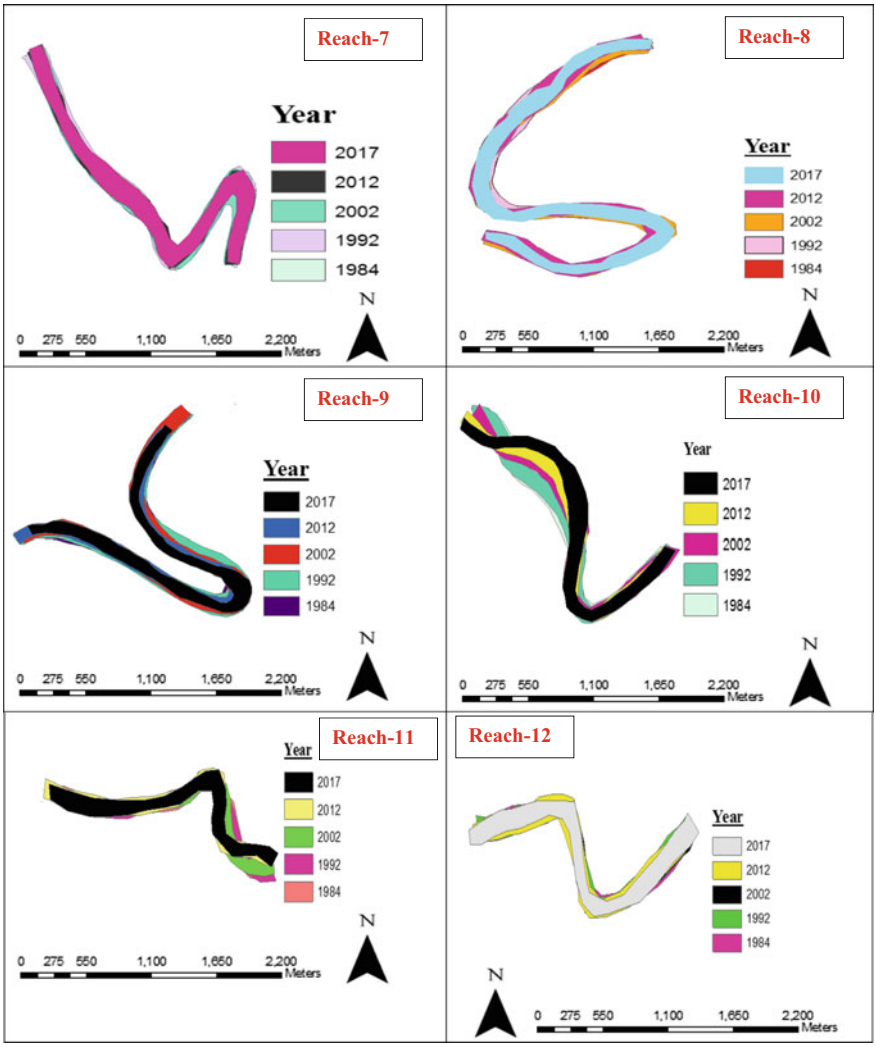

Fig. 6 (continued)

References

1. Dente E, Lensky NG, Morin E, Dunne T, Enzel Y (2019) Sinuosity evolution along an incising channel: new insights from the Jordan River response to the Dead Sea level fall. Earth Surf Proc Land 44(3):781–795
2. Batalla RJ, Iroumé A, Hernández M, Llena M, Mazzorana B, Vericat D (2018) Recent geomorphological evolution of a natural river channel in a Mediterranean Chilean basin. Geomorphology 303:322–337
3. Zaimes GN, Schultz RC, Isenhart TM (2004) Streambank erosion adjacent to riparian forest buffers, row-crop fields, and continuously-grazed pastures along Bear Creek in central Iowa. J Soil Water Conserv 59(1):19–27
4. Heitmuller FT, Hudson PF, Kesel RH (2017) Overbank sedimentation from the historic AD 2011 flood along the Lower Mississippi River, USA. Geology 45(2):107–110
5. Rosgen DL (2001) A hierarchical river stability/watershed-based sediment assessment methodology. In: Proceedings of 7th federal interagency sedimentation conference, March, Reno, Nevada
6. King AJ, Townsend SA, Douglas MM, Kennard MJ (2015) Implications of water extraction on the low-flow hydrology and ecology of tropical savannah rivers: an appraisal for northern Australia. Freshw Sci 34(2):741–758
7. Nanson GC, Hickin EJ (1983) Channel migration and incision on the Beatton River. J Hydraul Eng 117(7):942–946 (Discussion and Closure), ASCE, Reston, Virginia, USA
8. Ganguly S (1983) Geology and hydrocarbon prospects of Tripura Cachar-Mizoram region. Petrol Asia J 6(4):105–110
9. Ganguly S (1984) Tectonic evolution of the orogenic belt of Tripura. Q J Geol Min Metall Soc India 56(3):128–137
10. Brunnschweiler RO (1966) On the geology of the Indo-Burma Ranges. J Geol Soc Austral 13(1):137–194
11. Dutta TK, Saikia MM (1976) The eastern limit of the Himalayan Orogenic Belt—the Indo-Burman Orogen and its geodynamic development. Himalayan Geol 6:303–313
12. Evans P (1932) Tertiary succession in Assam. Trans Min Geol Inst India 27:155–260
13. Evans P (1964) Tectonic framework of Assam. J Geol Soc India 5:80–96
14. Mathur LP, Evans P (1964) Oil in India: International Geological Congress, 22nd session, India
15. Raju ATR (1968) Geological evolution of Assam and Cambay Tertiary basins of India. Bull Am Assoc Pet Geol 52(12):2422–2437
16. Seshavataram BTV, Nandi PK, Choudhury S (1998) Petroleum geology of Cachar fold belt. In: Proc. Reg. Sem. Dev. Geol. Res. in N.E. India, Gauhati University, pp 327–348
17. Nandy DR, Das Gupta S, Sarkar K, Ganguly A (1983) Tectonic evolution of Tripura-Mizoram fold belt, Surma Basin, northeast India. Q J Geol Min Metall Soc India 55(4):186–194
18. Hooke JM (1980) Magnitude and distribution of rates of river bank erosion. Earth Surf Process 5(2):143–157
19. Brice JC (1982) Stream channel stability assessment. Report No. FHWA/RD-82/021. Federal Highway Administration, Washington, DC, USA, p 41
20. Lagasse PF, Spitz WJ, Zevenbergen LW, Zachmann DW (2004) Handbook for predicting stream meander migration. Ayres Associates Inc., Fort Collins, Colorado, p 107

Identification of groundwater recharge potential zones using AHP and Fuzzy Logic: A blockwise study of western Purulia district, India

Sauvik Santra and Sujata Biswas

Abstract Managing groundwater resources, particularly under data-scarce and dry regions, involves a lot of difficulties and problems which have driven the planners to apply remote sensing (RS) and geographic information system (GIS) based procedures. In the present study, groundwater recharge potential zones are delineated by integrating the Analytic Hierarchy Process (AHP), GIS, and RS methods in five blocks of Purulia district, India. At first, the adequate thematic layers of factors impacting the groundwater recharge potential, such as drainage density, geomorphology, soil types, land use, geology, rainfall, slope, and lineament density, are extracted from sources like satellite imagery and collateral data. The AHP method is utilized to estimate the weights of different layers for applying the hierarchical fuzzy logic to identify potential zones for groundwater recharge. It is found that about 186.35 km^2 area has very good groundwater recharge potential (GRP), which is only 12.13% of the total study area. The area with good, average, and low GRP are about 359.08, 455.29, and 415.44 km^2 respectively. Analyzing the blockwise distribution of potential zones, it is found that Baghmundi block having 21.9% and 27.76% of its area under very good and good GRP zones respectively, is most suitable for blockwise implementation of groundwater recharge sites.

Keywords Groundwater · Fuzzy logic · AHP · India

1 Introduction

Water is one of the most vital resources for the existence of life on earth. From ancient times, groundwater is preferred over surface water as it is free from most of the pollutants, and its availability is more homogeneous than surface water. A

S. Santra
Department of Civil Engineering, Indian Institute of Technology Kharagpur, Kharagpur, India

S. Biswas (✉)
Department of Civil Engineering, Indian Institute of Engineering Science and Technology, Shibpur, Howrah, India
e-mail: sujata@civil.iiests.ac.in

C. Bhuiyan et al. (eds.), *Water Security and Sustainability*,
Lecture Notes in Civil Engineering 115,
https://doi.org/10.1007/978-981-15-9805-0_12

constant increase in demand for water leading to rapid growth in water consumption can be seen in recent years, whereas a relatively massive growth in consumption of groundwater over the surface water can be seen prior to 1990 [1].

This extracted groundwater must be recharged to maintain a steady groundwater level. Due to excessive usage, natural groundwater recharge has become insufficient to replenish the groundwater. As a result, the groundwater table has been depressed all over the world [2] and especially in India [3]. In some areas, it has even gone out of the feasible extraction range. This depression of groundwater level affected surface water, resulting in drying up of many rivers, lakes, and shallow water bodies in the last few decades. This has become an international crisis and an alarming concern for today's environmental scientists and water resources engineers. In India, specifically over the northern India, a steady lowering of the groundwater table is observed in the past few decades [4].

As a remedial step, we may use technology to replenish the depleted water level by using the concept of artificial groundwater recharge. Today many researchers are trying to find a proper place, method, and amount of groundwater recharge to mitigate the crisis. As a handy tool for analyzing the large area, remote sensing (RS) and geographic information system (GIS) are playing an important role in these studies.

Utilization of remote sensing and GIS for the exploration of groundwater and the identification of artificial recharge sites can be found in much earlier studies. Data from Linear Imaging Selfscanning Sensor (LISS-II) onboard Indian Remote Sensing Satellites (IRS-1A, 1B and P2) was combined with the information derived from digital elevation model (DEM) using GIS to find the suitable sites for groundwater recharge over the hard rock terrain in the Sironj area of Vidisha district of Madhya Pradesh, India [5]. A similar technique was used to determine groundwater recharge potential zones in Lebanon, where lineament and drainage density, karstic domains, land cover, and lithologic character were determined using satellite images (Landsat 7 ETM & SPOT) and aerial photographs, further integrating them in GIS [6]. Thematic maps constructed merging LISS-III and panchromatic (PAN) remote sensing data and aquifer parameters from field data were integrated using GIS to create a map of groundwater recharge potential zones over the Jammu district, India [7]. Weighted thematic layers of five contributing factors, lithology, land cover, lineaments, drainage, and slope derived using aerial photographs, geology maps, and a land-use database were combined using GIS to delineate groundwater recharge potential zones in Taiwan [8]. With the development of modern computational techniques and the availability of updated computational resources, a scope was created to refine the results from the approaches mentioned above using soft computing. One of the initial studies using an integrated approach to combine GIS with a decision support system (DSS) for the delineation of groundwater recharge potential sites was carried out by [9] over the Meimeh Basin, Iran.

The next big change took place when GIS was combined with numerical modeling techniques to delineate the groundwater recharge potential zones in the arid region of Maknassy basin, Tunisia [10]. A combination of RS, GIS, and multi-criteria decision-making (MCDM) techniques using normalized weights computed using

Saaty's Analytic Hierarchy Process (AHP) was used to delineate artificial recharge zones as well as to identify favorable artificial recharge sites in the West Medinipur district of West Bengal, India [11]. A study over a sub-watershed of River Kanhan, in Nagpur District, Maharashtra, India, was carried out in GIS using the land use, soil types, topography, and rainfall-runoff model data, where AHP with expert's judgment was used for ranking the sites [12]. The next advancement in the method came when [13] coupled GIS with MCDM using fuzzy rules to yield more precise results in selecting the site for managed aquifer recharge.

Later on, [14] used modern satellite imagery to revise the GIS and AHP coupling techniques. In current years, software to process high-resolution satellite data has been improved drastically. [15] used high-resolution layers to find out groundwater (GW) recharge potential zones using AHP. A combination of state-of-the-art groundwater potential mapping (GPM) tool C5.0 along with random forest (RF), and multivariate adaptive regression splines (MARS) algorithms were used recently for generating GPMs in the eastern part of Mashhad Plain, Iran [16]. Other known machine learning-based methods adopted in recent studies include boosted regression tree (BRT), classification and regression tree (CART), support vector machine (SVM), and genetic algorithm optimized random forest (RFGA) [17, 18]. A sensitivity analysis of the effect of sample size on the accuracy of different individual and hybrid models (i.e., adaptive neuro-fuzzy inference system (ANFIS), ANFIS-imperial competitive algorithm (ANFIS-ICA), alternating decision tree (ADT), and random forest (RF)) was carried out by [19].

Although very effective and accurate machine learning and artificial intelligence-based GIS techniques are adopted in current studies, the accuracy and efficiency of most of the approaches heavily depend on the available data size and accuracy. However, most of the areas of acute groundwater depletion problem in the Indian subcontinent suffer from the scarcity of accurate and updated spatial data of most of the critical parameters. Hence, we wanted to evaluate the applicability of a relatively simple and computationally inexpensive approach to delineate the groundwater potential zones with minimal available data. For the present study, AHP is used as a scientific tool to estimate weightage, coupled with a simple Mamdani-based hierarchical fuzzy controller to delineate groundwater recharge potential zones over a data-scarce area.

Purulia district of West Bengal is one of the most water-scarce areas of India. Although this district receives 1400 mm of average rainfall during the monsoon season, most of the precipitation disappears through Kumari and Kangsabati river systems as runoff. Low retention capacity of the soil and the presence of hard crystalline rocks beneath the ground create constraints to groundwater development in the area. In the present study, an endeavor has been made to delineate groundwater recharge potential zones in some severely water-scarce blocks of Purulia district of West Bengal using GIS and fuzzy logic techniques to overcome the limitations due to unavailability of ground-based observational data.

2 Study Area

The study area mainly follows the river Subarnarekha, a major river on the western part of Purulia district. Subarnarekha flows through two blocks of Purulia district, Jhalda-I and Baghmundi. In the present study, three adjacent blocks, Jhalda-II, Joypur, and Balarampur are also taken, as these blocks also have groundwater scarcity [1]. The areal extent of the study area is 1549.13 km^2 lying between 23º North to 23º36" North in latitude and 85º48'36" East to 86º19'12" East in longitude.

Subarnarekha is known for its flash floods during the monsoon season. But with contrast, it is also the river basin having the lowest groundwater potential with a groundwater potential of 1.82 bcm (lowest among all the rivers of India) [20]. Average rainfall in the area remains minimal throughout the year except during the monsoon period. Residents of the area, therefore, depend mostly on the available groundwater for their daily needs as well as irrigation. As a natural outcome, groundwater is being depleted very fast [21, 22]. In the past few years, irregularity of rainfall joined the fleet, and the area is going through a severe groundwater crisis [23].

3 Methodology

Some physical methods like groundwater depth, bore well data, soil type, slope, local status, availability of land, presence of harmful metals and chemicals nearby, presence of industry, and presence of harmful organic substances are used for selection of appropriate recharge site in localized studies. But to select those recharge sites on a large scale, the analysis may be done using GIS. Among the different aspects of using GIS, the basic difference is in the selection of layer used and method adopted to obtain the final output.

In the present study, soil type, drainage density, lineament density, geology, geomorphology, land-use type, and rainfall data are used as layers, and analytic hierarchical process (AHP) [24] is used to calculate the weight of each of the individual layers as the input of the hierarchical fuzzy logic. Finally, hierarchical fuzzy logic is used through a total of seven steps to finding the output layer.

The district block boundary map of Purulia is collected from [24] at a scale of 1:2,50,000. From this map, an area has been extracted, taking five blocks (Fig. 1).

3.1 Analysis of Digital Elevation Model

3.1.1 Digital Elevation Model

Digital elevation model (DEM) is a 3D representation of a terrain's surface created from terrain elevation data. From satellite data, latitude and longitude of the

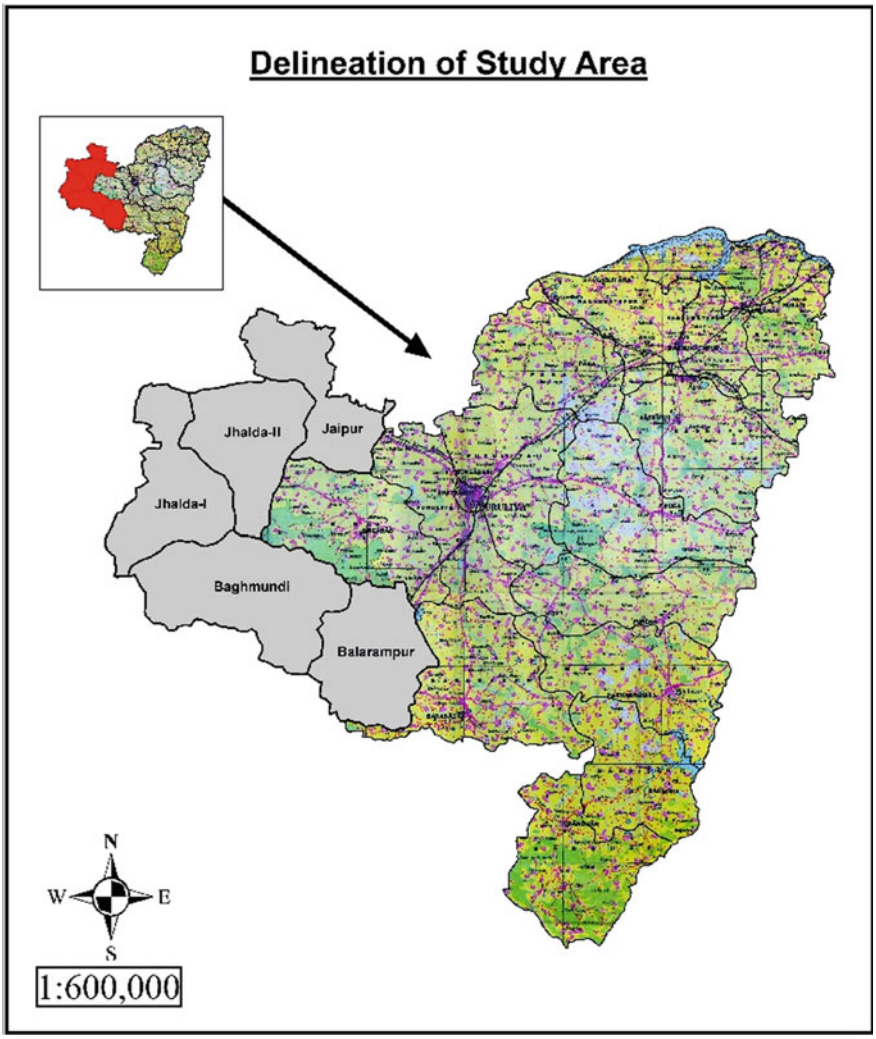

Fig. 1 Selected study area

boundary points are calculated. Using these coordinates, the digital elevation model is downloaded from [25]. This DEM is then geo-corrected and mosaicked together (Fig. 2).

3.1.2 Preparation of Slope Map

The slope is the measure of steepness or the magnitude of inclination of a plane relative to the horizontal plane, typically expressed as a percentage. Slope plays

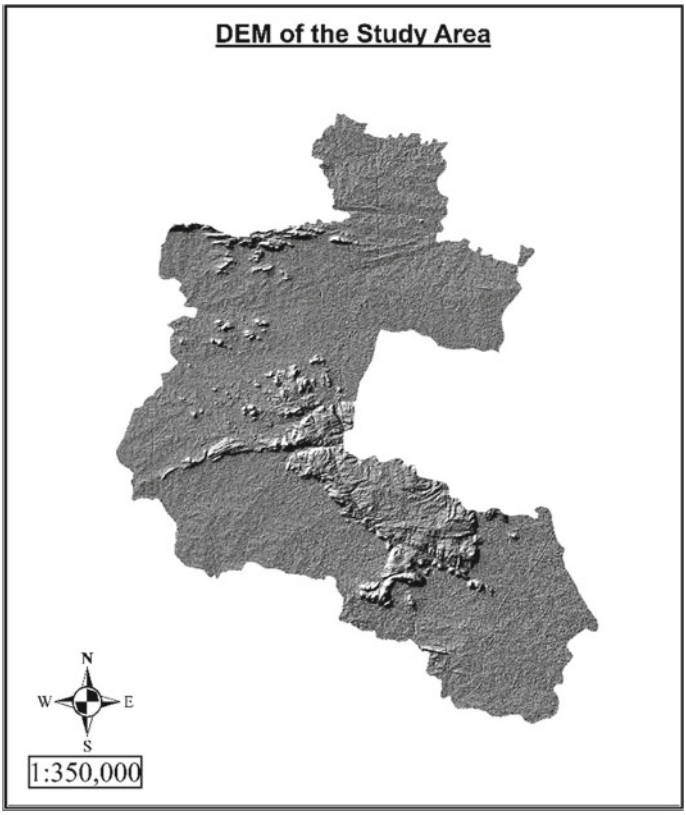

Fig. 2 DEM of the study area

a significant part in governing the hydrological balance of terrain, influencing the orientation and volume of surface runoff and subsurface drainage approaching a site. It also determines the duration and velocity of surface flow, subsurface flow, and amount of infiltration [26]. Steep slope generates more runoff, and less infiltration takes place. However, if the slope is less, more infiltration or recharge will take place, decreasing the runoff amount [27]. DEM is used to generate a slope map to observe the topographic attributes (slope aspects and steepness), which facilitate the evaluation of the variables affecting the presence and flow of groundwater in the area. The slope (Fig. 9), ranging from 0 to 57°, is categorized into five classes.

3.1.3 Preparation of Drainage Map

The drainage map of the study area is derived from DEM using ArcGIS software. This obtained drainage map shows that rivers and channels flow toward east and west from the central axis of the study area. This drainage map is then validated by lying it

over the satellite image of the study area to see if the generated river channels overlap with the actual ones. The process of generating a drainage map starts with the creation of 'Fill'. After the DEM is extracted, it had to be ensured that it had no erroneous depressions. So it is filled using GIS software tools. The depressionless DEM is then used to calculate the probable flow direction in the region. Flow direction is important while working with hydrological modeling, because in order to calculate the drainage network in a watershed, it is essential to determine the direction of flow in each cell of the area. This is done by calculating the relative slope between each cell of the DEM.

The cells with the greatest accumulated flow have been chosen and then converted into a flow accumulation grid, based on the flow direction (Fig. 3). The drainage

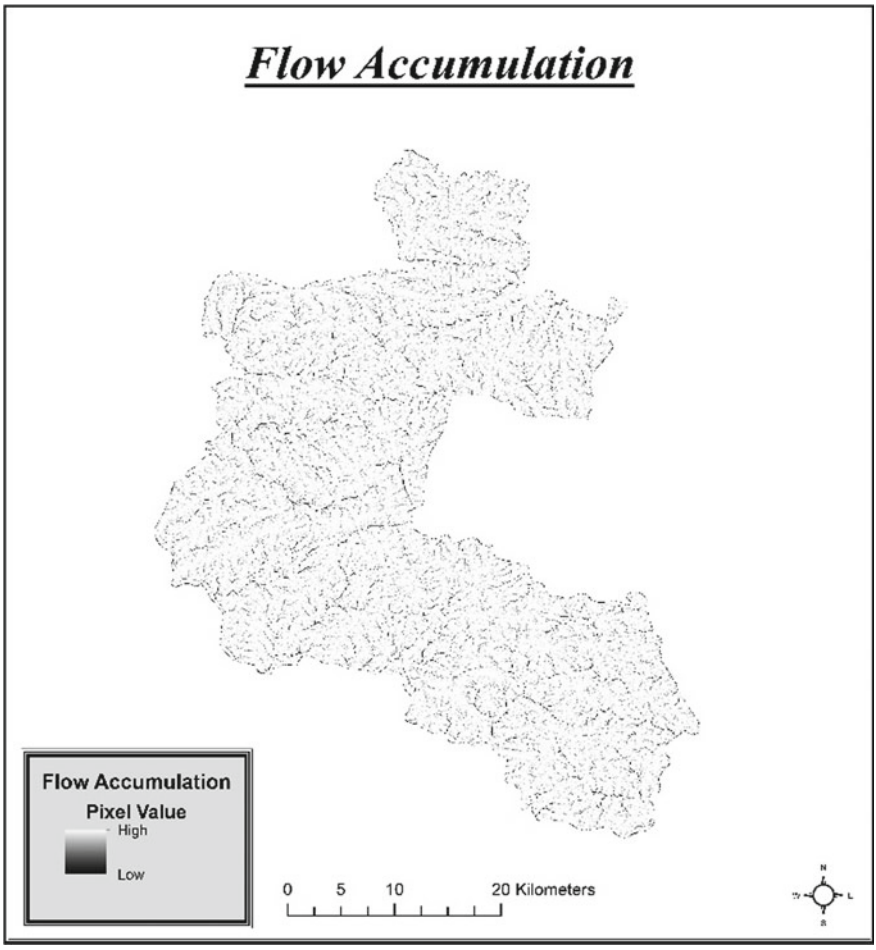

Fig. 3 Flow accumulation map of the area

network in the area is derived from the flow accumulation layer. This method for the creation of a drainage map from flow accumulation works on the probabilistic approach and gives value for each possible flow line. These flow lines are used to delineate possible streamlines. These generated rivers are then validated using the satellite datasets [28]. After the validation, the GIS-based approach is used to classify the rivers into ascending orders (Fig. 4, as rivers having higher-order have a higher contribution in drainage through that area leading to a high rate of infiltration. Universal Transverse Mercator Coordinate system (WGS 1984 UTM Zone 45N) is used to vectorize the flow features in order to quantify the streamflow feature according to respective lengths.

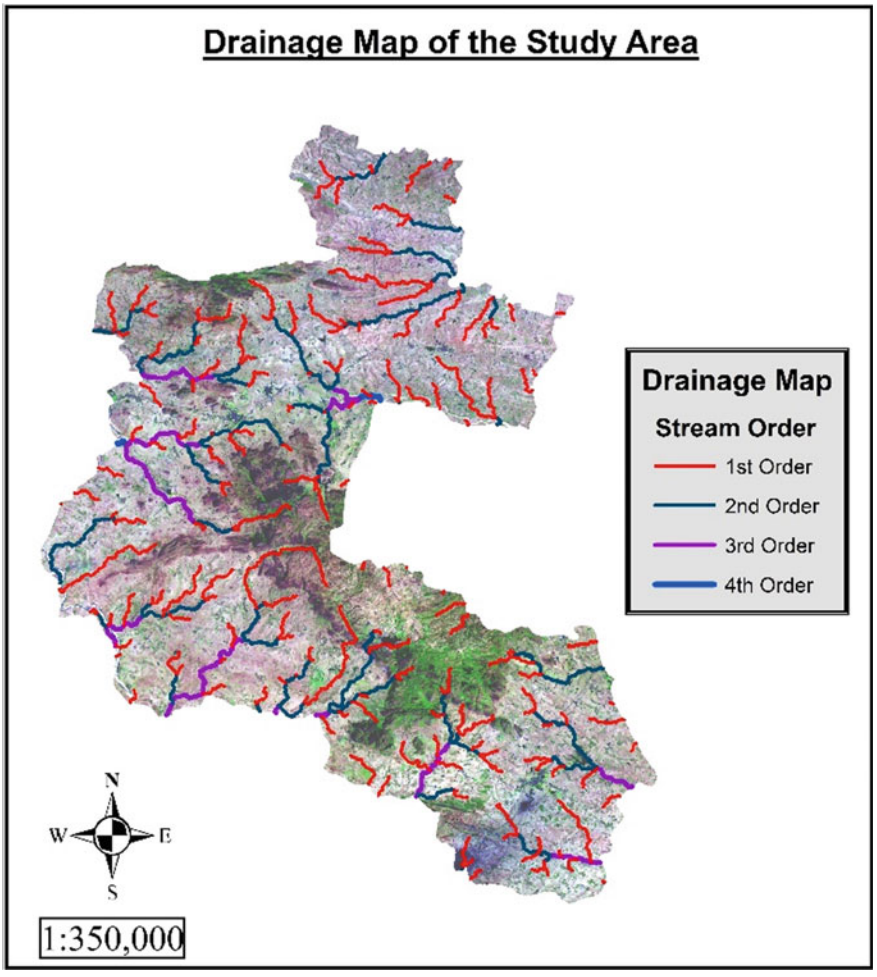

Fig. 4 Drainage map of the area

3.1.4 Preparation of Drainage Density Map

Drainage density is the length of all the streams per unit area of a drainage basin. $D_d = L/A$, where D_d = drainage density of the area, L = total length of the drainage channel in the study area (m), and A = areal extent of the study area (m^2). It reflects how properly or how poorly a watershed is drained by stream channels. The impact of drainage density on infiltration can be considered from two different aspects. If the river is of a lower order, it contributes mainly to drainage, leading to a lower rate of infiltration. On the other hand, for higher-order rivers, more infiltration takes place due to less slope of the terrain and more availability of water. Drainage density for the area is calculated using GIS (Fig. 10).

3.1.5 Preparation of Lineament Density Map

In the rocky areas, the occurrence and movement of groundwater depend mainly on the permeability resulting from the lineament of the area due to faulting, fracturing, etc. Lineament is an essential parameter in calculating the groundwater recharge potential as it indirectly gives knowledge about the storage and movement of groundwater. Straight stream valleys and aligned segments of a valley are typical geomorphological expressions of lineaments. In this study, after stream ordering, a surface lineament map is prepared from the drainage map. The drainage lines having stream order one, which is parallel to each other, are delineated as features of lineament.

In the present study area, the lineament density ranges from 0 to 3 m/m^2. Particularly in the north, south, and southwest parts of the study area, the density range from 0.5 to 2.5 $m/m^{2,}$ and these sites are considered as potential zones for groundwater recharge as these sites are most suitable for infiltration of surface water into the ground. Those areas, which have a lineament density of less than 0.5 m/m^2, are not suitable for groundwater recharge (Fig. 11).

3.2 Mapping with Remote Sensing and GIS Techniques

IRS-P6 LISS-III satellite image of Purulia district (dated March 8, 2011) is collected (Fig. 5). Satellite images can be used to verify several artificially generated data. It can also be used as an input to generate some further map layers.

3.2.1 Preparation of Land-Use Map

The extracted satellite image is classified according to land use. For this, we followed a supervised classification technique. In supervised classification, some training polygons are created to train computer about the type of land cover. The maximum likelihood supervised classification technique is then applied using ArcGIS to get an

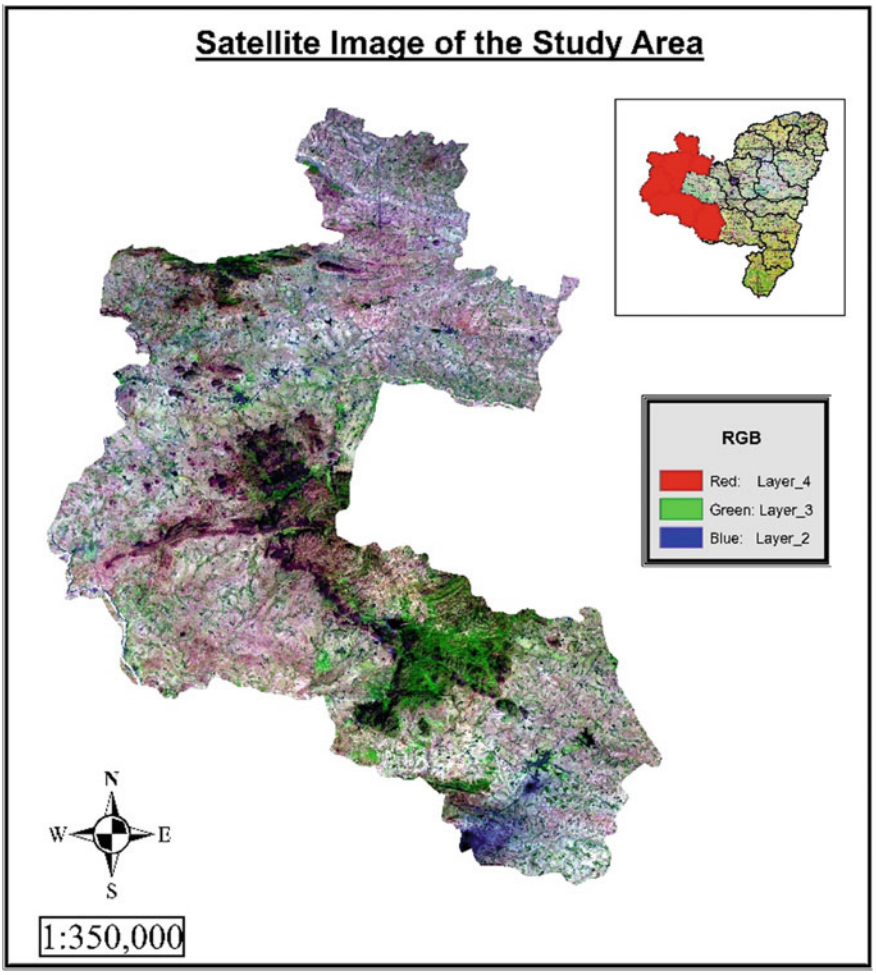

Fig. 5 Satellite image of the area

output image that is classified into four sets of land-use types (Fig. 12; Table 1), 1. dense forest, 2. agricultural land, 3. water bodies, and 4. bare land.

Table 1 Land-use type

Land-use type	Dense forest	Agricultural land	Water body	Bare land
Area (km^2)	472.5	545.17	3.33	521.33

3.2.2 Preparation of Soil Map

Soil plays an important role in the infiltration rate of an area. This again directly affects groundwater recharge potential of that area. Different soils have different infiltration rates. So, it is important to prepare a soil map of the study area, which has been derived from the National Bureau of Soil Survey and Land Use Planning (ICAR) at a scale of 1:500,000. There are five types of soil (Fig. 6) present in the area,

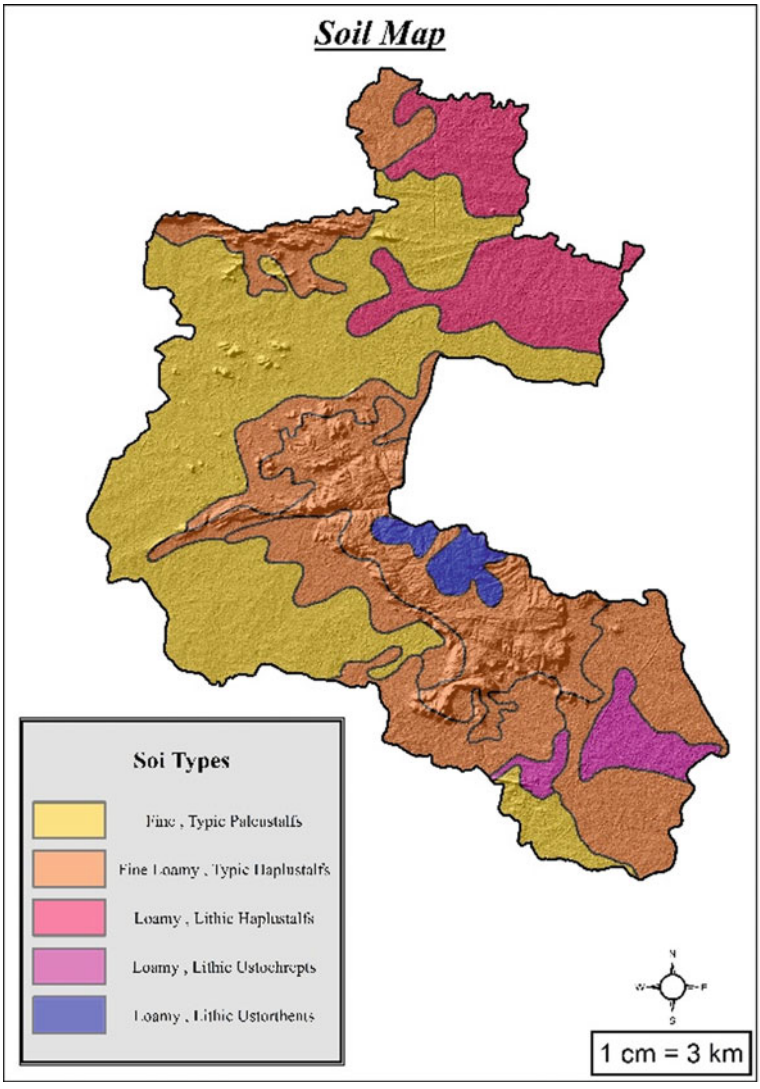

Fig. 6 Soil map of the area

Table 2 Soil types of the area

Type of soil	Soil code as per ICAR	Area covered (km^2)
Ustochrepts (Loamy)	W093, W095	64.02
Haplustalfs (Loamy)	W096	191.15
Haplustalfs (Fine Loamy)	W091, W094, W102	657.71
Paleustalfs (Fine)	W104	602.54
Ustorthents (Loamy)	W092	32.74

i.e., Paleustalfs (Fine), Haplustalfs (Fine Loamy), Haplustalfs (Loamy), Ustochrepts (Loamy), and Ustorthents (Loamy) (Table 2).

3.2.3 Preparation of Geology Map

Geology of an area plays a vital role in this study. Several rock formations give an idea about the groundwater depth and subsurface flow characteristics. The map has been prepared from the Geological Survey of India at a scale of 1:250,000. After extracting the study area from the map, a vector layer is created over it to get the characteristics and area of each geology type (Fig. 7).

3.2.4 Preparation of Geomorphology Map

Geomorphology tells us about the creation and transformation of topographic and bathymetric features created by physical, chemical, or biological processes operating at or near the earth's surface. Geomorphology map is obtained from the Geological Survey of India at a scale of 1:1,000,000, which is then georeferenced, and the study area is extracted. After vectorization, the final geomorphology thematic layer map is prepared (Fig. 8).

3.2.5 Rainfall Distribution Map

Rainfall is the main contributor for artificial recharge. Areas with more rainfall are naturally more suitable for artificial recharge sites. Rainfall data for the area is downloaded from ECMWF [29]. This is utilized to develop the rainfall distribution map using the Inverse Distance Weighted (IDW) interpolation technique in the ArcGIS spatial analyst tool.

Inverse distance weighted (IDW) interpolation is a technique based on the assumption that objects closer to each other are more identical than those which are more separated. The measured values around the prediction location have a more significant impact on the forecasted value than those farther away. It gives higher importance to points closest to the forecast location, and the weights decrease as a function

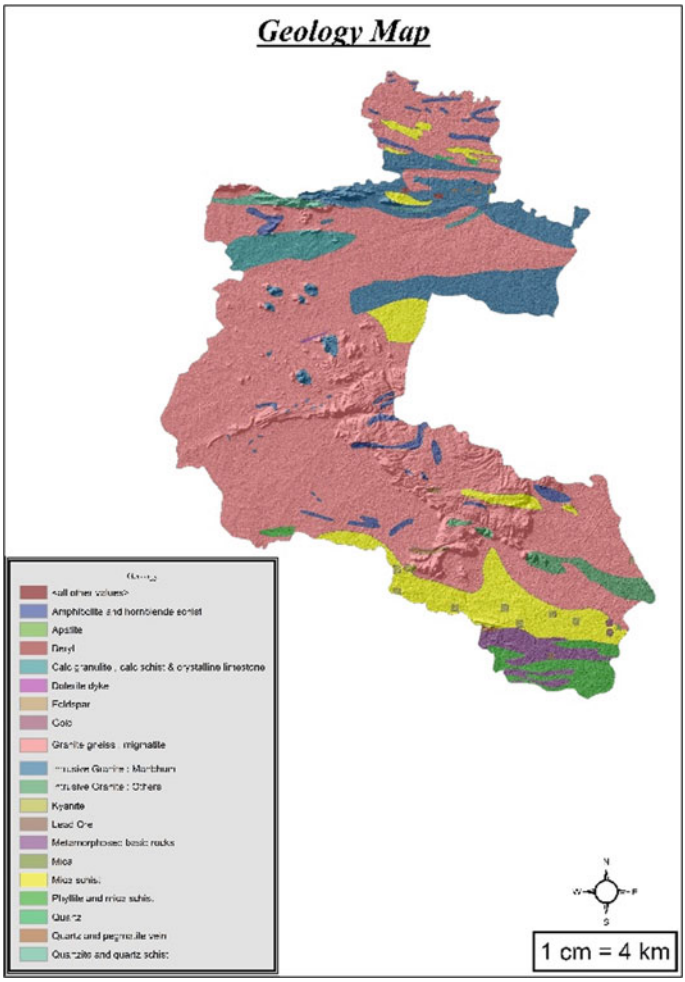

Fig. 7 Geology map of the area

of distance. Result of the IDW analysis of rainfall distribution is further used as a thematic layer in the calculation (Fig. 13).

3.3 Hierarchical Fuzzy Logic

Fuzzy logic is a tool to deal with uncertainty where normal probability theory fails to work due to large computational expensiveness. Fuzzy logic takes into account all the possible combinations of inputs and possible outcomes for each case. It then considers the possible fuzziness of the output and gives a more humanlike response

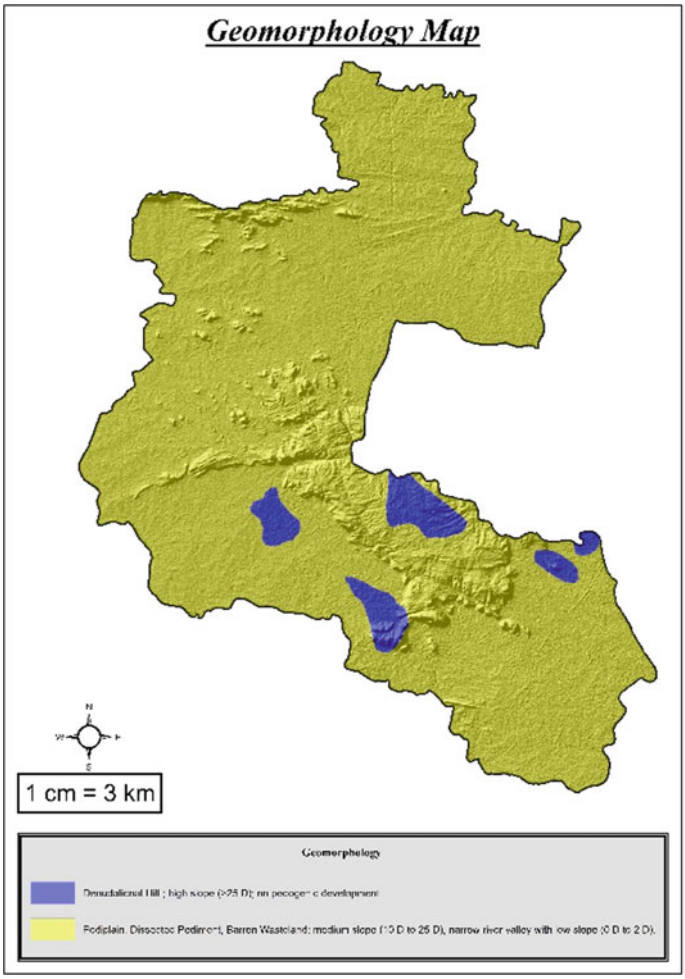

Fig. 8 Geomorphology map of the area

toward the problem. The main problem with the fuzzy sets is the number of rules (predefined relations between input set and output) increase exponentially with the number of inputs used. To overcome this shortcoming, hierarchical fuzzy logic (HFL) is introduced where inputs are sorted according to relative importance, and then fuzzy logic-based calculations are carried out stepwise. Here, we have used the same approach, and to find the initial relative weights among the parameters, AHP is used.

3.3.1 Analytic Hierarchy Process (AHP)

AHP is a mathematical, matrix-based technique, widely used as a decision-making tool in various complex methods. It helps to capture both subjective and objective aspects of a decision. Hierarchical structures have been used here to represent a complex problem and develop local priorities for alternatives based on the judgment of the user, and then synthesizes the results for the calculation of global priorities [24].

AHP, as a weight estimating technique, enables decision-makers to derive weights rather than assign them arbitrarily. AHP maintains complexity and suitable judgment while allowing both objective and subjective considerations to be incorporated in the decision-making process [30].

(i.) The dominant objective is specified first as a goal
(ii.) The goal is then broken down step by step into more specific objectives that can further be broken down into subobjectives:
(iii.) The attributes lie at the tip of the hierarchy.

3.3.2 Applying AHP in Present Study

In the present study, AHP proposed by [24] is applied to determine the weights. The AHP method used here has four steps of calculations.

- Creating pairwise comparison matrix;
- Finding highest eigenvalue and then right eigenvector for each criterion;
- Normalizing right eigenvector to delineate weight for individual layers;
- Checking for consistency.

3.3.3 Deriving Pairwise Comparison Matrix

The AHP pairwise matrix is developed by putting relevant importance value for each criterion involved in the present study. The relative importance values are defined with the Saaty's 1 to 9 scale, where a score of 1 denotes equal weight between the two cases, and a score of 9 means the absolute importance of one case compared to the other one [24]. An unbiased opinion is taken from each of the individuals of a three-member expert panel. The average of three individual datasets is then used as the base pairwise comparison matrix. Table 3 represents the pairwise comparison matrix obtained based on average expert opinion using Saaty's nine-point importance scale used to calculate relative weights for the thematic layers.

Table 3 Pairwise comparison matrix

	Drainage density	Geomorphology	Soil	Land use	Geology	Rainfall	Slope	Lineament density
Drainage density	1	¼	3	6	1/2	4	5	2
Geomorphology	4	1	6	9	3	7	8	5
Soil	1/3	1/6	1	4	1/4	2	3	½
Land use	1/6	1/9	1/4	1	1/7	1/3	½	1/5
Geology	2	1/3	4	7	1	5	6	3
Rainfall	¼	1/7	1/2	3	1/5	1	2	1/3
Slope	1/5	1/8	1/3	2	1/6	1/2	1	¼
Lineament density	½	1/5	2	5	1/3	3	4	1

Table 4 Right eigenvectors of the thematic layer parameters

	Eigenvector	Normalized weight
Drainage density	−0.299	0.144
Geomorphology	−0.804	0.3867
Soil	−0.137	0.0658
Land use	−0.046	0.0221
Geology	−0.434	0.2087
Rainfall	−0.092	0.0442
Slope	−0.064	0.0309
Lineament density	−0.203	0.0976
Sum	**−2.08**	**1**

3.3.4 Evaluation of Eigenvalue Analysis

AHP captures the idea of uncertainty in judgments through the principal eigenvalue and the consistency index [31]. In the present study, maximum eigenvalue and corresponding right eigenvector are calculated for the pairwise comparison matrix shown above; the maximum eigenvalue is 8.3458721. The resultant right eigenvector is shown in Table 4.

3.3.5 Normalizing Right Eigenvector to delineate weight for individual layers

In the final step of AHP analysis, the normalized weights are computed from the corresponding eigenvector values using the formula as mentioned below.

$$Normalized\ Weight = \frac{Eigenvector\ value\ of\ a\ feature\ class}{Sum\ of\ all\ the\ Eigenvectors}$$

These normalized weights are then used for sorting the inputs for calculations using HFL.

3.3.6 Checking for Consistency

Saaty's eigenvector method is used to find out the consistency ratio (CR) for errors in the judgment of parameter weights. CR is calculated using the formula:

$$C.R. = \frac{C.I.}{R.I.} \tag{1}$$

where CI represents for consistency index, derived using the formula.

$$C.I. = \frac{\lambda_{\max} - n}{n - 1} \tag{2}$$

and RI stands for ratio index, the value of which is specified by Saaty (Table 5), where n is the number of parameters, hence 8.

If the value of CR is less than 0.1, then it is accepted, whereas for CR values greater than 0.1, reconsideration of judgments is required. In our case, the CR value is 0.035, which is well below the permissible limit.

Table 5 Saaty's ratio index for different number of parameters (n)

n	R.I.
1	0
2	0
3	0.58
4	0.89
5	1.12
6	1.24
7	1.32
8	1.41
9	1.45
10	1.49

Table 6 Design of hierarchical fuzzy logic controller

Stage	INPUT 1	INPUT 2
Stage 1	Geomorphology	Geology
Stage 2	Output of Stage 1	Drainage density
Stage 3	Output of Stage 2	Lineament density
Stage 4	Output of Stage 3	Soil
Stage 5	Output of Stage 4	Rainfall
Stage 6	Output of Stage 5	Slope
Stage 7	Output of Stage 6	Land use

3.3.7 Applying Hierarchical Fuzzy Logic

After the satisfactory estimation of the final weighted sequence for the input parameters through the application of AHP, calculation through HFL is implemented. As discussed earlier, to reduce the computational load, the total fuzzy logic controllers are divided into a total of seven stages to form an HFL, namely stage 1 through stage 7.

Gaussian distribution is applied to each of the stages, and two stages are fuzzified using the Mamdani approach at each level. The distribution of levels is presented in Table 6. Each of the feature maps is classified in a total of five levels of groundwater potential, namely very poor, poor, average, high, and very high. Final values are calculated by defuzzification of the fuzzy membership values from the output of stage 7 using the small of maximum (SOM) method of defuzzification. Defuzzified fuzzy membership values (FMV) corresponding to the suitability of groundwater recharge range from 0 to 1 (‘0’ being the least suitable and ‘1’ being the most suitable). The study area is categorized into five groundwater recharge potential zones, namely very poor ($0 \leq \text{FMV} \leq 0.125$), poor ($0.125 < \text{FMV} \leq 0.375$), moderate ($0.375 < \text{FMV} \leq 0.625$), good ($0.625 < \text{FMV} \leq 0.875$), and very good ($0.875 < \text{FMV} \leq 1$).

4 Results and Discussions

The spatial distribution map of slope, drainage density, and lineament density using the digital elevation model is presented in Figs. 9, 10, and 11, respectively. The spatial distribution map of land-use types estimated through the application of remote sensing using a high-resolution satellite image of the study area is presented in Fig. 12. The spatial map of IDW analysis of rainfall distribution is shown in Fig. 13. The final output from the fuzzy AHP analysis is plotted in GIS to obtain the spatial map showing different types of potential zones (Fig. 14).

From the output map (Fig. 14), it is observed that most of the high groundwater recharge potential zones lie in the northeast and central part of the study area. In Table 7 below, the area under each potential zone is shown, and the blockwise distribution

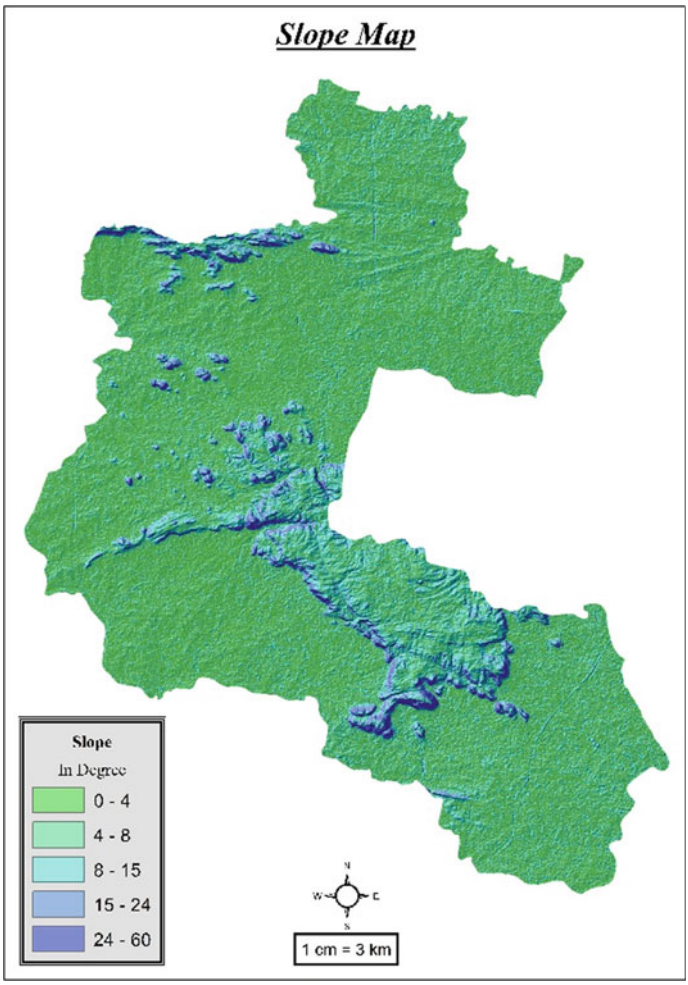

Fig. 9 Slope map of the area

of area is shown in Table 8. The table highlights that the recharge potential zones are spread among all the blocks, though Baghmundi block has the best potential for groundwater recharge having 21.9% and 27.76% of its area under very good and good recharge potential zone, respectively.

In this study, a fuzzy-based method that maintains the relativistic influence of various thematic layers and their corresponding classes affecting groundwater has been adopted to predict groundwater recharge potential zones of the area. Five blocks of Purulia district of West Bengal are chosen as the study area and eight thematic layers, viz. geomorphology, land use, density of drainage network, soil types, geology, rainfall, slope, and lineament density, have been incorporated for estimating groundwater recharge potential zones. Results indicate that 12.13% of

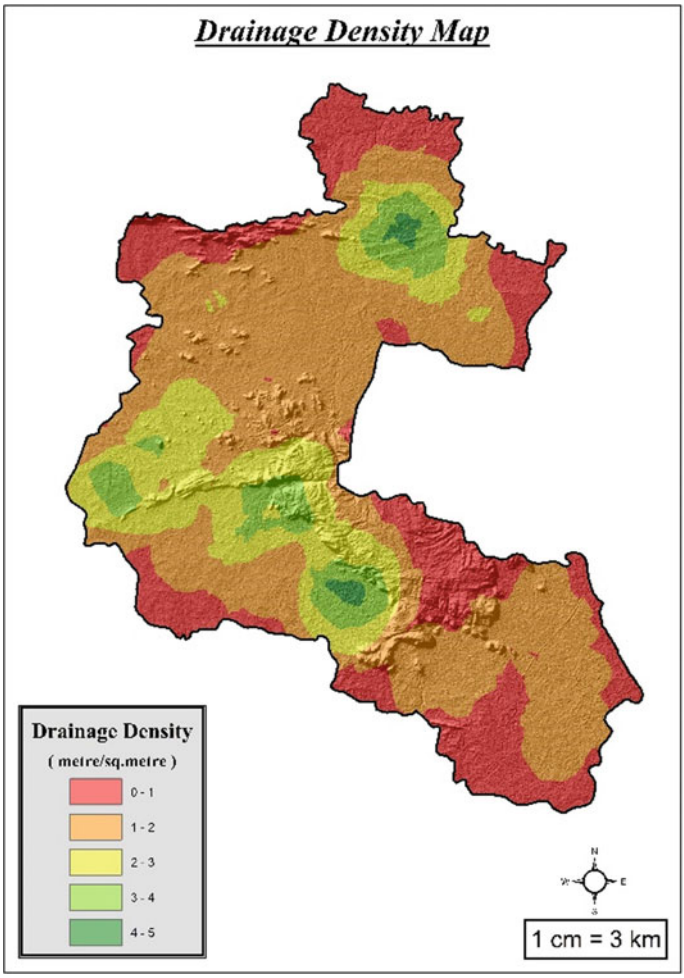

Fig. 10 Drainage density map of the area

the area has very good groundwater recharge potential, and 29.37% of the area is designated as having good groundwater recharge potential, with over 29.64% being moderate and 27.04% area has poor groundwater recharge potential. 7.82% of the area has very poor groundwater recharge potential.

From blockwise statistics, it is seen that Baghmundi block has the highest percentage of area suitable for groundwater recharge. This block has 21.9% of its area, having very good and 27.76% of its area having good groundwater recharge potential. It can be seen that areas with dense forest, higher lineament density, and soil type having a high infiltration rate have been detected to be having very good recharge potential.

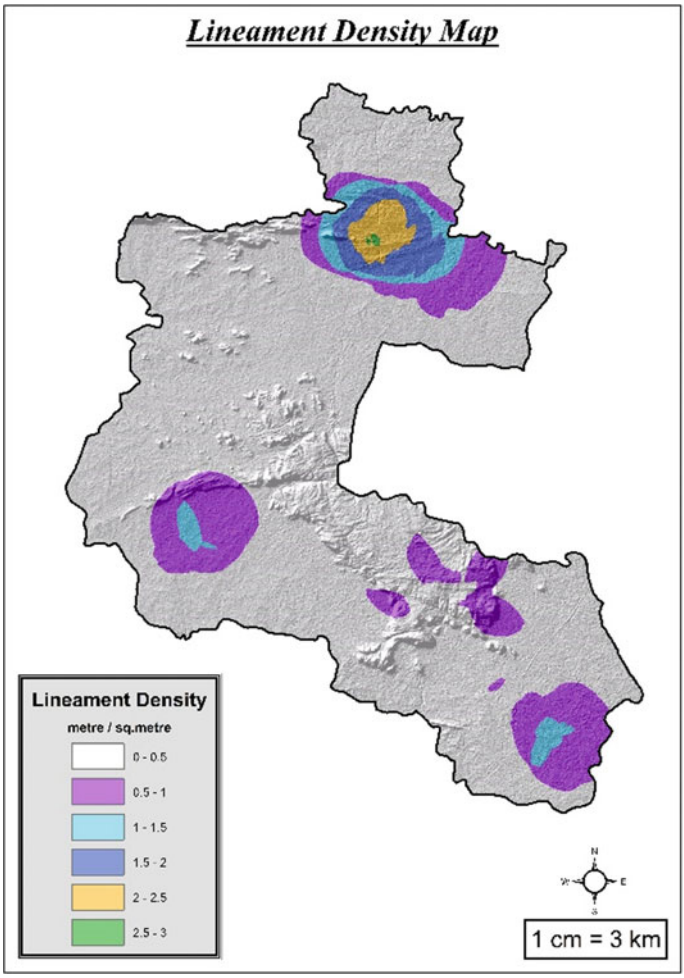

Fig. 11 Lineament density map of the area

The area under study is one of the areas to have the minimal presence of ground-based data, thus inhibiting any past study over the region. Although this study exhibits the efficacy of a coupled yet simple numerical approach to delineate groundwater potential zones, the availability of more observational data over the region is expected to aid the approach in both the accuracy and viability aspect.

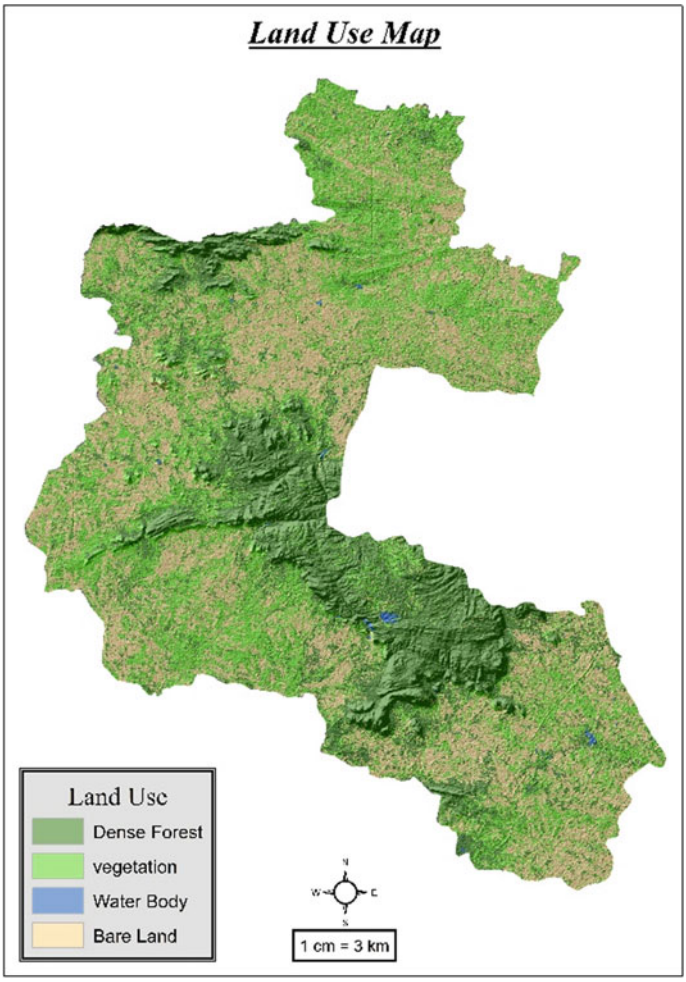

Fig. 12 Land-use types over the area

5 Conclusion

The present research has shown the abilities of AHP with geoinformatics coupled with fuzzy logic techniques for the identification of groundwater recharge potential zones, specifically over a data-scarce region. Based on the results of this research, it can be concluded that the applied methodology is a valuable framework for the prompt evaluation of groundwater recharge potential and can be suggested to be implemented in other areas, especially in areas having insufficient ground data. Therefore, the outcome of this study can also be utilized for developing irrigation facilities in the future, which in turn will accelerate the crop production. The study

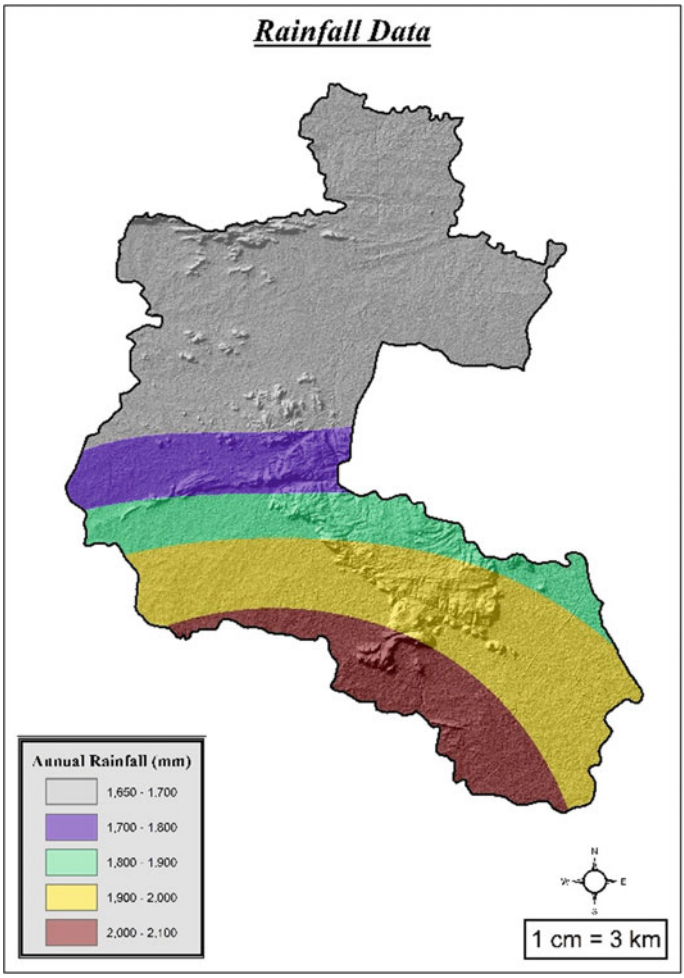

Fig. 13 Rainfall distribution map of the area

will be helpful for adopting suitable sites for water harvesting structures. Thus, the study is expected to lead to a good path for future planning of water resources in the blocks of the Purulia district.

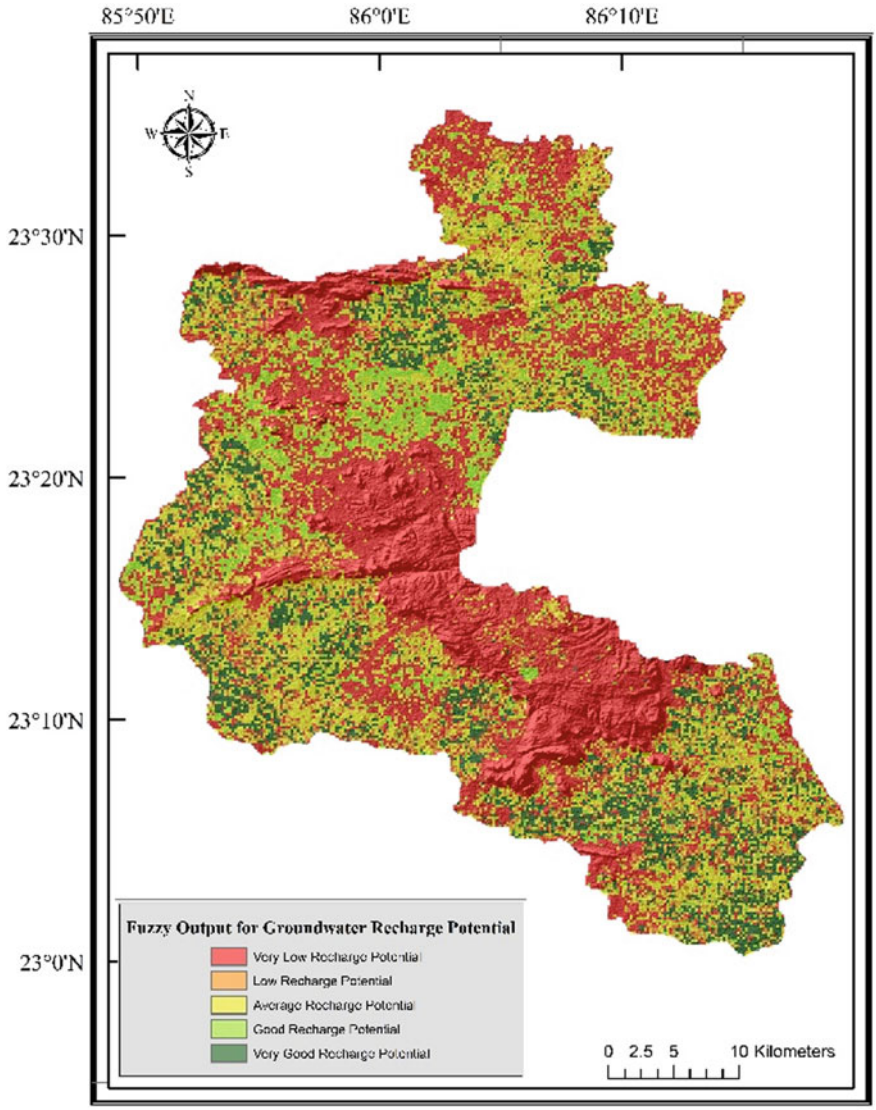

Fig. 14 Final fuzzy output for the area

Table 7 Percentage and area under each potential zone

Potential zones	Area (km^2)	Percentage of area
Very low	120.08	7.82 %
Low	415.44	27.04 %
Average	455.29	29.64 %
High	359.08	23.37 %
Very high	186.35	12.13 %
Total area = 1536.24 km^2		

Table 8 Blockwise area statistics

	Balarampur (%)	Baghmundi (%)	Jhalda-I (%)	Jhalda-II (%)	Jaipur (%)
Very low	8.22	6.04	6.32	6.11	14.08
Low	27.51	18.43	25.64	34.05	34.96
Average	37.82	25.87	34.32	32.81	16.71
High	24.58	27.76	29.09	13.63	18.93
Very high	1.87	21.9	4.63	13.40	15.32

References

1. Wada Y, Wisser D, Bierkens M (2014) Earth Syst Dyn 5:15
2. Wada Y, van Beek LP, van Kempen CM, Reckman JW, Vasak S, Bierkens MF (2010) Global depletion of groundwater resources. Geophys Res Lett 37(20)
3. Rodell M, Velicogna I, Famiglietti JS (2009) Nature 460:999–1002
4. Tiwari V, Wahr J, Swenson S (2009) Dwindling groundwater resources in northern India, from satellite gravity observations. Geophys Res Lett 36(18)
5. Saraf A, Choudhury P (1998) Int J Remote Sens 19:1825–1841
6. Shaban A, Khawlie M, Abdallah C (2006) Hydrogeol J 14:433–443
7. Jasrotia A, Kumar R, Saraf A (2007) Int J Remote Sens 28:5019–5036
8. Yeh HF, Lee CH, Hsu KC, Chang PH (2009) Environ Geol 58:185–195
9. Ghayoumian J, Ghermezcheshme B, Feiznia S, Noroozi AA (2005) Environ Geol 47:493–500
10. Chenini I, Mammou AB (2010) Comput Geosci 36:801–817
11. Chowdhury A, Jha MK, Chowdary V (2010) Environ Earth Sci 59:1209
12. Sargaonkar AP, Rathi B, Baile A (2011) Environ Earth Sci 62:1099–1108
13. Mahmoud SH, Alazba A et al (2014) Water Resour Manag 28:3319–3340
14. Kaliraj S, Chandrasekar N, Magesh N (2014) Arab J Geosci 7:1385–1401
15. Mahmoud SH (2014) Environ Earth Sci 72:3429–3442
16. Golkarian A, Naghibi SA, Kalantar B, Pradhan B (2018) Environ Monit Assess 190:149
17. Naghibi SA, Pourghasemi HR, Dixon B (2016) Environ Monit Assess 188:44
18. Naghibi SA, Ahmadi K, Daneshi A (2017) Water Resour Manag 31:2761–2775
19. Moghaddam DD, Rahmati O, Panahi M, Tiefenbacher J, Darabi H, Haghizadeh A, Haghighi AT, Nalivan OA, Bui DT (2020) Catena 187:104421
20. IWRS 2015 Indias water resources at a glance. http://www.iwrs.org.in/iwr.html
21. Nag S, Kundu A (2018) Appl Water Sci 8:38
22. Ghosh PK, Jana NC (2018) Sustain Water Resour Manag 4:583–599
23. Ghosh MK, Dutta MK, Saaty T (1977) J Math Psychol 15:234–281

25. GSI S EH, Rajarajan K (1976) A manual of the geology of India and Burma (Manager of Publications)
26. Eosdis N (2015) Aster GDEM of spatial resolution 30m from earth observation system data and information system. NASA. http://reverb.echo.nasa.gov/reverb
27. Ng C, Zhan L, Bao C, Fredlund D, Gong B (2003) Geotechnique 53:143–157
28. Ibbitt R, Henderson R, Copeland J, Wratt D (2000) J Hydrol 239:19–32
29. ISRO 2011 Irs-p6 liss-iii satellite image of Purulia district from Bhuvan. ISRO. http://bhuvan.nrsc.gov.in/bhuvan_links.php. Accessed 8th Mar 2011
30. Dee DP, Uppala S, Simmons A, Berrisford P, Poli P, Kobayashi S, Andrae U, Balmaseda M, Balsamo G, Bauer P et al (2011) Q J R Meteorol Soc 137:553–597
31. Forman EH (1983) Proceedings of the IEEE Computer society
32. Saaty TL (2004) J Syst Sci Syst Eng 13:1–3511

Simulation of Runoff for Subarnarekha Catchment Using SWAT Model

R. Murmu and S. Murmu

Abstract This paper is based on Soil and Water Assessment Tool (SWAT) which is a hydrological model that integrates the Geographic Information System (GIS) with the attribute database to simulate runoff. SWAT Model is basically executed in association with ArcGIS as ArcSWAT. The study area taken is Subarnarekha River which flows through the eastern part of India over the states of Jharkhand, West Bengal, and Odisha. In this paper, Digital Elevation Model (DEM) has been used for delineating the catchment area. Remote sensing data has been used as input in ArcSWAT for delineation of catchment area determination of drainage pattern, land use/land cover, slope, etc. To develop landuse/landcover map the satellite imagery from Landsat 8 was acquired and the soil map for the study area was obtained from Harmonized World Soil Database (HWSD) Raster world soil map. Hydrological Response Unit (HRU) analysis was performed which resulted in 25 subbasins and 194 HRUs. Then by using 11 years of daily rainfall data, SWAT simulation has been performed to estimate the monthly and yearly runoff for their respective rainfall. The annual rainfall-runoff of the Subarnarekha River from 2005 to 2015 has been plotted and found the maximum rainfall of 1811.62 mm and runoff of 595.65 mm is in the year 2007. The reliable accuracy of the model has been checked with the assessment of the model performance as with the rainfall-runoff correlation coefficient which was found to be 0.971.

Keywords Hydrologic modelling · SWAT · Rainfall · Runoff

1 Introduction

Runoff received by a stream from its catchment area is a crucial water resources planning and management. The runoff from catchments of rivers may be determined either by direct measurement of discharge through rivers or it may be estimated in an

R. Murmu · S. Murmu (✉)
Department of Civil Engineering, Indian Institute of Engineering Science and Technology, Shibpur, Howrah 711103, WB, India
e-mail: sneha@civil.iiests.ac.in

C. Bhuiyan et al. (eds.), *Water Security and Sustainability*,
Lecture Notes in Civil Engineering 115,
https://doi.org/10.1007/978-981-15-9805-0_13

indirect manner. For estimation of quantity and rate of the surface runoff accurately from land surface into streams and rivers is difficult and time consuming. The estimated runoff can be used further to assess the likelihood and aspects of flooding. The manner in which different variables affecting runoff interacts with time and space makes the direct determination of runoff very difficult. Therefore, we estimate runoff using methods that reflect the combine effect of the variables on an individual catchment. The conventional methods of predicting runoff can be augmented by incorporation of satellite imaging technology in the field of hydrology. Remote sensing technology is the most reliable and potent technique to derive spatial information on land use, soil, vegetation, drainage, etc., from satellite data which can be used to interpret runoff. These data can be incorporated with the conventionally measured topographic and climatic parameters like precipitation and temperature to contribute the rainfall-runoff models as inputs. Additionally, Geographical Information System (GIS) is a powerful tool for input of remotely sensed data into database, further processing and retrieval of selected information which can analyze/manipulate the data to generate useful spatial information on specific format. Thus, the emergences and advances of remote sensing and GIS in a combined manner can provide a new perspective to rainfall-runoff studies. This paper aims to simulate runoff for Subarnarekha catchment using Soil and Water Assessment Tool (SWAT) Model. This model is capable of forecasting the possible impacts of climate change, and the effects that cause changes on water resources due to human activities, in form of both quantity and quality [1]. GIS-based ArcSWAT model has been used for simulation of runoff with the required weather parameters of 30 years with a good correlation coefficient result [2]. Development of watershed simulation models with reliable accuracy including calibration and validation of the results is a challenging task [3]. Accurately validated SWAT Models can be useful for decision making problems for watershed planning [4]. This model can also help in predicting hydrologic variables like coefficient of runoff, baseflow and evapotranspiration as well as comparative analysis with the observed data can be done after successful outcome [5]. Performances of SWAT and Xinanjiang (XAJ) models have been compared using ten year daily runoff data from four different gauging stations, which shows reasonably good runoff simulation from both the models [6].

2 Materials and Methods

2.1 Area Under Study

The present study has been conducted for the upper part of Subarnarekha river basin which is a part of the Chotanagpur River system, a plateau in the eastern part of India. The river Subarnarekha originates near Nagri village in the Ranchi district and flows over the states of Jharkhand, West Bengal and Odisha before joining the Bay of Bengal. The river is having a total catchment area of 18,951 km^2 surrounded by

the Chotanagpur plateau, Baitarani river catchment, Kangsabati river catchment and the Bay of Bengal. A part of Subarnarekha basin has been chosen for the present study covering its gauging station of Gopiballavpur, located in the West Midnapur District of West Bengal. The gauging station at Gopiballavpur has been considered as the outlet of the catchment area. The total extent of the catchment under study covers 11,394.152 km^2 area which ranges from longitude 85° 31′ to 87° 22′ E and from latitude 22° 7′ to 23° 28′N. The geographical location of the study area is shown in 'Fig. 1.'

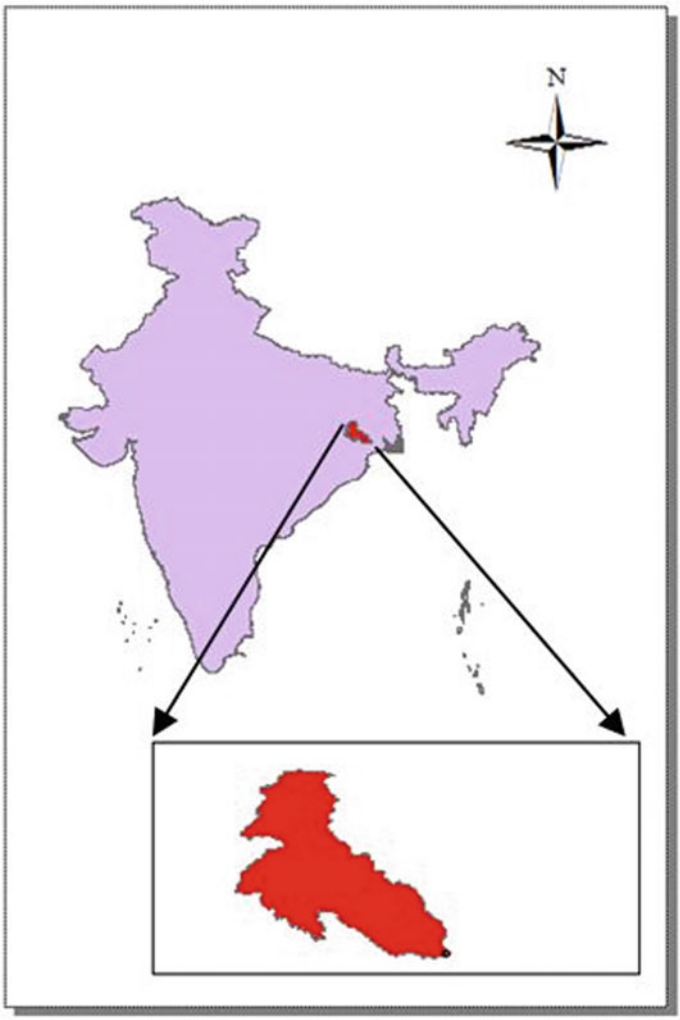

Fig. 1 Location of study area

The Subarnarekha basin falls in the tropical monsoon climate region with a marked hot and dry season, with a pronounced monsoon season, and a mild winter season. Rainfall received by the river comes during the monsoon, which spans from the month of June to August. The season of the retreating monsoon experiences mild rainfall and sometimes tropical cyclones that occur from September to November.

3 Model Setup

The SWAT model is a physically based distributed parameter model which has been developed to predict runoff, erosion, sediment and nutrient transport from a catchment developed by the USDA Agricultural Research Service. In this model, prediction of runoff as well as pre and post-processing of runoff is carried out using a number of spatially varied dataset, i.e., topography, soils, land cover, and weather. The ArcSWAT interface package in ArcGIS was used to setup the model. The model simulation was conducted on the basis of delineation of catchment area using the Digital Elevation Model (DEM) data, preparation of the input data using soil, slope, land use, Hydrologic Response Unit (HRU) definition weather data definition. Finally, it was run to obtain the output.

3.1 Watershed Delineation

For delineating the catchment area ASTER GDEM acquired from https://earthexplorer.usgs.gov/ with spatial resolution 30 m has been used. The watershed delineator tab in ArcSWAT was used to define the basin and subbasins for the river under study based on the DEM as input. At this stage, few steps were followed in which flow direction, flow accumulation, stream definition maps were developed to obtain subsequent stream network utilizing DEM, and finally, the outlet point was defined (at Gopiballavpur gauging station) to for the development of the catchment. The entire catchment with a total area of 11,394.152 km^2 has been divided into twenty-one sub-catchments to represent its spatial variability 'Fig. 2.'

3.1.1 Landuse Classification

Analyzing the effect of land use and land cover (LULC)practices on the hydrological response of a watershed is important as the distribution and land cover class affect the rate of infiltration, runoff, and thus the volume of total surface runoff at the outlet. Image classification is done using supervised classification technique using Landsat 8 image. The landuse are classified into five classes, i.e., Sand, Forest, River, Reservoir, Agricultural land and Fallow land. In 'Fig. 3,' the classified LULC map has been shown.

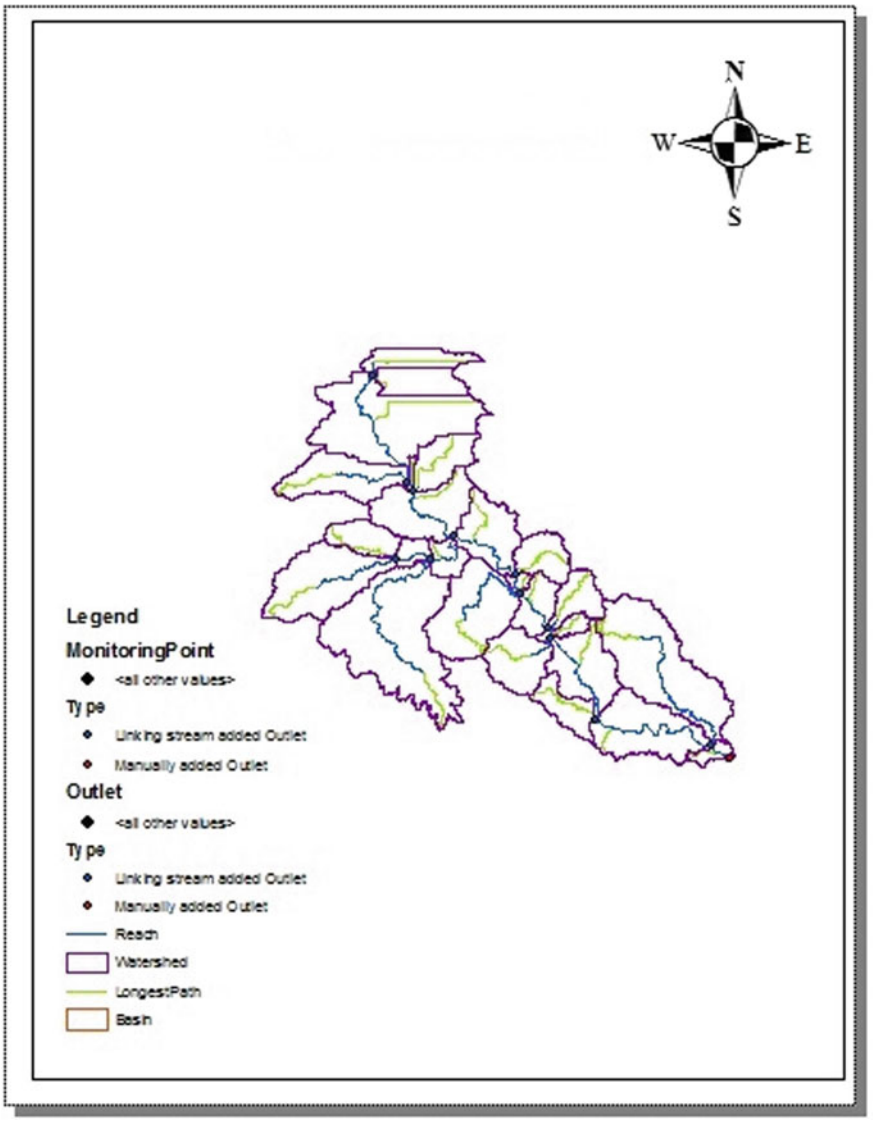

Fig. 2 Sub-catchments of Subarnarekha

3.1.2 Soil Classification

In the catchment, red sandy soil and lateritic soils are found to be the dominant soil types. Soil map is prepared using Harmonized World Soil Database (HWSD)

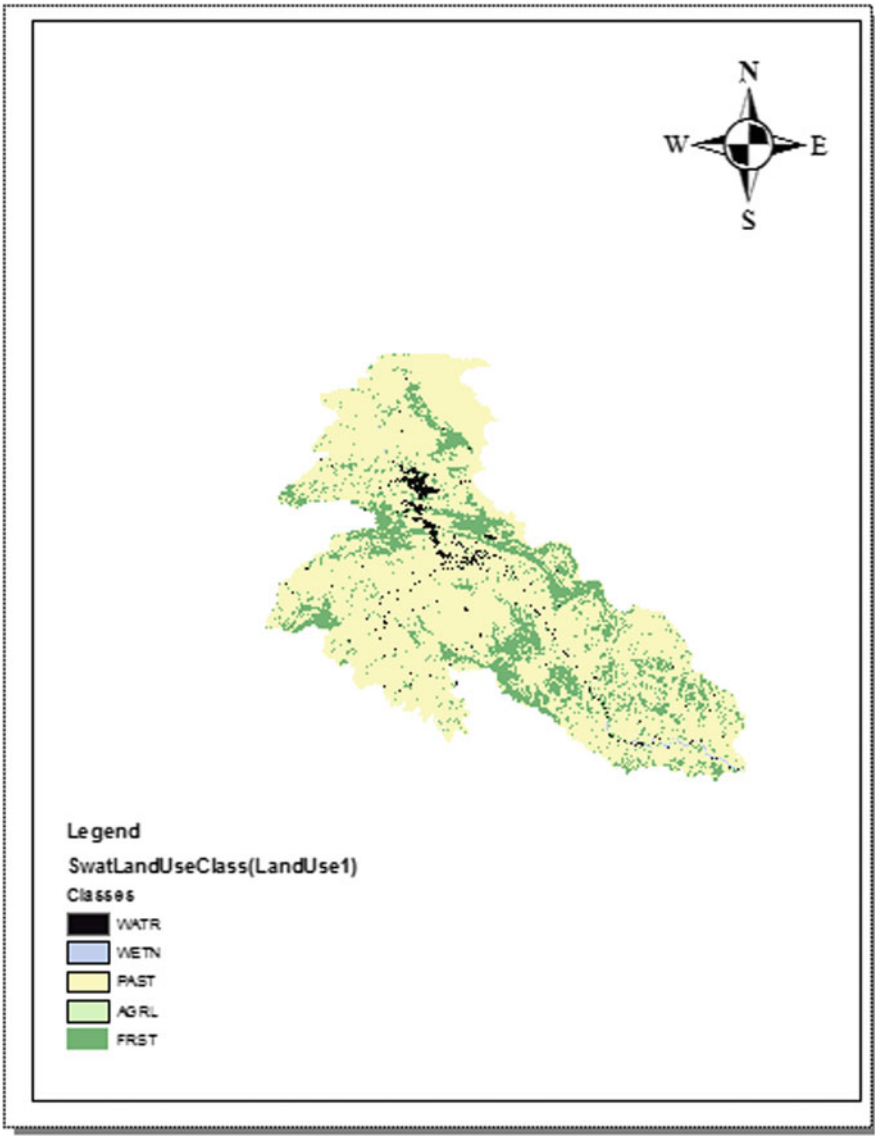

Fig. 3 Landuse map

data from http://webarchive.iiasa.ac.at/Research/LUC/External-Worldsoil-database/HTML/ shown in 'Fig. 4.' Four types of soil were identified in the study area based on their infiltration rates.

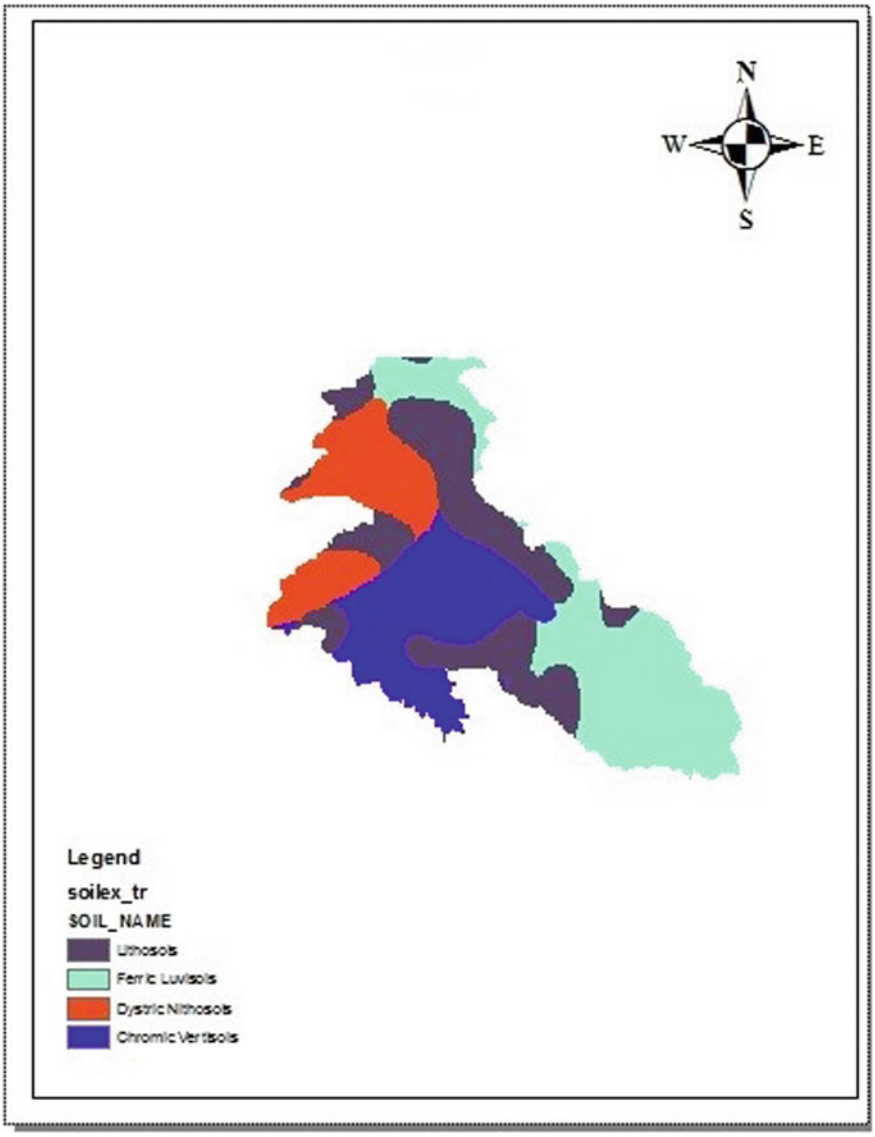

Fig. 4 Soil map

3.1.3 Slope Classification

As the study area is comprised of different slope characteristics in between the beginning and the end point upto its outlet at Gopiballavpur of the river divided by the length of the river. The slope map is prepared using DEM in five different classes 'Fig. 5.' The slope of this catchment is divided into five classes, that is 0–3%,

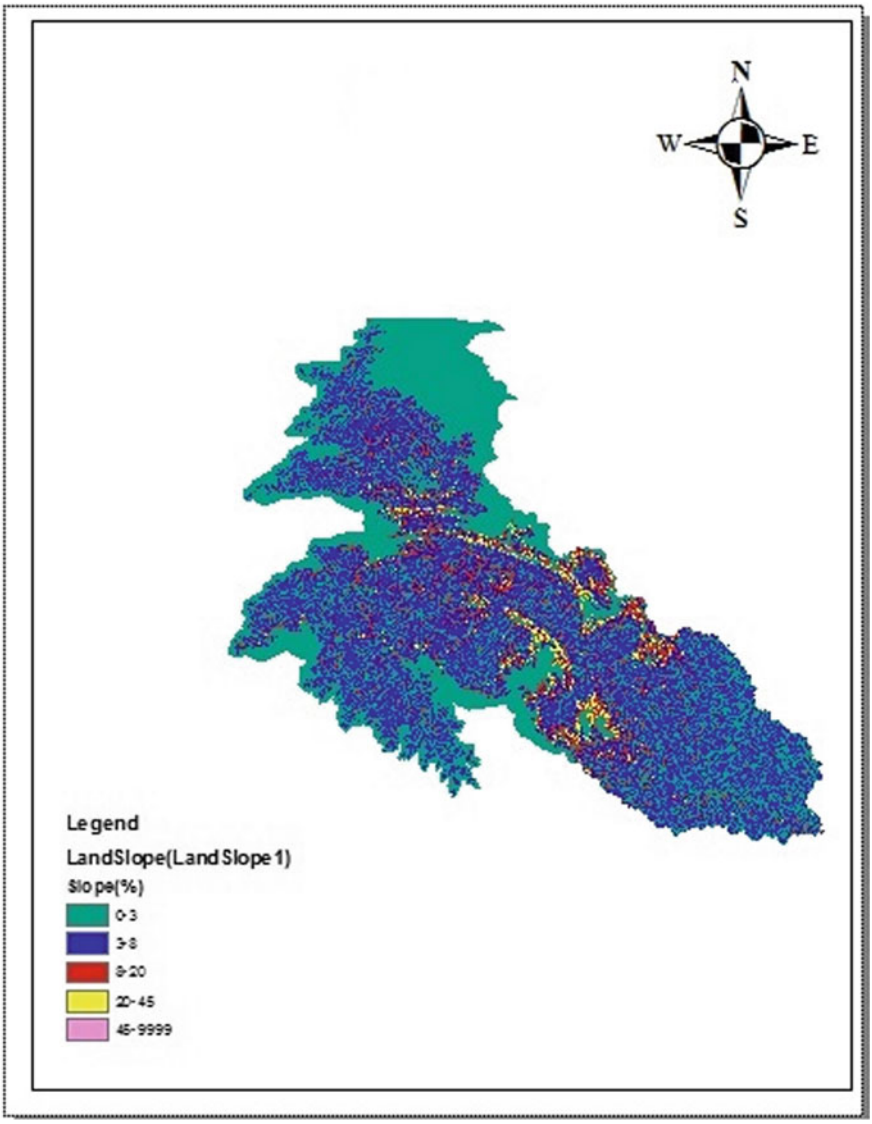

Fig. 5 Slope map

3–8%, 8–20%, 20–45% and above 45%. Threshold value for all landuse, soil class, and slope class is taken as 10% to create HRU analysis report. In the HRU analysis report, the watershed is divided into 25 subwatersheds and 194 HRUs.

3.2 Hydro-Meteorological Data

The model uses daily weather data of rainfall, maximum and minimum temperature, solar radiation, relative humidity and wind speed for modeling and simulation. Here 11 years' (1976 to 2005) daily rainfall data has been collected from Indian Meteorological Department (IMD) at an interval of 0.5° for 90 stations. In ArcSWAT, the user is allowed to load the spatial location of each weather station and allocate the data to the sub-catchments. The other weather parameters, i.e., maximum and minimum temperature, wind speed, solar radiation, and humidity, have been acquired through the weather generator tool of ArcSWAT model while weighted average of the gridded rainfall data over the catchment area was fed into the model.

Prediction of runoff in SWAT model can be performed either using the Soil Conservation Services Curve Number method (SCS, 1972) or Green and Ampt infiltration method (1911). In the present study, SCS CN method has been applied. Finally, SWAT simulation was performed to accomplish the input database for ArcSWAT model and run the model for monthly as well as yearly basis.

4 Results and Discussion

The relationship between hydrologic process like a rainfall event and its relationship with the runoff resulting from it is a complex one because of the presence of a number of climatic and catchment factors affecting the transformation of runoff from rainfall. This paper aims to represent the framework of SWAT model for modeling of the rainfall-runoff process. 11 years (2005–2015) of 0.25 gridded daily rainfall data of 90 stations is used in this study. SWAT simulation was performed in yearly and monthly basis. The annual average runoff for given annual average rainfall is shown in Table 1. In the present study, the maximum runoff has been found in the year 2007 and the minimum runoff in the year 2010. The monthly average rainfall for the 11 years data and the corresponding runoff has also been estimated with the help of this model is shown in Table 2. The graphical representation of the annual and monthly average rainfall-runoff values has been shown in 'Figs. 6 and 7.' The correlation between rainfall-runoff has been performed with the 11 years data resulting in a remarkable correlation with r^2 value of 0.9716.

5 Conclusion

SWAT model produced good simulation results of the study area for both monthly and annual runoff. Assessment of the model performance has been accomplished in conjunction with the statistical coefficients with observed correlation coefficient of 0.971. In this study, remote sensing data helped a lot by serving the input data

Table 1 Annual average rainfall-runoff

Year	Rainfall mm	Runoff mm
2005	1151.52	220.73
2006	1673.39	519.3
2007	1811.62	595.65
2008	1521.09	410.62
2009	1312	286.3
2010	943.38	123.14
2011	1732.25	543.72
2012	1367.92	269.93
2013	1784.57	525.9
2014	1302.44	282.97
2015	1341.98	311.77

Table 2 Monthly average rainfall-runoff

Year	Rainfall mm	Runoff mm
Jan	16.0	0.94
Feb	18.48	0.59
Mar	19.53	0.26
Apr	38.35	2.04
May	105.94	16.32
Jun	234.61	71.86
Jul	347.86	99.26
Aug	291.67	73.71
Sep	265.79	80.73
Oct	92.61	25.00
Nov	10.65	0.62
Dec	9.60	0.56

for obtaining the catchment and sub-catchments of the river under study through drainage pattern of the area. Also satellite data from Landsat 8 has been classified to prepare the land use/land cover map for the catchment. These data can be integrated with GIS and can be effectively used for projects related to watershed planning and management. In this model, GIS came across as a dynamic tool for the construction of the input, i.e., land use, soil, weather data needed by ArcSWAT and also for simulation of runoff. Validation of the results for monthly and annual runoff values could have been executed with observed runoff during that period. The annual rainfall-runoff of the Subarnarekha River catchment in 11 years has been estimated and found the maximum rainfall of 1811.62 mm and runoff of 595.65 mm is in the year 2007. This river had crossed its previous Highest Flood Level (HFL) of 12.2 m (40 ft) in 2007 in

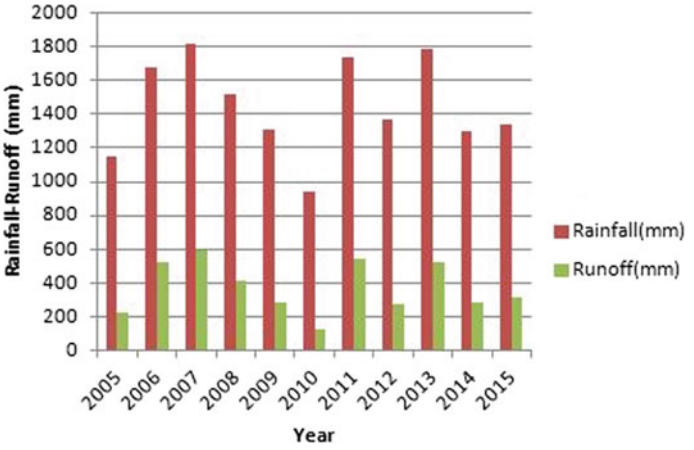

Fig. 6 Annual average rainfall-runoff

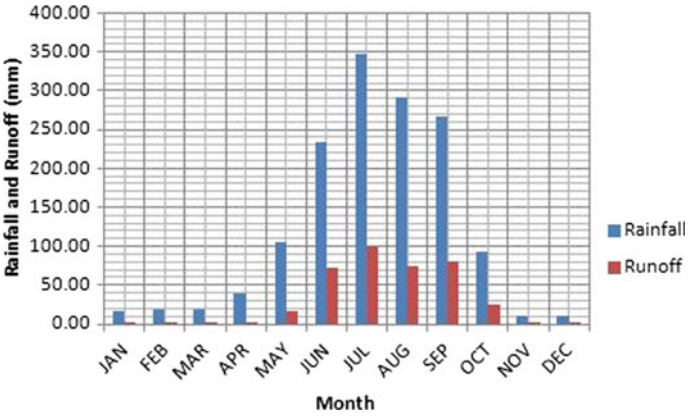

Fig. 7 Monthly average rainfall-runoff

Odisha, exceeding its previous record of 1997 which is even reflected in the results of this study. So, in spite of the model validation due to the unavailability of observed discharge data from the gauging station and the runoff obtained at the outlet can be stated as reliable.

References

1. Bouslihim Y, Kacimi I, Brirhet H, Khatati M, Rochdi A, Pazza N, Miftah A, Yaslo Z (2016) Hydrologic modeling using SWAT and GIS, application to subwatershed Bab-Merzouka (Sebou, Morocco). J GIS 8:20–27

2. Kangsabanik S, Murmu S (2017) Rainfall-runoff modelling of Ajay river catchment using SWAT model. IOP Conf Ser Earth Env Sci 67:1755–1315
3. Khare D, Singh R, Shukla R (2014) Hydrological modelling of Barinallah watershed using ArcSWAT model. Int J Geol Earth Env Sci 4(1):224–235
4. Patil NS, Raikar RV, Manoj S (2014) Runoff modelling for Bhima river using SWAT hydrological model. Int J Eng Res Technol 3(7):923–928
5. Amathya DM, Jha MK (2011) Evaluating the SWAT model for a low gradient forested watershed in coastal South Carolina. Trans ASABE 54(6):2151–2163
6. Shi P, Chen C, Srinivasan R, Zhang X, Cai T, Fang X, Qu S (2011) Evaluating the SWAT model for hydrological modeling in the Xixian watershed and a comparison with the XAJ model. Water Resour Manag 25:2595–2612

Spatial Disparity in Access to Improved Source of Drinking Water and Sanitation Facility: A District-Level Assessment in India

Amitha Puranik, Nilima, and Sushmitha Prabhu

Abstract More than one billion people worldwide are deprived of basic facilities including clean water sources and sanitation. Although many countries achieved progress through the millennium development goal, countries in South Asia like India still face the problem. More than 163 million people in India do not have access to clean water. Out of the 60% of the world population without access to drinking water, India tops the list by contributing 19.33%. Poor sanitation not only has a direct influence on well-being but also has an indirect impact on the living conditions, reduced education outcomes, and poverty. As of 2018, about 8% of the population in India still do not have access to an improved sanitation facility. The present study aims to assess the presence of spatial clustering in the proportion of households with access to an improved source of drinking water and sanitation facility at the district-level in India, using the data from national surveys. The study also aims at the temporal assessment of the clustering pattern during the period of 2007–2008 and 2015–2016. Spatial analytical techniques such as exploratory mapping and spatial cluster analysis are performed. The findings of this study are useful in locating the districts that lack access to an improved source of drinking water and sanitation facility. This information can further help in implementing targeted intervention programs to achieve the sustainable development goal of clean water and sanitation by 2030.

Keywords Drinking water · Getis-Ord Gi* · Public health · Sanitation · Spatial analysis

A. Puranik (✉)
Department of Data Science, Prasanna School of Public Health, Manipal Academy of Higher Education, Manipal, Karnataka, India
e-mail: amitha.puranik@manipal.edu

Nilima
Department of Biostatistics, All India Institute of Medical Sciences, Delhi, India

S. Prabhu
Department of Community Medicine, Sri Siddhartha Institute of Medical Sciences and Research Centre, Bengaluru, Karnataka, India

C. Bhuiyan et al. (eds.), *Water Security and Sustainability*,
Lecture Notes in Civil Engineering 115,
https://doi.org/10.1007/978-981-15-9805-0_14

1 Background

More than one billion people worldwide are deprived of basic facilities including clean water sources and sanitation [1]. Most places in India are characterized by overcrowding, inadequate water supply, and inadequate facilities of disposal of human excreta, wastewater, and solid wastes [2]. Individual and domestic hygiene practices can be improved if water supply, wastewater disposal, and waste management are proper [2]. Poor sanitation not only has a direct influence on well-being but also has an indirect impact on the living conditions, reduced education outcomes, and poverty [3].

Drinking water is a key source of microbial pathogens, and poor sanitation is integral to enteric pathogen exposure [4]. Poor water quality, sanitation, and hygiene account for more than 1.6 million deaths a year worldwide mainly due to diarrhea. Nine out of 10 such deaths are in children, and virtually all of the deaths are in developing countries [5]. Mode of water transportation, the existence of excess water in the street, domestic water storage conditions, feces disposal, and the presence of vectors predispose the children to several gastrointestinal infections [6, 7]. Diarrhea, a gastrointestinal infection is caused by pathogenic microorganisms including E. coli, Rotavirus, Salmonella typhimurium, Campylobacter, and Shigella present in water [8, 9].

About 2.4 billion people lack access to a proper sanitation facility, and four out of five of these underprivileged people lived in Asia alone [3, 10]. The millennium development goal (MDG) to halve the proportion of people without access to water and basic sanitation by 2015 [3] remains unmet. Over 2600 million of the 2015 population gained access to an improved water source during the MDG period. However, more than 660 million people across the globe and one-fifth of them in South Asia still use an unimproved source of drinking water [11]. Despite working hard to achieve the MDG goal, low baseline and high population density country like India has almost 163 million people with no access to clean water [11]. To respond to these public health concerns, urban India needs to have universal access to water and toilets with safe collection and treatment of human excreta [12].

India has set its way to achieve the sustainable development goal of clean water and sanitation by 2030 making the review of current status more important [13, 14]. India has a highly heterogeneous structure making spatial analysis an integral technique. Generating evidence through spatial analysis will help target the locations requiring attention. Spatial statistics are fundamental in mapping the condition of interest, [1, 15–18] to identify the hot spots/cold spots and provide the information on significant clusters of locations [18]. The spatial assessment will enable civil engineers for strategic planning to improve the present situation of water and sanitation facilities.

To the best of our knowledge, the spatial-temporal presentation of water and sanitation facilities in India at a gap of eight years has not been previously presented. In the present study, the spatiotemporal mappings of regions affected by the poor sanitation and water supply are reported for instituting the understanding of the

locations of concern. This preliminary study aims at mapping that will further assist in the formulation and implementation of tailored strategies.

2 Objective

The study aims to assess the presence of spatial clustering in the proportion of households with an access to improved source of drinking water and sanitation facility in the districts of India, using the data from national surveys. The study also aims at the temporal assessment of the clustering pattern during the period of 2007–2008 and 2015–2016.

3 Materials and Methods

This is an ecological study that utilized aggregate level data from District-Level Household and Facility Survey-3 (DLHS-3) conducted during 2007–2008 and National Family Health Survey-4 (NFHS-4) conducted during 2015–2016. Data on Nagaland is not available for the period of 2007–2008 (DLHS-3) and hence not included in the analysis.

Table 1 provides the definitions of improved source of drinking water and sanitation facility in the two surveys, DLHS-3 and NFHS-4.

The data on proportion of households with access to an improved source of drinking water and sanitation facility for the districts of India were retrieved. The spatial analysis was performed using the ArcGIS 10.3 (ESRI, Redlands, CA, USA) software package. The exploratory maps were generated to depict the spatial distribution of the proportion of households with access to drinking water and sanitation facility based on the data obtained from DLHS-3 and NFHS-4, for the period of 2007–2008 and 2015–2016, respectively. The data on proportion were categorized

Table 1 Definitions of improved source of drinking water and sanitation facility as provided in the surveys

Survey	Drinking water	Sanitation
DLHS-3	Piped into dwelling, piped to yard/plot, public tap/stand, pipe/hand, pump/tube, well/bore well/well covered/spring tanker, cart with small tank and bottled water	Flush to piped sewer system, flush to septic tank, flush to pit latrine with slab, pit ventilation
NFHS-4	Piped water, public taps, stand pipes, tube wells, boreholes, protected dug wells and springs, rainwater, and community reverse osmosis (RO) plants	Non-shared toilet of the following types: flush/pour flush toilets to piped sewer systems, septic tanks, and pit latrines; ventilated improved pit(VIP)/biogas latrines; pit latrines with slabs; and twin pit/composting toilets

based on quartiles. Each category was color coded; darker shade represents higher proportion, and lighter shade represents low proportion.

The global spatial autocorrelation in the percentage of households with access to drinking water and sanitation obtained from the two surveys was estimated using Moran's I statistic, with Queen's contiguity weight matrix. A Moran's I value of zero indicates the null hypothesis of no clustering, a positive Moran's I indicates positive spatial autocorrelation (i.e., clustering of areas with similar attribute values), and a negative coefficient indicates negative spatial autocorrelation (i.e., neighboring areas tend to have dissimilar attribute values).

The local spatial clusters were identified using the spatial analysis technique called Getis-Ord *Gi** statistic [19]. The null hypothesis for the cluster detection technique is spatial randomness of proportion of event of interest in the geographic units under consideration. The Getis-Ord *Gi** statistic and the associated p value will determine whether to reject or not reject the null hypothesis. If the null hypothesis is rejected, it implies that the spatial clustering is statistically significant and has not occurred due to chance.

The formula to compute Getis-Ord *Gi** statistic is given as

$$Gi^* = \frac{\sum_{j=1}^{n} w_{ij}x_j - \bar{X}\sum_{j=1}^{n} w_{ij}}{S\sqrt{\frac{n\sum_{j=1}^{n} w_{ij}^2 - \left(\sum_{j=1}^{n} w_{ij}\right)^2}{n-1}}}$$

where n is the number of areas within the region of interest and x_j is the observed value for area j ($i \neq j$), and $\bar{X}$ the mean of the attribute under investigation. w_{ij} is a measure of the closeness of areas i and j represented using the weight matrix.

$$\bar{X} = \frac{\sum_{j=1}^{n} x_j}{n}$$

$$S = \sqrt{\frac{\sum_{j=1}^{n} x_j^2}{n} - \left(\bar{X}\right)^2}$$

$\boldsymbol{E(Gi)} = 0$ and $\boldsymbol{Var(Gi)} = 1$ and the distribution of *Gi** under the null hypothesis of no spatial association among the observed values is approximately normal. Getis-Ord *Gi** statistic is a z-score which is computed for every geographic unit under consideration. The value of statistic for each geographic unit is compared with the value of sum of statistic of all geographic units. If the value of statistic for each geographic unit is different from the expected value of statistic, and if that difference is too large to be the result of random chance, the resultant z-score of statistic is considered to be statistically significant.

A positive value of the statistic indicates clustering of high values of attribute, and a negative value of the statistic indicates clustering of low values of attribute. Larger the value of statistic, the more intense is the clustering. The districts with high proportion of access to drinking water form hot spots (high-high) if they are

surrounded by districts with high proportion. Cold spots (low-low) are formed by districts with low proportion surrounded by districts with low proportion of access to drinking water. Patterns such as high-low and low-high indicate clustering of districts with high proportion surrounded by districts with low proportion and vice versa. Similar interpretation is applicable for spatial clustering of the proportion of access to sanitation facility. The districts contributing to the formation of cold spots were of interest in this study.

4 Results

The proportion of households with access to an improved source of drinking water and access to sanitation facility varied during the period of 2007–2008 and 2015–2016. Table 2 provides a description of the proportion observed during two different surveys. The average percentage of household with an improved water facility is close to 38 in the period of 2007–2008 which is considerably improved to 88 in the period of 2015–2016. The distribution of percentage of an improved water source was skewed with only 0.1 in the districts namely Araria, Banka, Begusarai, Gopalganj, Supaul, Sheohar, Sitamarhi, and Siwan of Bihar state and 3.1% of households had improved sanitation facility in the district Sidhi of Madhya Pradesh state during the period of 2007–2008. The minimum is observed to have improved to 32% and 7%, respectively, in the period of 2015–2016. Moran's I values were indicative of the presence of spatial clustering in the district-wise percentage of households with access to drinking water and sanitation facility.

The exploratory maps generated to depict the spatial distribution of the proportion of households with access to an improved source of drinking water and sanitation facility are presented below (Figs. 1, 2, 3, and 4).

Table 2 Descriptive of the percentage of households with access to an improved source of drinking water and sanitation facility in the districts of India during the period of 2007–2008 (n = 601) and 2015–2016 (n = 636)

		DLHS-3	NFHS-4
Drinking water (%)	Min	0.1	32.2
	Max	100	100
	Mean (standard deviation)	38.12 (32.04)*	88.12 (12.54)
	Moran's I	0.72	0.56
Sanitation (%)	Min	3.1	6.9
	Max	99.9	99.5
	Mean (standard deviation)	44.35 (29.08)#	47.94 (22.59)
	Moran's I	0.76	0.75
Median (Q_1,Q_3) = 30.35 (8.05,69.33)*; 37.65 (18.40,67.93)#			

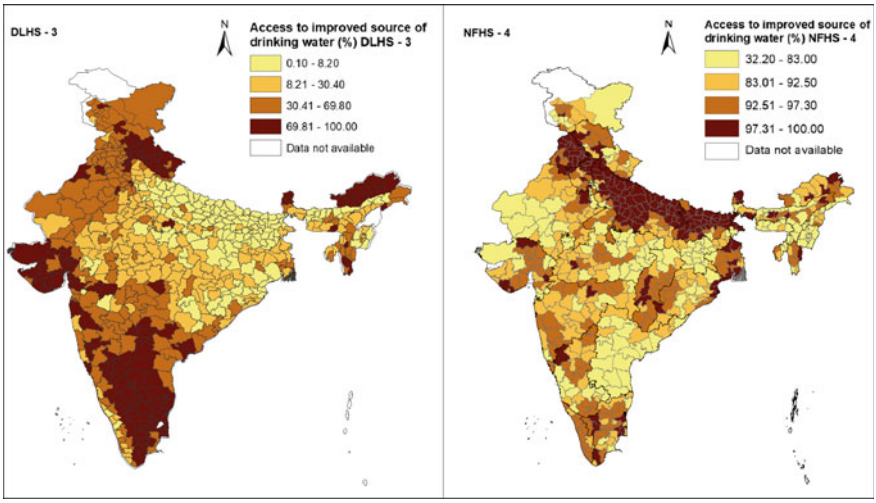

Fig. 1 Exploratory map depicting the proportion of households with access to an improved source of drinking water during the period of 2007–2008 and 2015–2016

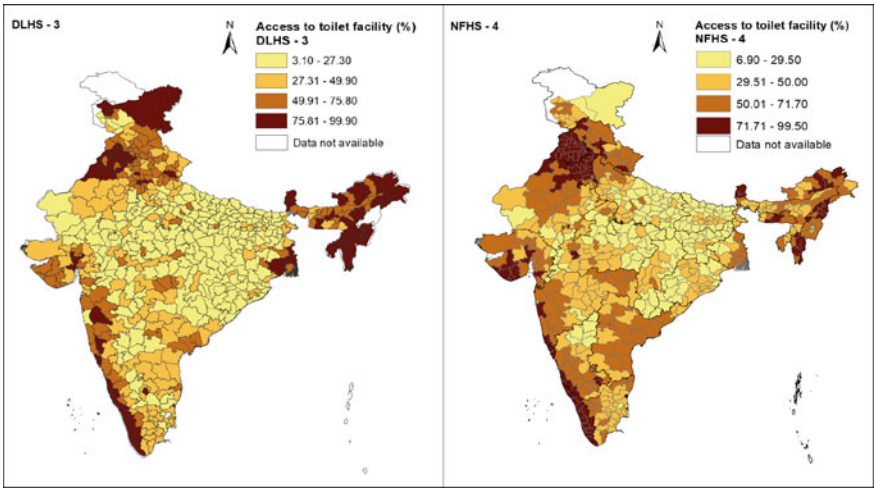

Fig. 2 Exploratory map depicting the proportion of households with access to sanitation facilities during the period of 2007–2008 and 2015–2016

5 Discussion

The present study findings provide valuable insights into persistent locations with poor water and sanitation facility at a gap of eight years. The data on sanitation facilities in India reveals numerous facts to be stressed. After a significant eight

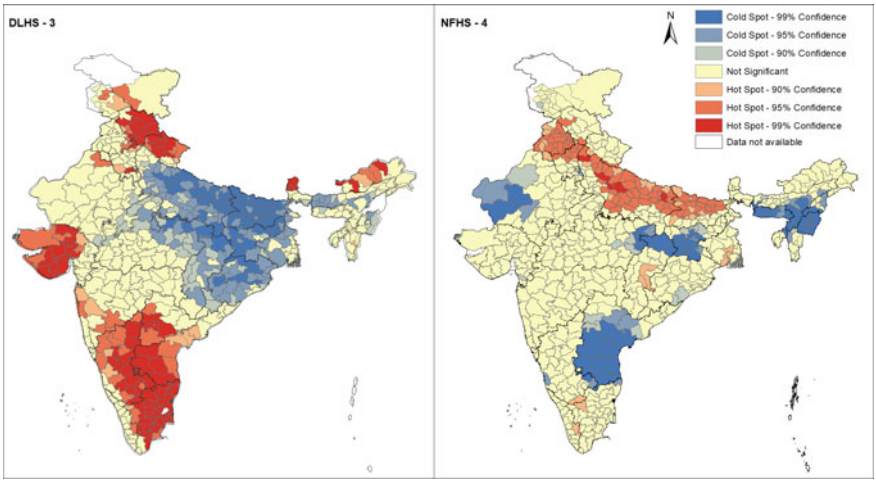

Fig. 3 Local indicators of spatial association cluster map for the proportion of households with access to an improved source of drinking water during the period of 2007–2008 and 2015–2016

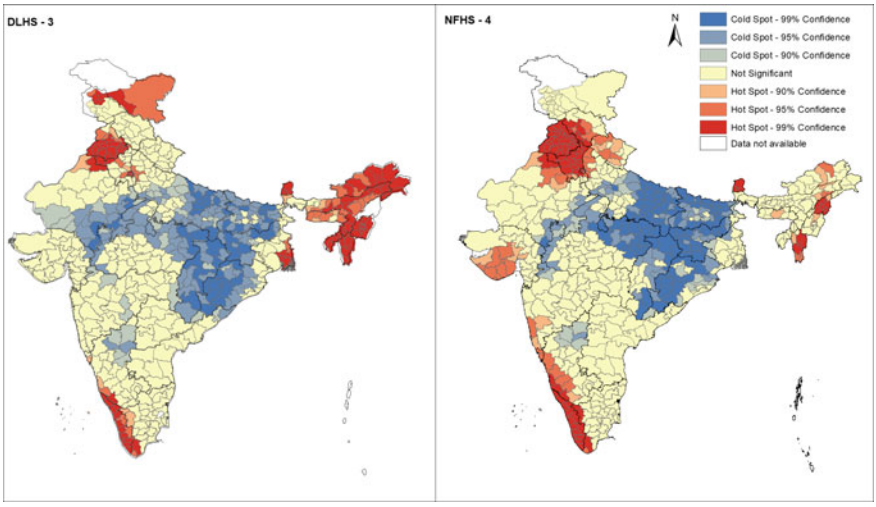

Fig. 4 Local indicators of spatial association cluster map for the proportion of households with access to sanitation facilities during the period of 2007–2008 and 2015–2016

years gap, the district of Bihar, Jharkhand, Odisha, Uttar Pradesh, Chhattisgarh, and Madhya Pradesh are observed to have persistently poor sanitation facilities (Table 3). Rajasthan is the only state with a visible improvement in the sanitation facility over the two time period. The situation for the water facility was almost similar to that of sanitation facilities in the period of 2007–2008. However, this seems to have changed drastically in 2015–2016. It is important to note that in the period of 2015–2016,

Table 3 List of districts forming cold spots of the proportion of improved source of drinking water and sanitation facility at 99% confidence level, in the districts of India during the period of 2007–2008 and 2015–2016

Data source	Improved source of drinking water		Sanitation facility	
	State	District	State	District
DLHS-3	Bihar	Araria, Banka, Bhagalpur, Begusarai, Saran, Darbhanga, Gopalganj, Jamui, Muzaffarpur, Purnia, Khagaria, Madhubani, Lakhisarai, Madhepura, PurbaChamparan, Munger, Nalanda, Nawada, PashchimChamparan, Patna, Samastipur, Saharsa, Gaya Sitamarhi, Siwan, Supaul, RohtasBhojpur, Buxar, Jehanabad	Bihar	Araria, Bhagalpur, Gopalganj, Jamui, Muzaffarpur, Madhepura, Saharsa, Supaul, Gaya, Rohtas
	Chattisgarh	Surguja	Chattisgarh	Bastar, Raigarh, Raipur, Surguja, Bilaspur, Kawardha
	Jharkhand	Deoghar, Dumka, Giridih, Godda, Gumla, Ranchi, Sahibganj, Palamu, Kodarma	Jharkhand	Deoghar, Dumka, Giridih, Godda, Gumla, Ranchi, Palamu
	Madhya Pradesh	Chhatarpur, Satna, Sidhi	Madhya Pradesh	Satna, Sidhi, Shahdol
	Orissa	Anugul, Baudh, Balangir, Kendujhar, Cuttack, Sundargarh	Orissa	Anugul, Baudh, Balangir, Bargarh, Kalahandi, Koraput, Nuapada, Kandhamal, Rayagada, Sundargarh, Sonapur
	Uttar Pradesh	Azamgarh, Budaun, Allahabad, Ambedkar Nagar, Basti, Bahraich, Ballia, Barabanki, Deoria, Faizabad, Ghazipur, Gonda, Gorakhpur, Farrukhabad, Hardoi, Kannauj, Kheri, Kushinagar, Mau, Shahjahanpur, Sultanpur, Sonbhadra, Siddharthnagar	Uttar Pradesh	Ambedkar Nagar, Basti, Bahraich, Ballia, Faizabad, Gonda, Gorakhpur, Pratapgarh, Sultanpur, Sonbhadra, Siddharthnagar
			Rajasthan	Banswara, Chittaurgarh, Karauli, Kota

(continued)

Table 3 (continued)

Data source	Improved source of drinking water		Sanitation facility	
	State	District	State	District
NFHS-4	Andhra Pradesh	Anantapur, Chittoor, Y.S.R, Guntur, Krishna, Kurnool, Mahbubnagar, Nalgonda, Sri PottiSriramulu Nellore, Prakasam	Andhra Pradesh	Vizianagaram
	Assam	Cachar, Dhubri, Hailakandi, KarbiAnglong, Karimganj, DimaHasao	Bihar	Araria, Banka, Bhagalpur, Supaul, Jamui, Nawada, Darbhanga, Gopalganj, Gaya, Muzaffarpur, Rohtas, Purnia, Khagaria, Madhubani, Madhepura, Purba and PashchimChamparan, Saharsa, Buxar, Sitamarhi, Kaimur
	Chattisgarh	Jashpur, Koriya, Surguja	Chattisgarh	Bastar, Dantewada, Jashpur, Koriya, Raigarh, Surguja
	Jharkhand	Bokaro, Gumla, Hazaribagh, Khunti, Latehar, Lohardaga, PashchimiSinghbhum, Ranchi, Simdega	Jharkhand	Deoghar, Dumka, Giridih, Godda, Gumla, PashchimiSinghbhum, Ranchi, Garhwa, Palamu, Chatra, Kodarma
	Karnataka	Chikkaballapura	Madhya Pradesh	Chhatarpur, Guna, Jabalpur, Umaria, Panna, Satna, Rewa, Sagar, Sidhi, Dindori, Mandla, Shahdol,
	Madhya Pradesh	Anuppur, Shahdol, Sidhi	Orissa	Anugul, Baudh, Balangir, Bargarh, Kendujhar, Kalahandi, Ganjam, Gajapati, Koraput, Nayagarh, Nuapada, Kandhamal, Rayagada, Sundargarh, Sonapur

(continued)

Table 3 (continued)

Data source	Improved source of drinking water		Sanitation facility	
	State	District	State	District
	Manipur	Bishnupur, Chandel, Churachandpur, Imphal East, Imphal West, Senapati, Tamenglong, Thoubal, Ukhrul	Rajasthan	Banswara, Udaipur
	Meghalaya	East Garo Hills, Jaintia Hills, South Garo Hills, West Garo Hills, West Khasi Hills	Uttar Pradesh	Azamgarh, Allahabad, Ambedkar Nagar, Basti, Bahraich, Ballia, Balrampur, Banda, Barabanki, Chitrakoot, Deoria, Faizabad, Ghazipur, Gonda, Gorakhpur, Farrukhabad, Sultanpur, Mau, Jaunpur, Kaushambi, Mirzapur, Rae Bareli, Lalitpur, Pratapgarh, SantKabir Nagar, Shrawasti, Sonbhadra, Siddharthnagar
	Nagaland	Dimapur, Kohima, Peren, Phek		
	Rajasthan	Barmer, Jodhpur		
	Tripura	North Tripura		

Rajasthan and Andhra Pradesh were observed to have poorer water facilities. Uttar Pradesh, Bihar, Jharkhand, Odisha, Madhya Pradesh had poor water facility in the period of 2007–2008, however, all of them showed significant improvement in the facility after eight years. The results indicate that the strategic approach of the administration and the sweats of focusing on low performing states are paying off. These notable accomplishments are the effect of countless initiatives of the Government [14]. The community-wide National Rural Health Mission effective in the period of 2005–2012 might have assisted in reducing the spatial disparities. The noted reduction may also be an outcome of the state government schemes like Punjab rural water supply and sanitation project [20]. The solid waste disposal concessions awarded to 50 municipal corporations including the one in Kolhapur District of Maharashtra would have contributed to the improvement in the water and sanitation facilities in Maharashtra [3]. The influence on improved water and sanitation could be a result of numerous other national and international schemes including the second phase of community-led infrastructure finance facility-2015 [21] and sulabh international [22]. Studies [23] reveal that a substantial percentage of underprivileged was found interested to invest in water and sewer network connection reflecting the alert and informed behavior of residents. This information can further help in implementing targeted intervention programs to achieve the sustainable development goal.

Although the present study tried to address the spatial disparity in access to drinking water and sanitation facility at the district level based on the available data and spatial analytical techniques, there are certain limitations in this study. The use of aggregate district-level data can lead to ecological fallacy and hence the findings cannot be generalized at an individual or household level. The limitations associated with the data collection method of DLHS-3 and NFHS-4 are also the limitations of this study.

The present study has attempted to provide a visual description of the spatial disparity in accessibility of drinking water and sanitation facility in the districts of India. The exploratory maps and spatial cluster analysis performed in this study are useful in locating the districts that lack access to drinking water and sanitation facility. On a priority basis, interventions should be channeled to the most affected districts in India, as revealed in the presented study.

References

1. Bessong PO, Odiyo JO, Musekene JN, Tessema A (2009) Spatial distribution of diarrhoea and microbial quality of domestic water during an outbreak of diarrhoea in the Tshikuwi community in Venda, South Africa. J Health Popul Nutr 27(5):652
2. Nath K (2003) Home hygiene and environmental sanitation: a country situation analysis for India. Int J Environ Health Res 13(supp 1):S19–S28
3. Van MH, Hung NV (2011) Economic aspects of sanitation in developing countries. Environ Health Insights 5:63–70
4. Nilima, Kamath A, Shetty K, Unnikrishnan B, Kaushik S, Rai SN (2018) Prevalence, patterns, and predictors of diarrhea: a spatial-temporal comprehensive evaluation in India. BMC Public

Health 18(1):1288
5. Ashbolt NJ (2004) Microbial contamination of drinking water and disease outcomes in developing regions. Toxicology 198(1–3):229–238
6. Simiyu S (2010) Water risk factors pre-disposing the under five children to diarrhoeal morbidity in Mandera district, Kenya. East Afr J Public Health 7(4)
7. Kumar SG, Subita L (2012) Diarrhoeal diseases in developing countries: a situational analysis. Kathmandu Univ Med J 38(2):83–88
8. Yongsi H (2008) Pathogenic microorganisms associated with childhood diarrhea in low-and-middle income countries: case study of Yaoundé-Cameroon. Int J Environ Res Public Health 5(4):213–229
9. Kaushik S, Tiwari U, Nilima, Prashar S, Das B, Sinha RK (2019) Label-free detection of E scherichia coli bacteria by cascaded chirped long period gratings immunosensor. Rev Sci Instr 90(2):025003
10. World Health Organisation (2006) The global water supply and sanitation assessment. World Health Organisation, Geneva
11. World Health Organisation (2015) Supply WUJW, Programme SM: Progress on sanitation and drinking water: 2015 update and MDG assessment. World Health Organization
12. Wankhade K (2015) Urban sanitation in India: key shifts in the national policy frame. Environ Urbanization 27(2):555–572
13. UNDP: undp.org [Internet].Sustainable Development Goals, New York. http://www.undp.org/content/undp/en/home/sustainable-development-goals/goal-3-good-health-and-well-being.html
14. Interventions WE (2012) Commodities and guidelines for reproductive, maternal, newborn and child health. World Health Organization, Geneva
15. Njemanze PC, Anozie J, Ihenacho JO, Russell MJ, Uwaeziozi AB (1999) Application of risk analysis and geographic information system technologies to the prevention of diarrheal diseases in Nigeria. Am J Trop Med Hygiene 61(3):356–360
16. Fang L, Yan L, Liang S, de Vlas SJ, Feng D, Han X, Zhao W, Xu B, Bian L, Yang H (2006) Spatial analysis of hemorrhagic fever with renal syndrome in China. BMC Infect Dis 6(1):77
17. Sarkar R, Prabhakar AT, Manickam S, Selvapandian D, Raghava MV, Kang G, Balraj V (2007) Epidemiological investigation of an outbreak of acute diarrhoeal disease using geographic information systems. Trans R Soc Trop Med Hyg 101(6):587–593
18. John A, Nilima, Binu V, Unnikrishnan B (2019) Determinants of antenatal care utilization in India: a spatial evaluation of evidence for public health reforms. Public Health 166:57–64
19. Getis A, Ord J (1992) The analysis of spatial association by use of distance statistics. Geograph Anal 24:189–206
20. Singh J (2017) Punjab rural water supply and sanitation project: problems faced by RWSS committees. Soc ION 6(1):76–87
21. Jack M, Morris R (2005) The community led infrastructure finance facility (CLIFF). International Association of Local and Regional Development Funds in Emerging markets. http://www.citiesalliance.org/doc/resources/financing/cliff/articleIADF(FullVersionFinal)_Jun05.pdf
22. Pathak B (2011) Sulabh sanitation and social reform movement. Int NGO J 6(1):014–029
23. Davis J, White G, Damodaron S, Thorsten R (2008) Improving access to water supply and sanitation in urban India: microfinance for water and sanitation infrastructure development. Water Sci Technol 58(4):887–891

Extreme Hydrology

Flood Hazard Mapping and Vulnerability Analysis Along Seti River in Pokhara Metropolitan City

Anup Shrestha, Saraswati Thapa, and Bhola Nath Sharma Ghimire

Abstract Flood is frequent during every monsoon in Nepal which poses threat to life and property in lowland areas. Among 6000 rivers and rivulets, most are prone to floods in Nepal. Seti River flows from Machhapuchhre Rural Municipality in the north, along the center of Pokhara Metropolitan City, and toward Tanahu which meets with Madi River there. Seti flood of 2012 was one of the devastating floods which took the life of many people and destroyed infrastructures along its way. So, Pokhara Metropolitan City lies at a high risk of flood impacts. Hydrodynamic simulation using HEC-RAS and GIS is one of the important methods of estimating the probable loss due to flood of various scenarios quantitatively. In this study, flood hazard maps of Seti River across Pokhara Metropolitan City has been prepared for different flood scenarios. The flood frequency analysis was performed using Gumbel, Log-Pearson, Log Normal, and Fullers Method. The goodness of fit was performed using chi square test, and results of Gumbel method was used as it was found more appropriate than other methods for this basin. One-dimensional steady hydrodynamic modeling was done to create water surface profile which was used to prepare hazard maps and vulnerability maps for various return periods. The model was evaluated using statistical parameters, coefficient of determination R^2), and Nash–Sutcliffe efficiency (NSE) whose values were found to be 0.951 and 0.819, respectively. The maps prepared can be used for planning the built-up areas along the river sides and may help in decision making for flood mitigation measures.

Keywords Flood · Hazard · Seti River · Pokhara Metropolitan City · HECRAS · GIS

A. Shrestha (✉) · S. Thapa · B. N. S. Ghimire
Department of Civil Engineering, Institute of Engineering, Pulchowk Campus, Lalitpur, Nepal
e-mail: anoopstha50@gmail.com

S. Thapa
e-mail: saraswati.thapa@pcampus.edu.np

B. N. S. Ghimire
e-mail: bholag@ioe.edu.np

C. Bhuiyan et al. (eds.), *Water Security and Sustainability*,
Lecture Notes in Civil Engineering 115,
https://doi.org/10.1007/978-981-15-9805-0_15

1 Introduction

Flood is a natural and perennial phenomenon which is beneficial for enhancing the soil fertility [1] and also a hazard endangering the human life, property, and environment which is induced by natural or anthropogenic activities [2]. Due to fragile topography and young geology, active seismic plates, occasional glacier lake outburst floods, and concentrated monsoon rains, Nepal is observing significant water-induced disasters such as soil erosion, landslides, debris flow, flood, and bank erosion. Globally, Nepal lies in 13th rank in terms of flood vulnerability [3].

This study concentrates on the Seti Sub-river basin and its impact in the Pokhara Metropolitan City. The city is located nearly at the middle of the Gandaki Province (Province No. 4), which lies between latitude 28°4′50″N to 28°20′40″N and longitude 83°48′00″E to 84°09′00″E, and has an area of 464.24 km^2 and population of 4,02,995. Pokhara Metropolitan City has Madi and Rupa Rural Municipality on the east, Annapurna Rural Municipality on the west, Machhapuchre Rural Municipality on the north, and Tanahu and Syangja on the south direction as shown in Fig. 1 [4].

The number of flood events and its impact on people and economy are increasing each year. Though the fatalities have decreased in some of the regions of Nepal, the number of affected people due to flood has an increasing trend. Hence, the vulnerability in the urban areas is also increasing. The encroachment of river corridor, disturbance of natural pathway due to anthropogenic activities, excessive extraction

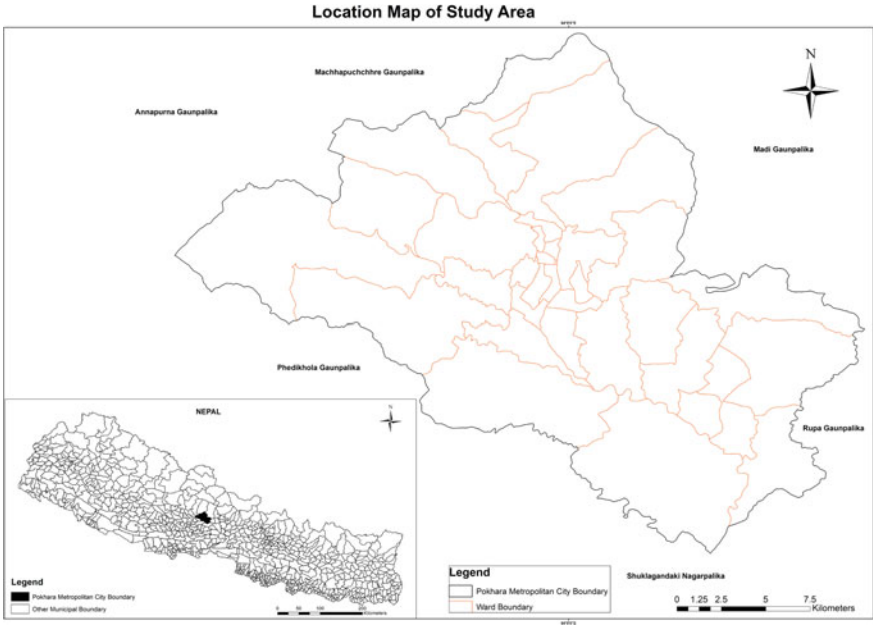

Fig. 1 Location map of study area

of sediments from river, and change in land use are increasing the vulnerability of people during floods.

To reduce the vulnerability due to flood hazards, mitigation is a must. Mitigation can be done by structural or non-structural measures. Flood hazard mapping is one of the non-structural measures of mitigation to estimate the areas which are at a risk of flooding under extreme flooding conditions under different scenarios. This study aims to prepare flood hazard map of Pokhara Metropolitan City using one-dimensional hydraulic model HECRAS, Arc GIS, and HEC-Geo RAS. Various scenarios are considered to quantify the flooding and flood/inundation, and hazard prone areas along Seti River would be identified and processed to prepare hazard maps.

2 Methodology

One-dimensional steady hydrodynamic modeling was used using HECRAS 5.0 to calculate the water surface profiles for various return periods. The geometry was created using HEC-GeoRAS extension in Arc GIS, and Arc GIS was used to prepare the hazard and vulnerability maps. The details of the methodology are shown in Fig. 2. To obtain the flood hazard maps, DEM ALOS Palsar 12.5 m resolution [5], hydrological data (Discharge Data from DHM), land use data of 2010 (Obtained from ICIMOD [6]), population data (obtained from Central Bureau of Statistics), household data (Obtained from Open Street Map) were used.

Flood frequency analysis for the return periods of 2, 5, 10, 50, and 100 years was carried out using Gumbel's method, Fuller's Method, Log-Pearson-III method and Log Normal method. For the ungauged tributaries, catchment area ratio method was used to calculate the discharge which was used as input to HEC-RAS. The manning's roughness coefficient 'n' was used by using trial and error method and comparing the rating curve obtained from Department of Hydrology and Meteorology, Nepal data and output of HEC-RAS. The value of n was taken as 0.045 for channel and 0.06 for left and right over banks.

The goodness of fit test was performed for the given values using chi square test, and Gumbel distribution was found to be suitable for the basin, and hence, the discharge for the various return period was used from Gumbel's method. The discharge used in the study for 2, 5, 10, 50, and 100 years return periods was 401.38 m^3/s, 706.34 m^3/s, 908.25 m^3/s, 1353.62 m^3/s, and 1540.48 m^3/s, respectively.

3 Preparation of Flood Hazard and Vulnerability Maps

Flood depth is considered as the most important indicator of intensity of flood hazard [8]. So, to quantify the flood hazard; three levels of hazards, low, moderate, and high are categorized in this study according to the flood depth. Flood depth less than 1 m

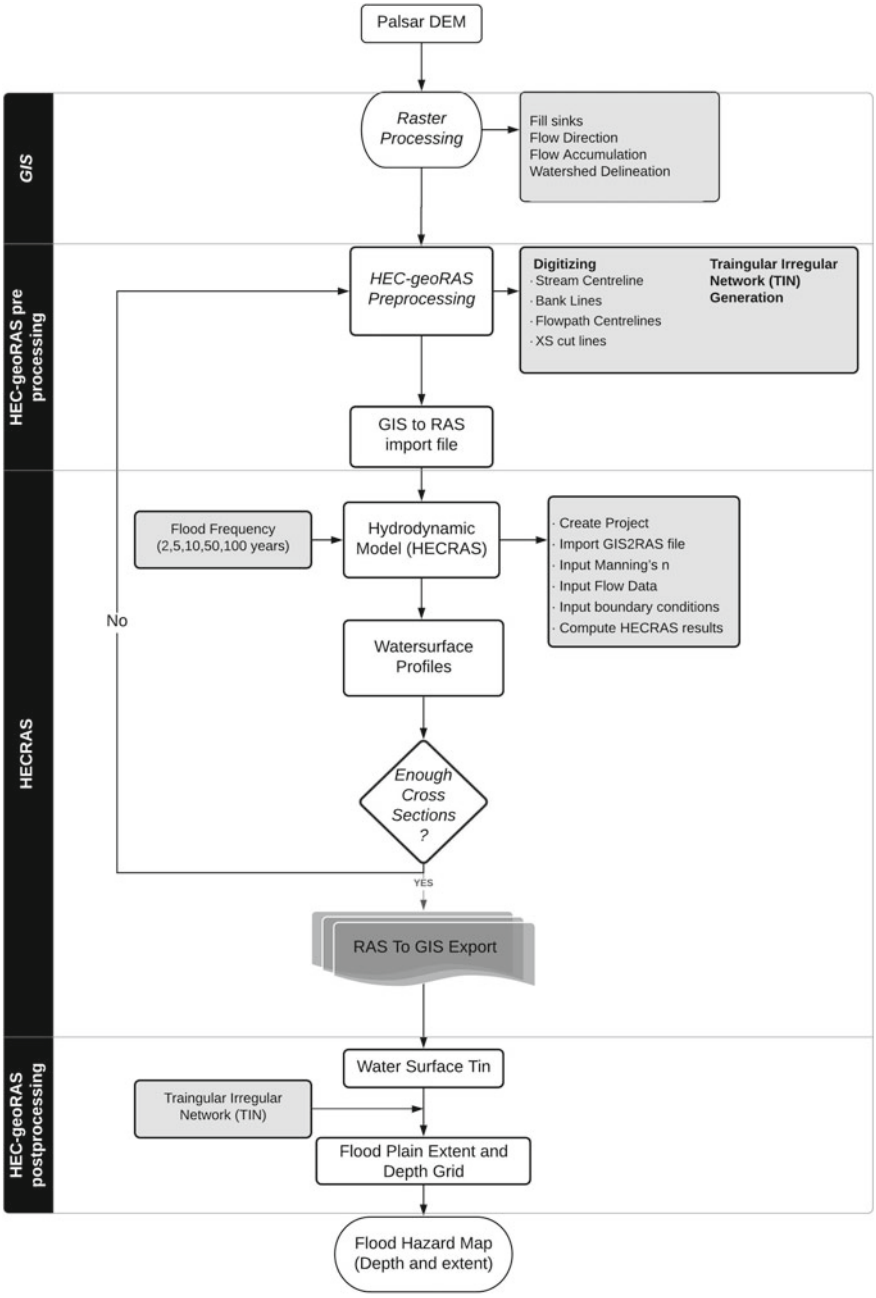

Fig. 2 Flowchart of methodology [7]

is considered low hazard, 1–3 m is considered moderate, and greater than 3 m is considered as high hazard class.

It is assumed that lesser flood depth has less effect on the people and properties, and higher ones have larger effect. The flood hazard map for 50 years return period is shown in Fig. 3a.

To prepare flood vulnerability maps, landuse map was used. The landuse map of the study area is clipped by the flood depth boundary polygon to prepare the flood vulnerability maps. The flood vulnerability map for 50 years return period is shown in Fig. 3b.

4 Results

The performance of the one-dimensional steady hydrodynamic model was evaluated by comparing the flood depth observed at the Seti–Phoolbari hydrological station with the simulated depth. The statistical parameters used for the model performance evaluation were coefficient of determination R^2) and Nash–Sutcliffe efficiency (NSE), and their values were found to be 0.951 and 0.819, respectively.

The flood hazard and vulnerability analyses along with exposed people and buildings are summarized in terms of affected area in Tables 1 and 2.

5 Conclusions and Recommendations

This study was done to prepare hazard and vulnerability map and exposure information using HECRAS for one-dimensional steady hydrodynamic modeling, Arc GIS as the interface for spatial data analysis and processing and HEC-GeoRAS to link Arc GIS and HECRAS. The values of R^2 and NSE show that the performance of the model can be rated as very good [9].

The result shows that the area, population, and buildings affected by the floods in 2, 5, 10, 50, and 100 years return periods for Pokhara Metropolitan City are increasing. The assessment of flood hazard shows that the flood intensity increases as lower flood depth decreases and higher flood depth area increases. The hazard map for 50 years return period shows that specific areas along the Seti River like Shri siddhi box gadh, Pokhara Rangashala, Manipal College, Ramghat area, Kaskeri Chautari, and some part of Prithvi and Pokhara Baglung Highway as well as many street roads are at high risk. Hence, river training works are recommended for those high risk areas. The result of flood vulnerability further shows that the most vulnerable area is agricultural area for all return periods which might have direct impact on the food security for the area.

Landcover of 2010 was used in this study, and on the contrary, recent landcover could represent the present scenario more reliably. Though 12.5 m resolution DEM

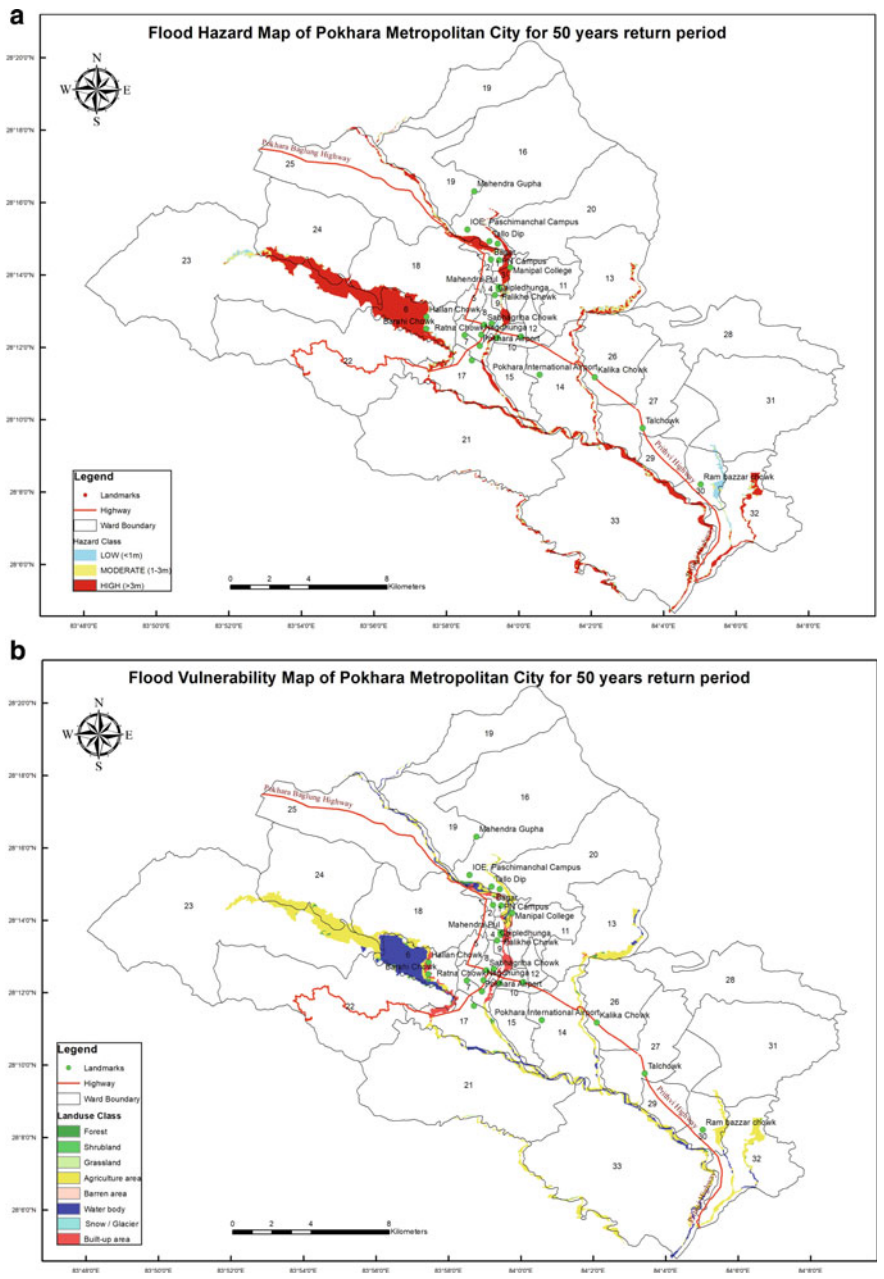

Fig. 3 **a** Flood hazard map for 50 years return period and **b** flood vulnerability map of 50 years return period

Table 1 Total area affected according to hazard class

Hazard class	Flood depth	Return period/total flooded area (sq. km)				
		2 yrs	5 yrs	10 yrs	50 yrs	100 yrs
Low	<1 m	2.476	1.195	1.125	2.052	0.953
Moderate	1 to 3	3.946	4.526	4.29	3.588	4.093
High	>3	12.09	14.52	15.564	16.883	22.368
	Total	**18.512**	**20.242**	**20.98**	**22.522**	**27.414**

Table 2 Landuse vulnerability for different return periods

S.N.	Land cover	Total vulnerable area (sq. km)				
		2 yrs	5 yrs	10 yrs	50 yrs	100 yrs
1	Forest	0.374	0.428	0.455	0.488	0.515
2	Shrubland	0.02	0.023	0.023	0.023	0.026
3	Grassland	0.036	0.05	0.05	0.059	0.06
4	Agriculture area	10.881	12.125	12.614	14.024	14.617
5	Barren area	0.131	0.133	0.133	0.136	0.138
6	Water body	5.384	5.573	5.65	5.81	5.897
7	Built-up area	1.211	1.512	1.658	1.973	2.124
	Exposure	**Number**				
1	Population exposed	4390	4833	5011	5517	6716
2	Buildings exposed	2206	2934	3260	4017	4474

(uploaded in 2009) was used which is the high resolution freely available, higher resolution and more recent DEM would produce better results.

References

1. Ghosh A, Kar SK (2018) Application of analytical hierarchy process (AHP) for flood risk assessment: a case study in Malda district of West Bengal, India. Nat Hazards: J Int Soc Prev Mitig Natural Hazards 94(1):349–368, Springer, October. https://ideas.repec.org/a/spr/nathaz/v94y2018i1d10.1007_s11069-018-3392-y.html
2. Godschalk DR (1991) Disaster mitigation and hazard management. Emergency management: principles and practice for local government, 132
3. UNDP N UNDP Nepal. http://www.np.undp.org/content/nepal/en/home/energy-environment-climate-and-disaster-risk-management/in-depth.html. Accessed 29 July 2019
4. Pokhara Metropolitan City (2019) Pokhara Metropolitan City. http://www.pokharamun.gov.np/. Accessed 30 Aug 2019
5. ASF DAAC (2015) ALOS PALSAR_Radiometric_Terrain_Corrected_ high_res; Includes Material. Accessed through ASF DAAC. https://doi.org/10.5067/JBYK3J6HFSVF. Accessed 25 Apr 2019
6. ICIMOD (2013) Landcover of Nepal 2010. ICIMOD. Retrieved from ICIMOD, Kathmandu

7. Thapa S, Shrestha A, Lamichhane S, Adhikari R (2020) Catchment-scale flood hazard mapping and flood vulnerability analysis of residential buildings: the case of Khando River in eastern Nepal. J Hydrol Reg Stud 30(March):100704. https://doi.org/10.1016/j.ejrh.2020.100704
8. Islam MM, Sado K (2002) Development priority map for flood countermeasures by remote sensing data with geographic information system. J Hydrol Eng 346–355. https://doi.org/10.1061/(ASCE)1084-0699(2002)7:5(346)
9. Moriasi DN, Arnold JG, Bingner RL, Harmel RD, Veith TL (2007) Model evaluation guidelines for systematic quantification of accuracy in Watershed simuaalations. ASABE 50(3):885–900

Bed-Bank Relationship and Flood Characterisation in the Upper Reach of the Brahmaputra Valley, Assam

Siddhartha Kumar Lahiri, Angkuran Sarma, and Robert James Wasson

Abstract Brahmaputra valley relief of upper Assam in India bears plenty of evidences to suggest active structural control as well as remarkable unevenness in sediment budgeting. These two major forcings cause highly variable bed-bank relationships along different reaches of the Brahmaputra's channel belt. Under steady average annual precipitation in decadal scale, flood vulnerability can be taken as directly proportional to the decreasing rate of bed-bank elevation difference. Normally, average bed elevation of the highest order river of a given valley reach is the base level of the reach. Bed-bank architecture over the years shows different reach scale possibilities. A big braided river like the Brahmaputra shows alternating narrower 'nodes' and wider 'internodes'. Usually, nodes are deeper and anti-nodes are shallower. Reach scale widening of rivers over time on many occasions is accompanied by shallowing tendency as well. For the upper reach of the Brahmaputra River and the valley, reach scale plano-temporal variability for the period 1915–2015 was monitored. From the confluence of three major rivers, the Siang, the Dibang and the Lohit, up to 230 km downstream, 23 reaches each of 10 km width were chosen. Essentially we have four findings. First, by measuring plano-temporal variability of sandbar/channel areas we could locate reaches having steady rate of aggradation; secondly, two indices for depths and widths were developed which help to identify normalised deeper zones and zones showing normalised widening tendency over three different average widths (1915, 1975 and 2015). This also helps to test the validity of the general assumption whether shallower reaches show a general trend of widening or not for the upper reach of the Brahmaputra valley. Thirdly, by assuming discretisation of the flow into equal width reaches, probable flood inundation areas were identified for incremental jumps of water levels over

S. K. Lahiri (✉) · A. Sarma
Department of Applied Geology, Dibrugarh University, Dibrugarh 786004, Assam, India
e-mail: siddharthalahiri@dibru.ac.in

R. J. Wasson
ANU, Canberra, Australia

JCU, Singapore

UKM, Bangi, Malaysia

C. Bhuiyan et al. (eds.), *Water Security and Sustainability*,
Lecture Notes in Civil Engineering 115,
https://doi.org/10.1007/978-981-15-9805-0_16

the average bank elevations by 0.5, 1.0, 1.5, 2.0 and 2.5 m assuming absence of embankments. Lastly, assuming complete embankments for both the banks exclude the possibility of immediate flooding but accelerate thereby the river bed construction and practically zero bank construction which can be interpreted in terms of disaster incubation. For uniform aggradation all along the river bed of the study area, reaches having river bed elevation equal or higher than the bank elevation will be more prone towards embankment breaches. Accordingly, for different aggradation thickness values of 0.5, 1.0, 1.5, 2.0 and 2.5 m within the channel belt, the incubation of vulnerability for different reaches of both the banks was identified.

Keywords Geomorphic relief · Flood vulnerability · Brahmaputra · Nodes · Internodes · Aggradation

1 Introduction

Big rivers show considerable degree of reach scale variability in the bed-bank relationship from source to sink. Thus, rivers even during peak flood season seldom flood all the banks. Mountain fed rivers, acting as conduits between the high elevation source zones and the sinks in seas or oceans, run across reaches having variable slopes. Moreover, tributaries of different size join the rivers at different places. Slope, discharge and the load (both bedload and the suspended load) together play more significant components to determine the stream power as well as the channel patterns [1] of a river at a given reach. There are reaches where slopes are the principal factor, and there are reaches where the discharge can play the main role to determine the stream power [2]. Thus, the response of a river for equal slopes near the source zone where it is rich mainly in bedload and before approaching the sink where it is usually rich in suspended load needs different explanations.

2 Brahmaputra

Brahmaputra, having highly variable thalweg [3], the seventh-largest river in the world [4] and after being joined by the Ganges, the highest sediment carrier [5, 6], is also one of the worst flood causing rivers.

In recent times, the Brahmaputra came to headlines at least due to six major reasons. Firstly, a trans-boundary international issue relating the construction of big dams in the Chinese part; secondly, sudden influx of black clayey materials since the last quarter of the year 2017 through the Siang causing a prolonged change in the colour of the river water and drastic reduction in the fish population (the causes of which are yet to be ascertained and there might be a connection with the unreported dam failures in the upstream side); thirdly, changing characters of the floods in terms of frequency, suddenness, intensity and the magnitude of losses. The average annual

flood toll of human lives increased from 41 (during 1953–1995) to 63 (during 2001–2017) in Assam. In 2017, the number of deaths was 158. Most of these deaths were due to embankment breaches; fourthly, unprecedented magnitude of bank-line migration; the fifth factor was related to a grand design of river linking project of exporting surplus water from the northern India to the water starved southern provinces and the sixth factor was related to a massive dredging project of the Brahmaputra channel belt apparently aimed at improving the navigability of the river as a part of an ambitious planning to expand the length of waterways along with the roadways as a part of raising a robust infrastructure of communications. A common factor that runs under all these issues is the hydro-sedimentary budgeting, its spatio-temporal variability annually and over different cycles. To refresh a few information and general statistics, the Brahmaputra River is approximately 3848 km in length and runs through Tibet (autonomous region of China) in between the great Himalayan ranges in the south and the Kailash range to its north for nearly 1650 km in west to east direction. The river is also known as the Tsangpo (purifier) in China. It enters India (Arunachal Pradesh) after taking a southward direction near the Namcha Barwa mountain range in the Upper Siang district. One school [7–11] likes to call the Brahmaputra as Dihang or Siang River in the Arunachal Pradesh which flows along the north-south direction through Upper Siang and east Siang districts covering a total of 400 km of Arunachal Pradesh before it enters Assam. The river runs for 650 km from east to west through Assam and acts as a valley divider before entering Bangladesh (rechristened as the Jamuna) and ultimately drains into the Bay of Bengal. The other school [12–14] puts the name Brahmaputra after three major rivers, the Siang, the Dibang and the Lohit confluence (at a place called Kobo as could be seen in the topographic map prepared during 1912–1926 having the scale 1inch = 4miles). Present study covers only the upper reach of the Brahmaputra River and the adjacent banks, a 230 km long stretch (Fig. 1).

3 Bed-Bank Relationship

Flood characterisation essentially means spatio-temporal variability study in the bed-bank relationship of a river system which due to changing hydro-sedimentary budgeting makes different reaches of a valley susceptible to inundation due to the ‘excess water’ over the ‘bankfull condition’. A simple model of flooding is first to visualise an inclined trough having an inlet and outlet at the opposite ends, sediment loaded water flowing through it. When the rate of influx (water or/and sediment) is more than the outflow, height of the water column keeps on increasing and a stage comes when the spill-over happens. Now, the question is wherefrom the spill-over begins first? For the analogy taken up in the present discussion, the obvious answer will be the downstream side. However, for a river valley, when the flood prone areas are mapped, a considerable degree of arbitrariness is observed (Fig. 2). For example, (i) both the banks of a river may not be reaching ‘bankfull condition’ at the same point

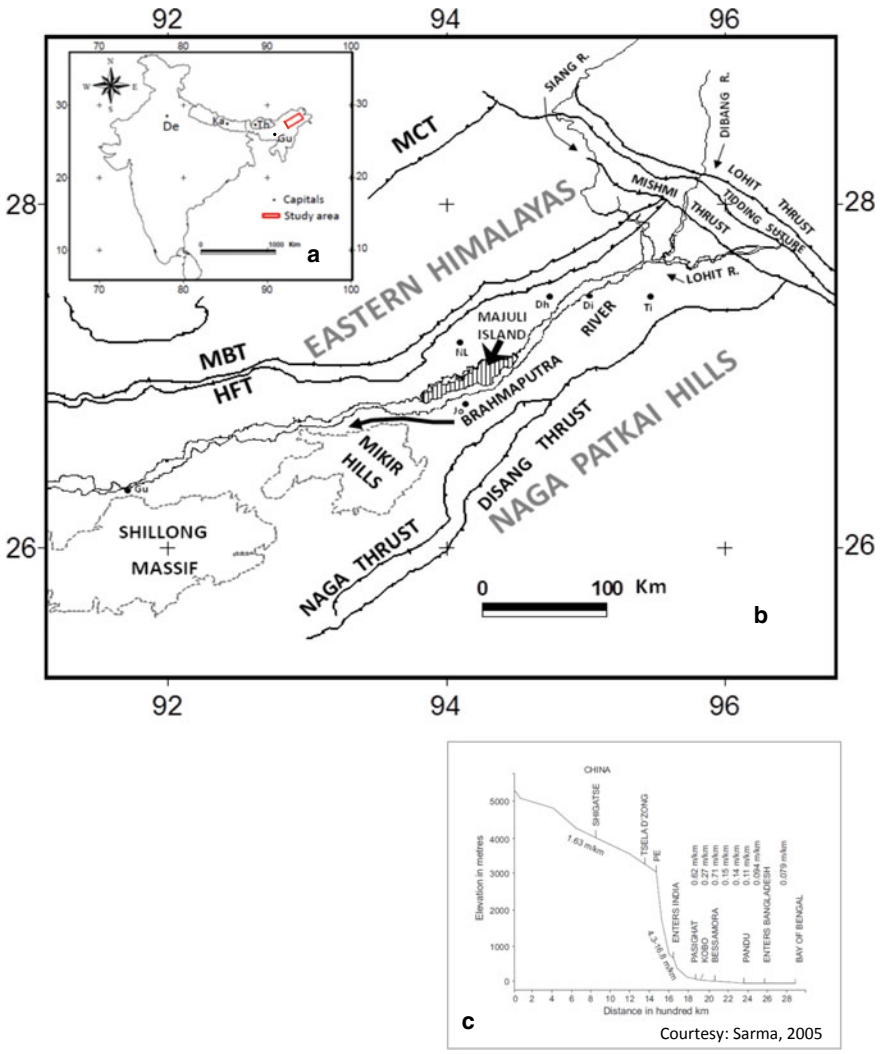

Fig. 1 **a** Study area is shown on the outline of India. De-Delhi, Ka-Kathmandu, Th-Thimpu, Gu-Guwahati. **b** Location map of the upper reach of the Brahmaputra valley. Some of the prominent geological elements are shown. MCT-Main Continental Thrust, MBT-Main Boundary thrust, HFT-Himalayan Frontal thrust. Some of the important townships of upper Assam: Di-Dibrugarh, Ti-Tinsukia, Dh-Dhemaji, Jo-Jorhat, NL-North Lakhimpur. The Brahmaputra River shown in the figure represents its status in 1915. **c** Changing elevation of the Brahmaputra River which covers source to sink. From the Tibetan part at a place called PE to the first time entry in the Indian territory, the high variability in slope 4.3–16.8 m/km is remarkable which reduces to 0.62 m/km at PASIGHAT

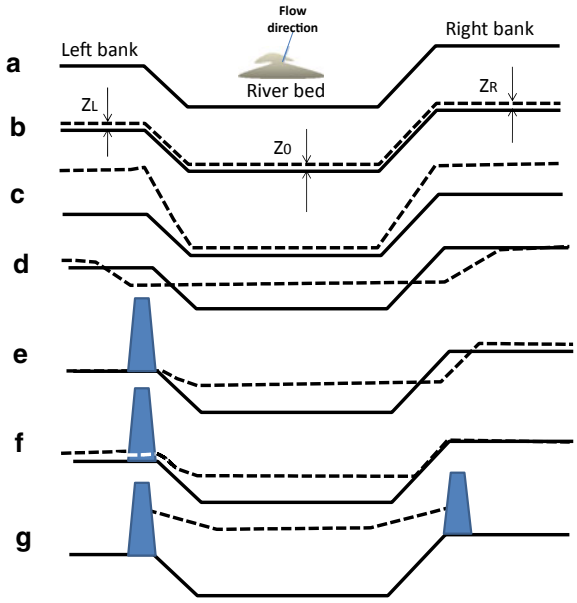

Fig. 2 Bed-bank relationship showing some of the many possibilities. **a** The directional convention and nomenclature followed. It has been assumed that the average elevation of right bank is higher than the left bank **b** A situation for which rate of formation for the bed and the banks is more or less uniform that is, $Z_L = Z_0 = Z_R$; **c** Rate of river bed aggradation is much lesser than the rate of flood plain construction and $Z_L > Z_R \gg Z_0$. This may be due to higher slope reaches, mostly 'nodes'; **d** Asymmetric rate of river bank construction with $Z_0 \gg Z_L > Z_R$. These are typical reaches of aggradation which causes bank-line migration, mostly 'anti-nodes'; **e** This type of situation can happen when there is embankment in the left bank that is $Z_0 \gg Z_R$. Left bank construction stopped; **f** Rate of river bed aggradation is much higher that the flood plain construction that is $Z_0 \gg Z_L > Z_R$ This is due to leaky embankment **g** Embankments in both the sides temporarily stops flooding as well as the construction of banks. Rate of bed construction advances at a much faster rate and a stage comes when the river bed no more represents the 'base level'. In spite of good quality embankments, river can change its course in a highly unpredictable manner

of time due to variable bank elevations; (ii) thalweg of the river might have considerable degree of reach scale variability due to uneven distribution of the sediments; (iii) Different reaches of the river show different degrees of aggradation which might have structural implications; (iv) the channel belt might show alternate 'nodes' and 'internodes' (Fig. 3) where stream power might be guided principally by the valley slope or the discharge or perhaps a continuously variable proportion of both which in turn determines whether the rate of lateral erosion will be more or vertical incision; (v) a big river like the Brahmaputra flows in certain reaches as a single flow, or a multichannel, or in anabranching mode and even showing sometimes highly anastomosing tendency. Thus, what constitutes reach scale 'flow efficiency' of a channel is definitely a complex problem of hydro-dynamics which attains greater complexity if the influence of different tributaries is taken into account. This article explores a simple geomorphological approach for flood characterisation.

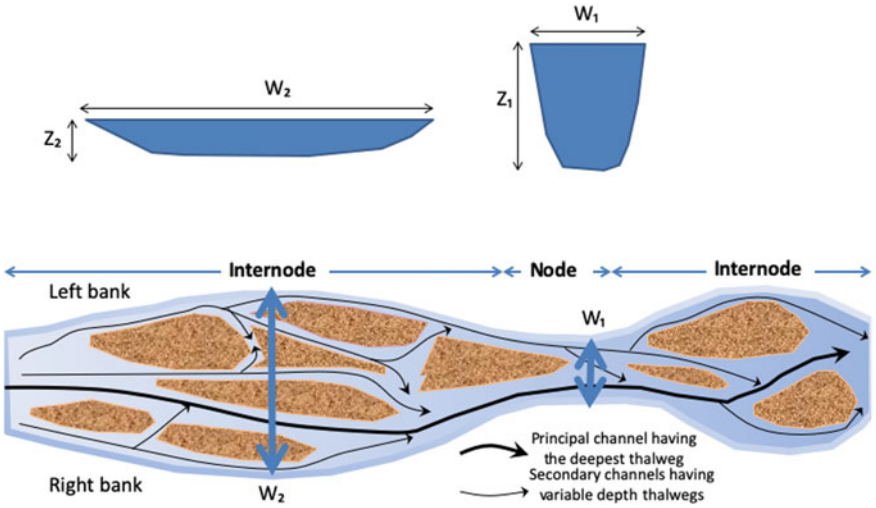

Fig. 3 Cartoons showing assumptions on channel morphology, **a** Wider reaches are shallower **b** Narrower stretches of the channel belts are usually deeper, **c** Planform representation of a braided river showing the tapered zones marked as 'Nodes' and the widened stretches marked as 'Internodes' where the aggradation potential is more and the number of sand bar deposits are also more. In the multichannel internode segment, the bolder arrow shows the deepest and the widest of all channels and can be treated as the representative thalweg of the river

Observations of river bank stratigraphy show that river bed aggradation and the riverbank formation aided by the flood plain deposits can take diverse forms in different reaches. Some of the possibilities are shown in Fig. 2. In essence, the fact that matters is for a given reach whether the effective accommodation space is increasing or decreasing. Increase in the accommodation space means for a given discharge, possibility of flooding reduces and if the effective accommodation space decreases, flood vulnerability for that reach increases. Flood plain construction might follow symmetrical characteristics, and in other circumstances, it can be grossly asymmetrical. There is no doubt about it, raising embankments arbitrarily along the river banks introduces higher degree of reach scale asymmetry and the river bed aggradation rate becomes faster. As a result, accommodation space decreases at a much faster rate and even for normal or reduced precipitation than the average of the past decades, flood vulnerability increases.

Assumptions for flood characterisation

Brahmaputra shows alternate widening and narrowing pattern in the planform. We have made two basic assumptions:

Assumption 1 Narrower the channel belt deeper it is.

Assumption 2 For the multichannel reaches of the braided rivers, wider channels have deeper thalweg. Accordingly, for a braided channel belt, the location of the deepest thalweg can be assumed to be the median path of the widest channel (See Fig. 3).

Apparently, these two hypotheses oppose each other! However, it can be explained by the fact that the stream power is basically proportional to the product of the slope and the discharge and the constant of proportionality can be a factor of bank material consolidation.

For valleys having strong structural controls, slopes show considerable lateral variability ('kinks' in the elevation variability profile). High slope segments witness increases in the stream power which helps greater bed incision and lesser aggradation potentiality and hence increased depth and narrower widths (Nodes). On the other hand, zones of subsidence, showing enhanced aggradation tendency, more numbers of sandbars and multichannels. Stream power is determined mainly by the discharge volume—accordingly, wider the channel, higher the stream power and higher the rate of bed incision (for 'Internodes').

Thus, for 'Nodes', slopes play the decisive role, whereas for 'internodes', relative discharge volume plays more important role to determine the depth of the thalweg. Moreover, average stream power at 'Nodes' is more than the 'Internodes'.

Assumption 3 We have further assumed that the continuous flow of the river from its upstream to downstream end can be replaced by 'cascade flow' (discrete) which essentially means that when the bankfull condition of a given reach is surpassed and inundation of the banks take place, the turn of the next downstream reach comes immediately afterwards as if 'flooding in succession'. However, the delay time is so small that the process becomes closer to the continuous flow condition. The advantage of the assumption is that bed-bank relationship of individual reaches can be treated as principally responsible for inundation of that reach. Impact of inundation in the upstream reaches on the downstream reaches is neglected.

4 Data and Interpretation

To introduce comparability in the morpho-dynamics of the Brahmaputra River in terms of the reach scale variability in the depths (for the present situation only) and the widths (for 1915, 1975 and 2015) two indices were used which are given below.

$$\text{Depth Index} = \frac{\text{Reach depth} - \text{Average depth}}{\text{Maximum depth} - \text{Minimum depth}}$$

And,

$$\text{Width Index} = \frac{\text{Reach width} - \text{Average width}}{\text{Maximum width} - \text{Minimum width}}$$

'+'ve values of both the indices mean higher than the average.

Our general expectation, as discussed earlier, reaches showing widening tendency will also undergo a shallowing tendency principally due to increased rate of aggradation. We have latest status (not the earlier situations like 1915 and 1975) to reach scale average elevation differences between the river bed and two banks. We are interested to investigate the temporal changes in width associated with those reaches which are deeper compared to the average depth. We have identified five zones (shown by boxes in Fig. 4) where we find the channel is deeper compared to the average depth value.

In **Box 1**(Fig. 4b), width index during 1915 and 1975 were showing the opposite trend (fitting nicely with the assumptions we made). However, the trend during 2015 shows similar trend.

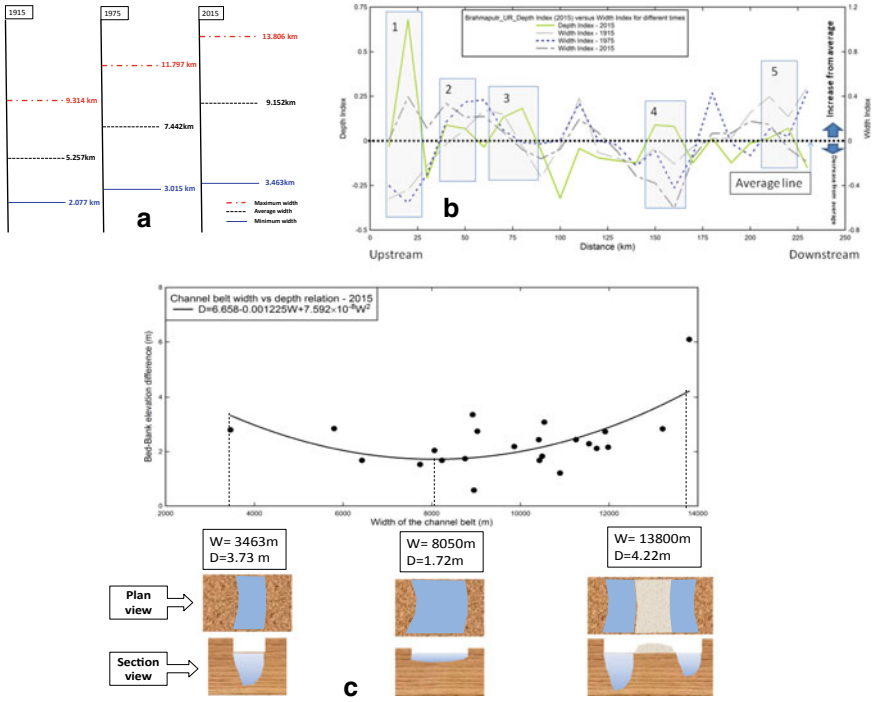

Fig. 4 Depth-width relations **a** The boundary and the average values at three different times about which width index were calculated for different reaches **b** A comparative study of the depth index and temporal variability of the width index. Boxes 1–5 show the zones where depth index increases over the average depth. **c** A second-order approximation of polynomial fit gives an empirical equation showing bed-bank relation during 2015 where difference in average elevation between the bank and bed (expressed as depth D) has been treated as the function of width of the channel belt (expressed by W). The qualitative significance of the equation has been explained in the plan and section views below

Explanation: While considering the depth index, the channel belt included newly evolved relict island the Dibru-Saikhoa. This was essentially due to the course correction of the Lohit River which helped to increase by jump the width of the Brahmaputra channel belt. Thus the reach scale width index is showing much higher value.

In **Box 2**, deeper reaches are also associated with increasing width index.

Explanation: This is probably due to the massive erosion of the banks constituted of loose bank materials. Some of the shallow subsurface loose sand units help rapid 'toe cutting'. Massive lateral erosion helped to redistribute the sediments in the downstream but did not cause effective shallowing tendency at the place of erosion itself.

Box 3 represents a transition zone where some of the higher depth reaches (in the upstream side) are wider and some are narrower (in the downstream side).

Explanation: The river beyond these reaches is going back to its normal logic of aggradation

For **Box 4,** the reaches of the river show the standard opposite characteristics—'Deeper the reach narrower it is'.

Box 5 representing downstream end of the Majuli Island, shows a mixed behaviour which is most probably due to anthropogenic intervention of various kinds of river management schemes operational in this area since a long time.

The anomalous situations arising due to high degree of variability in the sandbar/channel ratio can influence the bed-bank relation which is shown in Fig. 4c by a second-order approximation of depth variation as a function of variation in width during the year 2015.

4.1 Flood Characterisation

The flood characterisation done is mainly based on the areal extent of inundation due to flooding with respect to an unit increase of head in the water level in full bank condition. Each of the reaches selected every 10 km interval was further subdivided into five sub-reaches and every incremental rise was identified in the DEM of the Google Earth and the final equal interval contours of probable inundation were plotted in the ArcGIS platform.

Using the DEM data areal extent of flooding is delineated (Fig. 5) and simple volumetric calculations are being done. To keep the calculation simple the presence of ridge and swale geomorphological features of the flood plain are not considered.

Areal extent of the inundation areas had been calculated as shown in Table 1.

From the data thus obtained and calculated assuming no difference in elevation between both the banks, following observations are made (Table 2).

- A 0.5 m increase in the water level head can cause a great areal extent of flooding than its preceding increase ranging between the minimum 490 to maximum 1500 km^2.

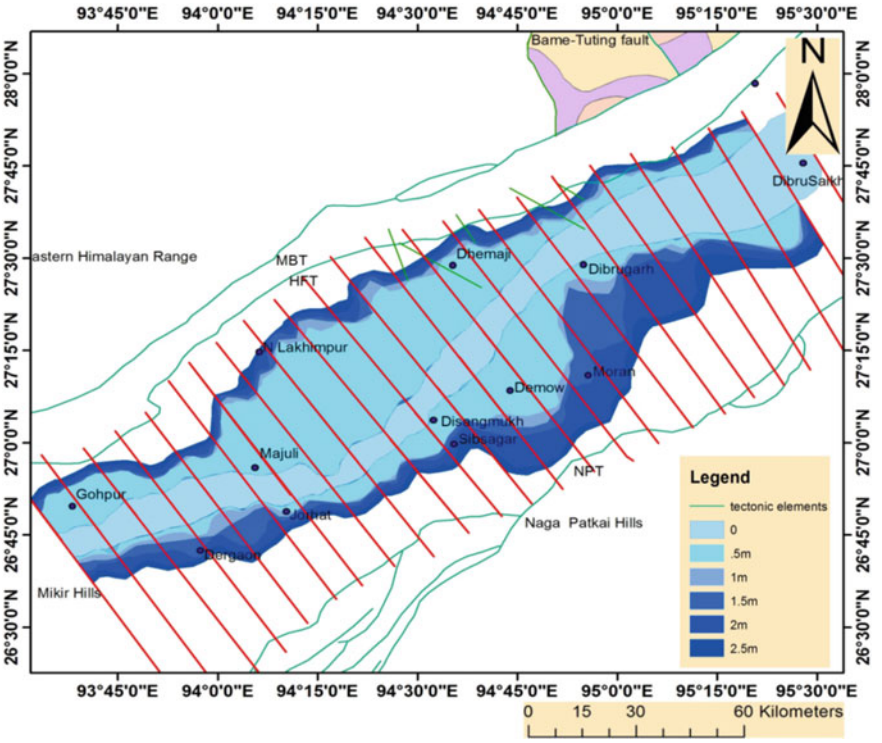

Fig. 5 Map showing areal extent of flooding with 0.5 m, 1 m, 1.5 m, 2 m and 2.5 m decrease in depth of river bed and reach scale average bank elevation does not change, and also there is no embankment. Every incremental change of water elevation over the bankfull condition is supposed to inundate all those bank areas having less or equal the said elevation

Table 1 Areas of inundation calculated for incremental increase in water level

Increment in water level (m)	Right bank (km^2)	Left bank (km^2)	Left +right bank (km^2)
0.5	2919.3	1309.5	4228.9
1	3114.2	1604.8	4719.0
1.5	3312.5	2260.0	5572.5
2	3666.8	3404.9	7071.8
2.5	3945.8	3935.7	7881.6

- In the upstream part, the left bank is more prone to flooding and its areal extent is much larger than the corresponding right banks (Fig. 5). This can be attributed to the impact of Himalayan orogeny near the frontal thrust belt in terms of upliftment as well as higher rate of sediment influx raising the effective elevation of the relief.
- However, in the middle part of the study area, both the right and the left bank are equally vulnerable to flooding.

Table 2 Incremental increase in areal extent due to every 0.5 m increase in water level than the bankfull condition

Increment in water level (m)	Right bank (increment in areal extent) (km^2)	Left bank (increment in areal extent) (km^2)	For both banks (increment in areal extent) (km^2)
0.5			
1	194.9	295.3	490.1
1.5	198.3	655.2	853.5
2	354.3	1145.0	1499.3
2.5	279.0	530.8	810.0

- In the downstream section, the right bank is more vulnerable to flooding. This is probably due to the sediment influx from some of the major south bank tributaries like the Burhi-Dihing, Disang, Dikhau and the Dhansiri which compensate the sediment influx due to the north bank rivers. Moreover, shifting aggradational tendency in the river bed reduces the bed-bank elevation difference.
- For 0.5 m to 1.5 m increase in water level head, the areal extent of flood inundation in the right bank is much higher than the left bank areas (Table 1).
- However, with increase in water level over 1.5 m, the areal extent of inundation in both banks almost tends to be equal (Table 1).

4.2 Flood Disaster Incubation

Flood incubation is a term used to define the growth of potentiality of flood in a region. Many anthropogenic as well as natural factors are responsible for intensifying the flood vulnerability of a region. Embankment construction, a major issue for the people of Assam is one of the most important attributes to increase the potentiality of flood vulnerability. Flood occurrence due to embankment breaching is a common cause of flood in Assam.

Embankments which are built for mitigation of flood increase the flood vulnerability by decreasing the accommodation space for sedimentation by the river, thus decreasing bed-bank depth which in turn greatly influences the flood vulnerability of the region (see Fig. 2). For a constant annual discharge of water, the river water overtops in the subsequent years thus flowing above the bank. This overtopping water on entering the pore spaces of the embankments decreases the stability of the embankments and hence acts as an incubator of flood.

By plotting average elevation of the bed with increase in unit amount of sediment from present-day elevation of the river bed versus distance and the present-day reach scale elevation of both the banks (Fig. 6), following observations were made:

- For 0.5 m to 1 m increase in river bed due to sediment deposition, the water level overtops left bank at a particular reach.

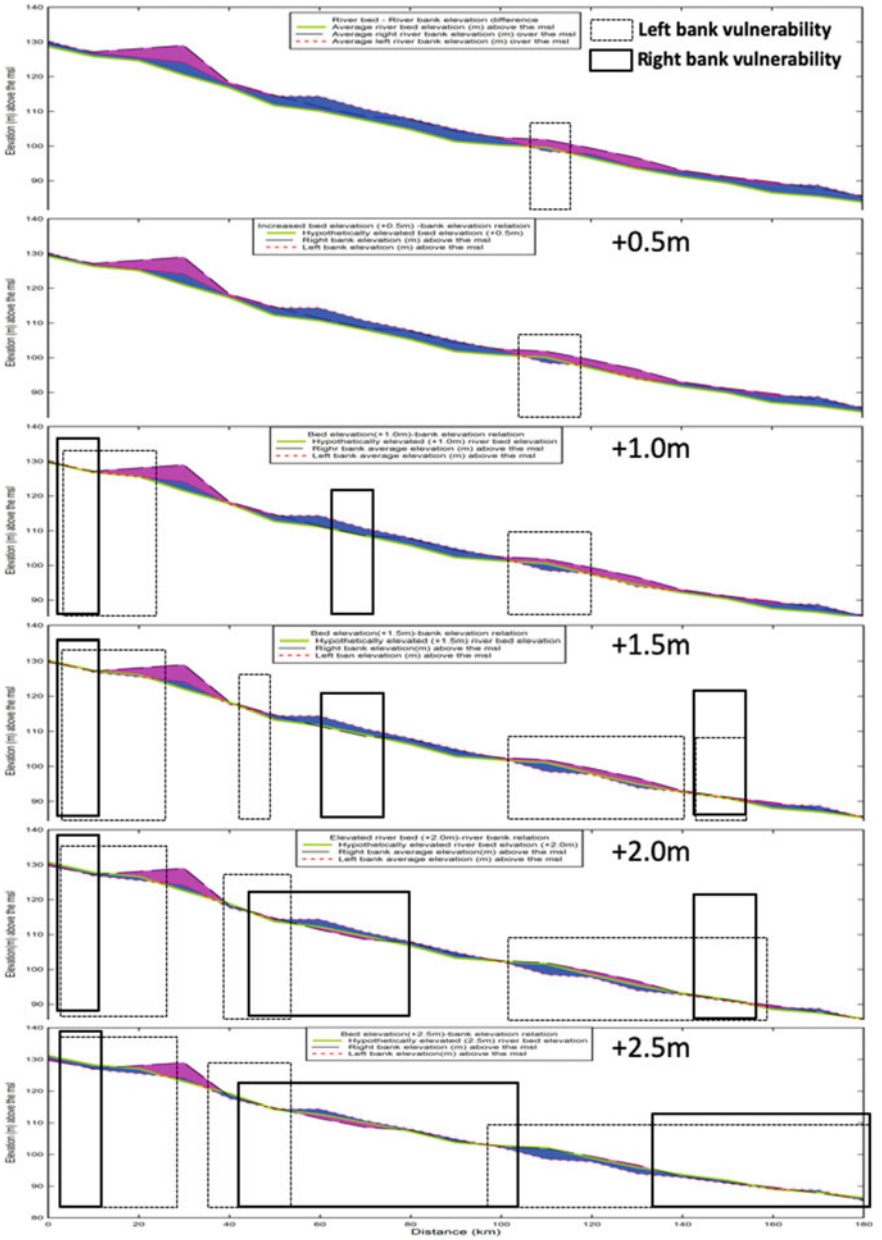

Fig. 6 Graph showing relationship between unit increase of sediment deposition in the river bed with flood disaster incubation and the associated vulnerability of the respective zones

- With further increase in the sedimentation of the river bed, it can be seen that much of the bank-line both right and left become susceptible to flooding or the reach scale flood vulnerability increases with increase in sediment deposition.
- From the present position of the river bed elevation, if the rapid rate of aggradation due to the construction of embankments causes 2.5 m rise, the threshold is reached which makes both the banks equally vulnerable for flash flood due to embankment breaching.

4.3 Flood Triggering

There are ample evidences of paleo mega-flood events in the higher Himalayas (Fig. 7a) which are usually called as the Glacial Lake Outburst Floods (GLOFs) and Landslide Lake Outburst Floods (LLOFs). These were mostly climate induced or large scale tectonic readjustment induced events. However, ever since big dams are constructed at different levels mostly to tap hydroelectric potential, possibilities of flood triggering due to dam outburst have started attaining similar and in certain situations much bigger proportions. We would like to present a modest estimation of flood triggering.

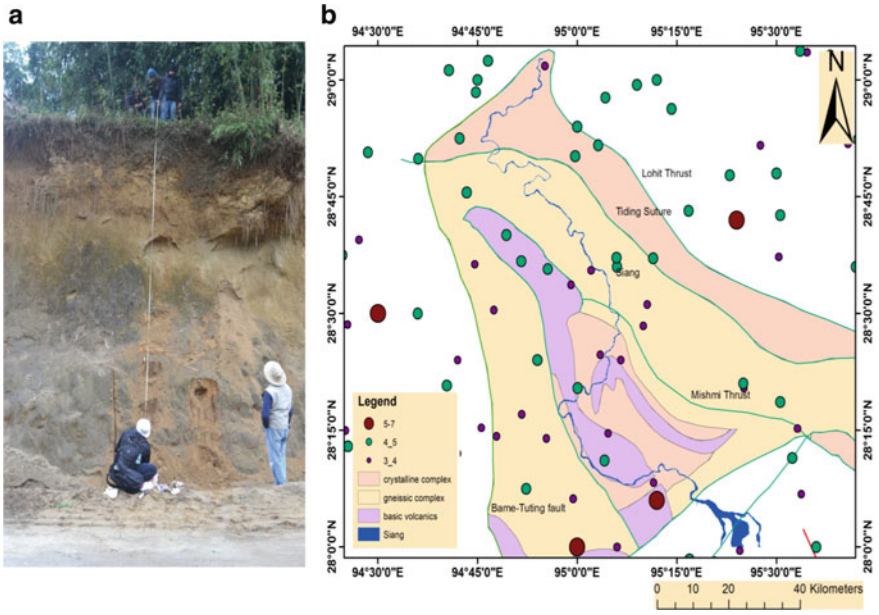

Fig. 7 **a** An evidence of paleo mega-flood deposits near Geku in the Siang Himalayas at the location N28°25′35.6″ E95°05′39.3″ Elev.278 m. This one-shot fining upward sequence was measured about 6.5 m. **b** Locations of epicentres of some of the recent (from the year 2000 onward) earthquakes in the Siang Himalayas (*Source* NEIST-CSIR, Jorhat)

• MWL	: EL 234.4 m
• Full Reservoir level (FRL)	: EL 230 m
• Min. Drawdown level(MDDL)	: EL 225.5 m
• Gross storage at FRL	: 1421.0 Mcum
• Gross storage at MDDL	: 1216.93 Mcum
• Live Storage	: 204.07 Mcum
• Area under submergence	: 51.51 sq km at FRL
• Length of reservoir	: 77.5 km along main Siang River and 28.5 km along Siyom River at FRL.

Power house is with installed capacity of (9×300) 2700 MW.

Box 1 Reservoir characteristics for the Siang hydrological project

From the data available from Siang hydrological project the reservoir characteristics are mentioned in Box 1.

A Central Electricity Authority, Govt of India Report (2001), identifies the north-east as the 'future powerhouse' and at least 168 large hydroelectric projects with a total installed capacity of 63,328 MW are either under construction or in the near-final stage of implementation.

Now, a simple calculation suggests that if the required volume of water held by the reservoir to produce 2700 MW of electricity = 1421.0 Mcum then for 63,328 MW of electricity volume of water required to be in the reservoir will be 33,329 Mcum which is much higher than the areal extent covered by a 2.5 m increase in water level. Recent seismicity status (Fig. 7b) since the year 2000, as monitored by the NEIST-CSIR, Jorhat shows that the Siang Himalayas is highly active and the current state of our knowledge is inadequate to guarantee that every possible factor causing dam outburst had been taken care of.

Besides the upstream side, high altitude causes of flood triggering, as discussed earlier every year frequency of embankment breaching is increasing. The life of an embankment is generally set at 25–30 years, but the field evidences suggest that the complete construction of embankments takes nearly 20–25 years as these are mostly built on piecemeal basis. Older stretches are more vulnerable than the newer ones. However, lack of reliability in the official records of the exact dates of commencement and completion of different stretches of embankments and hence the needs for additional monitoring and maintenance measures are simply absent. During bankfull condition, repairing works are mostly done on ad hoc basis when actual seepages are being reported.

5 Conclusion

For flood characterisation, sediment budgeting, spatio-temporal changes in the pattern of aggradation play crucial role. Reach scale study of river bed and the river bank relationship can give important clues to assess the trend of flood vulnerability. During 1915–1975, the principal site of aggradation was concentrated mostly in the upstream part of the Brahmaputra valley which is evident from the reach scale sandbar/channel area ratios computed for the length of 230 km. However, during 1975–2015, the site of aggradation has shifted further downstream in and around Majuli. A comparative study of width indices for different times (1915, 1975 and 2015) with the present depth index (2017 imagery) helps to understand the stream power variability of the river flow and its consequences on the bank erosion and bed incision. Raising embankments help to incubate flood vulnerability; five-stage increments in river bed thickness show clearly the spread of vulnerability along both the right and left bank of the Brahmaputra River. The areal extent of multi-stage flood inundation was generated in case of flood triggering due to single or multiple dam failures or embankment breaching. For flood head increases from +0.5 m to + 1.5 m, more of north bank areas are vulnerable; however, for +2.5 m increase in the flood water head, vulnerability of both the banks reaches uniformity.

Acknowledgements First two authors acknowledge the help extended by Dibrugarh University for providing financial and administrative support to conduct field visits.

References

1. Schumm SA (1981) Evolution and response of the fluvial system: sedimentologic implications. Soc Econ Paleontol Mineral Spec Publ 31:19–29
2. Robert, A.: River processes—an introduction to fluvial dynamics. Arnold, a member of the Hodder Headline Group, GB (2003)
3. Coleman JM (1969) Brahmaputra River channel processes and sedimentation. Sediment Geol 3:129–239
4. Hovius N (1998) Controls on sediment supply by larger rivers. In: Shanley KW, McCabe PJ (eds.) Relative role of eustasy, climate, and tectonism in continental rocks. Soc Sediment Geol SEPM Spec Publ 59:3–16 (1998)
5. Goswami DC (1985) Brahmaputra River, Assam, India: Physiography, basin denundation and channel aggradation. Water Resour Res 21:959–978
6. Latrubesse E (2008) Patterns of anabranching channels: the ultimate end-member adjustment of mega rivers. Geomorphology 101:130–145
7. Bracciali L, Najman Y, Parrish RR, Akhter SH, Millar I (2015) The Brahmaputra tale of tectonics and erosion: early Miocene river capture in the Eastern Himalaya. Earth Planet Sci Lett 415:25–37
8. Brookfield ME (1998) The evolution of the great river systems of southern Asia during the Cenozoic India-Asia collision: rivers draining southwards. Geomorphology 22:285–312

9. Cina SE, Yin A, Grove M, Dubey CS, Shukla DP, Lovera OM, Kelty TK, Gehrels GE, Foster DA (2009) Gangdese arc detritus within the eastern Himalayan Neogene foreland basin: implications for the Neogene evolution of the Yalu-Brahmaputra River system. Earth Planet Sci Lett 285:150–162
10. Lang KA, Huntington KW (2014) Antecedence of the Yarlung-Siang-Brahmaputra River, eastern Himalaya. Earth Planet Sci Lett 397:145–158
11. Seward D, Burg JP (2008) Growth of the Namche Barwa Syntaxis and associated evolution of the Tsangpo Gorge: constraints from structural and thermochrono-logical data. Tectonophysics 451:282–289
12. Lahiri SK, Sinha R (2012) Tectonic controls on the morphodynamics of the Brahmaputra River system in the upper Assam valley, India. Geomorphology 169–170:74–85
13. Sarma JN, Phukan MK (2004) Origin and some geomorphological changes of Majuli Island of the Brahmaputra river in Assam, India. Geomorphology 60:1–19
14. Sarma JN (2005) Fluvial process and morphology of the Brahmaputra river in Assam, India. Geomorphology 70:226–256

Innovative Techniques and Technologies

Control of Sediment Entry into Intake Canals Using Submerged Vanes with Collar

Sruthi Thazhathe Kalathil, Muralidharan Rethinam Murugesan, and Venu Chandra

Abstract Intake canals transport water and sediments from main rivers to power plants, irrigation fields, and for various other purposes. Increased sediment load in the intake canal leads to reduction in the quality and quantity of water. Submerged vanes are installed at the entrance of intake canals to counteract the secondary circulation and reduce the sediment entry into the intake canals. In the present study, collars have been introduced to submerged vanes to test its performance in the reduction of both sediment entry and local scour around vanes. The vane angles tested are 15°, 35°, 40° and 45°. The ratio of vane spacing to vane height is 5 and the two collar diameters considered are three and four times the vane height, respectively. It is found that 40° is the optimum vane angle for maximum reduction in sediment entry into the intake canal of 85.36%. Collars reduced the local scour and sediment entry (%) by a maximum of 69.08% and 24.84%, respectively, for a 15° vane angle. However, introduction of collar reduced the performance for vane angles 35°, 40°, and 45° in controlling sediment entry into the intake canal.

Keywords Sedimentation · Secondary currents · Vane angle · Local scour · River training

1 Introduction

Sediment transport is a hydraulic phenomenon that has emerged as a significant problem in river-intake canals. River flow, which enters into an intake canal, carries a lot of sediment along with it due to centrifugal action at river-intake junction [1]. The transport of sediment can be in the form of suspended and bed loads. The movement of the sediments through the river-intake structures is a major challenge for the

S. T. Kalathil · V. Chandra (✉)
Department of Civil Engineering, Indian Institute of Technology Madras, Chennai 600036, India
e-mail: vc@iitm.ac.in

M. R. Murugesan
TANGEDCO Ltd., Uppur, Ramanathapuram 623525, India

C. Bhuiyan et al. (eds.), *Water Security and Sustainability*,
Lecture Notes in Civil Engineering 115,
https://doi.org/10.1007/978-981-15-9805-0_17

operation and maintenance of intake canals, power plants, and irrigation fields. As a consequence of sediment entry and subsequent deposition in these intake structures, there is also a reduction in the water carrying capacity of these canals.

Submerged vanes have been used as a control measure at river intakes since 1990 [2]. Submerged vanes are small flow-training structures designed to modify the near bed flow pattern and re-distribute the flow in the channel cross section. The vanes function by influencing bed shear stress and cause a change in the distribution of velocity, depth, and sediment transport in the area affected by the vanes. The performance of submerged vanes is based on the formation of helical vortices at the river canal junction, which reduces the effect of naturally occurring secondary circulation near the intake structure [3]. The sediment is picked up from the vane's negative pressure side and gets deposited on the positive pressure side. The strength of the helical vortex induced by the vanes depends on spacing between the vanes, vane height, vane angle, and longitudinal arrangement of the vanes [4–7]. In addition to reduction of sediment entry into the intake canal, care should be taken to ensure that the local scour around the vane is minimal. Increase in local scour would result in the dislodgement of vane and failure of the flow-training mechanism.

The optimum values for the vane parameters over the years have been identified based on studies related to intake canals, river bed, and river bank protection [8–11]. Vane height-to-water depth ratio can range from 0.2 to 0.5 and vane height-to-vane length ratio can be varied from 0.1 to 0.5 [9]. A vane angle of 15° produces the least scour depth around the vanes and lowest sedimentation percentage in the intake canal [12]. However, the effect of vane angle on the sediment entry is different for different vane configurations [13]. At $S/H_v \leq 3$ (where, S is spacing between the vanes and H_v is the height of vanes), volume of sediments entering the intake increases with an increase in vane angle. On the contrary, at $S/H_v \geq 4$, as the vane angle increases, the volume of sediments entering the intake is reduced. The present work introduces a collar at the vane bottom to investigate its effectiveness in reducing the local scour around the vane. The value for S/H_v is equal to 5 for all the scenarios tested.

2 Experiments

The experiments were conducted in the Hydraulics Laboratory of Indian Institute of Technology Madras, India. The experimental setup consists of a mobile bed main channel and a rigid bed lateral channel. The main channel is rectangular with a width of 57.5 cm and a depth of 33 cm. The d_{50} of sediment in the main channel is 0.28 mm. The intake canal is considered as trapezoidal with a bottom width of 18 cm, top width of 88 cm, height of 33 cm, and side slopes of 1:1. The intake canal takes diversion from the main channel at an angle of 45°. The sediment bed in the main channel is kept at the same level with the intake canal bottom [12]. A discharge of 10 Lps and a flow depth (H_m) of 5.5 cm with a corresponding Froude number of 0.426 was maintained in the main channel. Submerged vanes of thickness 4 mm, height (H_v) $0.4H_m$, and length $1.2H_m$ were fabricated from stainless steel. Depth of vane

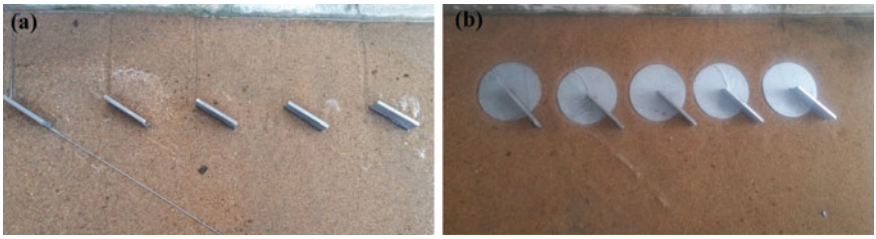

Fig. 1 Arrangement of vanes in the main channel (flow from left to right): **a** without collar, and **b** with collar

insertion into soil and spacing between vanes (S) were considered as H_m and $2H_m$, respectively. The different vane angles used were 15°, 35°, 40º, and 45°. Diameter of collars was varied as $3H_v$ and $4H_v$. Figure 1 shows the arrangement of vanes in the main channel at the entrance of the intake canal.

A digital point gauge was used to measure the water and bed surface levels. Triangular notches were placed at the upstream and downstream of the main channel to ensure constant flow throughout. Local scour around vanes was measured at an interval of 10 min up to first 30 min and then at 30 min interval till equilibrium scour is attained. Equilibrium scour depth is said to be attained when the rate of scouring equals the rate of deposition. Quantification of the total sediment eroded from the main channel and those deposited in the intake canal was done by volume measurement from the downstream collection tanks.

3 Results and Discussion

The experimental results are expressed in terms of sediment entry percentage into the intake canal (S_{ic}) and the maximum local scour depth ratio ($S_{r,max}$) around vanes, where $S_{r,max}$ is the ratio of maximum scour depth around vane to the flow depth in the main channel. The initial percentage of sediment entry into the intake canal (S_{ic}) without the use of vanes was 50.42%. Submerged vanes of $H_v = 0.4H_m$ and $S = 2H_m$ installed at vane angles (α) 15°, 35°, 40°, and 45° reduced S_{ic} to 26.81%, 16.21%, 7.38%, and 14.50%, respectively. The lowest S_{ic} is obtained for $\alpha = 40°$ (85.36% reduction), in contrary to the optimum vane angle of 15° suggested by Kalathil et al. [12], where S/H_v tested were equal to 2.67 and 4. In the present study, S/H_v is equal to 5. This supports the finding of Beygipoor et al. [13] that reduction in S_{ic} with respect to α depends on the value of S/H_v. In addition to S_{ic}, another critical factor determining the efficiency of a submerged vane is its local scour. The maximum local scour ratio has to be less in order to avoid failure of the vanes.

3.1 Effect of Submerged Vanes on Local Scour Depth Ratio

Figure 2 shows the temporal variation of $S_{r,max}$ for different vane angles. It is found that maximum local scour always occurs at the trailing edge of the vane for any given experiment. All curves follow a crest and trough pattern which shows sediment deposition and erosion from the main channel bed. The pattern continues until the equilibrium point where rate of erosion and deposition becomes equal. Equilibrium scour was attained at around 120 min for all the experiments conducted. Equilibrium maximum local scour depth ratio for $\alpha = 35°$ coincides with $\alpha = 45°$. The curve corresponding to $\alpha = 40°$ shows the highest equilibrium maximum local scour depth ratio while the least is observed for $\alpha = 15°$ with a value of 0.72.

It can be concluded that equilibrium maximum local scour depth ratio increases with an increase in vane angle. On the contrary, the least sediment entry into intake canal was observed for $\alpha = 40^0$. It is inferred that although local scour around vanes placed at higher vane angle is more, the eroded sediment is carried to the downstream of main channel, instead of entering into the intake canal. In an attempt to reduce the local scour around vane edges together with least sediment entry into intake canals, experiments have been conducted by installing collars to vanes. The concept is inspired from the use of collars to reduce local scour around bridge piers.

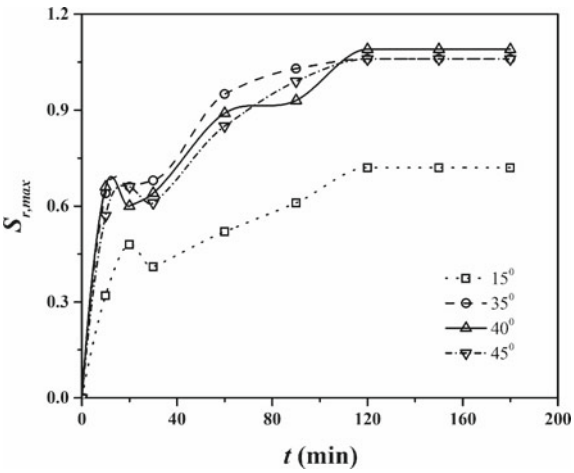

Fig. 2 Temporal variation of maximum scour depth ratio $S_{r,max}$ with different vane angles

3.2 *Effect of Collar Diameter on the Maximum Local Scour Depth Ratio*

Collars of diameters (D) $3H_v$ and $4H_v$ were installed to the leading edge of vanes at the bed level. Figure 3 shows the variation of $S_{r,\,max}$ with time for vanes with and without collars for different vane angles. Earlier, it was seen that vanes without collar attained equilibrium after 120 min. Typically, flow happens around vanes with the formation of a helical vortex, a phenomenon which has been long established. However, in the case of vanes with collar, the mechanism is bound to be different with the collar restriction at the bed level, and the equilibrium scour was attained after 180 min. Nevertheless, the local scour at the downstream end of each vane has reduced as can be seen from the figure. The $S_{r,\,max}$ values for $D = 3H_v$ reduced by 68.06%, 14.15%, 13.76%, and 8.49% for $\alpha = 15°$, 35°, 40° and 45°, respectively. For $D = 4H_v$, $S_{r,\,max}$ reduced by 36.11%, 4.72%, 5.5%, and 1.89%, respectively. Also, it is inferred that the effect of collar is prominent at lower vane angles. For $\alpha = 35°$, 40° and 45°, the effect is considerably less. In all cases, the lowest equilibrium $S_{r,\,max}$ is observed for $D = 3H_v$. At $D = 4H_v$, the increased collar diameter results in closer

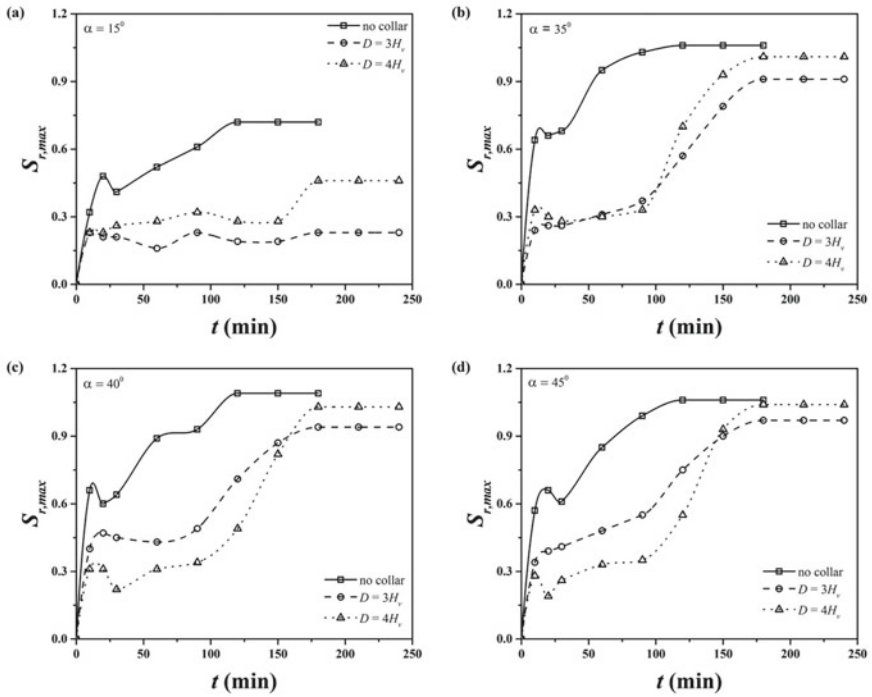

Fig. 3 Comparison of temporal variation of maximum scour depth ratio $S_{r,\,max}$ for vanes with and without collar at different vane angles: **a** 15°, **b** 35°, **c** 40°, and **d** 45°

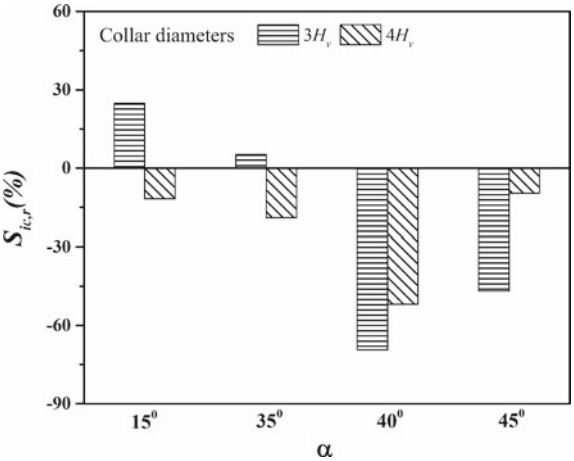

Fig. 4 Percentage reduction of sediment entry into the intake canal ($S_{ic,r}$) for different vane angles and collar diameters

proximity of the collar edge to the trailing edge of vane. This might be the cause for less reduction in $S_{r,\,max}$ for $D = 4H_v$.

3.3 Effect of Collar Diameter on the Percentage of Sediment Entry into the Intake Canal

The percentage reduction in sediment entry into the intake canal ($S_{ic,r}$) with α for vanes with collars is shown in Fig. 4. The pattern of variation in S_{ic} for vanes with collar follows that of vanes without collar with an optimum at $\alpha = 40°$ for both $D = 3H_v$ and $D = 4H_v$. The values of S_{ic} for $\alpha = 15°, 35°, 40°$, and $45°$ with $D = 3H_v$ are 20.15%, 15.36%, 12.5%, and 21.3%, respectively. The corresponding values for $D = 4H_v$ are 29.97%, 19.29%, 11.21%, and 15.9%, respectively. However, comparing the variations with respect to the collar diameters, the pattern is not consistent. Moreover, it is observed that sediment entry into the intake canal increased in most cases with a maximum increase of 69.38% for $\alpha = 40°$ and $D = 3H_v$. This reveals that although the collars result in lowering the local scour around vanes, the presence of collar at the bed level induces higher bed erosion in the test section which eventually resulted in increased sediment entry into the intake canal.

4 Conclusion

Intake canals divert water from main rivers for various purposes. Transport of sediment along with water causes reduction in the quality and quantity of water transported. Use of submerged vanes as river training structures at the entrance of intake canals has been in existence since 1990. The present study introduces collars to submerged vanes to reduce its local scour and prevent the collapse of vanes. An optimum vane angle of 40° resulted in the lowest percentage of sediment entry into the intake canal of 7.38%. On the contrary, maximum local scour for vanes with 40° vane angle was found to be the highest with a value of 1.09 times the main channel flow depth. Collars of diameters $3H_v$ and $4H_v$ were installed at the vane bottom to reduce the local scour, where H_v is the height of the vane. It is found that collar is efficient in reducing local scour for all vane angles with a maximum reduction of 68.06% for 15° vane angle and $3H_v$ collar diameter. Also, use of vanes with collars at 15° vane angle resulted in a decrease of sediment entry into the intake canal by 24.84% and 5.24% for collar diameters $3H_v$ and $4H_v$, respectively. However, the collars reduced the performance of the optimum vane angle of 40° in terms of the sediment entry percentage. It is concluded that collars are efficient in reduction of sediment entry into intake canal for only lower vane angles. Perhaps the study of collars could be extended for cases with lower vane spacing to vane height spacing ratio, where the optimum vane angle is 15°.

References

1. Bosman DE, Prestedge GK, Rooseboom A, Slatter P T (2002) An investigation into the removal of sediments from water intakes on rivers by means of jet type dredge pumps Water Research Commission Report, 1187/1/02
2. Nakato T, Kennedy JF, Bauerly D (1990) Pump-station intakes hoaling control with submerged vanes. J Hydraul Eng 116(1):119–128
3. Barkdoll BD, Ettema R, Odgaard AJ (1999) Sediment control at lateral diversions: limits and enhancements to vane use. J Hydraul Eng 125(8):862–870
4. Odgaard AJ, Wang Y (1991) Sediment management with submerged vanes. I: theory. J Hydraul Eng 117(3):267–283
5. Marelius F, Sinha SK (1998) Experimental investigation of flow past submerged vanes. J Hydraul Eng 124(5):542–545
6. Yonesi HA, Omid MH, Haghiabi AH (2008) A study of the effects of the longitudinal arrangement sediment behavior near intake structures. J Hydraul Res 46(6):814–819
7. Tan SK, Yu G, Lim SY, Ong MC (2005) Flow structure and sediment motion around submerged vanes in open channel. ASCE J Waterw Port Coast Ocean Eng 131(3):132–136
8. Odgaard AJ, Kennedy JF (1983) River-bend bank protection by submerged vanes. J Hydraul Eng 109(8):1161–1173
9. Odgaard AJ, Spoljaric A (1986) Sediment control by submerged vanes. J Hydraul Eng 112:1164–1180
10. Michell F, Ettema R, Muste M (2006) Case study: sediment control at water intake for large thermal-power station on a small river. J Hydraul Eng 132(5):440–449
11. Ouyang HT, Lai JS, Yu H, Lu CH (2008) Interaction between submerged vanes for sediment management. J Hydraul Res 46(5):620–627

12. Kalathil ST, Wuppukondur A, Balakrishnan RK, Chandra V (2018) Control of sediment inflow into a trapezoidal intake canal using submerged vanes. ASCE J Waterw Port Coast Ocean Eng 144(6):04018020
13. Beygipoor G, Bajestan MS, Kaskuli HA, Nazari S (2013) The effect of distance from submerged vanes to the intake at different angles of vanes on controlling the sediment entering the intake branching from a 90° convergent bend. Int J Farm Allied Sci 2(17):591–598

Effectiveness of River Bed Filtration in Pollutant Removal Along the River Tel, India

Rajiv Lochan Sahu, Rakesh Roshan Dash, Pradip Kumar Pradhan, and Sourava Sahu

Abstract Riverbank filtration (RBF) is a cost-effective water treatment technology. In this method, infiltrated surface water is extracted through a pumping well which is located nearby alluvial aquifer. In the process of infiltration surface water is treated by various mechanisms like biological, chemical, and physical processes; hence, water extracted from pumping well is free from pollutants. Although riverbank filtration (RBF) was used extensively in United States and Europe, but there are no proven scientific researches done related to RBF use in Odisha. This paper is aimed to present a concise summary of the theoretical foundations of the RBF technique and its benefits. The paper also reports the effectiveness of bed filtration in reducing turbidity, phosphates, coliform, and nitrates from water of River Tel at Belagaon, Balangir District, in Odisha.

Keywords RBF · Turbidity · Phosphates · Coli form and nitrates

1 Introduction

Riverbank filtration provides a sustainable and cost-effective means which improves the quality of surface water [1]. Mechanisms like physicochemical filtration, biodegradation, and sorption usually occur in the aquifer and the river bed, during river bank filtration process. RBF helps in attenuating the pollutants like micropollutants, parasites, viruses, bacteria, suspended particles, and other organic, and inorganic compounds usually present in surface water [2, 3]. Some researchers studied

R. L. Sahu (✉) · R. R. Dash · P. K. Pradhan · S. Sahu
Department of Civil Engineering, Veer Surendra Sai University of Technology, Burla, Odisha, India
e-mail: robinsahu1@gmail.com

R. R. Dash
e-mail: rrdash@gmail.com

P. K. Pradhan
e-mail: pkpradhan1@yahoo.co.in

C. Bhuiyan et al. (eds.), *Water Security and Sustainability*,
Lecture Notes in Civil Engineering 115,
https://doi.org/10.1007/978-981-15-9805-0_18

the removal of turbidity, organics, and bacteria at RBF site at Haridwar alongside the Ganga River [4]. RBF technique was reported as an effective method for attenuating pollutants like turbidity and bacteria present in surface water of four rivers of Uttarakhand [5]. River bed material plays a vital role in the treatment of river water during RBF. Potential RBF sites like Badamadhapur and Kuchinda present in Odisha were analyzed, and it was seen that RBF technique was helpful in enhancing the surface water quality parameters making it suitable for drinking purposes [6]. Riverbank filtration has been extensively studied across the world, but very limited research has been done on River bed filtration in Odisha. As the Belgaon site was near to our University and easily accessible, hence in the present study, the effectiveness of River bed filtration in Odisha was evaluated in removing pollutants from surface water.

2 Study Area and Methodology

2.1 Study Area and Hydrology

Out of 29 states in India, Odisha is situated in the eastern part; it extends from 17.31° N latitude to 22.31° N latitude and from 81.31° E longitudes to 87.29° E longitude. The state's six major rivers are Subarnarekha, Budhabalanga, Baitarani, Mahanadi, Brahmani, and Rusikulya. Odisha generally has sub-humid climatic conditions, and precipitation is approximately 1491 mm and gets approximately 75–80% of rainfall during June to September.

3 Site Selection

River Tel with water supply scheme at Belgaon, Balangir District, was selected for the study.

Belgaon is situated at outskirts of Balangir district, Odisha 50 km away from Balangir headquarter. It is situated in the western part of Odisha. Its latitude is 20° 19′ 08.8″ N and longitude is 83° 18′ 57.5″ E, and is located near River Tel. Figure 1a shows sampling locations at river bank filtration site. The production well (Fig. 1b) is situated on the river bank (within 2 m from River Tel) which is getting water through the laterals connected to it. Water from the river is entering into the laterals after passing through the river bed. The depth of production well below bed level is 20 m, and its diameter is 2 m. It originates from the plains in Koraput district. Discharge at the production well was around 0.2 m^3/min. In the present study, the water samples were collected directly from Tel river as well as from production well (river bed filtrated water), and tube wells (groundwater) near the river. Collected

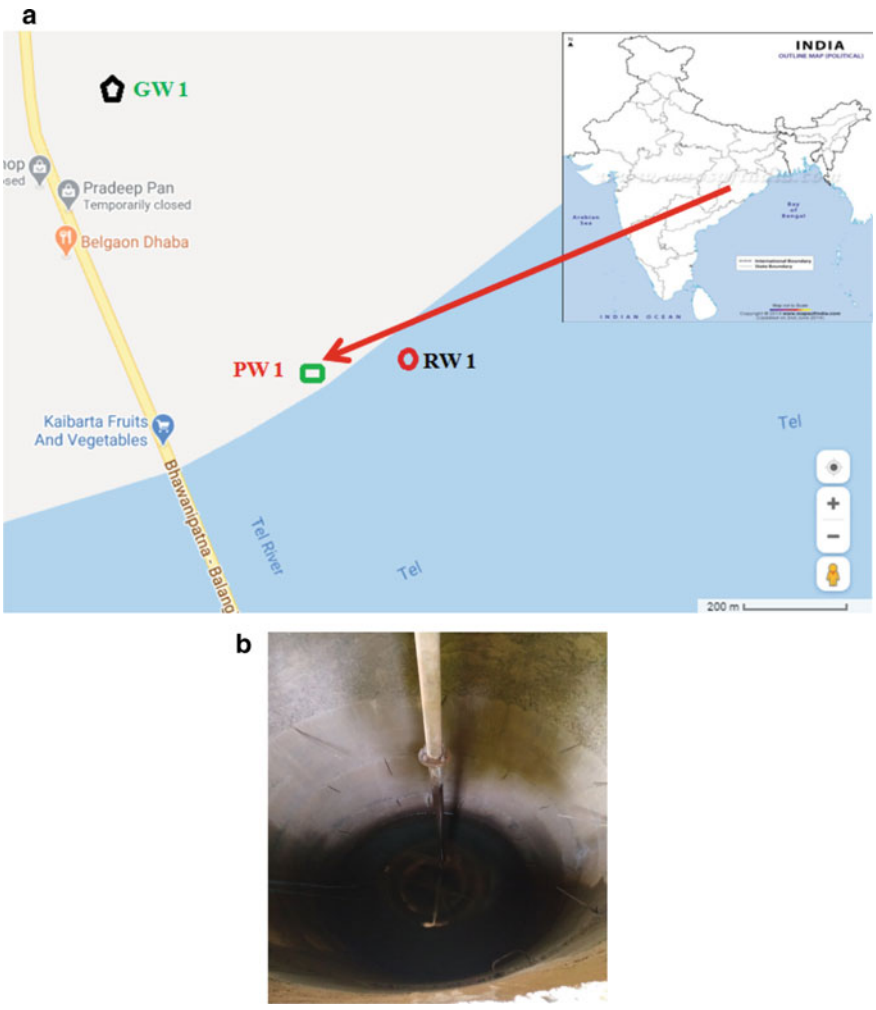

Fig. 1 **a** Sampling locations at river bank filtration site. **b** Inside view of the production well

water samples were tested in the laboratory. In addition, soil samples taken from the river bed at a depth of 1 m were subjected to sieve analysis for gradation of soil.

4 Sieve Analysis of Soil Collected from River Bed

IS code was used for grain size analysis of the soil sample [7]. The soil sample was collected at a depth of 1 m from the river bed. Dry sieve analysis was done at laboratory, and the percentage finer and particle size graph was plotted (Fig. 2).

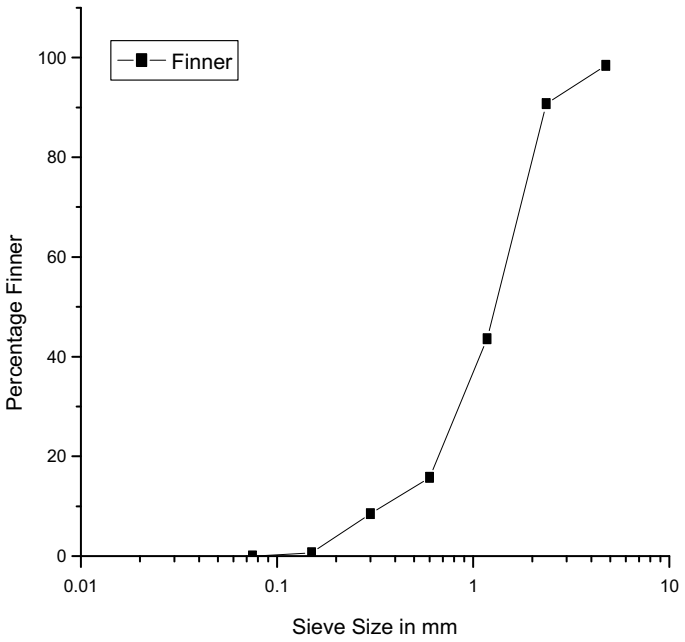

Fig. 2 Particle size distribution curve

5 Methodology

The water samples were collected from surface water, i.e., the Tel river RW1 (Belgaon) as well as from the production well PW1 (river bed filtrated water), tube well GW1 (groundwater) during different seasons/time using clean and sterilized bottle (sampling location are shown in Fig. 1a). All the water sample tests were performed in the laboratory of environmental engineering. The standard methods like [8] were used in the collection of water samples. Various tests like sieve analysis [7], pH (pH meter), total dissolved solids, and temperature (TECH TEST water quality tester TDS meter and temperature), e-conductivity (HM digital conductivity meter), turbidity (turbidity meter), hardness (Wanklyn solution method), alkalinity [9], chlorides [9], fluoride (pH/ISE meter-thermo scientific Orion Star), total coli form (MPN test) and phenol, phosphate, nitrate, UV absorbance (UV spectrophotometer) were done as per respective standards using appropriate instruments.

6 Results and Discussion

The results obtained from the analysis of different water quality parameters and aquifer characterizations are discussed in subsequent paragraphs.

6.1 Water Quality and Soil Analysis

Water samples are collected from different locations of Belgaon and analyzed in the laboratory for different water quality. Here, the river water was raw water (RW), production well water (PW1) was the river bed filtered water, and ground water was the tube well water. Water quality monitoring was done in 15 phases for the year 2018–19, considering time periods like monsoon, post-monsoon, and summer. Each time period comprised of five phases. Water samples were collected from River Tel (RW1; surface water), production well (PW1, riverbank filtered water), and one deep bore well which is at a distance of more than 1 km from the Tel River (GW1, groundwater) at Belgaon. Water sample results from different sources, i.e., river water, production well, and tube well are given in Table 1.

7 Percentage Removal of Pollutants

From Fig. 3, it can be noticed that phosphate removal percentage varied between a lowest (minimum) value of 10.53% to a highest (maximum) value of 35.91%. The average removal percentage was reported as 17.94%. Similarly, it can be noticed that phenol removal percentage varied between a lowest value of 14.15% to a highest value of 28.71%. The average removal percentage was reported as 20.63%. It can be noticed that turbidity removal percentage varied between a lowest value of 99.62% to a highest value of 99.86%. The average removal percentage was reported as 99.76%. It can be noticed that total coliform removal percentage varied between a lowest value of 96.17% to a highest value of 99.73%. The average removal percentage was reported as 98.69%. It can be noticed that nitrate removal percentage varied between a lowest value of 3.15% to a highest value of 6.15%. The average removal percentage was reported as 4.92%. It can be noticed that UV absorbance removal percentage varied between a lowest value of 10.43% to a highest value of 30.36%. The average removal percentage was reported as 16.91%. From Fig. 3, it can be concluded that pollutants like turbidity and total coliform removal percentages were more compared to other pollutants like phosphate, phenol, nitrate, and UV absorbance.

Figure 4 shows the relative values of water quality parameter for the production well water and the river water. The parameters such as TDS, conductivity, alkalinity, chloride, fluoride, and hardness values are greater than 1, i.e., the values of production well water are greater than river water. From Fig. 5, it was found that the parameters such as turbidity, nitrate, total coliform, phenol, phosphate, and UV absorbance values are less than 1, i.e., the values of river water is greater than production well water. Here, we found that the TDS and conductivity of the production well water is more than that of the river water because the production well water is mixture of river water (having lower TDS and conductivity) and ground water (having higher TDS and conductivity). From the above results, we found that bed filtration has effectively removed turbidity, coliform bacteria, organics (UV abs. and total coliform), and

Table 1 Comparison of different parameters of river water, production well water, and tube well water (ground water)

	River water			Production well water			Tube well water		
Parameter	Min	Max	Avg	Min	Max	Avg	Min	Max	Avg
pH	9.5	9.8	9.65	7.4	7.4	7.4	6.6	7	6.8
TDS in mg/l	78	78	78	131	135	133	302	352	327
Electrical conductivity in μs/cm	160	165	162.5	288	296	292	674	713	693.5
Temperature in °C	30	32	31	29	29	29	31	32	31.5
Turbidity in NTU	26.5	74	45.48	0.1	0.1	0.1	NA	NA	NA
Hardness in mg/l as $CaCO_3$	46	86	65.73	116	140	127.2	108	108	108
Alkalinity in mg/l as $CaCO_3$	165	190	175	185	215	198.8	170	450	310
Chloride in mg/l	2.58	7.8	4.9	5.24	11.36	8.4	29.82	56.8	43.31
Fluoride in mg/l	0.46	0.64	0.576	0.71	0.78	0.74	1.9	3.1	2.5
Total coli form MPN	16,000	110,000	48,766.67	300	920	380	NA	NA	NA
Phenol in mg/l	0.22	0.26	0.24	0.18	0.20	0.19	NA	NA	NA
Phosphate in mg/l	1.69	2.47	1.98	1.32	1.76	1.61	1.60	2.28	1.94
Nitrate in mg/l	6.58	6.93	6.76	6.25	6.59	6.42	6.15	6.44	6.30
UV Abs (254 nM)	0.784	1.007	0.851	0.693	0.715	0.704	0.7	0.686	0.693

phosphate and reduce hardness. In this process, we remove some amount of phenol, but it remains above the Indian drinking water standards, i.e., 0.001 mg/l. The river bed filtration at Tel River, Belgaon, was found to be efficient for the removal of turbidity, organics (UV abs, phenol), nutrients (phosphate and nitrate), and bacteria (total coliform). Bed filtration is effective in removal of turbidity and total coliform for all the collected samples. This may be due to combination of several processes, including physicochemical filtration, dispersion, advection, and straining. Among above-mentioned processes, physicochemical filtration play a major role in attenuating the pollutants like turbidity and coliform from the river water. The removal of organics at the site may be due to a combination of several mechanisms, including

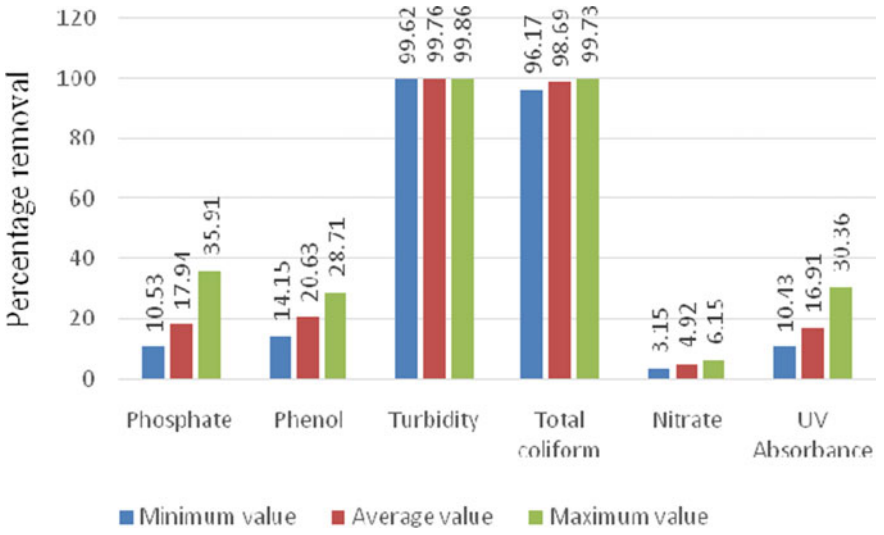

Fig. 3 Maximum, minimum, and average percentage removal of different water quality parameters

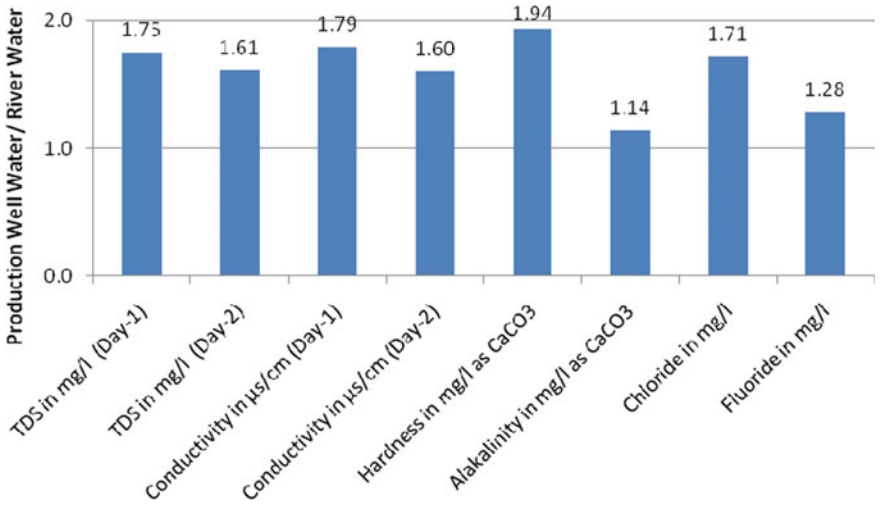

Fig. 4 Quality of production well water relative to river water parameter

dilution with other water; microbiological, chemical, and physical degradation. For other parameters such as TDS, total hardness, anions, and cations of well water is more than that of the river water because the water in the well is mixture of river water (having lower TDS, cations, anions, hardness), and ground water (having higher TDS, cations, anions, and hardness). The aquifer bed at Tel river is found to

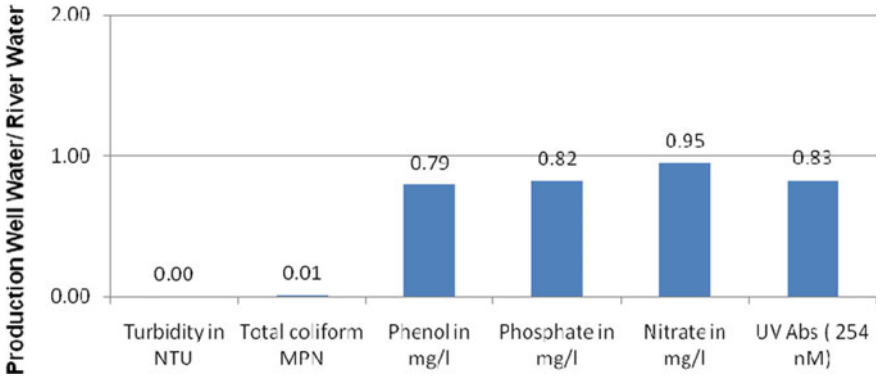

Fig. 5 Turbidity, organics, nutrients, and coliform counts of production well water relative to river water

be sandy and aquifer possesses high hydraulic conductivity which is good in getting sufficient yield (0.2 m^3/min) for the infiltration wells.

8 Conclusions

The study concludes that at the RBF study site in Belgaon, the pH of production well water are within the limit [10], i.e. 6.5–8.5. The electrical conductivity and TDS of the production well water is greater than the river water, whereas it is less than the tube well water. This concludes that the ground water mixing is taking place along with river bed filtration. The RBF in Belgaon (Tel River) efficiently removes turbidity, phosphates, and nitrates. The most probable number (MPN) value of the river water is more than the production well water and the removal efficiency of bacteria is more than 99% during bed filtration. The UV absorbance value of the production well water is less than the river water, which is conclusive of the removal of organic matter. The RBF does reduce the phenol content but not up to the Indian drinking water standard. The results of this work have demonstrated the benefits of bed filtration which is a natural purification technique to enhance the quality of surface water in terms of removal of pathogens, organics, and turbidity for drinking water supply. As natural attenuation process like filtration requires low routine maintenance, hence RBF is a cost-effective alternative for water supply schemes which relies on surface water supplies. RBF method possesses some limitations. These limitations depend on parameters like permeability and high organic pollution. It can be noted that change in temperature can change the permeability of the aquifer and hence the performance of RBF. Similarly, high organic pollution can reduce the RBF treatment efficiency.

References

1. Tufenkji N, Ryan JN, Elimelech M (2002) The promise of bank filtration. Environ Sci Technol 36(21):422A–428A
2. Kuehn W, Mueller U (2000) Riverbank filtration—an overview. J Am Water Works Assoc 92(12):60–69
3. Sacher F, Brauch HJ (2002) Experiences on the fate of organic micro pollutants during riverbank filtration. In: Ray C (ed) Riverbank filtration: understanding contaminant biogeochemistry and pathogen removal. Kluwer, Dordrecht, pp 135–151
4. Dash RR, Prakash EVPB, Kumar P, Mehrotra I, Sandhu C, Grischek T (2010) River bank filtration in Haridwar, India: removal of turbidity, organics and bacteria. Hydrogeol J 18(4):973–983. https://doi.org/10.1007/s10040-010-0574-4
5. Tyagi S, Dobhal R, Kimothi PC, Adlakha L, Singh P, Uniyal DP (2013) Studies of river water quality using river bank filtration in Uttarakhand, India. Water Qual 5. https://doi.org/10.1007/s12403-013-0097-z
6. Sahu RL, Dash RR, Pradhan PK, Das P (2019) Effect of hydrogeological factors on removal of turbidity during river bank filtration: laboratory and field studies. Groundwater Sustain Dev 9:100229. https://doi.org/10.1016/j.gsd.2019.100229
7. IS 2720 (1985) Indian standard on methods of test for soils, part 4. Grain size analysis (second revision). Bureau of Indian Standards, New Delhi, India
8. APHA, AWWA, WPCF Standard methods for the examination of water and wastewater, 19th, 20th and 21st eds. American Public Health Association, Washington, DC (1995, 1998, 2005)
9. IS 3025 (1986, 1988) Methods of sampling and test for water and waste water. Bureau of Indian Standards, New Delhi, India
10. IS 10500 (2012) Indian standard on drinking water: specifications. Bureau of Indian Standards, New Delhi, India

Removal of Organic Matters and Nutrients by Using Bio-balls and Corn Cobs as Bio-film Carrier in MBBR Technology

Akankshya, Rakesh Roshan Dash, and Siprasthiti Mohanty

Abstract Water is our life's most significant component. It is used to cook, bathe, drink, wash, and for various industrial purposes. Due to urbanization, over exploitation and industrialization of water bodies throughout the world lead to degradation of water quality. Therefore, high water quality is needed, resulting in the need to develop modern and cost-effective techniques to remove organic matter and nutrients from wastewater. Moving-bed bio-film reactor (MBBR) method is one of those methods that are used effectively in this situation. The purpose of this research was to explore the effectiveness of the MBBR method in removing chemical oxygen demand (COD), nitrate, phosphate from wastewater using bio-balls and corn cobs as bio-film media. Synthetic wastewater was prepared in laboratory by taking different concentration of COD, nitrate, and phosphate. By using bio-balls as a bio-film carrier, the maximum removal efficiency of COD, nitrate, and phosphate was obtained to be 84%, 95.48%, and 96.93%, respectively, whereas for corn cobs, the maximum removal efficiency of COD, nitrate, and phosphate was found to be 72.39%, 94.63%, and 93.7%, respectively. The result obtained from the experiment confirmed that this process can be effectively used to treat domestic and industrial wastewater containing different pollutants.

Keywords MBBR · Bio-balls · Corn cobs · Nitrate · Phosphate · COD

1 Introduction

Many types of sewage treatment methods are available. Generally, physio-chemical and biological treatments are useful to treat wastewater for the removal of organic, inorganic, and nutrients present in that. The treatment methods are generally classified as component processes and component operations. Unit operation includes the removal of contaminants by physical services. The main treatments methods

Akankshya · R. R. Dash (✉) · S. Mohanty
Department of Civil Engineering, VSS University of Technology, Burla, Burla, Sambalpur, Odisha, India
e-mail: rrdash@gmail.com

C. Bhuiyan et al. (eds.), *Water Security and Sustainability*,
Lecture Notes in Civil Engineering 115,
https://doi.org/10.1007/978-981-15-9805-0_19

are screening, skimming, sedimentation, grit chamber, etc. Conventional wastewater treatment consists of a combination of physical, chemical, and biological processes and operations to remove solids, organic matter, and, sometimes, nutrients from wastewater. General terms used to describe different degrees of treatment, in order of increasing treatment level, are preliminary, primary, secondary, and tertiary and/or advanced wastewater treatment. There are many different biological wastewater treatment options are available. Biological processes are two types, i.e., suspended growth process and attached growth process. Examples of suspended growth processes are various types, i.e., activated sludge process, aerobic lagoon, aeration pond, aerobic and anaerobic sludge disaster, etc., and attached growth processes are trickling filter, bio-towers, RBC, etc. Every process has its own set of advantages and disadvantages. Based on the requirements and availability of resources, we need to choose the suitable treatment process. Research is still going on to find out the more effective and accessible method for the treatment and reuse of wastewater.

RBC is a bio-reactor that is primarily used for biological wastewater treatment, containing largely organic waste products. It is one of the attached growth processes. Attached growth means the microorganisms will be attached to a surface and the wastewater has to pass through it for a certain period of time. It mainly consists of several disks mounted on the surface of a rotating shaft and partially submerged in the wastewater. The disks are usually made up of different forms of plastic such as polypropylene or polyurethane. As the shaft rotates, the disks that are attached to it also start rotating through the wastewater.

Moving-bed bio-film reactor (MBBR) technology combines both the benefits of suspended growth system which is activated sludge process and attached growth system which is trickling filter. Among all the bio-film reactors, MBBR technology uses entire tank volume for the enlargement of biomass, as happens in an activated sludge process (ASP). But MBBR does not need sludge recirculation as required in ASP. This is attained due to biomass that grows on the media which are moved freely in the reactor by aeration or by automatic mixing. The media are reserved inside the reactor by installing a strainer at the reactor outlet. Separation of surplus biomass has taken place as there is no sludge recirculation occurred. So, it is a big advantage of MBBR technology over ASP [1]. Medias can differ from each other in treatment capabilities, material composition, shape, and specific surface area. The filling ratio of the carrier plays an important role as it provides sites for the growth of microbes. The carriers are produced using plastic with a thickness close to 1 g/cm^3 giving them a chance to move easily inside the reactor surely when the limit comes to 70%. The moving bed shapes originate from the flow float in wastewater treatment that offers an extended specific surface inside the reactor for the advancement of the biomass, accomplishing basic reduction surrounded by the natural reactor volume. A few components have been detailed to influence the execution of MBBR. The high particular range of the carrier media controls the framework execution which is as a result of exceptionally high bio-film concentrations nearness in a little reactor volume [2]. It was detailed that common place bio-film concentrations extend from

3000 to 4000 g TSS/m^3. The rate of reactor volume comprised of media is controlled to 70%, with 67% being normal. In any case, wastewater attributes and specific treatment targets are the most parts choosing the level of media required inside the reactor. As a general rule, a life of bio-carriers opens inside the market changes from 11 to 40 years [2].

Literature survey suggests that different hybrid bio-reactors have been developed for the removal of different pollutants from wastewater and landfill leachate. Different carriers have also been used in MBBR process. Research work has been carried out to explore the performance of MBBR process for treating commercial wastewater by using three different types of carrier viz media-1 BI16, media-2 PP22, and media-3 mutag biochip 25TM [3], for removal of the phenol and microbial community shift during pH shock in MBBR [4], for the treatment of industrial food processing wastewater [3], for nutrient removal by using polyurethane foam carrier [5], for nitrogen removal from mine effluents using a 2 staged MBBR [2], for phenol removal using two reactors, and for the removal of organic carbon, nitrogen, and phosphate by using sequencing MBBR [6].

The objective of this research work is to check the efficiency of MBBR technology in removing organic matter, i.e., COD, nitrate, and phosphate, from municipal and industrial wastewater by using bio-balls and corn cobs as bio-film carriers.

2 Materials and Methods

2.1 Properties of Bio-film Carriers

Bio-balls are made up of polyurethane material and inside that active carbon foam is present. The diameter of the bio-ball used for the study was 16 mm and purchased from Aquarium House, Bhubaneswar, Odisha. These are spherical in size and black in color. These are specially intended to provide plenty of surface area for bacterial growth. Density of bio-ball is 0.9 gm/cc, and surface area is 2.02×10^{-3} m^2. Picture of bio-balls is shown in Fig. 1.

The corn cobs have a calcareous structure that can cause the pathogenic population to be quickly attached and developed. Density of corn cob is 1.18 g/cm^3, and the surface area is 50.67 cm^2. It provides considerable high void ratio, specific surface area, and small specific gravity. Initially, corn cobs were dried in the oven at 105 °C for 24 h and cut into parts of roughly equal size (h) and (d) length of 5.0 cm and 2.5 cm, respectively. Prepared cobs of corn are submerged in sterile water and thoroughly washed. Cleaned cob shells of corn are then dried for 5 h in an oven at 150 °C. Picture of raw corn cobs is shown in Fig. 2.

Fig. 1 Bio-balls (not to scale)

Fig. 2 Corn cub after drying

2.2 Composition of Synthetic Wastewater

Synthetic wastewater was prepared which consists of glucose used as source of carbon and a main ingredient to organic matter. Potassium nitrate and potassium di-hydrogen phosphate were added in wastewater to provide enrichment as nitrogen and phosphorus source, respectively. Synthetic wastewater was seeded with bacteria culture that was aerated for 15 days for microbial growth. Growth of the bacteria also depends on the availability of oxygen. Supply of oxygen was done by air diffuser. Detailing of five batches used for different concentration of COD, nitrate, and phosphate is given in Table 1.

Table 1 Characteristics of synthetic wastewater

Batches	COD in mg/l	Nitrate in mg/l	Phosphate in mg/l
1	100	15	5
2	200	20	10
3	400	25	15
4	800	30	20
5	1000	35	25

2.3 Operating Procedure of MBBR

For the study, MBBR was run under continuous flow system. Model setup of MBBR was shown below in Fig. 3a, b. The filling ratio of media was kept 50% of the volume of the tank, and for agitation of media, air diffuser was used which supply oxygen to synthetic wastewater for the survival of bacteria. Experiments were performed under aerobic condition in five batches for both the media individually which includes both nitrification and denitrification process. Reactor was continuously operated for 24 h, and sample was collected in every two hours interval, i.e., 2, 4, 6, and 8 h, and the end of 24 h. After collection of each sample, experiments of TDS, pH, COD, nitrate, and phosphate were performed to determine the final concentration and to calculate the percentage removal.

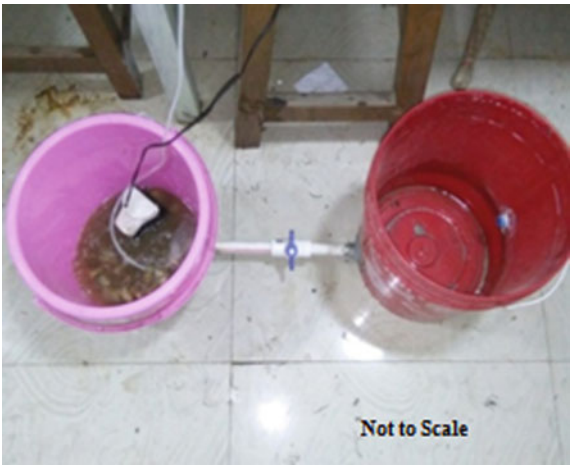

Fig. 3 MBBR setup

3 Results and Discussions

3.1 Comparison of Removal Efficiency of Nitrate for Different Batches

Figure 4a, b shows the variation of removal efficiencies for bio-balls and corn cobs as media for different concentration of nitrate and different operating time. For both the media, removal efficiency increases with increase in concentration and increase in operating time. For bio-balls, with increase in concentration from 15 to

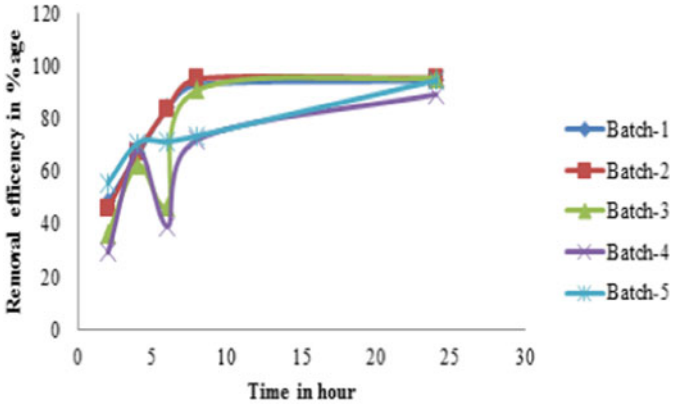

(a) Bio-balls

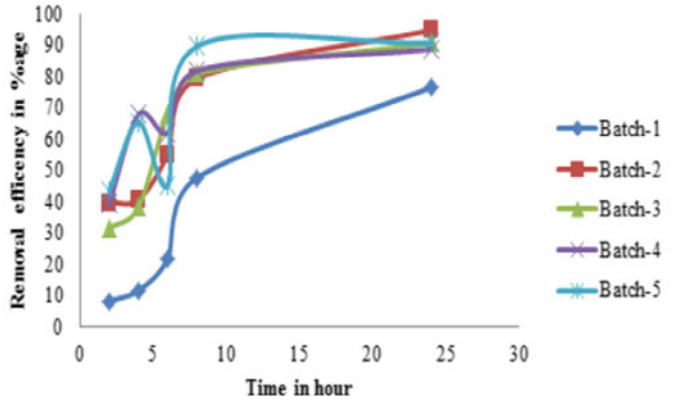

(b) Corn cobs

Fig. 4 Nitrate removal efficiency with respect to operating time

25 mg/l, efficiency increases from 89.2 to 94.48%, and for corn cobs, with increase in concentration from 15 to 35 mg/l, efficiency increases from 76.37 to 94.63%.

For bio-balls with initial concentration of 25 mg/l and corn cobs with initial concentration of 20 mg/l (optimum condition), the efficiency increases with increase in operation time from 6 to 24 h. The nitrate concentration in the effluent was relatively stable during the surface loading stage, but there were fluctuations during the sludge concentration and temperature stages which takes place around operation time of 6 h. Best removal efficiency was achieved in 24 h for all the five batches for both the media. So for optimum removal, the reactor must have a hydraulic retention time of minimum one day.

The nitrogen removal in this process most commonly as well as economically accomplished in two stages: nitrification and denitrification [7]. Nitrification converts ammonia to oxidized nitrogen, i.e., nitrite and nitrate, and then, it is converted to a nitrogen gas in the next denitrification process. The step produces nitric oxide (NO), nitrous oxide (N_2O), and nitrogen gas (N_2). All the products are gaseous in nature which can be released in atmosphere. Generally, nitrosomonas and nitrobacter are responsible for the nitrification in the wastewater. For denitrification, denitrifying organisms and an organic carbon source are responsible for decomposition. The nitrification rate is determined by the load of organic matter, ammonium concentration, and oxygen concentrations. Nitrification rate depends on mixture and heterotrophs distribution. The rate limiting substrate for nitrification may be ammonia or oxygen. According to a study, for nitrification, DO level in aerated reactor is sufficiently high which penetrates through outer layer of the oxygen-consuming hetrotroph and in nitrifying bacteria. The nitrification dependS upon oxygen concentration. For MBBR, the liquid film diffusion was an essential parameter.

3.2 Comparison of Removal Efficiency of Phosphate for Different Batches

Figure 5a, b shows the variation of removal efficiencies for bio-balls and corn cobs as media for different concentration of phosphate and different operating time. For both the media, efficiency increases with increase in concentration and increase in operating time. For bio-balls, with increase in concentration from 5 to 25 mg/l, efficiency increases from 60.1 to 96.9%, and for corn cobs, efficiency increases from 73.2 to 93.7%.

For bio-balls with initial concentration of 20 mg/l and corn cobs with initial concentration of 10 mg/l (optimum condition), the efficiency increases with increase in operation time from 6 to 24 h. Best removal efficiency was achieved in 24 h for all the five batches for both the media.

Phosphorus is removed biologically in this process by moving bed bio-film process [8]. The biological phosphorus removal is done by phosphate-accumulating organisms (PAO) because they have the ability for accumulating phosphate which

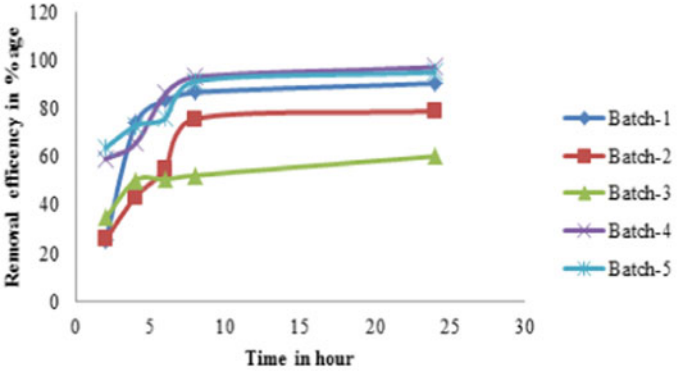

(a) Bio-balls

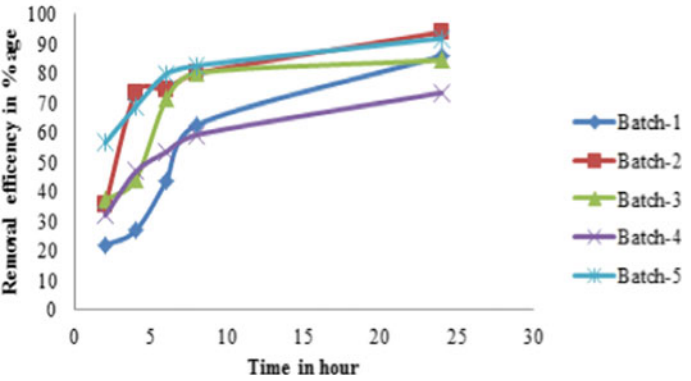

(b) Corn cobs

Fig. 5 Phosphate removal efficiency with respect to operating time

are required for growth. This biological process is enhanced biological phosphate removal (EBPR). The EBPR consists of assimilating the phosphorus which is present in sample into biomass of cell which finally is removed from the system as a result of sludge wasting. Phosphorus accumulating organisms are responsible for this process for assilimilation of phosphorus into cell biomass.

3.3 Comparison of Removal Efficiency of COD for Different Batches

Figure 6a, b shows the variation of removal efficiencies for bio-balls and corn cobs as media for different concentration of COD with different operating time. For bio-balls, for low concentration of COD, removal efficiency is high. For batch-1 and bio-ball as media, at COD concentration of 100 mg/l, the removal efficiency is 84%

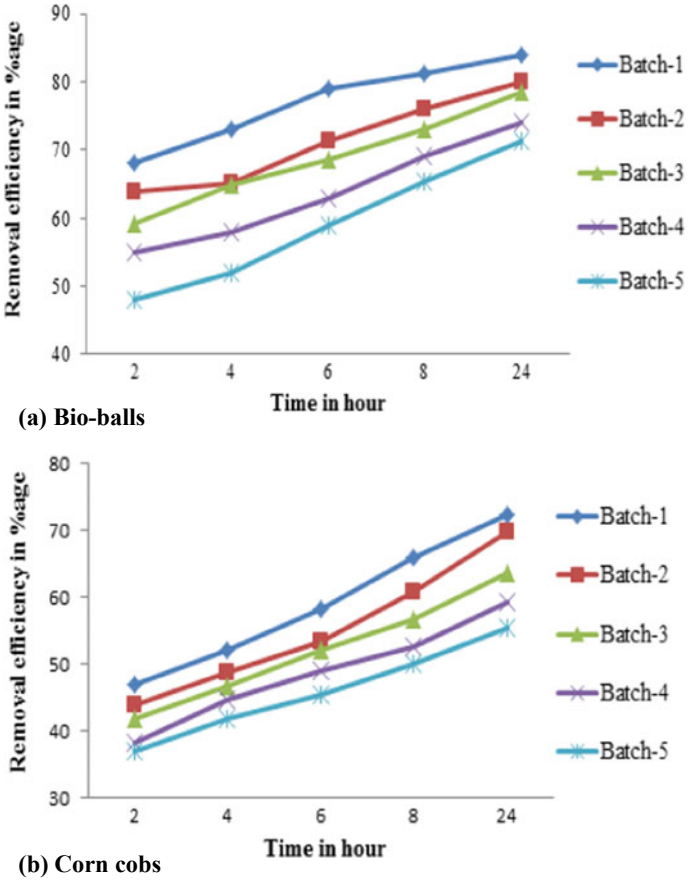

Fig. 6 COD removal efficiency with respect to operating time

at operation time of 24 h. At initial lower concentration of COD, biomass is very active as supply of food is low. For their survival, they consume as much as organic matter they can, which yield in higher removal efficiency. For batch-5 and bio-ball as media, at COD concentration of 1000 mg/l, the removal efficiency is 71.3% at operation time of 24 h. In higher COD concentration, degradation of microbes occurs in inner layer of bio-film which is in the state of anaerobic condition. Due to high F/M ratio, the removal efficiency is low.

Similar observation was found for corn cobs as media. In addition to it, with increase in operation time, the removal efficiency increases for both the media.

By increasing the operation time, enough time to start the activity of the microorganisms is provided, which yields in higher removal efficiency.

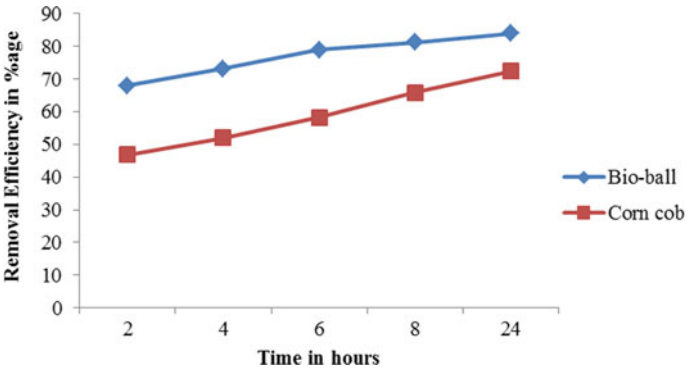

Fig. 7 COD removal efficiency comparison between bio-balls and corn cobs

3.4 COD Removal Efficiency Comparison Between Bio-balls and Corncobs

Figure 7 shows COD removal between bio-balls and corn cob for batch-1, i.e., initial COD concentration of 100 mg/l. At operation time of 24 h, maximum removal efficiency was achieved for both the media. Removal efficiency of bio-ball and corn cob is 84% and 72.39%, respectively. So, bio-ball is more efficient than corn cob when other conditions are same.

4 Conclusion

In the present research, attempts have been made to remove different pollutant from synthetic wastewater prepared in laboratory. Some of important parameter of influent and effluent of wastewater was tested in laboratory such as biodegradable organics, nitrate, and phosphate removed by MBBR technique. According to this analysis, the use of MBBR scheme for organic carbon and nutrient removal from wastewater is achieved by a laboratory scale study. Complete nitrification occurred in optimal condition in the presence of oxygen in the reactor, i.e., aerobic reactor with an average efficiency of 95.8 percent for bio-balls and 94.6 for corn cobs in nitrate removal. Highest phosphate removal efficiency for bio-ball and corn cob was 96.9% and 93.7%, respectively. The removal of COD increases with decrease in concentration and increase in operation time, i.e., from 100 to 1000 mg/l, and the efficiency achieved 84% for bio-balls and 72.4% for corn cob. It can be concluded that MBBR process is a technique of wastewater treatment that is economically, environmentally, and technically effective to remove distinct pollutants from industrial and domestic wastewater, and bio-film media plays an important role in this treatment process.

Acknowledgements The authors wish to acknowledge Department of Civil Engineering, VSS University of Technology Burla and TEQIP-III, VSSUT Burla, for felicitating the research work.

References

1. Pastorelli G, Canziani R, Pedrazzi L, Rozzi A (1999) Phosphorus and nitrogen removal in moving-bed sequencing batch bio-film reactors. Water Sci Technol 40(4):169–176
2. Biswas K, Michael WT, Susan JT (2014) Successional development of bio-films in moving bed bio-film reactor systems treating municipal wastewater. Appl Microbiol Biotechnol 98:1429–1440
3. Mane S, Kotwal R, Mandave S, Landge N, Kedari H (2018) Performance evolution of different MBBR media in wastewater treatment
4. Hao Z, Wang G, Wu M, Xu W, Zhang X, Liu L (2018) Phenol removal performance and microbial community shift during pH shock in a moving bed biofilm reactor (MBBR). J Hazard Mater. https://doi.org/10.1016/j.jhazmat.2018.02.055
5. Poojashri RN, Thanushree M, Manoj BK (2016) Studies on nutrient removal using polyurethane foam (PUF) in moving bed bio reactor (MBBR). IRJET 3(8):1854–1872
6. Hosseini SH, Borghei SM (2005) The treatment of phenolic wastewater using a moving bed bio-reactor. Process Biochem 39(10):1177–1181
7. Dale C, Laliberte M, Oliphant D, Ekenberg M (2015) Wastewater treatment using MBBR in cold climates. In: Proceedings of mine water solutions in extreme environments, 12–15 Apr, Vancouver, Canada
8. Emara MM, Amir A, Ahmed AMS (2017) Industrial food processing wastewater treatment by modified moving bed biofilm reactor (MBBR). Int J Sci Eng Res 8(1):929–934

An Overview on the Photocatalytic Application of Transition Metal–ZnO Nano-Photocomposites for Degradation of Textile Effluents in Water

Parita Basnet and Somenath Chatterjee

Abstract Water remediation has become an urgent requirement to meet the growing need of water scarcity. Organic dyes emanating from the textile industries without proper treatment are a major source of water pollution and, therefore require urgent treatment. This overview is based on one such strategy of converting organic dyes present in aqueous medium into inorganic components by the process of photocatalysis. Photocatalytic dye degradation has been considered with transition metal–zinc oxide (ZnO) nano-photocomposites (NPC) owing to their excellent photo-physical properties. This overview covers three important aspects of photocatalysis using transition metal–ZnO NPC: (i) requirement of photocatalytic dye degradation and photocatalysis, (ii) need for an optimum transition metal dopant/deposit percentage and (iii) the underlying mechanism occurring during photocatalysis upon UV, visible and UV–Visible light irradiations.

Keywords ZnO Photocomposites · Transition-metal incorporation · Water remediation · Dye degradation · Photocatalysis

1 Introduction

In regards to the technological importance of ZnO nanoparticles (NP) [1], owing to their inexpensive synthesis, mechanical durability, innoxious nature and stability under room temperature ambiance as well as under reducing hydrogen atmosphere [2–6], improvement in their properties is progressing rapidly. Photocatalytic activity of ZnO NP is extensively investigated to carry out several applications such as wastewater detoxification, hydrogen gas evolution and others [2, 7, 8]. The photo-absorbing ability of ZnO NP, otherwise confined to the ultraviolet (UV) region, may be enhanced by the introduction of metal NP [6]. Such type of metal introduction may be grouped into doping and deposition [6]. Both these types help in widening the

P. Basnet · S. Chatterjee (✉)
Centre for Materials Science and Nanotechnology, Sikkim Manipal Institute of Technology, Sikkim Manipal University, Sikkim, India
e-mail: somenath@gmail.com; somenath.c@smit.smu.edu.in

C. Bhuiyan et al. (eds.), *Water Security and Sustainability*,
Lecture Notes in Civil Engineering 115,
https://doi.org/10.1007/978-981-15-9805-0_20

range of light absorption by ZnO NP from the solar light radiation. Influence on the ability of photon absorption, which subsequently affects the photocatalytic activity, is further dependent upon the type of metal used as a dopant or deposit. Generally, the common type of metals used is either noble metals or transition metals [6, 9, 10]. Although, both these categories suffice the requirement of broadening the region of light absorption, high cost associated with noble metal precursors may pose a restriction while considering cost effectivity. Thus, transition metals are more preferred unless the requirement of noble metals is irreplaceable.

A significant amount of the textile dyes as effluents is released during their manufacture and processing into the water bodies (or water treatment plants) [11]. These dye molecules are readily reduced into environmentally harmful aromatic amines under anaerobic conditions [11]. Therefore, for generating risk-free products from these effluents, photocatalysis has been considered as a highly advanced and simple process, which operates in an economic environment. Over the past many years, various photocatalysts have been proposed to perform the efficient photo-degradation of organic dyes present as water waste [6]. Amongst them, ZnO photocatalyst was selected as a potential candidate as it is environmentally safe and a very promising semiconductor nanomaterial [2]. Research related to the enhancement of its photocatalytic activity is still under progress, and many reports suggest the functionalization of transition metal with ZnO NP to be highly beneficial [9, 10]. Therefore, herein, authors have considered the study related to this domain. In this overview, authors have highlighted the effect of transition metal concentration and the ongoing mechanism over ZnO nano-photocomposite (NPC) during the photocatalytic process.

2 Photocatalytic Activity of Transition Metal–ZnO NPC

2.1 Effect of Transition Metal Content upon Photocatalysis

Several studies dedicated to uncover the fundamentals of transition metal–ZnO NPC report alteration in the photocatalytic activity of ZnO after transition metal functionalization [12–14]. The primary reason resulting in this phenomenon may be attributed to the decrease in the band gap energy, and thereby, increase in the absorption range. Another important factor resulting in such changes is the introduction of various defect states in ZnO crystal structure [12–14]. Majority of the research articles based on studies related to defect states and the corresponding photo-physical properties of transition metal–ZnO NPC are conclusive of the synergistic effect between the metal and ZnO NP to exhibit enhanced photocatalytic behaviour [9, 10, 12, 13]. However, certain reports suggest the reduction in photocatalytic activity of bare ZnO after metal incorporation, thereby channelizing the concept of antagonistic effect between them [15, 16]. Nevertheless, these effects ultimately depend upon the morphology, defect states and the type of metal used during synthesis.

According to Bloh et al. [16], an optimum doping percentage exists up to which the photocatalytic activity of ZnO increases, and after which, it drastically decreases. They reported that lower doping concentration of titanium (Ti) was favourable for enhancing the photocatalytic degradation efficiency of ZnO, while its higher concentration diminished the activity. They explained that the introduction of Ti cations led to effective charge separation, wherein the cations acted as trap centres for electrons and/or holes. However, at higher concentration, the authors explained a detrimental effect of the same mechanism, wherein the nearest cationic neighbourhood of the two dopant cations acted as a recombination centre. Jongprateep et al. [15] explained the high photocatalytic performance of Ti-doped ZnO NPC for methylene blue (MB) dye degradation which was related to the solubility limit, where, below the solubility limit, enhancement in the photocatalytic performance was observed and vice versa. The concept of trapping sites creation (as before) was considered for the excitonic diminution while formation of titanium compound was regarded as an antagonistic agent for lowering the degradation efficiency. The possible reasons for such reduced photocatalytic MB dye degradation activity of TiO_2-ZnO coupled nanocomposite (NC) were ascribed to the uniform bonded heterostructure with random adhesion of particles at the surface and to the obstruction of the reactive surface by the secondary phase. Lu et al. [10] explained that Mn ions substitute the Zn ions in ZnO lattice due to their similar ionic radii (Mn^{2+}—65 pm and Zn^{2+}—74 pm). This creates a change in the electronic configuration of ZnO resulting from diversity in the ionic radii. For restoration of its stable electronic configuration, adsorption of more number of oxygen (O_{2ads}) and hydroxide ions (OH^-) occurred while undergoing the following reactions (1–4).

$$Mn^{2+} + e^- \rightarrow Mn^+ \tag{1}$$

$$Mn^+ + O_{2ads} \rightarrow Mn^{2+} + O_2^- \tag{2}$$

$$Mn^{2+} + h^+ \rightarrow Mn^{3+} \tag{3}$$

$$Mn^{3+} + OH^- \rightarrow Mn^{2+} + OH \tag{4}$$

Through these reactions, it may be interpreted that the exchange interaction occurring between Mn^{2+}-Mn^{3+} prolongs the lifetime of captured photo-generated e^--h^+ pairs in ZnO. Consequently, these excitons may easily participate in photocatalytic reactions. Following this discussion, authors concluded that the incorporation of Mn dopants proved to be beneficial in terms of effective charge separation and reduced recombination leading to enhanced photocatalytic activity. Sutka et al. [9] considered the enhancement in the photocatalytic degradation efficiency of ZnO by cobalt (Co) doping due to the widening of the absorption wavelength and increased charge separation. Through absorption and photoconductivity studies, they confirmed the transfer of photo-generated electrons from ZnO VB to the localized Co energy states

with the simultaneous occurrence of d-d transitions amongst the Co dopant levels. The analogous excited states were near to the vicinity of CB minimum leading to ligand charge transfer, and consequently, promoting exciton separation. Similar to the aforementioned decrease in the photocatalytic efficiency of Ti-doped ZnO induced by the higher dopant concentration, in this study also, increase in the Co concentration led to parallel results. Authors explained that high content of Co stimulated rise in the energy of CB minimum, which favoured the Co 3D excited states to become energetically more secluded, subsequently resulting into the generation of an energy barrier for ligand exciton transfer. This phenomenon ultimately resulted into lower photocatalytic activity of the Co-doped ZnO photocatalyst (possessing higher Co content). Ashebir et al. [17] found that the photocatalytic degradation of methyl violet (MV) by ZnO significantly enhanced in the present of dopants such as Mn or Ag. Authors suggested that the observed synergistic effect may be attributed to the increased surface area and oxygen defect sites. Qi et al. [18] reported the photocatalytic degradation of MB dye with different transition metal ions such as Mn, Fe, Co, Ni or Cu as the dopant in ZnO. They observed that the highest degradation efficiency was achieved with Cu-doped ZnO nanoparticles mainly because in Cu-doped ZnO, the electronic transitions of Zn 3p, O 2p and O 2p Cu 3D states are significantly stronger as compared to other ZnO-doped systems which led to an enhancement in the visible light absorption. Ong et al. [19] reported that the metal-doped ZnO may enhance the photocatalytic activity by increasing the magnitude of trapping sites of the photo-induced charge carriers, and thereby, decrease their recombination. Vaiano et al. [20] studied the photocatalytic degradation of MO dye simultaneously with the photocatalytic hydrogen generation by ruthenium (Ru) modified ZnO photocatalyst. They observed that although the Ru doping content largely determined the amount of hydrogen production, the degradation of MO dye was not much affected. They observed that in order to meet both these applications, the amount of Ru to be doped must be 0.25% to ZnO. Ebrahimi et al. [21] reported the degradation of direct blue 15 (DB-15) dye with Ag, Cu or Mn-doped ZnO under UV as well as visible light irradiations. They concluded that the enhanced activity of doped ZnO as compared to bare ZnO was possible as a result of (i) reduction in the electron–hole pair recombination, (ii) increased generation of (•OH) radicals in the system and (iii) development of impurity states after doping. All these factors contributed to enhanced photocatalytic activity of metal-doped ZnO NPC. Therefore, while considering transition metal–ZnO NPC, an optimum concentration of the dopant/deposit and higher trapping sites are the necessary requirements for achieving higher photocatalytic degradation efficiencies.

2.2 Mechanism of Photocatalysis

The mechanism of dye degradation occurs through three main pathways: (i) dye-sensitized mechanism, (ii) N-deethylation and (iii) destruction of conjugated structure. The dominance of a particular mechanism depends upon the nature of light

source used (sunlight, UV light or visible light), which in turn is related to the type of material employed as a photocatalyst. Since this overview is based on transition metal–ZnO NPC, mechanism related to this material will only be emphasized. Most of the organic dyes absorb in the visible region, therefore, dye-sensitized mechanism simultaneously occurs with the other two above-mentioned mechanisms, while in the absence of visible light, there is no scope for this mechanism to take place. Since organic dyes (e.g., MB, rhodamine B, methyl orange, acridine orange, etc.) contain π-conjugation, the incident photons from the visible light source get absorbed resulting into the release of charge carriers. These electrons then transfer to the lowest unoccupied molecular orbital and finally relocate to the photocatalyst's CB [22].

The oxygen molecules adsorbed at the surface of the photocatalyst react with these electrons and generate superoxide radical anions. These CB electrons may also interact with the adsorbed water molecules and produce hydroxyl radicals. The as-generated radicals are responsible for initiating the dye degradation phenomenon, which may then occur through either N-deethylation or conjugated structure breakdown or both. In case of transition metal–ZnO NPC, visible light is absorbed by both the dye molecules as well as the photocatalyst. The extent of dye degradation is initially monitored using UV–Vis spectroscopy by observing the decrease in the temporal absorption over a fixed interval of time. As the degradation proceeds, the absorbance maximum of the dye decreases and may reach a minimum. The percentage difference in the initial and final concentrations of the dye provides the degradation efficiency of the photocatalyst. The decrease in the absorbance maximum of the dye, as observed from UV–Vis spectrum, may be of two types [23–26], as shown in Fig. 1a [18] and b [2]. In one type, decrease in the absorption maximum without wavelength shifts is observed, as in case of Fig. 1b while in the other type, decrease is accompanied by hyposochromic shift of the absorption maximum (Fig. 1a). The former reveals the dominance of conjugated structure destruction and N-deethylation is the predominant process in the latter. The difference in these two degradation pathways is only realized upon the generation of intermediate products during the course of the reaction. However, the complete mineralization of the respective dye eventually forms carbon dioxide, water and inorganic salts, irrespective of the degradation pathway followed.

Thein et al. [12] have led forward the mechanism of photocatalytic degradation of rhodamine B (RhB) dye by Ni coupled ZnO NC under UV light as follows: under UV light irradiation, electron–hole pairs are generated in ZnO. Due to the effect of localized surface plasmons from Ni metal, electrons present in the defect levels of ZnO are transferred into Ni particles, which functioned as electron trapping centres. Thus, mobilization of holes increased and these diffused onto the surface of the photocatalyst. Finally, the redox reactions of holes and escaped electrons present at the surface with adsorbed oxygen and water molecules led to the formation of reactive oxidative species (ROS). These ROS then underwent a chain reaction to degrade the dye molecules. The underlying mechanism for the photocatalytic degradation of MB dye under visible light by ZnO: Mn^{2+} has been elaborately discussed by Ullah et al. [14]. According to the authors, illumination of the photocatalyst with visible light generated electron–hole pairs located at the tail states within the proximity of the

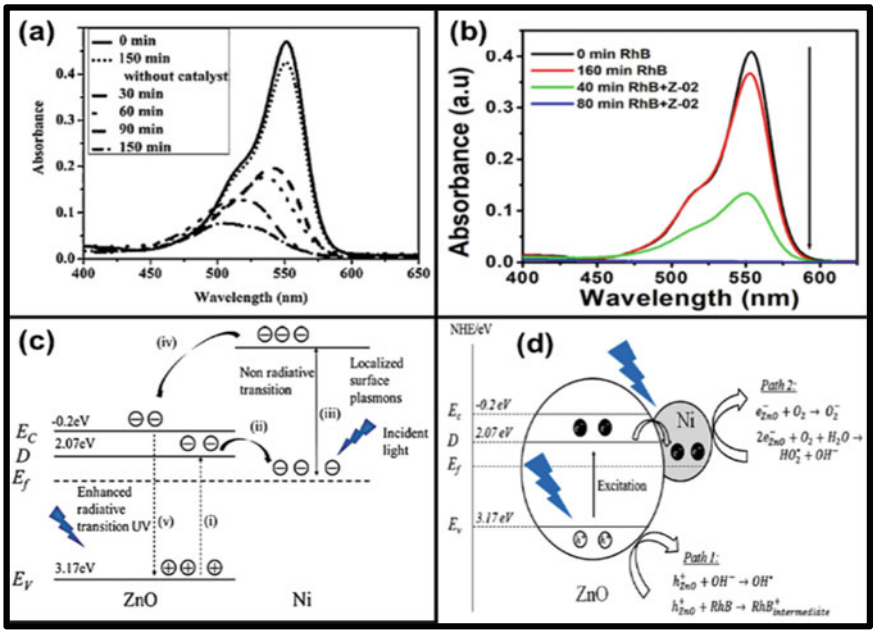

Fig. 1 **a** UV–Vis spectra depicting the dominance of N-deethylation process [18], **b** UV–Vis absorption spectra depicting the dominance of chromophoric group's destruction [2], **c** SPR effect on enhancement of UV emission and suppression of visible light emission in Ni–ZnO NC [11], and **d** Mechanism of RhB degradation upon UV light illumination by Ni–ZnO NC [11]

corresponding CB and VB. The excited electrons are then transferred from the CB into the adsorbed MB molecules, thereby, disrupting the complex conjugated system and consequently, leading to its decomposition. The holes present at the VB then react with water molecules to form hydroxyl radicals, which further participate in the oxidation reaction. Finally, Mittal et al. [13] have given a reasonable explanation for the photocatalytic degradation of crystal violet (CV) dye by Mn-doped ZnO NC under UV–Vis light irradiation. When Mn-doped ZnO NC is irradiated with UV–Vis light, the photo-generated electrons in the VB of ZnO transfer to the localized Mn energy states with the simultaneous occurrence of d-d transitions amongst the Mn dopant levels. Thus, these excited electrons get trapped by the Mn dopant sites. On the other hand, the photo-generated holes in the VB of ZnO migrate to the surface of the photocatalyst and form ROS, which then breakdown the complex organic structure of the CV dye. Therefore, from these mechanisms, an important point may be emphasized: ROS are the main species responsible to carry out the degradation process irrespective of their generation/source. However, higher or lower concentration of ROS may pose better and poor photocatalytic degradation results, respectively. SPR effect on enhancement of UV emission and suppression of visible light emission in Ni-ZnO NC and the mechanisms of photocatalytic degradation of RhB dye by Ni-ZnO NC have been presented in Fig. 1c and d, respectively.

3 Conclusion

To minimize the problems associated with water scarcity, one of the methods is to recycle the existing water sources and improve water quality. Dyeing stuffs or dyes emanating from the textile industries must be properly treated before ultimately disposing into water bodies. Although, several conventional methods are adopted to combat this issue, photocatalytic degradation using semiconductor nanomaterials require fewer resources and is relatively a more efficient process. Therefore, this method must be developed and used as an alternative to the existing traditional methods.

Acknowledgements Ms. Parita Basnet is obliged to receive scholarship from Pai Endowment Fund, Ref SMU/VC/2015-70, dated 17/11/2016.

References

1. Vaseem M, Umar A, Hahn Y (2010) ZnO Nanoparticles: Growth, Properties, and Applications 5:1
2. Basnet P, Inakhunbi Chanu T, Samanta D, Chatterjee S (2018) J Photochem Photobiol B Biol. 183:201
3. Basnet P, Samanta D, Inakhunbi Chanu T, Mukherjee J, Chatterjee S (2019) SN Appl Sci **1**:633
4. Sharma R, Shishodia PK, Wakahara A, Mehra RM (2009) Mater Sci Pol 27:225
5. Basnet P, Chanu TI, Samanta D, Chatterjee S, Mukherjee J (2019) Dae solid state physics symposium 2018, p 030204
6. Basnet P, Samanta D, Chanu TI, Mukherjee J, Chatterjee S (2019) Mater Res Express 6:085095
7. Liu H-L, Yang TCK (2003) Process Biochem 39:475
8. Lu X, Wang G, Xie S, Shi J, Li W, Tong Y, Li Y (2012) Chem Commun 48:7717
9. Šutka A, Käämbre T, Pärna R, Juhnevica I, Maiorov M, Joost U, Kisand V (2016) Solid State Sci 56:54
10. Lu Y, Lin Y, Xie T, Shi S, Fan H, Wang D (2012) Nanoscale 4:6393
11. Vinodgopal K, Wynkoop DE, Kamat PV (1996) Environ Sci Technol 30:1660
12. Thein MT, Pung S-Y, Aziz A, Itoh M (2016) J Taiwan Inst Chem Eng 61:156
13. Mittal M, Sharma M, Pandey OP (2016) Sol Energy 125:51
14. Ullah NR, Thiringer T, Karlsson D (2008) IEEE Trans Power Syst 23:601
15. Jongprateep O, Deedit P, Puranasamriddhi R, Meesombad K (2018) J Met Mater Miner 28:104
16. Bloh JZ, Dillert R, Bahnemann DW (2013) ChemCatChem 5:774
17. Ashebir ME, Tesfamariam GM, Nigussie GY, Gebreab TW (2018) J Nanomater 2018:1
18. Qi K, Xing X, Zada A, Li M, Wang Q, yuan Liu S, Lin H, Wang G (2020) Ceram Int **46**:1494
19. Ong CB, Ng LY, Mohammad AW (2018) Renew Sustain Energy Rev 81:536
20. Vaiano and Iervolino (2019) Catalysts 9:964
21. Ebrahimi R, Hossienzadeh K, Maleki A, Ghanbari R, Rezaee R, Safari M, Shahmoradi B, Daraei H, Jafari A, Yetilmezsoy K, Puttaiah SH (2019) J Environ Heal Sci Eng 17:479
22. Choi YI, Lee S, Kim SK, Kim Y-I, Cho DW, Khan MM, Sohn Y (2016) J Alloys Compd 675:46
23. Samanta D, Chanu TI, Basnet P, Chatterjee S (2018) J Mater Eng Perform 27:2673
24. Chanu TI, Samanta D, Tiwari A, Chatterjee S (2016) Appl Surf Sci 391:548
25. Samanta D, Basnet P, Chanu TI, Chatterjee S, Chatterjee SG, Mukherjee J (2019) Dae Solid State Phys Symp 2018(2115):030203
26. Samanta D, Chanu TI, Chatterjee S (2017) Mater Res Bull 88:85

An IoT-Based Water Management System for Smart Cities

Immanuel Savio Donbosco and Udit Kr. Chakraborty

Abstract Water conservation is one of the prime concerns in the current scenario where environmental conditions are deteriorating at an alarming rate. Smart cities, unlike the conventional system of living, are in the frontline of innovation in terms of both connectivity and technological advancement. The main idea is to use the available technology to make life easy with lesser harm to the environment. An Internet of Things (IoT) and data analytics (DA) based water management system will be a basic ground for implementation and future research on how data and IoT can be used to make this happen. This paper proposes an Internet of Things (IoT) and data analytics (DA) based water distribution cum management system that would help in optimal distribution of water based on user consumption at the plot holding level. The proposed system would not only save water misuse but also help in storing usage data for analysis and town planning at a macro-level.

Keywords Water management · Data analytics · Internet of Things · Smart city

1 Introduction

Smart cities combine technology and innovation in day-to-day living. The idea behind every smart city is that the application of IoT and intelligent techniques in regular everyday activities can increase the ease of living and efficiently perform these activities with less effort [1]. In a smart city, the basic idea of IoT is implemented which is "anything that can be automated will be automated". One very important task in a smart city or any city for that matter is water distribution and conservation. In traditional cities and housing communities, water is distributed manually with the use of traditional pipe and motor systems [2]. This being very inefficient in terms

I. S. Donbosco (✉) · U. Kr. Chakraborty
Department of Computer Science and Engineering, Sikkim Manipal Institute of Technology, Majitar, Sikkim, India
e-mail: immanuelsavio@gmail.com

U. Kr. Chakraborty
e-mail: udit.c@smit.smu.edu.in

C. Bhuiyan et al. (eds.), *Water Security and Sustainability*,
Lecture Notes in Civil Engineering 115,
https://doi.org/10.1007/978-981-15-9805-0_21

of availability and also conservative management of this valuable resource, planned and efficient water management is required. A water management system with the implementation of IoT and data analytics is expected to decrease water wastage and also be more efficient in terms of water availability and also from a conservation point of view [3]. This paper presents a plot holding level plan for smart water management. Applicable in upcoming smart cities [4], this IoT- and DA-based system uses user consumption behavior to optimize the water distribution. Using smart sensors, the proposed system also presents a plan to harvest rainwater at the plot level. The following sections of the paper will give detailed explanation on the basic terminologies used in this paper. It gives the specifications of the sensors and their usage. The next section will give the architecture of the water supply block. Following, it is the structure of the water tank and how its structure will help the rainwater harvesting mechanism and how the sensors are placed on the tank. The final part is the description of the water distribution of the water in the smart city and how it is optimized with the use of DA. In the end, the conclusions and future works summarize the paper and the methodologies proposed and present the possible research and advancement in the proposed methodology.

2 Existing Distribution Method

Urban water distribution methods, or the conventional method of water distribution which is being followed in cities all around the world, work but are inefficient and have a lot of opportunities for development. It has a one-way cycle, consisting of the reservoir/any water body, treatment plants, water storage, homes/consumers, finally to the waste management/treatment facility and send back to nature as groundwater or natural water (Fig. 1). This method of water distribution can have certain downfalls like inefficient water supply or unavailability of the resource at times due to unwanted

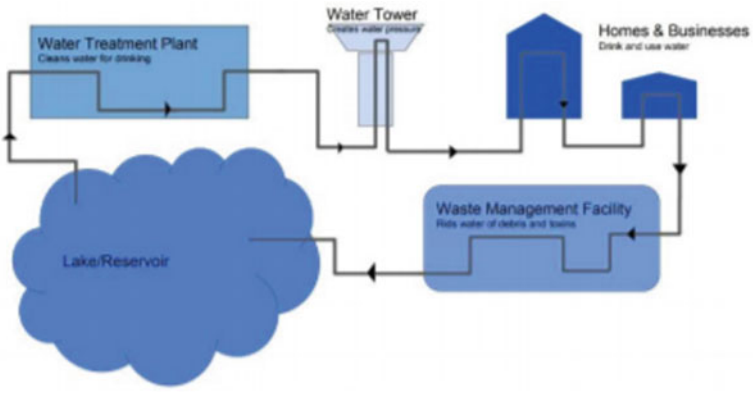

Fig. 1 Conventional water distribution architecture

usage or an architectural failure in the system. This paper has been targeted to overcome some of these basic failures that might occur in the conventional method of water distribution.

The aim of this paper is to optimize the distribution method, to achieve better, faster distribution and also better use of technology to conserve water, which is the need of the hour.

3 Basic Terminology

This section presents in brief the terminologies and technologies used in this paper. This includes IoT, data science, the different sensors and its purpose.

3.1 Internet of Things (IoT)

The growth in computing power, miniaturization of components and higher bandwidth for faster communication has helped in the development of Internet technologies. What was initially envisaged as only a digital mailing system has now grown to be the World Wide Web. Taking full advantage of such technologies, an exciting new field has emerged which allows unprecedented control over devices spread over distant locations and enables data gathering for analysis and intelligent control. Termed as Internet of Things and better known as IoT, this is the systematic interrelation or interconnection of devices for different machines, objects or even humans each with a unique identifier and all interconnected with each other all through the Internet [5]. The main aim of Internet of Things is automation, human–computer interaction and data collection and analysis. Concepts like embedded systems, automation, wireless sensor networks and control systems, etc. contribute to Internet of Things.

IoT has found widespread applications in home automation, security systems, elder and child care, personal health care, telemedicine, transportation and traffic control, livestock tracking and farming management, wild life and defense to name a few. Applications are growing by the day and are limited only by imagination and sensor availability. One such application on water management is presented herein below.

3.2 Smart City

A smart city is an urban area where sensor-based Internet of Things is used to aid in management of resources and civil life. The sensors are used to collect data from various sources to be analyzed and used for better utilization of assets and services. This data may include citizen count, traffic data, electricity usage data, rainfall data,

etc. which can later be used in analytical models to draw inferences to significantly change the quality of life for the citizens. “Smart city” or a “digital city” is the use of modernized techniques in communication, sensing, analysis and integration to run everyday living conditions [6].

Smart implementation of technology can give intelligent and prompt responses to different needs including but not limited to commute and traffic management, public safety, resource distribution and management and commercial trade and activities. In layman terms, a smart city is a way of living with and aided by technology and data. Unlike conventional cities, smart cities integrate technology with governance and that is what makes smart cities different. Automation is made from the smallest entities such as a simple traffic light to more complex infrastructure such as water supply, energy transfer, governance and emergency situation handling. A smart city is therefore portrayed as being better equipped to face growth-related changes through a simple transnational relationship of governance with citizenry and resource usage patterns.

3.3 Data Analytics (DA)

Increasing environmental awareness among people and the desire to work fast and effectively through the reduction of time spent on unproductive activities is forcing the realization on governments toward building smart cities. While one important aspect of this lies in connectivity through sensors, the other is data analytics.

Data analytics (DA) is the basic science of analyzing trends and features in data. As the name suggests, it deals with analyzing patterns in data to derive information on which decisions can be based. Data analytics is a sub-section of machine learning, as it uses several machine learning techniques to analyze the data including regression, classification techniques and also bagging and boosting techniques such as XGBoost and AdaBoost [6]. Use of analytical techniques in IoT and smart city-based applications can improve their performance [7]. Analysis of traffic patterns can help in deciding traffic flow regulation. Weather data analysis can help in street light control, which may additionally also depend on the traffic density saving power. Analysis of carbon emission data may help in devising means of reduction of emission. A host of such application can be found through intelligent sensor usage and data analytics. Data analytics in IoT is almost always clubbed with cloud techniques to improve data retrieval management so that the data is safely stored and accessible for use. The current paper proposes an IoT-based water management technique, which augmented with data analytics can be used in smart cities for effective water management and sustainable town planning.

3.4 Sensors and Transmitters

The data for the analysis obtained from the water supply mechanism and the water reservoir and tanks present in the city is collected continuously using sensors and transmitted to the cloud [8]. This following section has the basic description of the technology used. This project uses the Arduino UNO is an open-source microcontroller to connect and coordinate the different sensors. Arduino UNO is an open-source microcontroller developed by the Arduino group [9]. This board has 14 I/O pins to connect different sensor and transmitter to collect the data and transmit the data to the cloud. It is programmed using the Arduino IDE and a simple USB cable. This board is powered by a 9volt power supply. Different sensors are used to measure the water conditions and levels for data collection [8]. The microcontroller, sensors and transmitters used are:

- Arduino UNO
- SRF-05 sensor (ultrasonic sensor)
- YF-S201 Hall effect sensor (Water flow sensor)
- LM393 chip-based sensor (Rain sensor)
- ESP-8266 Wi-Fi transmitter
- Stepper motor

1. RF-05 sensor (ultrasonic sensor): The SRF-05 ultrasonic sensor (Fig. 2) is a wide range distance sensor which uses the SONAR technology [10]. The SRF-05 sensor has a range of 4 m in total.
   It is used in the top of the water tank in this project to measure the amount of water present in the tank. Let x be the height measured from the top of the tank to the surface of water level and h, r be the height and radius respectively of the cylindrical tank. So, the volume of water in the tank can be calculated using the following formula.

$$\pi r^2(h - r) \tag{1}$$

2. YF-S201 Hall effect sensor: Accurate flow measurement is an essential step in terms of both qualitative and economic points of view. Flow meters have proven excellent devices for measuring water flow, and now it is very easy to build a water management system using the renowned water flow sensor YF-S201 [11]. This sensor sits in line with the waterline and contains a pinwheel sensor to measure how much water has moved through it. There is an integrated magnetic Hall effect sensor that outputs an electrical pulse with every revolution.
3. LM393 chip-based rain sensor: The LM393 chip-based rain sensor is a sensor used to sense whether there is rain or not. This sensor uses the principle of resistance. It is basically connected to the Arduino board to sense the presence of moisture on the rain board. If there is moisture, then a signal is sent back to the microcontroller.

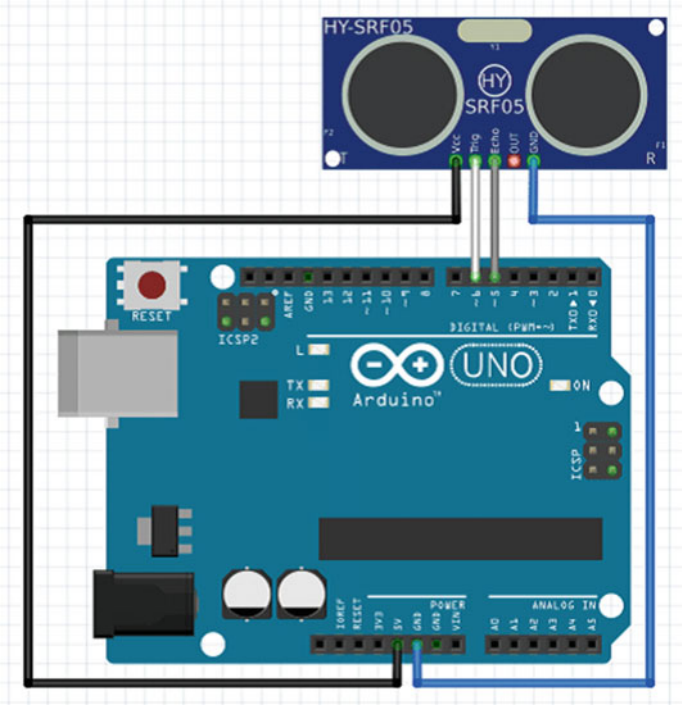

Fig. 2 SRF-05 ultrasonic sensor with Arduino UNO

4. ESP-82866 Wi-Fi transmitter: The ESP-8266 [12] (Fig. 3) Wi-Fi transmitter is the low-cost wireless microchip with a fully integrated TCP/IP stack ready for deployment with any microcontroller such as Arduino for experimental purposes.

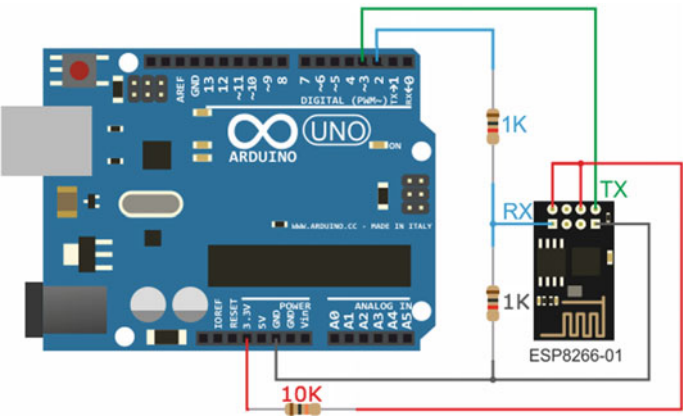

Fig. 3 ESP-8266 Wi-Fi transmitter connected to Arduino

The ESP8285 is an ESP8266 with 1 MiB of built-in flash, allowing for single-chip devices capable of connecting to Wi-Fi.

4 Blocks of Water Supply Architecture

This section gives a brief overview of the architecture of the smart city and how the basic blocks of the city are laid out for the water transmission.

4.1 Block Structure of Smart City

The water management system in the smart city is solely based on the fact that the city is divided into several blocks, and each block consists of several houses to which the water is supplied. The paper assumes this block structure to ease the explanation. The entire city is seen as a collection of blocks which are again recursively organized as sub-blocks. The recursion can go up to a suitable level as would be required for efficient and effective management. Individual houses would be the atomic constituents of such blocks. As shown in Fig. 4, initially the water is stored in the reservoir, from where the water for the smart city is obtained. From the reservoir, it is directly sent to the water treatment plant as it is treated to make it ready for use. Every outlet in the water supply architecture is monitored using motorized valve for ease of activation.

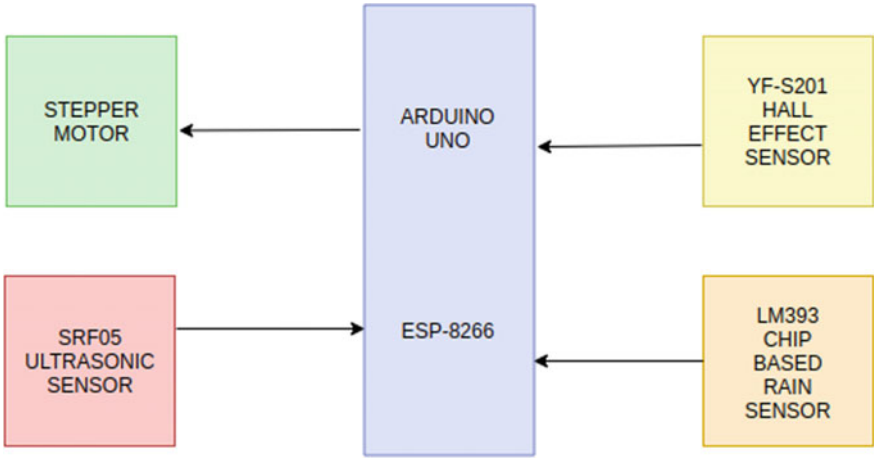

Fig. 4 Microcontroller setup

4.2 Server and Data Control Room

One of the main components of this architecture is the server and data control room where the data from every sensor in the block is collected and sent to the cloud and also a main hub for the maintenance of the valve and sensor mechanisms. The sent data is then used in the cloud to perform different extrapolation and feature modeling methods to find the water consumption and usage rate and predict the values for the future use.

4.3 Underwater Storage Facility

Water from the treatment plant is taken to the underwater storage facility [1]. This facility is present near every block of the city, and the water in this storage unit is used for immediate consumption on demand [11]. The water from this facility is sent to different blocks and houses using the sensors and the motor-controlled valve and smart water pumping systems.

4.4 Water Tanks and Pressure Control Systems

The water from the underwater facility is sent to every house in a block using pumps and sensors [5]. The specially designed water tanks are used to measure parameters like current water level and amount of water used to make the water supply more efficient [13], and conservation and management of the resource become easier. The structure and organization of the tank are explained in the further section.

5 Structure of the Water Tank

The water tank present in every house is of a specific structure. Firstly, the water tank is fully customized to suit our requirements of the smart city [14]. It mainly takes care of three functions:

1. Senses the shortage of water to release water into the tank.
2. Records the amount of water used by the person/house on a daily basis.
3. Uses a rainwater harvesting method to smartly open the valve to capture falling rainwater.

5.1 Build of the Water Tank

As mentioned above, the water is stored and supplied to each house through a smart water tank fitted on top of each house [6]. The smart water tank has several features as mentioned below.

5.1.1 Microcontroller Setup

The water tank is fitted with the Arduino UNO microcontroller, and it is powered with a battery which is recharged with a solar panel. The board is kept in a waterproof container to keep it from moisture which might cause short-circuiting. This microcontroller will control all the sensors connected in and around the tank. The UNO is connected with an ESP-8266 Wi-Fi transmitter which is used to connect with the nearest access point which in turn is connected to the server room to transmit data [9].

The basic architecture is mentioned in Fig. 5. The second sensor is the SRF-05 ultrasonic sensor. This sensor is used to measure the amount of water in the tank. The sensor is fitted, face down inside the tank. The sensor emits ultra-sonic waves and sends it in the tank. The waves are reflected back to the sensor, and it senses the height h meters. Assuming that the radius of the base of the cylindrical tank is r meters, the volume of water in the tank volume would be:

$$\text{vol} = \pi r^2 h \tag{2}$$

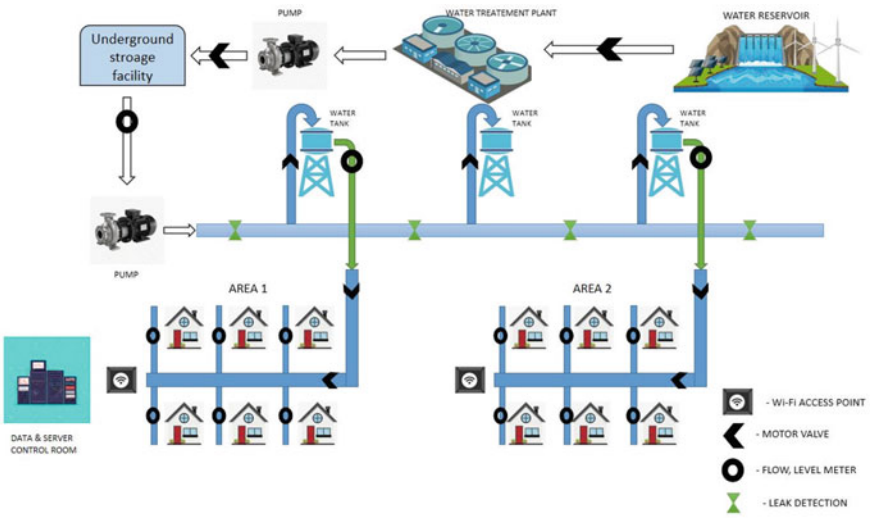

Fig. 5 Smart city water distribution architecture

This measure would help find the amount of water in the tank. If the measured amount is lesser than the minimum threshold, the automated motorized valve opens filling the tank with water. This also helps in supplying the house with the required amount of water. If the tank is having enough water for the home's usage, the valve is kept closed until required later. The amount of water used by the house (data) is collected using the YF-S201 Hall effect sensor. The tank has the outlet into the house on its base. The Hall effect sensor is placed on the outlet. The amount of water used up from the tank is calculated using Eq. (2), using the flow rate, average velocity of the water and the cross-sectional area of the pipe. This gives the essential data to analyze the data to identify and find out the rate of usage of water with the historic data.

5.1.2 Rainwater Collection

The water tank is designed in a way not only to make the water distribution efficient but also to collect rainwater during a shower in order to maximize the water conservation. To facilitate this, a funnel-like structure is placed on top of the tank's opening with a door like structure which can be flipped and a water filter on its base. The door of the funnel is connected to a stepper motor. This stepper motor is used to force open and close the opening of the funnel. This is placed as keeping the funnel always open might lead to evaporation of the water from the tank. The top of the tank is fitted with the LM393 chip-based rain sensor connected to the Arduino board. When there is rain, the sensor senses it and sends a signal to Arduino. Once it receives the signal from the sensor, it sends a signal to the stepper motor to open the door of the funnel to capture the oncoming rainwater and passes through the filter into the tank for storage. This in turn increases the water ready for use in the tank. Once the rain subsides, and the rain sensor dries out, the Arduino sends another signal to the stepper motor to close the door of the funnel.

6 Water Distribution

The water distribution is also fully monitored and controlled with the help of sensors and fully connected valve systems. The water from the reservoir is sent to the treatment plant from which it reaches the underwater storage. From the underwater storage, the water is sent to each block in a specific manner. All the monitoring from when the valve opens, to how much water is sent, everything is controlled from the server and data control center. The underwater storage facility sends the required amount of water to separate distribution tanks in each block.

From the analysis of the data received and the predicted amounts of water, the water is sent through pipelines with motorized valves to each house. The water sent to each house depends on two things:

1. The signal from the sensors of the tank.
2. The requirement calculated from the data.

6.1 Signal from the Sensors

As mentioned in section IV, the water tank placed on top of every house is fitted with different sensors. These sensors keep sending the data to the control center. This data is used to determine when the water should be supplied and when not. When signals are received from the sensor that the water level is low, the motorized valve at the outlet of the pipe is opened and water is sent in. In case the sensor shows that enough water is present in the tank adequate for the consumption of the household (obtained from the historic data collected), then the water is not sent to the house. This helps to divert that water to another area or block where it is actually required. Following this method will reduce the wastage or unwanted supply of water to the houses in the city.

6.2 Supply on Demand

The water supply to the houses as mentioned above also depends on another factor, i.e., supply on demand. This means that the water is supplied only to an extent which the household requires. This requirement is calculated by the analysis of the historic data [15]. Extrapolating from usage patterns already recorded YF-S201 Hall effect sensor, future requirement can be predicted. This would allow regulated water supply in exact quantity as required by a household and prevent wastage. In case of excess requirement, special requests can be arranged for individual household delivery. The obtained value and the actual value are kept and later the error is used to tune the model better. Storage of such information and excess supply needed by individual households would help in tuning the predictive models for better analysis including error margins in prediction. The same information can also be utilized for taxing individuals for excess use beyond set limits. This application of data analysis differentiates this method of supply from the regular distribution methods. Regular tuning of the model can keep the prediction in range and can help optimize the distribution better. Even seasonal variations in usage patterns can be tracked and included in the model. Administrative decisions taken at times of water scarcity caused by lack of rain can also be handled through such models.

7 Conclusion and Future Works

The water distribution can be optimized, and the water can be conserved better by the application of the above method in a real-life scenario. The proposed methodology can be improved with the application of better sensors and industry grade materials which would make it efficient. Motorized valves can be replaced with a better alternative and the Arduino with the ESP-8266 upgraded with a NodeMCU or even better ones. This can make the working faster and better. Improvements in the analytics can be done by using advanced ML algorithms with neural networks or similar techniques for a better outcome.

In the current paper, as already mentioned, simplifying assumptions have been made about the layout and plan of the city where it can be implemented. This has been done purely for ease of identification of the individual households, as analysis of the data gathered plays a pivotal role in the proposed model. It becomes essential therefore to pinpoint every holding and regulate the supply accordingly. The scalability of the proposed model in its current form is limited only by the organization of the cities household. The same may however be implemented on any scale, small or big, provided a proper distinction can be made between individual houses to enable the analysis to be based on that identity.

Another novelty of the proposed model is its flexibility. The same model can be used for farmland water management, wherein the identification of every household would be replaced by individual farm plots. The analytics can be appropriately tuned without major changes.

References

1. Mohanasundaram SV, Joyce A, Naresh SK, Gokulakrishnan G, Kale A, Dwarakanath T, Haribabu P (2018) Smart water distribution network solution for smart cities: Indian scenario. 2018 Global Internet of Things Summit (GIoT). https://doi.org/10.1109/GIOTS.2018.8534524
2. Agarwal N, Agarwal G Role of cloud computing in development of smart city. Int J Sci Technol Eng (IJSTE), (online) ISSN: 2349-784X
3. Merchanta A, Mohan Kumar MS, Ravindra PN, Vyas P, Manohar U (2013) Analytics driven water management system for Bangalore city. In: 12th International conference on computing and control for the water industry, CCWI2013, Procedia Engineering, vol 70, pp 1137–1146
4. Karwot J, Kaźmierczak J, Wyczolkowski R, Paszkowski W, Przystałka P (2016) Smart water in smart city: a case study, conference: SGEM 16th international scientific conference on earth and Geosciencesat: Albena, Bulgaria vol 3/I. https://doi.org/10.5593/sgem2016B31.
5. Kaur MJ, Maheshwari P (2016) Building smart cities applications using IoT and cloud-based architectures. In: Proceedings of 2016 international conference on industrial informatics and computer systems (CIICS). https://doi.org/10.1109/GIOTS.2018.8534524.
6. Su K, Li J, Fu H (2011) Smart city and the applications. In: Proceedings of the 2011 international conference on electronics, communications and control (ICECC). https://doi.org/10.1109/ICECC.2011.6066743
7. Koo D, Piratla K, John Matthews C (2015) Towards sustainable water supply: Schematic development of big data collection using internet of things (IoT). Procedia Eng 118:489–497

8. Karwati K, Kustija J (2018) Prototype of water level control system. In: International symposium on materials and electrical engineering (ISMEE) 2017, materials science and engineering 384:012032. https://doi.org/10.1088/1757-899X/384/1/012032
9. Priya R, Rameshkumar GP (2017) A novel method to smart city's water management system with sensor devices and arduino. Int J Comput Intell Res 13(10):2391–2406 ISSN 0973-1873
10. Varun KS, Kumar KA, Chowdary VR, Raju CSK (2018) Water level management using ultrasonic sensor (automation). Int J Comput Sci Eng 6(6):799–804. E-ISSN: 2347-2693
11. Paska D (2018) Digitalized water and smart cities—how can telecommunication networks be used for environmental resilience? International Telecommunication Union, 2018, ICT Discoveries, Special Issue No. 2
12. https://www.hackster.io/jeffpar0721/add-wifi-to-arduino-uno-663b9e
13. Mulyana Y, Hakim DL (2017) Prototype of water turbidity monitoring system. In: Proceedings of the international symposium on materials and electrical engineering (ISMEE). https://doi.org/10.1088/1757-899X/384/1/0120512
14. Karray F, Triki M, Jmal MW, Abid M, Obeid AM (2018) WiRoTip: an IoT-based wireless sensor network for water pipeline monitoring. Int J Electr Comput Eng (IJECE) 8(5):3250–3258, ISSN: 2088-8708. https://doi.org/10.11591/ijece.v8i5.pp3250-3258
15. Immanuel SD, Chakraborty (2019) UK Genetic algorithm: An approach on optimization. In: 2019 International Conference on Communication and Electronics Systems (ICCES), Coimbatore, India, pp 701–708. https://doi.org/10.1109/ICCES45898.2019.9002372

Comparative Study of Scouring Around Bridge Piers

P. Sreeja and Supradeep Singh

Abstract Excessive scouring around bridge piers is one of the main causes for bridge failures. Scour is not easily noticeable because it is hidden under the channel flow. Scour around a bridge pier is a challenging problem to planners and hydraulics researchers because of the adaptation of some empirical formulas. The basic reason of such adaptation of empirical formulas is due to lack of monitoring of such complex problem, and hence, the mechanism of scouring is not fully understood. Most of these scour prediction empirical formulas was based primarily on flume experiments. Thus, the knowledge of precise maximum scour depth for a given hydraulic and geotechnical condition is essential for proper design of foundation of the bridge piers as under predicted scour depth will lead to bridge failures, and over prediction of scour depth will lead to unnecessary construction costs. Since most of the scour prediction equations are based on laboratory experiments, it is important to analyse the hydraulic characteristics of the river before and after the construction of the bridge. In this study, analysis has been carried out to understand the influence of different parameters such as sediment size and the shape of the pier using different empirical equations. In India, Indian codes for scour estimation uses Lacey's regime equation for scour depth estimation for the hydraulic design of bridges, which are having certain limitations. Thus, the objective of this study is to obtain a better understanding of the mechanism which causes scouring by considering hydraulic and geotechnical characteristics. Therefore, in the present study, an attempt has been made to investigate the effect of different parameters on scour around bridge piers. The results obtained were compared with equations and models used by other researchers and found that Lacey's equation is giving over predicted values than other empirical equations.

P. Sreeja
Water Resource Engineering and Management, Department of Civil Engineering, IIT Guwahati, Guwahati, Assam, India

S. Singh (✉)
Department of Civil Engineering, Sikkim Manipal Institute of Technology, Majitar, Sikkim, India
e-mail: Supradeep.s@smit.smu.edu.in

C. Bhuiyan et al. (eds.), *Water Security and Sustainability*,
Lecture Notes in Civil Engineering 115,
https://doi.org/10.1007/978-981-15-9805-0_22

Keywords River hydraulics · Local scour depth · Clear-water scour · Saraighat bridge · Bridge piers

1 Introduction

Scour at a bridge pier is the formation of a hole around the pier due to erosion of soil by flowing water [1]. The scour depth around the bridge piers may vary depending upon the flow depth, angle of attack, pier size, pier shape and characteristics of the sediments. Numerous researchers have studied the scour mechanism but mostly, the model studies were made with lot of simplifications and empirical formulas associated with it [2]. But field investigations in this area are needed to understand the actual scouring mechanism. Such a study would be helpful in the efficient design of bridge foundations and strengthening of bed material if required.

1.1 Critical Appraisal of the Reviewed Literature

In laboratory model studies, internal flow characteristics do not truly represent prototype bridge pier scouring in rivers in view of large-scale distortion of the models [3, 4]. Hence, there is a need to evaluate the applicability of empirical scour equations to different site conditions and check its generality. There is also a need to evaluate whether the predicted maximum scour depth results in highly uneconomical and over conservative results.

1.2 Objective of the Study

The present research is concerned with the study of local scour around a bridge pier. The main aim of the study is to understand the scouring pattern for a river-bridge system in India (Saraighat Bridge, Guwahati). To address this objective, the present research has the following scope:

1. To model the river reach under unsteady flow conditions using computer software package HEC-RAS.
2. To critically evaluate the empirical equations for scour depth determination for its generality.

2 Methodology

The primary concern is pier scour which is calculated using one dimensional model (Hec-Ras) for high flood discharge. Aggradation and degradation are long-term

stream bed elevations which change due to natural or manmade causes. Contraction scour in the bridge channel involves the removal of materials from the bed, where the flow area of the stream is reduced either by natural contraction of the stream channel or by a bridge. General scour is the general decrease of the stream bed during the passage of the flood wave. Local scour involves the removal of bed materials around the structure located in the moving water.

2.1 River Flow Modelling

The river flow modelling is done for scour depth determination around bridge piers using Hec-Ras. Upstream end of the river system is modelled by using stage hydrograph, flow hydrograph and boundary conditions of stage and flow hydrograph. In unsteady flow model, the Saint-Venant equation is used.

Some of the commonly used equations for scour depth determination can be summarised as follows:

Lacey's [5] equation is given by

$$d_s = 0.47k\left(\frac{Q}{f}\right)^{0.33} - h \tag{1}$$

where d_s is the scour depth, Q is the discharge, h is the depth just upstream of the pier, k is the correction factor for local scour depth, and f is the silt factor.

Laursen and Toch [6] equation is given by

$$d_s = 1.35b^{0.7}y^{0.3} \tag{2}$$

where d_s is the maximum predicated depth of local scour, b is the pier width, and y is the flow depth.

Jain (1981) equation is given by [7]

$$d_s = 1.84b\left(\frac{y}{b}\right)^{0.3}(\mathrm{Fr_c})^{0.25} \tag{3}$$

where d_s is the scour depth, $\mathrm{Fr_c}$ is the critical Froude number, y is the depth flow b, and is the pier width.

CSU equation [8] will give maximum pier scour depth and is recommended for both live and clear-water pier scour computation, which is given by

$$\frac{Y_S}{a} = 2.0K_1K_2K_3K_4\left(\frac{Y_1}{a}\right)^{0.35}\mathrm{Fr}_1^{0.43} \tag{4}$$

where Y_S is the scour depth, Y_1 is the flow depth directly upstream of the pier (m), K_1 is the correction factor of the pier nose shape, K_2 is the correction factor for the angle

of attack of the flow, K_3 is the correction factor for bed condition, $K_4 = 0.4(V_R)^{0.15}$ is the correction factor for armouring by bed material size, and a is the pier width.

Froehlich's pier equation [9] is given by

$$y_s = 0.32\varnothing \left(a'\right)^{0.62} y_1^{0.47} \mathrm{Fr}_1^{0.22} D_{50}^{-0.99} + a \tag{5}$$

where y_s is the pier scour depth; $\varnothing$ is the correction factor for pier nose shape; a' is the projected pier width with respect to the direction of the flow; y_1 is the depth immediately at upstream of the pier; Fr_1 is the Froude number at the upstream of pier; D_{50} is the bed material grain size at which 50 per cent is finer; a is the pier width.

Gumbel's method is used for determining the design flood for different return periods, and the corresponding flood values are used in the river flow modelling for the determination of scour depth.

$$x_T = \bar{x} + K\sigma_{n-1} \tag{6}$$

where x_T is the value of T year flood event; $\bar{x}$ is the mean of the maximum instantaneous flow; σ_{n-1} is the standard deviation of the maximum instantaneous flow.

3 Results and Discussion

The various results obtained from the work done for the determination of depth of scour around bridge piers of Saraighat Bridge in Brahmaputra river for a high flood flow condition at different sections using Hec-Ras software.

The peak flow in the Brahmaputra River from a single gauging station at Pandu Port has been determined using the Gumbel's method and found to be 74,856.736 m^3/s corresponding to return period of 50 years. Water surface profile and velocity profile of the river corresponding to these flows have been computed using Hec-Ras for three conditions, namely (i) without the bridge, (ii) with the existing bridge and (ii) with two parallel bridges.

3.1 River Flow Analysis for the Existing Data

Velocity profile of the river without any bridge, with the existing bridge and the two bridges together are determined for the existing data obtained from Gammon India Ltd and return period 50 years. Figure 1 represents the comparison of velocity profile of the river without bridge, with the existing bridge and the two bridges together.

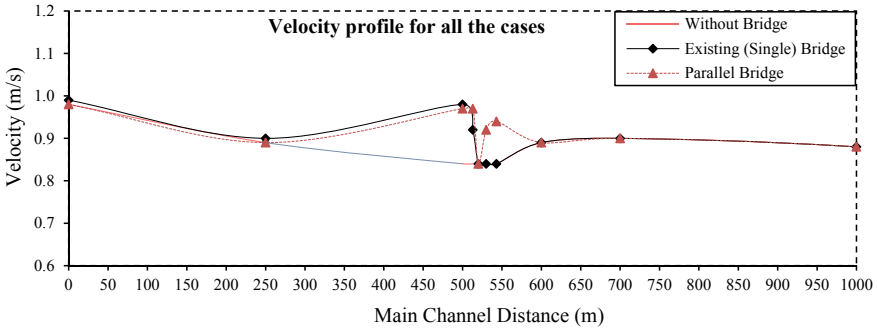

Fig. 1 Comparison of longitudinal velocity profiles in the river with different cases

From Fig. 1, it is seen that for cross-sectional area (without bridge), the velocity is reducing from 0.89 to 0.84 m/s for the channel with a chainage of 250–543 m. This is so caused because the natural flow area is increasing from 19,183.8 to 22,555 m^2. Now, for the existing bridge that is at the channel distance of 500 m, the velocity is increasing from 0.90 to 0.98 m/s and again decreasing to 0.90 m/s at a channel distance of 513 m. This abrupt change in the velocity is caused due to the sudden contraction of the flow area due to the presence of piers. After crossing the piers, the velocity reduces as the flow area increases and finally attains its stability. Again some variation of velocity is also seen in the downstream direction this is caused because of the variation of the cross-sectional area of the Saraighat River. For the parallel bridge, it is seen that the velocity is abruptly increasing twice that is at channel distance 500 m and again at channel distance 530 m. This is so occurring because the flow area is contracted by the piers due to the presence of multiple bridges.

3.1.1 River Flow Analysis for a Return Period of 50 Years

From Fig. 2, it is seen that for cross-sectional area (without bridge), the velocity is reducing from 0.92 to 0.89 m/s from the channel distance 250 to 543 m. This is so caused because the natural flow area is increasing from 19,183.8 to 22,555 m^2. For the existing bridge that is at the channel distance of 500 m, the velocity is increasing from 0.92 to 1.01 m/s and again decreasing to 0.97 m/s at a channel distance of 513 m. This abrupt change in the velocity is caused due to the sudden contraction of the flow area due to the presence of piers. After crossing the piers, the velocity reduces as the flow area increases and finally attains its stability. Again some variation of velocity is also seen in the downstream direction; this is caused because of the variation of the cross-sectional details of the river. For the parallel bridges, it is seen that the velocity is abruptly increasing at channel distance 500 and 530 m because the flow area is contracted by the piers due to the presence of multiple bridges

The scouring around the bridge piers have been computed using different empirical equations in the case of cohesionless soil with different sediment particles as listed

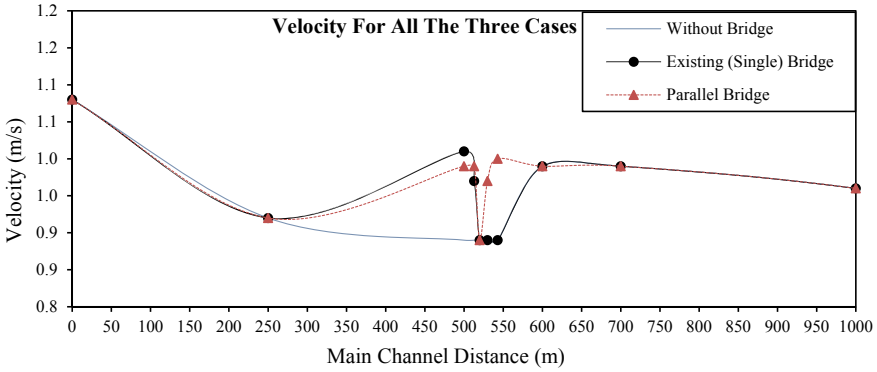

Fig. 2 Comparison of longitudinal velocity profiles in the river with different cases

in table. Different scours such as local scour, contraction scour and total scours have been estimated.

Different grain sizes at different piers of Saraighat Bridge

Pier number	1	2	3	4	5	6	7	8	9	10	11	12
Particle size d_{50} (mm)	0.38	0.37	0.28	0.02	0.32	0.32	0.25	0.32	0.32	0.08	0.71	0.32
Particle size d_{95} (mm)	0.88	0.68	0.62	0.07	0.71	0.75	0.48	0.52	0.48	0.32	1.6	0.63

The total scour calculated for observed flow data and 50 years return flow for the existing bridge have been shown in Figs. 3, 4, 5, 6, 7 and 8 which show the total scour depth for the parallel bridge.

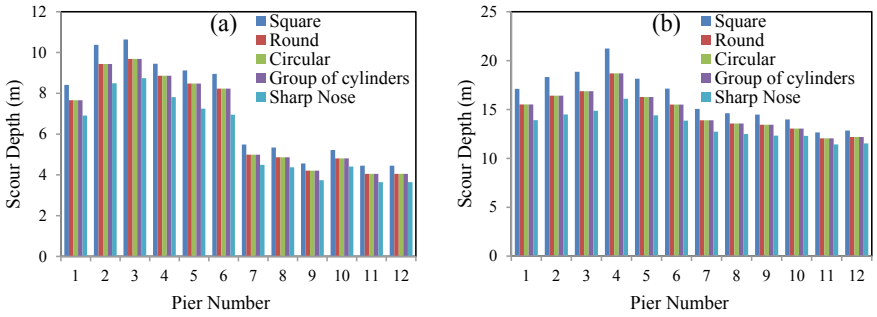

Fig. 3 Total scour depth around the existing bridge using the observed flow data with **a** CSU equation and **b** Froehlich equation

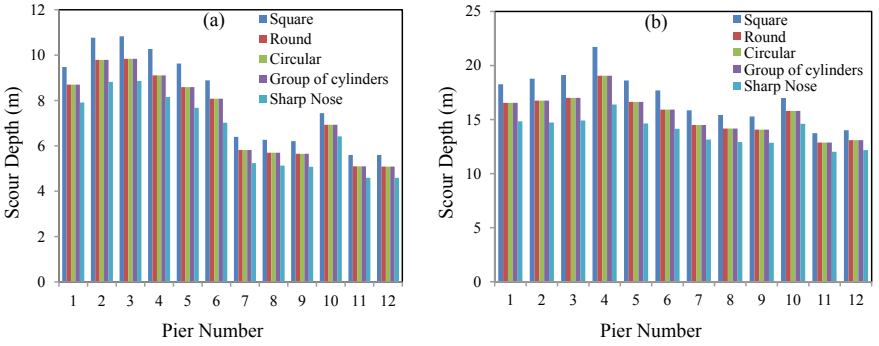

Fig. 4 Total scour depth around existing bridge using the 50 years return period flow with **a** CSU equation and **b** Froehlich equation

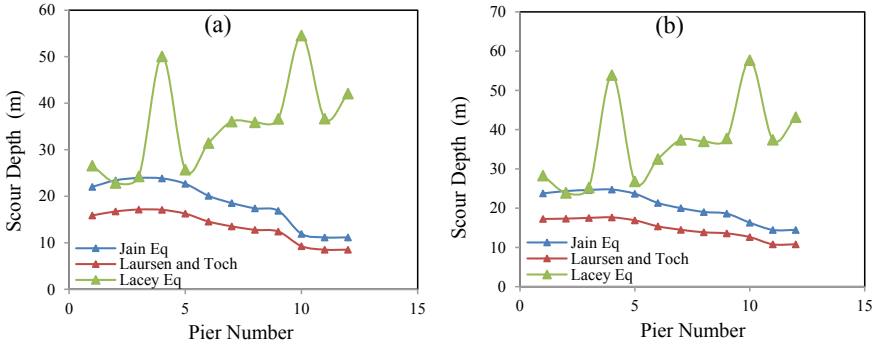

Fig. 5 Total scour depth around the existing bridge using the **a** observed flow **b** 50 years return period flow

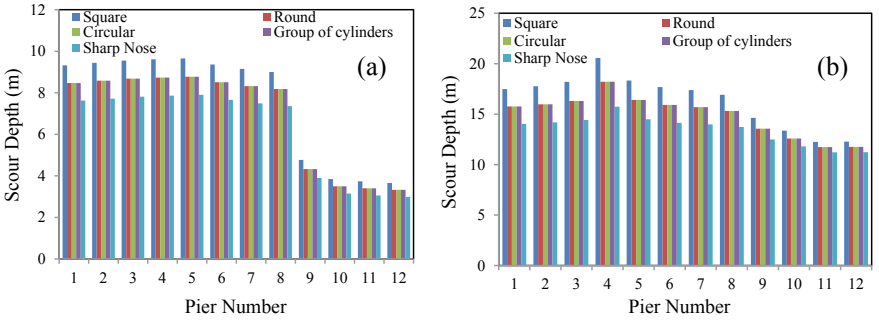

Fig. 6 Total scour depth around parallel bridge using the observed flow data with **a** CSU equation and **b** Froehlich equation

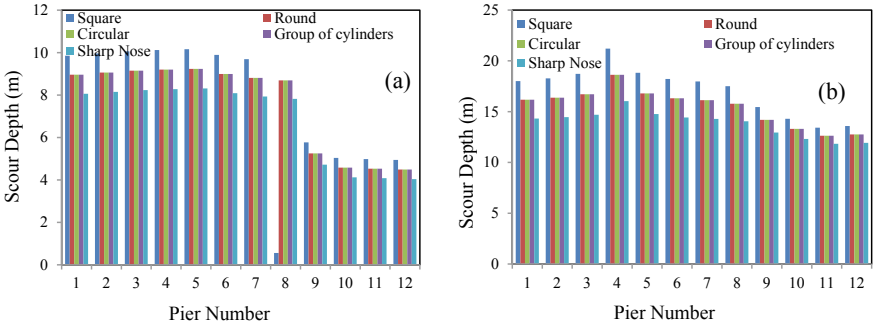

Fig. 7 Total scour depth around parallel bridge using the 50 years return flow with **a** CSU equation and **b** Froehlich equation

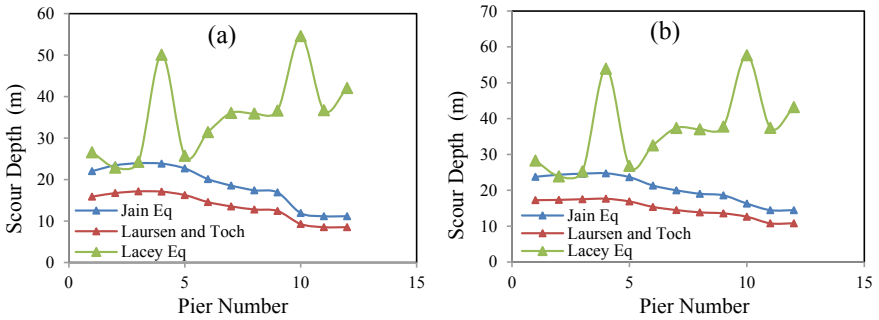

Fig. 8 Total scour depth around the parallel bridge using the **a** observed flow and **b** 50 years return period flow

Hence, it is seen that there is a variation of scour depth at different location of the piers for various kind of data's that is for existing data and 50 years return period using different empirical equations. It is also seen that the scour depth does not follow the same pattern for all the piers at different flow conditions that is for existing data and 50 years return period. This is due to the fact that the contraction scour has also been added with the local scour which is different for different types of piers.

4 Conclusion

In the present study, the empirical equation for scour depth determination has been critically evaluated; the determination of scour depth has also been done for different types of piers with different bed sediments with different pier shapes,; the change in scouring and flow characteristics in a river due to presence of multiple bridges has

also been evaluated. The important observations from the study are summarised as follows:

1. It has been found that while using CSU equation, the grain size effect is not influenced when diameter of the sediments is less than 2 mm.
2. Froehlich considers the effect of grain size when the diameter are less than 2 mm.
3. Jain and Fischer and Larsen and Toch does not considers the effect of grain size of the sediments.
4. It has been also seen that by using Lacey's equation over predicted values are obtained compared to other formula.

From the numerical study, it has been noted that the scour depth increases with the increase in approach flow depth and decreases at greater rate with decrease in flow depth. The decrease in scour depth is due to the interference of the eddies formed around the pier with the downward flow into the scour hole.

4.1 Future Scope of Work

Since the observed data for the scour depth was not available, the validation of the results could not carry out. Study has to be carried out for improving Lacey's equation for using the same for scour determination in the case of cohesive soils.

References

1. Shen HW, Schneider VR, Karaki SS (1969) Local scour around bridge piers. J Hydraulics Div 95(HY6):1919–1940
2. Ghorbani B (2007) A field study of scour at bridges piers in flood plain rivers. Turkish J Eng Environ Sci 32:1–11
3. Ahmed F, Rajaratnam N (1998) Flow around bridge piers. J Hydrau Eng 24(3):288–300
4. Chiew YM (2004) Local scour and riprap stability at bridge in a degrading channel. J Hydrau Eng 130(3):218–226
5. Lacey G (1929) Stable channels in alluviums. J Inst Eng 4736:229
6. Laursen EM, Toch A (1956) Scour around bridge piers and abutments. Bull. No. 4, Iowa Hwy Res Board, Ames, Iowa
7. Jain SC (1981) Maximum clear water scour around cylindrical piers. JHE 107(5):611–625
8. U.S. Army Corps of Engineers (2008) Hydrologic Engineering Center, HEC-RAS river analysis system version 4.0.0, March 2008
9. Mueller DS (1996) Local scour at bridge piers in non uniform sediment under dynamic conditions. Fort Collins, Colo., Colorado State University, Ph.D. dissertation, 212p

Quantification and Characterization of Microplastics in Kanke Lake, a Freshwater System of Ranchi, Jharkhand, India

Vicky Singh and Sukalyan Chakraborty

Abstract Plastics of particle size less than 5 mm are termed as microplastics. These are one of the most influential emerging contaminants, in terms of sustainable water resource. The present study shows the degradation of quality of freshwater systems in terms of occurrence and abundance of microplastics in surface water and sediments of freshwater systems, which leads to degradation of drinking water quality. This study was executed on Kanke dam (a lake), located in Ranchi district, which is the prime source of drinking water for the population of urban settlements. The sampling was carried out in three stretches, i.e., pisciculture area, water supply area and Ranchi municipal park area. The sampling of surface water is done with the help of Manta net, fabricated using mesh size of 125 μm, and sediments were collected with the help of trawl in aluminum foil. The trapped particles in Manta net were collected and sieved through 63 μm sieve. The raw sample was purified using H_2O_2 in presence of Fenton's reagent which acts as catalyst, followed by density separation using NaCl. The supernatant was collected on filter paper and quantified using stereomicroscope (fluorescence microscopy). The concentration of microplastic particles was maximum in pisciculture area followed by park area and water supply area. The count of microplastics particles quantified was 300 particles in 100 m^3 of water. The chemical nature of the collected microplastics was identified using FTIR technique. Polystyrene, polypropylene, polyethylene (low-density and high-density) and polyurethane were common polymers observed in the samples. Identification of the chemical nature of the microplastics indicates their probable sources and thus can be a useful tool to minimize the abundance by source correction.

Keywords Microplastics · Abundance · ATR-FTIR · Freshwater systems · Sources

V. Singh · S. Chakraborty (✉)
Department of Civil and Environmental Engineering, Birla Institute of Technology, Mesra, Ranchi, Jharkhand, India
e-mail: sukalyanchakraborty@bitmesra.ac.in

V. Singh
e-mail: singhvickey2009@gmail.com

C. Bhuiyan et al. (eds.), *Water Security and Sustainability*,
Lecture Notes in Civil Engineering 115,
https://doi.org/10.1007/978-981-15-9805-0_23

1 Introduction

Plastic pollution is one of the most critical and challenging issues globally. The global production of plastics is increasing day by day due to its durability, lightweight, economical and can be easily processed [1]. According to World Economic Forum, plastic production in 1950 was 1.5 million tons per year, and in the year 2018, it becomes 400 million tons per year, in which 50% of the plastics produced were single-use plastics. Improper plastic waste disposal has now become an environmental concern across the globe [2].

Microplastics (MPs), an emerging contaminant, are defined as the plastic particles of size less than 5 mm with no definite lower size [3–5]. Plastic particles primarily manufactured of size less than 5 mm are termed as primary microplastics, whereas plastic particles which are the consequence of physical, chemical or biological interaction are termed as secondary microplastics [6]. These tiny particles are detected in various shapes such as pellets, fragments, films, fibers, microbeads and foams, and size ranges between 1 mm to 5 mm are termed as large MPs whereas size less than 1 mm are termed as small MPs [1]. The persistent nature of MPs makes them more vulnerable to the environment, especially freshwater systems. In India, many cities utilize freshwater lakes as the primary source of water consumption. If these MPs reach the human body through water consumption, it can cause serious problems to human health. These MPs may act as carrier of many toxic chemicals and heavy metals, can be carcinogenic and ultimately contaminate the food web [3, 6, 7]. Some studies reported the accumulation of pesticides, organic pollutants and biofilms on these tiny particles [6, 7]. As far as freshwater systems are concerned, the primary source of occurrence of MPs is the direct littering of plastic waste into these lakes and fishing activities carried out inside these lakes. The secondary sources of these MPs are the treated wastewater discharge, stormwater runoff or wind advection [8]. Freshwater systems are most vulnerable to the microplastic contaminants as these tiny particles cannot be removed easily with conventional treatment from water and the vulnerability and risks associated with microplastics are its persistent and toxic to living beings which ultimately leads to water quality degradation. Several studies show that these microplastic particles are detected in salt, packaged drinking water bottles and even in tea bags. These tiny particles can act as a carrier of many harmful chemicals which can be toxic or sometimes carcinogenic to humans. Freshwater systems are given less emphasis when it comes to the investigation of occurrence of MPs. Till date, very few studies are done on the quantification of MPs on freshwater systems, especially in India [7]. Most of the studies are carried out on oceans and estuaries, and the protocols have been standardized accordingly [9–13]. However, there is a lack of information about the standard protocols for the quantification and identification of MPs in freshwater systems. Various studies confirmed the presence of MPs in drinking water and bottled water, which is a major public health concern, globally [14–16]. The presence of these microplastic particles ultimately degrades the quality of drinking water. These freshwater systems are efficient to accumulate a lot of MPs, however. Biomonitoring of these particles is given less attention when

it comes to freshwater systems, as compared to seawater. A recent review of MPs in freshwater systems clearly depicts the presence of MPs in freshwater systems like lakes [3]. In terms of quantification and characterization, the presence of MPs in freshwater systems is less understood. This study focuses on the quantification of MPs in drinking water sources like lake and morphological characterization of MPs in freshwater systems using the attenuated total reflectance—Fourier transform infrared (ATR-FTIR) technique.

2 Materials and Methods

2.1 Study Area

Ranchi, the capital city of Jharkhand, has been selected as the study site for quantification and characterization of microplastics (MPs). The study was carried on Kanke lake, located in northwest part of the Ranchi city (Lat 23° 23′ N to 23° 24′ N and Long Lat 85°17′ N to 85°18′ N). Kanke lake has total of 11,78,040 m^2 area and approximately 6000 m of perimeter and acts as the primary source of drinking water for the settlements across the city. According to local administration, the lake is divided into three segments, i.e., pisciculture department, water supply department and Ranchi municipal park. The sampling location is shown in Fig. 1.

2.2 Sampling of Microplastics from Surface Water

The surface water of lake of depth 10 cm was sampled using fabricated net similar to *Manta net*, having pore size of 125 μm, mouth opening of 35 cm × 20 cm, 3 m long tail, trawled with the help of non-mechanized boat [17]. The whole process was repeated three times for every stretch. The net was washed thoroughly with the help of the water jet and the particles along with unwanted materials are collected in separate buckets for each stretch. The water sample was stored in the bucket and sieved through 63 μm sieves. The materials retained on sieves were kept for 30 min and allowed the water to percolate through sieve. The unwanted material was then removed from each sieve with the help of tweezers and forceps by washing with distilled water to prevent the loss of MPs. The retained materials on sieves were then transported to the laboratory for further analysis. The whole process was done for each stretch separately.

- Stretch 1 (dotted line): This is the pisciculture department area having a perimeter of 2000 m. It is located in southeast direction of the lake. As per Ranchi Municipal Corporation, this area is mainly surrounded by water hyacinth. Treated wastewater effluents enter the lake in this area.

Fig. 1 Study area and selected sampling locations along the periphery of Kanke lake

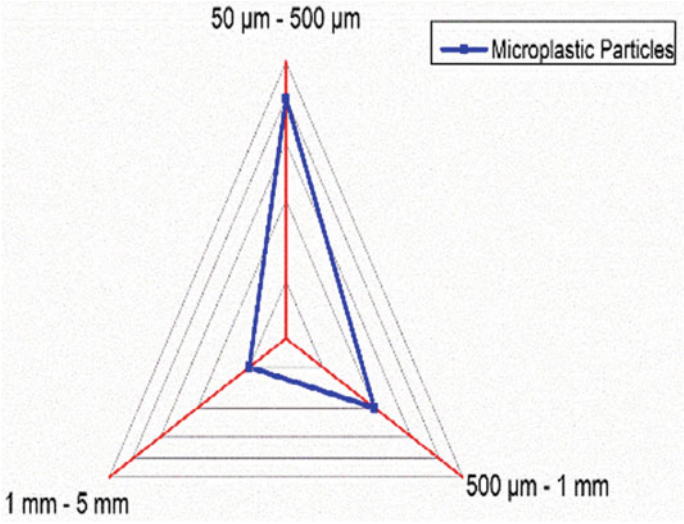

Fig. 2 Size classification of MPs detected

- Stretch 2 (double dotted line): This is the water supply department area having perimeter 1700 m. it is located at southwest direction of the lake. This area is surrounded by rural settlements and a service road for reservoir gate. A monsoon fed river stream discharge into this area.
- Stretch 3 (dashed line): This is the Ranchi municipal park area having a perimeter of 750 m. This area is surrounded by reinforced cement concrete stairs and stainless-steel fence. Recreational activities can be observed in this area.

2.3 Purification of Samples

The materials retained on the sieves were then transferred to beaker of 1 L capacity, separately for every stretch, with the help of distilled water. Wet peroxide oxidation (WPO) process was used to degrade organic matter from the sample in which hydrogen peroxide (30% H_2O_2) with Fenton's reagent was used in ratio 2:1, respectively [18]. The sample was kept on hot plate at 75 °C for 30 min and kept on the magnetic stirrer at 1000 RPM. The sample was then allowed to cool down for 30 min. If the organic matter was still visible, then further H_2O_2 was added and the whole process was repeated.

2.4 Extraction of MPs by Density Separation

After purification of the sample, the MPs particles were extracted by density separation using sodium chloride NaCl [19, 20]. The beakers containing samples were kept on a magnetic stirrer at 1000 RPM and 320 gm of NaCl was slowly added to 1 L of the sample. The sample was then stirred for 30 min, and then the solutions were kept for 24 h for significant density separation. MPs particles floated on the uppermost layer of the beaker due to differences in the densities. The uppermost layer was extracted and collected in Whatman filter paper. For each stretch, the extracted particles were distributed into seven replicates, stored in respective seven petri dishes and stored for further quantification.

2.5 Quantification of MPs

The filter paper containing MPs particles was quantified using a stereomicroscope (Olympus SZ-61) and a digital camera attached to it. The particles were counted manually, and shape, size and color were noted for each particle, and images were captured alternatively [19].

2.6 Identification of Functional Groups of the MPs

ATR-FTIR technique (Perkin Elmer Frontier™ FT-IR) has been adopted for the identification of polymer type, detected in water samples [6]. For every MPs type (fiber, microbeads, films and fragments), only one particle of each shape was analyzed under FTIR for polymer identification [21, 22]. Random particles were selected for the analysis of polymer type using tweezers and forceps. The particles were carefully removed from filter paper, wrapped in the butter paper and were transferred to Eppendorf tube. Before initiating the analysis process, the ATR diamond crystal probe attached with FT-IR was cleaned to prevent any contamination of the samples. For safety purpose, gloves and mask were put on the face to prevent distortion in the FT-IR spectral lines. The scanning was initiated for a blank to set up the reference. Then, the particles were taken out from Eppendorf tube and transferred to diamond crystal probe with the help of forceps and scanning of the particle was initiated. The absorption spectra obtained after scanning were analyzed by comparing with reference spectra and accepted with a match >80% [23].

3 Results and Discussion

3.1 Abundance of MPs in Water Samples

MPs abundance was determined as mean ±SD of items m^{-3} of sampled water, and the results have been presented in Table 1. MPs particles were detected in all the three stretches ranging from 29 ± 2 to 17 ± 2 particles m^{-3} of sampled water. The mean abundance detected in stretch 1 (pisciculture area) was 29 ± 2 particles m^{-3} of sampled water. In stretch 2 (water supply area), the mean abundance of MPs detected was 22 ± 2 particles m^{-3} of sampled water. In stretch 3 (park area), the mean abundance detected was 17 ± 2 particles m^{-3} of sampled water, which is minimum among all the three stretches. The overall abundance of MPs in the lake was 68 ± 2 particles m^{-3} of sampled water. Total MPs detected in the Kanke lake was 3 particles m^{-3}.

Table 1 MPs abundance, MPs types and polymer type

Stretch	Length (m)	MP abundance (No's/m^3) Mean ± SD	MPs type
1	2000	29 ± 1	Fiber, film, fragment, microbead
2	1700	22 ± 2	Fragment, fiber
3	750	17 ± 2	Film, fiber, fragment
Overall	4450	68 ± 2	Film, fiber, Fragment, microbead

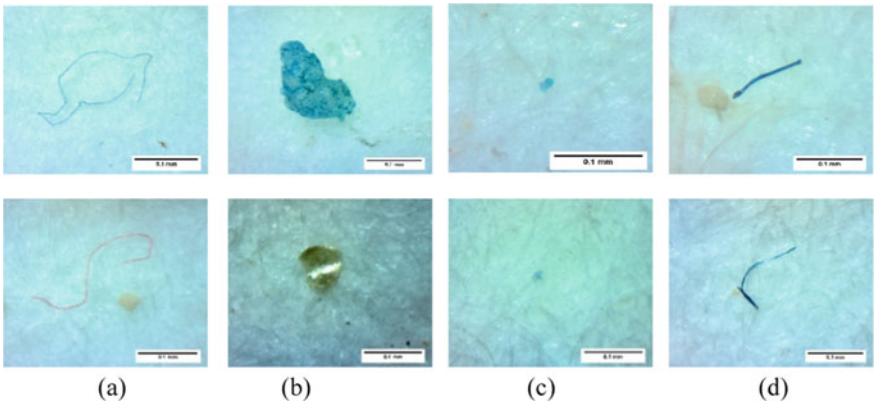

Fig. 3 Different shape of MPs detected **a** Fibers **b** Films **c** Microbeads **d** Fragments

3.2 Morphological Characterization of MPs

The morphological characterization is done based on size, shape, color and type. It has been observed that most of the particles were of fibers type followed by film, microbeads and fragments, in all the three stretches (Fig. 3). According to Sathish et al. [5], the abundance of fibers could be the fishing activity and wastewater effluent discharge into the lake. The particle size has been subdivided into three categories, i.e., (a) 50–500 μm, (b) 500 μm to 1 mm and (c) 1–5 mm. As shown in Fig. 2, relatively, most of the particles lie in the range 50–500 μm. It has been noticed that the order of color detected was blue > black > red > green > colorless > multicolor.

3.3 Polymer Type

The spectra obtained after scanning clearly show that polymer type of the plastic particles was polypropylene (PP), polyurethane (PU), polystyrene (PS), high-density polyethylene (HDPS) and low-density polyethylene (LDPE) (Fig. 4).

4 Discussion

The result of this study confirms that MPs are omnipresent in the Kanke lake. It can further be stated that this lake is acting as the sink for the MPs from various land-based activities. Insufficient solid waste management practice and improper fishing exercise can be accelerating the contribution to the abounding MPs in the freshwater system.

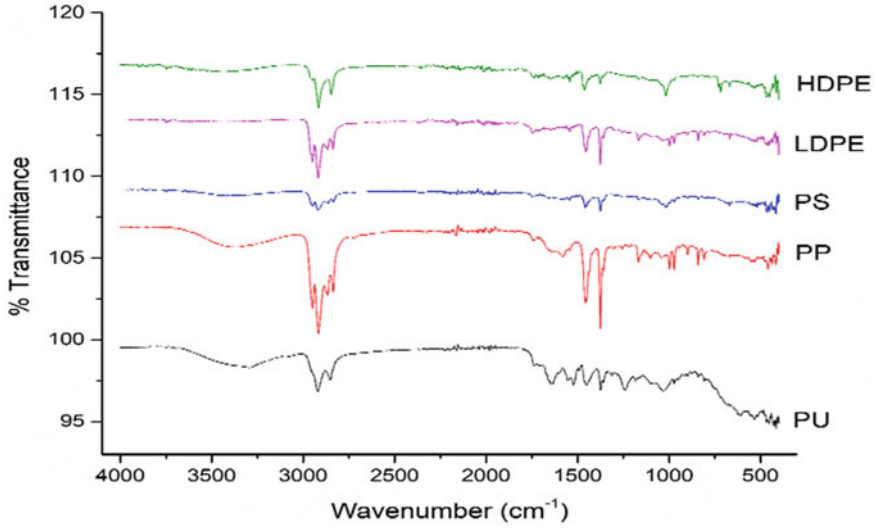

Fig. 4 FT-IR spectra of polymer type

The concentration of MPs detected in Kanke lake (300 particles 100 m^{-3}) was a clear indication that freshwater resources through this lake for the urban sprawl of Ranchi are vulnerable to plastic pollution. However, there is scarcely any study done on the freshwater systems of the study area or any other city except a few, in India. Globally, some studies have been carried out on freshwater systems for the detection of MPs. In Austrian Danube, Austria, Lechner et al. [15] reported that mean abundance of MPs was 0.317 particles m^{-3}, Three Gorges Dam, China, [16] reported that mean abundance of MPs was 4.70×10^3 particles m^{-3}, 29 Great Lake tributaries, USA, and [14] reported that mean abundance of MPs was 4.2 particles m^{-3}. The result of this study shows that the overall abundance of MPs in all the three stretches of Kanke lake is 68 ± 2 particles m^{-3} whereas total MPs detected in Kanke lake were 3 particles m^{-3}, which is a sign of significant plastic pollution.

Identification of MPs using ATR-FTIR techniques confirms that common synthetic polymers detected were PP, PS, PU, LDPE and HDPE. PP and HDPE are widely used in packaging applications whereas PS is mainly used for manufacturing spectacle frames, plastic cups and plates. Plastic carry bags are generally manufactured from LDPE [24]. The identification of these synthetic polymers indicates that presence of these microplastic particles is mainly due to human-induced activity.

Fibers were present in freshwater systems due to fishing net and synthetic textiles. Most of the fragment particles were originated from disposable cups and plates. Presence of primary MPs such as microbeads was due to discharge of wastewater into the lake. Wastewater originating from surrounding settlements contains kitchen wastewater and bathroom wastewater. Microbeads were mainly used to manufacture cosmetics, face wash and toothpaste. Thin synthetic polymers like sheets ultimately

result in films. These thin sheet-like particles originate from plastic carry bags and laminates [7].

Intake of MPs by the fishes can be a serious concern that can further contaminate the food web. There are several biological and chemical impacts which impact the flora and fauna. Chemical impacts include transfer of toxic chemicals which ultimately ends in consumption by organisms at the higher trophic level through the water. Biological impacts include colonization of microorganisms on the surface of microplastic particles, which gets transported along with these tiny particles [25, 26]. These particles can become a threat to the aquatic organisms of Kanke lake. There are several pathways which can cause toxic effects to humans and various mechanisms which impacts organisms of higher trophic levels [6]. Lu et al. [27] reported that human health gets effects on gut microbiota due to ingestion of MPs. Distribution of these particles may vary in terms of concentration which may affect the water quality of freshwater systems. The permissible limit of MPs ingestion by humans should be determined.

5 Conclusion

Freshwater systems have been less understood in terms of plastic pollution specifically in India. The current study focuses on the quantification and morphological characterization of MPs in Kanke lake. This lake serves as a primary water resource for water consumption for huge settlements in the Ranchi city; hence, MPs pollution can directly impact the aquatic organisms and human beings. At present, freshwater systems are continuously downgrading and can be the reason for water scarcity in terms of water quality. The morphological characterization produces clear evidence of the presence of these plastic particles due to anthropogenic activities by humans such as fishing activities and direct littering of plastic debris into the lake. Therefore, freshwater system such as Kanke lake used for human consumption of water needs continuous monitoring and should be restricted from plastic littering into the lake. At the same time, source reduction should also be considered to reduce MPs particles in the lake.

References

1. Saliu F, Montano S, Garavaglia MG, Lasagni M, Seveso D, Galli P (2018) Microplastic and charred microplastic in the Faafu Atoll. Maldives Mar Pollut Bull 136:464–471
2. Claessens M, Van Cauwenberghe L, Vandegehuchte MB, Janssen CR (2013) New techniques for the detection of microplastics in sediments and field collected organisms. Mar Pollut Bull 70(1–2):227–233
3. Koelmans AA, Nor NHM, Hermsen E, Kooi M, Mintenig SM, De France J (2019) Microplastics in freshwaters and drinking water: critical review and assessment of data quality. Water Res 155:410–422

4. Mintenig SM, Int-Veen I, Löder MG, Primpke S, Gerdts G (2017) Identification of microplastic in effluents of waste water treatment plants using focal plane array-based micro-Fourier-transform infrared imaging. Water Res 108:365–372
5. Sathish N, Jeyasanta KI, Patterson J (2019) Abundance, characteristics and surface degradation features of microplastics in beach sediments of five coastal areas in Tamil Nadu, India. Mar Pollut Bull 142:112–118
6. Li J, Liu H, Chen JP (2018) Microplastics in freshwater systems: a review on occurrence, environmental effects, and methods for microplastics detection. Water Res 137:362–374
7. Sruthy S, Ramasamy EV (2017) Microplastic pollution in Vembanad Lake, Kerala, India: the first report of microplastics in lake and estuarine sediments in India. Environ Pollut 222:315–322
8. Mason SA, Garneau D, Sutton R, Chu Y, Ehmann K, Barnes J, Rogers DL (2016) Microplastic pollution is widely detected in US municipal wastewater treatment plant effluent. Environ Pollut 218:1045–1054
9. Karthik R, Robin RS, Purvaja R, Ganguly D, Anandavelu I, Raghuraman R, Ramesh R (2018) Microplastics along the beaches of southeast coast of India. Sci Total Environ 645:1388–1399
10. Kumar VE, Ravikumar G, Jeyasanta KI (2018) Occurrence of microplastics in fishes from two landing sites in Tuticorin. South East Coast Ind Mar Pollut Bullet 135:889–894
11. Piperagkas O, Papageorgiou N, Karakassis I (2019) Qualitative and quantitative assessment of microplastics in three sandy Mediterranean beaches, including different methodological approaches. Estuar Coast Shelf Sci 219:169–175
12. Reddy MS, Basha S, Adimurthy S, Ramachandraiah G (2006) Description of the small plastics fragments in marine sediments along the Alang-Sosiya ship-breaking yard, India. Estuar Coast Shelf Sci 68(3–4):656–660
13. Vidyasakar A, Neelavannan K, Krishnakumar S, Prabaharan G, Priyanka TSA, Magesh NS, Srinivasalu S (2018) Macrodebris and microplastic distribution in the beaches of Rameswaram Coral Island, Gulf of Mannar, Southeast coast of India: a first report. Mar Pollut Bullet 137:610–616
14. Baldwin AK, Corsi SR, Mason SA (2016) Plastic debris in 29 Great lakes tributaries: relations to watershed attributes and hydrology. Environ Sci Technol 50(19):10377–10385
15. Lechner A, Keckeis H, Lumesberger-Loisl F, Zens B, Krusch R, Tritthart M, Schludermann E (2014) The danube so colourful: a potpourri of plastic litter outnumbers fish larvae in Europe's second largest river. Environ Pollut 188:177–181
16. Zhang K, Gong W, Lv J, Xiong X, Wu C (2015) Accumulation of floating microplastics behind the Three Gorges Dam. Environ Pollut 204:117–123
17. Stock F, Kochleus C, Bänsch-Baltruschat B, Brennholt N, Reifferscheid G (2019) Sampling techniques and preparation methods for microplastic analyses in the aquatic environment–a review. Trends Anal Chem 113:84–92
18. Prata JC, da Costa JP, Lopes I, Duarte AC, Rocha-Santos T (2019) Effects of microplastics on microalgae populations: a critical review. Sci Total Environ. 665:400–405
19. Hanvey JS, Lewis PJ, Lavers JL, Crosbie ND, Pozo K, Clarke BO (2017) A review of analytical techniques for quantifying microplastics in sediments. Anal Methods 9(9):1369–1383
20. Quinn B, Murphy F, Ewins C (2017) Validation of density separation for the rapid recovery of microplastics from sediment. Anal Methods 9(9):1491–1498
21. Dyachenko A, Mitchell J, Arsem N (2017) Extraction and identification of microplastic particles from secondary wastewater treatment plant (WWTP) effluent. Anal Methods 9(9):1412–1418
22. Mendoza LMR, Balcer M (2019) Microplastics in freshwater environments: a review of quantification assessment. Trends Anal Chem 113:402–408
23. Jung MR, Horgen FD, Orski SV, Rodriguez V, Beers KL, Balazs GH, Hyrenbach KD (2018) Validation of ATR FT-IR to identify polymers of plastic marine debris, including those ingested by marine organisms. Mar Pollut Bull 127:704–716
24. Xu P, Peng G, Su L, Gao Y, Gao L, Li D (2018) Microplastic risk assessment in surface waters: a case study in the Changjiang Estuary, China. Mar Pollut BUllet 133:647–654

25. Oberbeckmann S, Löder MG, Labrenz M (2015) Marine microplastic-associated biofilms–a review. Environ Chem 12(5):551–562
26. Thiel M, Gutow L (2005) The ecology of rafting in the marine environment. I. The floating substrata. Oceanogr. Mar. Biol: An Annu. Rev. 42:181–264
27. Lu L, Luo T, Zhao Y, Cai C, Fu Z, Jin Y (2019) Interaction between microplastics and microorganism as well as gut microbiota: a consideration on environmental animal and human health. Sci Total Environ 667:94–100

Numerical Simulation of Positive Surge Moving Upstream

Yatindra Kumar, Dhrubajyoti Sen, V. R. Desai, and Abhranil Adak

Abstract The study is focused on numerical simulation of one-dimensional unsteady flow in open channels using MacCormack Scheme. This scheme is an explicit numerical method for simulating one-dimensional and two-dimensional unsteady flow. This study is focused on depth and velocity variation in different sections of a rectangular flume at different time intervals. A series of experiments were performed on a multipurpose tilting flume on two different slopes viz., (a) nearly horizontal (zero slope) and (b) 3% slope. Experimental results are compared with the results of a computer program developed on the FORTRAN 90–95 programming language for simulating the MacCormack scheme. Results obtained from the developed code show comparable trends with the experimental result.

Keywords Depth variation · MacCormack scheme · Multipurpose tilting flume · Positive surge · Velocity variation

Notations

A Cross section area
F Vector comprising of A, g, V and $\overline{y}$
g Acceleration due to gravity

Y. Kumar (✉)
Punjab Engineering College (Deemed to be University), Chandigarh, India
e-mail: yatindra.iitcivil@gmail.com

D. Sen · V. R. Desai
Indian Institute of Technology, Kharagpur, India
e-mail: djsen.iit@gmail.com

V. R. Desai
e-mail: venkapd@gmail.com

A. Adak
Sikkim Manipal Institute of Technology, Sikkim, India
e-mail: abhranil2001@gmail.com

C. Bhuiyan et al. (eds.), *Water Security and Sustainability*,
Lecture Notes in Civil Engineering 115,
https://doi.org/10.1007/978-981-15-9805-0_24

q_l Lateral inflow
Q Flow discharge
S Vector comprising of A, g, q_l, $S_{0,}$ S_f and V_x
S_0 Slope of the channel
S_f Slope of the energy line
U Vector comprising of A and V
V Velocity of flow
V_x Component of the velocity of lateral inflow
$\overline{y}$ Distance from the water surface to the centroid of the area

1 Introduction

Flow in real world open channels is generally unsteady, with flow conditions varying with respect to time. Unsteady flows are also called transients. From an engineering perspective, a transient is referred as any pressure wave that is short-lived (i.e., not static pressure or pressure differential due to friction or minor inflow loss) [15]. The unsteadiness may be due to natural causes or due to human action. The unsteady flow conditions are a function of time and space. [4].

The partial differential equations delineate the unsteady flows, and except in very simplified cases, closed-form solutions are not available for these equations. Finite difference methods are numerical methods and used for obtaining solutions of partial differential equations using approximations for derivatives. The MacCormack finite difference scheme is an explicit numerical technique for analyzing one-dimension and two-dimensional unsteady flow problems [4].

The rapidly varied transient phenomenon in an open channel, generally known as "surge," occurs when there is a sudden change in depth or discharge or both. Such type of transients' situations occurs during the sudden closure or opening of a gate in flowing water. A surge with increasing depth is called positive surge while one with decreasing depth is known as negative surge [15]. Over the past century, hydraulicians and applied mathematicians studied positive surges. Mathematician Barré de Saint-Venant [1], Boussinesq [3], Swiss professor Favre [6] and several other researchers have discussed surge development [2, 6, 9, 10, 13, 14, 16, 18]. Garcia-Navarro and Saviron [7] uses MacCormack finite difference method as a predictive numerical tool for simulation of unsteady open channel flow. Gualtieri and Chanson [8] performed several experiments with six different gate opening using acoustic droppler velocimetry (ADV) and non-intrusive devices for observation of surge and experimental results matched with various theories. Leng and Chanson [11] experimentally studied upstream propagation of surges and bores in a large sized rectangular open channel with a smooth bed having Froude number ranging between 1.1 and 2.3. Viero et al. [17] analyze experimentally positive surge propagation in slopping open channels and compare experiment results with 0D model

predictions. Zheng et al. [20] experimentally studied various free surface characteristics of positive surge in an open channel flow and find a close agreement of maximum wave height at the first wave crest with McCowan theory.

2 Unsteady Flow

In unsteady flow, "flow waves" are generated. A wave may be defined as spatial (i.e., with respect to distance) and temporal (i.e., with respect to time). A wave is named as positive wave if water depth is higher behind the wave than the undisturbed flow depth and as negative wave if the lower water flow depth behind the wave than the undisturbed flow depth [4, 15]. The wave celerity is defined as relative wave velocity with respect to a flowing fluid, whereas absolute wave velocity with respect to a fixed frame of reference [4, 15].

2.1 Governing Equations for One-Dimensional Unsteady Flow

The two governing equations used to analysis unsteady, one dimensional, open channel flow are called the St. Venant equations. They are based on the principles of conservation of mass and momentum [4, 5, 12].

The conservative form of the continuity equation

$$\frac{\partial A}{\partial t} + \frac{\partial Q}{\partial x} = q_l \tag{1}$$

The conservative form of the momentum equation

$$\frac{\partial Q}{\partial t} + \frac{\partial}{\partial x}(QA + gA\bar{y}) = gA\left(S_0 - S_f\right) + V_x q_l \tag{2}$$

The conservation forms of the St. Venant equations for one-dimensional unsteady flow in vector form are

$$\frac{\partial U}{\partial t} + \frac{\partial F}{\partial x} + S = 0 \tag{3}$$

where $U = \begin{pmatrix} A \\ VA \end{pmatrix}$, $F = \begin{pmatrix} VA \\ V^2A + gA\bar{y} \end{pmatrix}$ and $S = \begin{pmatrix} -q_l \\ -gA(S_0 - S_F) - V_x q_l \end{pmatrix}$

3 MacCormack Method

The MacCormack method is an explicit scheme that utilizes two step predictor–corrector procedures for solving the governing equations at interior nodes. In predictor step, backward difference is utilized for the spatial partial derivative whereas in corrector step, forward difference is utilized for the spatial partial derivative [4, 19].

3.1 General Formulation

In the predictor step, the partials are defined as under:

$$\left.\begin{array}{l} \frac{\partial U}{\partial t} = \frac{U_i^* - U_i}{\Delta t} \\ \frac{\partial F}{\partial x} = \frac{F_i - F_{i-1}}{\Delta x} \end{array}\right\} \tag{4}$$

Substituting these values in the St. Venant equation, we obtain:

$$U_i^* = U_i - \frac{\Delta t}{\Delta x}(F_i - F_{i-1}) - \Delta t S_i \tag{5}$$

The computed value U_i^* gives A^* and V^*, which are used to compute F^* and S^*. In the corrector step, the partials are defined as:

$$\left.\begin{array}{l} \frac{\partial U}{\partial t} = \frac{U_i^{**} - U_i}{\Delta t} \\ \frac{\partial F}{\partial x} = \frac{F_{i+1}^* - F_i^*}{\Delta x} \end{array}\right\} \tag{6}$$

Substituting these values in the St. Venant equations, the following is obtained:

$$U_i^{**} = U_i - \frac{\Delta t}{\Delta x}\left(F_{i+1}^* - F_i^*\right) - \Delta t S_i^* \tag{7}$$

The value of the dependent variable at the next time unknown step $j + 1$ is finally obtained as:

$$U_i^+ = \frac{1}{2}\left(U_i^* + U_i^{**}\right) \tag{8}$$

3.2 Boundary Conditions

The channel is subdivided into N (in the present case, it is 50) reaches of equal length, and there are $N + 1$ computational nodes. Thus, there are $2(N + 1)$ unknowns for each new time step. For the interior nodes, $2(N-1)$ equations are obtained using finite difference techniques and two at boundary nodes, and remaining two equations are provided by applying principles of method of characteristics [19]. In case of subcritical flow, a boundary condition must be defined for both the upstream and downstream boundaries whereas for supercritical flow, none is required at the downstream boundary and two boundary conditions required for the upstream boundary. For subcritical flow, the minus characteristic equation will be applied at the upstream boundary, whereas the plus characteristic boundary equation at the downstream boundary [4]. In supercritical flow, both the plus and minus characteristics boundary equations will be applied at the upstream boundary. In the present simulation for downstream boundary, discharge is considered zero.

3.3 Initial Conditions

At the start of the simulation ($t = 0$), the values of the dependent variables (V and y or Q and A) for all nodes are referred to as initial conditions.

4 Experimentation

Experiments were conducted at the Hydraulic and Water Resources Engineering Laboratory, Department of Civil Engineering, Indian institute of Technology, Kharagpur in the multipurpose tilting flume apparatus (Fig. 1) having width, 0.075 m, depth, 0.3 m, and length, 4.9 m. An Agilent data acquisition system was connected to pressure sensors which were placed at different locations at the bottom of the flume. The pressure sensors were used to measure pressure variation during flow of water with respect to time, which in turn gave the changes in depths. Each pressure sensor had a capacity of 0.5 m. The Manning's roughness coefficient was estimated to be 0.008. The sidewalls of the apparatus were made of transparent material. In the experiments, the pressure sensors were calibrated initially, and a suitable equation relating the sensor output in millivolts (mV) versus water depth (m) was obtained which was used in converting the electrical signals to equivalent water depths. Figure 2 shows a photograph of a moving surge, and Fig. 3 indicates the location of the pressure sensors at the bottom of the hydraulic flume.

The experiments were conducted for the following two conditions:

Fig. 1 Experimental flume

Fig. 2 Movement of surge

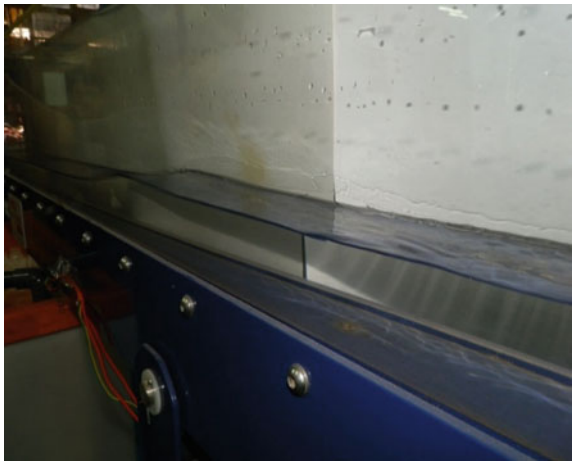

Experiment	Discharge (m^3/s)	Initial water depth (m)	Bed slope
1	0.00425	0.086	0.000
2	0.0030	0.055	0.003

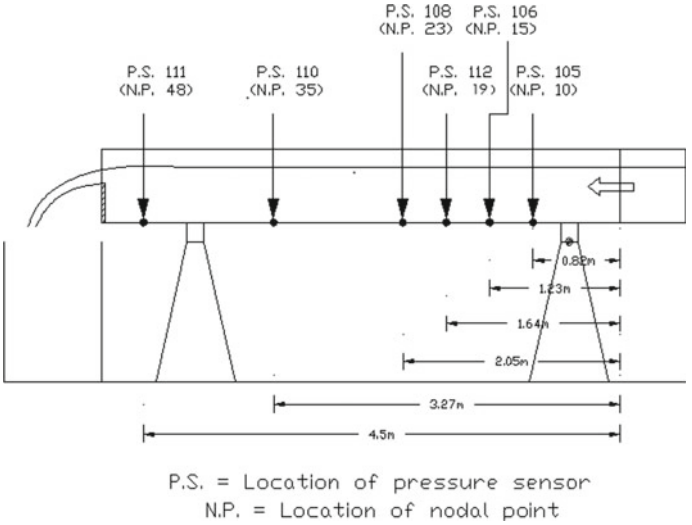

Fig. 3 Experimental setup in the experimental flume

In each case, initial steady state conditions were produced by running the flow for specified duration till steady state conditions are reached. Subsequently, transient conditions were produced by closing the downstream gate suddenly, and the data logger activated for measuring the transient pressure variation at each of the gauges.

The reading of pressure sensors was recorded with the help of bench link data acquisition unit. These readings (recorded in millivolts) were converted to depth with help of the respective calibration equations of the pressure sensors. Water depth in channel was measured with point gauge having accuracy ± 1 mm.

5 Simulation and Results

Experimental results are compared with results obtained from the FORTRAN code for McCormack scheme. From the experiments, water pressures are obtained at the different locations of sensors with respect to time. Simulation is carried out between water depth variation with respect to time at different location of pressure sensors. Water depth variation with respect to longitudinal distance and water velocity variation with respect to longitudinal distance is also obtained from MacCormack Numerical scheme and plotted the same.

5.1 Calibration Equations of Pressure Sensors

Calibration is performed for different pressure sensor locations in the channels for converting data logger reading to equivalent depth at that pressure sensor locations. After calibration of pressure sensors, the following equations are obtained for different pressure sensors.

Pressure sensor 105: $Y = 0.969\ X - 25.17$, Pressure sensor 106: $Y = 1.24\ X - 30.08$
Pressure sensor 112: $Y = 1.166\ X - 33.41$, Pressure sensor 108: $Y = 1.074\ X - 28.82$
Pressure sensor 110: $Y = 1.126\ X - 26.97$, Pressure sensor 111: $Y = 1.061\ X - 21.72$.

5.2 Results of the Flume Having Zero Bed Slope (Experiment Set 1)

5.2.1 Simulation Plot of Water Depth with Respect to Time

See Figs. 4, 5, 6, 7 and 8, and 9.

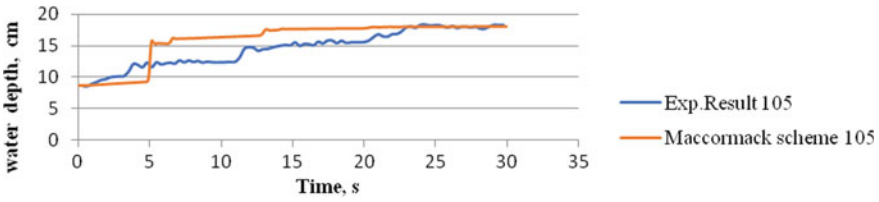

Fig. 4 Water level variation with respect to time at nodal point 10 (location of pressure sensor 105)

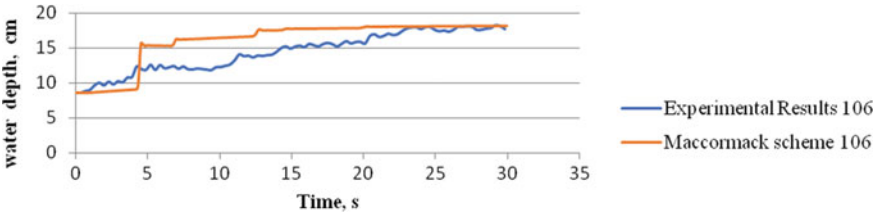

Fig. 5 Water level variation with respect to time at nodal point 15 (location of pressure sensor 106)

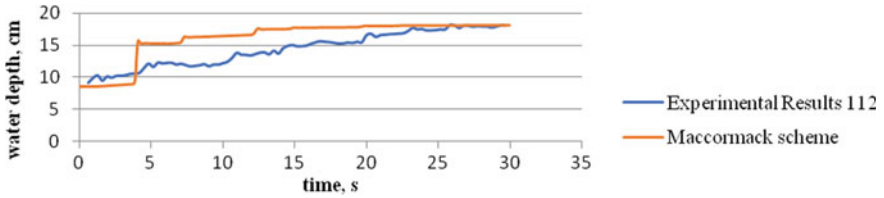

Fig. 6 Water level variation with respect to time at nodal point 19 (location of pressure sensor 112)

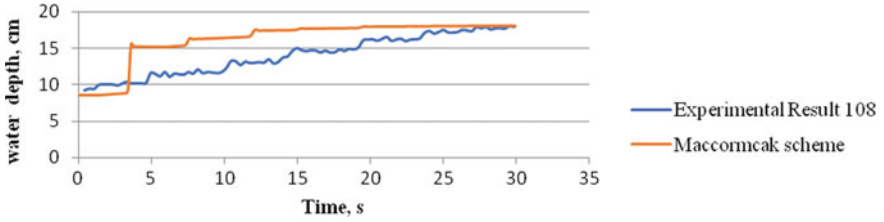

Fig. 7 Water level variation with respect to time at nodal point 23 (location of pressure sensor 108)

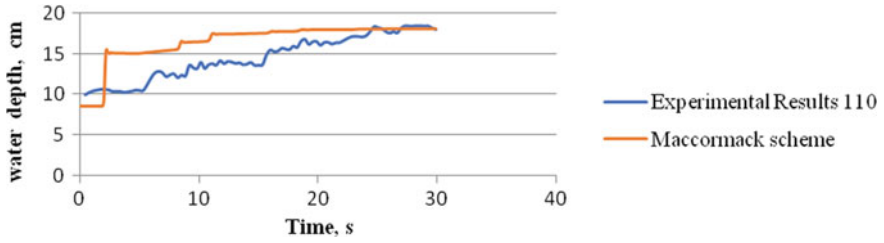

Fig. 8 Water level variation with respect to time at nodal point 35 (location of pressure sensor 110)

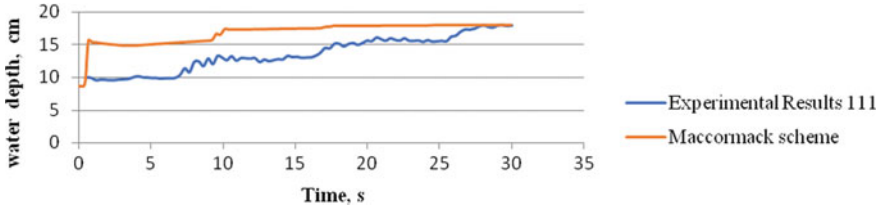

Fig. 9 Water level variation with respect to time at nodal point 48 (location of pressure sensor 111)

5.2.2 Plot of Water Depth with Respect to Longitudinal Distance from MacCormack Scheme Result

See Fig. 10.

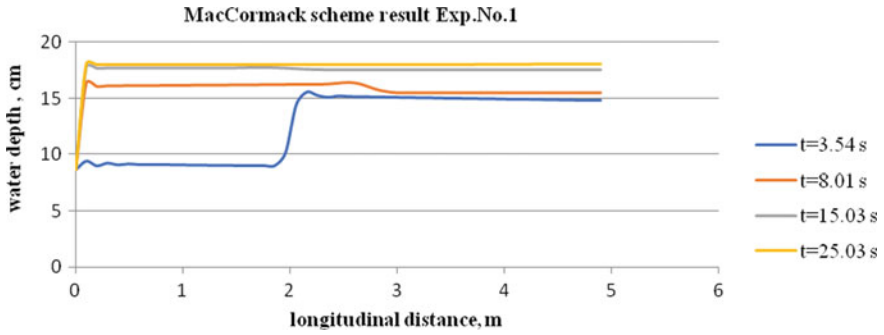

Fig. 10 Variation of water depth with respect to longitudinal distance

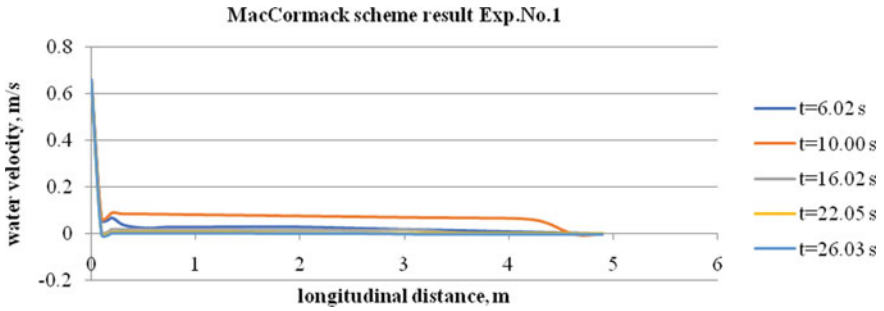

Fig. 11 Variation of water velocity with respect to longitudinal distance

5.2.3 Plot of Water Velocity with Respect to Longitudinal Distance from MacCormack Scheme Result

See Fig. 11.

5.3 Results of the Flume Having Slight Bed Slope (Experiment Set 2)

5.3.1 Simulation Plot of Water Depth with Respect to Time

See Figs. 12, 13, 14, 15, 16 and 17.

5.3.2 Plot of Water Depth with Respect to Longitudinal Distance

See Fig. 18.

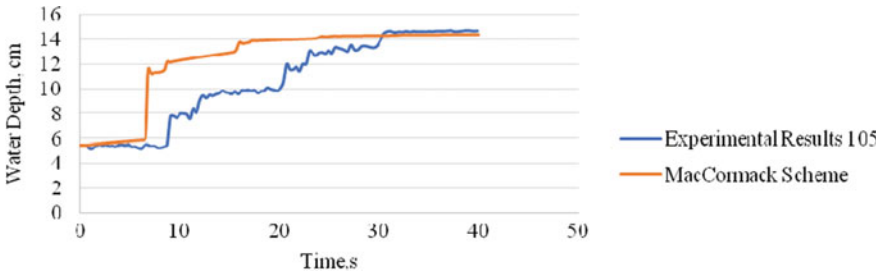

Fig. 12 Water level variation with respect to time at nodal point 10 (location of pressure sensor 105)

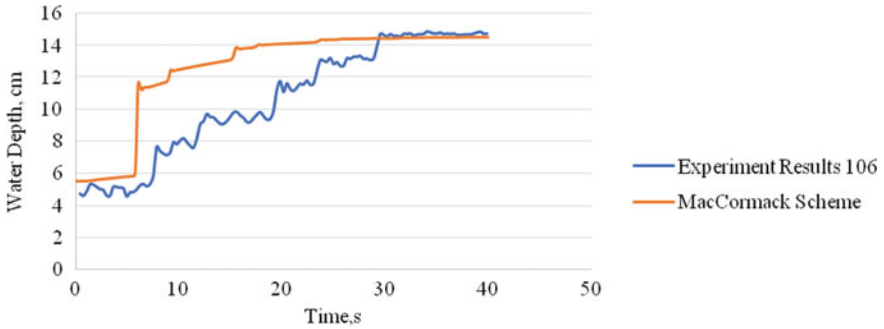

Fig. 13 Water level variation with respect to time at nodal point 15 (location of pressure sensor 106)

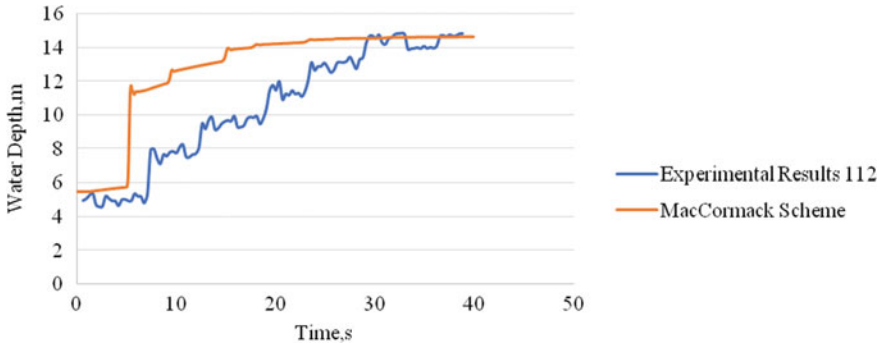

Fig. 14 Water level variation with respect to time at nodal point 19 (location of pressure sensor 112)

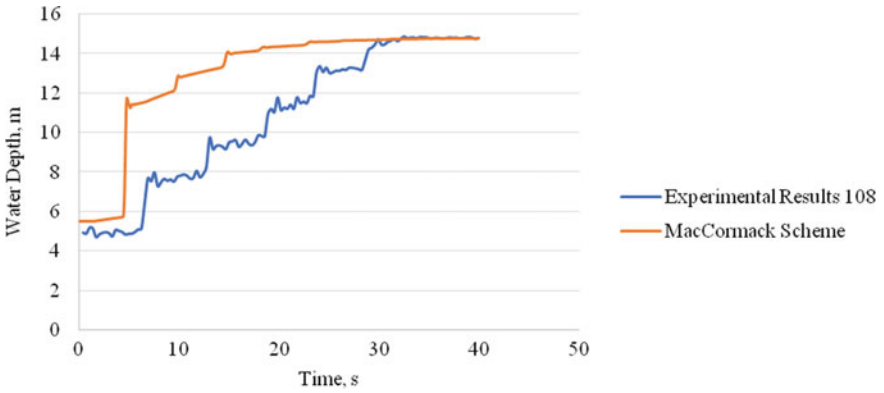

Fig. 15 Water level variation with respect to time at nodal point 23 (location of pressure sensor 108)

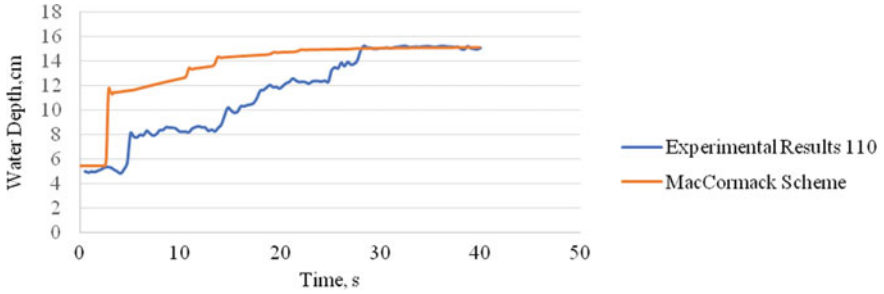

Fig. 16 Water level variation with respect to time at nodal point 35 (location of pressure sensor 110)

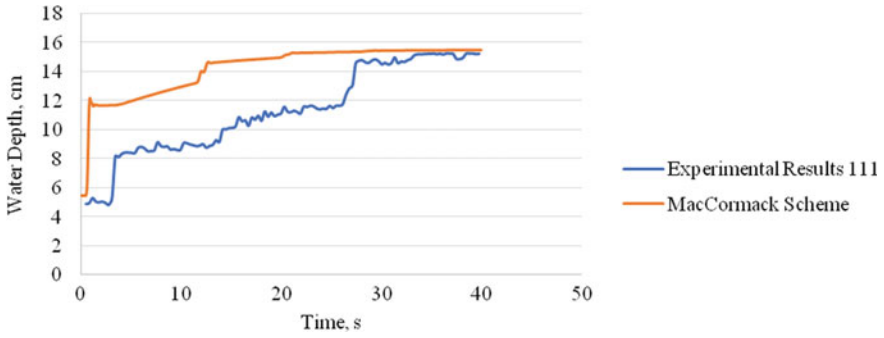

Fig. 17 Water level variation with respect to time at nodal point 48 (location of pressure sensor 111)

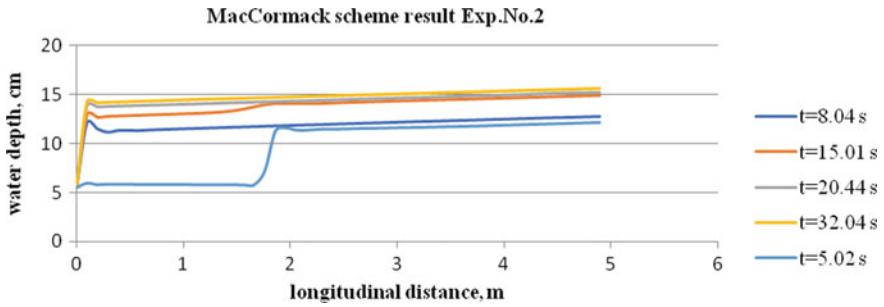

Fig. 18 Variation of water depth with respect to longitudinal distance

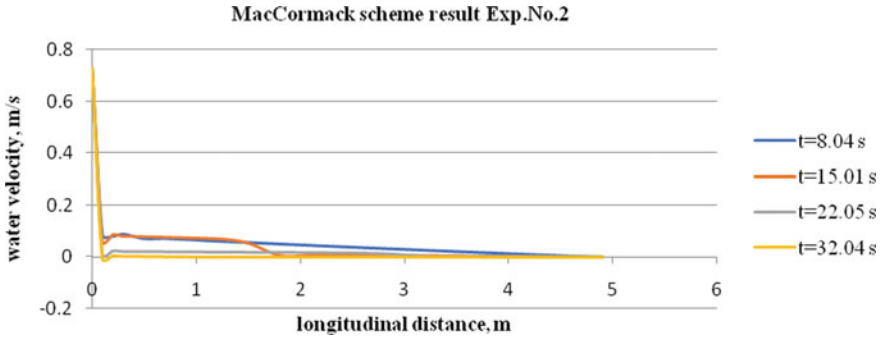

Fig. 19 Variation of water velocity with respect to longitudinal distance

5.3.3 Plot of Water Velocity with Respect to Longitudinal Distance

See Fig. 19.

6 Summary and Conclusions

6.1 Summary

The partial differential equations whose analytical solution either does not exist or is difficult to be solved may be done so by employing numerical solution techniques. The finite different methods are useful in solving nonlinear partial differential equations such as "Saint-Venant equations." The concept of characteristic curves is useful in visualization of wave propagation and the development of the boundary conditions for the case of explicit finite difference methods. In the present work, the MacCormack scheme is applied for analyzing one dimensional, unsteady open channel flow problems.

The main focus of the analysis is based on simulation of water depth calculated by MacCormack scheme and experimental result and variation of water depth with respect to nodal points and variation of water velocity and water depth with respect to time and nodal points located along the length of the flume.

7 Conclusions

The findings of the study may be summarized as follows:

1. The plots of the experimental observations and simulated values using numerical scheme follow approximately similar trends, within experimental error.
2. Unsteady flow conditions can be successfully simulated by numerical schemes like the finite difference method although the physical parameters like the channel roughness has to be carefully evaluated through standard physical experimental measurements under steady state conditions.
3. Electronic pressure sensors can be used to capture the transient conditions accurately but this has to be supplemented with accurate calibration charts relating electric voltage outputs from the sensors and the water pressure depths found out experimentally.
4. The results of this simulation conform that the technique may be used to predict numerically the transients which occur in open hydropower channels conveying water to hydroelectric stations, where load rejection may cause turbines to shut down resulting in surges traveling up along the channel.

References

1. Barré de Saint-Venant AJC (1871) Théorie et equations générales dumouvement non-permanent des eauxcourantes. Comptes Rendus des séances de l'Académie des Sciences, Paris, Séance 17 July 1871, 73:147–154 (in French)
2. Benjamin TB, Lighthill MJ (1954) On cnoidal waves and bores. Proc Roy Soc Lond A Math Phys Sci 224(1159):448–460
3. Boussinesq JV (1877) Essai sur la théorie des eaux courantes. (Essay on the theory of water flow). Mémoires presents par divers savants à l'Académie des Sciences, Paris, vol 23, Série 3, No. 1, suppl 24, pp 1–680 (in French)
4. Chaudhry MH (2008) Open channel flow, Springer, New York, USA
5. Chaudhry MH, Gharangik AM (1991) Numerical simulation of hydraulic jumps. J Hydraul Eng ASCE 117(9):1995–2010
6. Favre H (1935) Etude théorique et expérimentale des ondes de translation dans les canaux découverts (Theoretical and experimental study of travelling surges in open channels). Dunod, Paris (in French)
7. Garcia-Navarro P, Saviron JM (2010) McCormack's method for the numerical simulation of one-dimensional discontinuous unsteady open channel flow. J Hydraul Res 30(1):95–105
8. Gualtieri C, Chanson H (2012) Experimental study of a positive surge. Part 1: basic flow patterns and wave attenuation. Environ Fluid Mech 12(2):145–159

9. Lemoine R (1948) Sur les ondes positives de translation dans les canaux et sur le ressaut ondulé de faible amplitude (On the positive surges in channels and on the undular jumps of low wave height). La HouilleBlanche, Mar–Apr, pp 183–185 (in French)
10. Leng X, Chanson H (2017) Upstream Propagation of surges and bores: free-surface observations. Coast Eng J 59(1):1750003(1–32)
11. Leng X, Chanson H (2018) Transverse velocity profiling under positive surges in channels. Flow Meas Instrum 64:14–27
12. Machalinska-Murawska J, Szydłowski M (2013) Lax-wendroff and McCormack schemes for numerical simulation of unsteady gradually and rapidly varied open. Arch Hydro-Eng Environ Mech 60(1–3):51–62
13. Peregrine DH (1966) Calculations of the development of an undular bore. J Fluid Mech 25:321–330
14. Serre F (1953) Contribution à l'etude des ecoulements permanents et variables dans les canaux (Contribution to the study of permanent and non-permanent flows in channels), La Houille Blanche, pp 830–872 (in French)
15. Subramanya K (2009) Flow in open Channels, McGraw Hill Education (India) Private Limited, New Delhi
16. Teles da Silva AF, Peregrine DH (1990) Non steady computations of undular and breaking bores. In: Proceeding of the 22nd international congress coastal engineering, Delft. ASCE, New York, vol 1, pp 1019–1032
17. Viero Daniele P, Peruzzo P, Defina A (2017) Positive Surge propagation in sloping channels, Water, 9:518(1–13)
18. Wilkinson DL and Banner ML (1977) Undular bores. In: Proceeding of 6th Australasian hydraulic and fluid mechanics conference, Adelaide, pp 369–373
19. Wurbs RA, James WP (2002) Water resources engineering, Prentice Hall of India, pp 324–341
20. Zheng F, Li Y, Xuan G, Li Z, Zhu L (2018) Characteristics of positive surges in a rectangular channel. Water, 10(1–12):1473

Error Estimation for Forecasting of Orographic Rainfall Using Regression Method

Pooja Verma, Swastika Chakraborty, and Pragya Jaiswal

Abstract Forecasting model of monthly orographic rainfall, which is fundamentally characterized by a long occurrence period within a year not having much of maximum rain rate values, has been developed using regression approach. The analysis has been done on the basis of historical data of rainfall of two hill stations of different altitude, Majitar and Ghum. Performance of the developed model is evaluated through exhaustive error calculation. Goodness of fit value shows that the performance of the developed model is acceptable for the two stations having different altitude. F-test shows the statistical reliability of the prediction of rainfall. Lower root mean square error (RMSE) value indicates good prediction of stochastic-deterministic events like orographic rainfall.

Keywords Mean square error · Root mean square error · Mean absolute error · Orographic rainfall · Auto-regressive moving average · Auto-regressive integrated moving average

1 Introduction

Rainfall Modeling

Orographic rainfall is caused by lifting of moist air across the upslope of hills. As the air uplifts, it cools, resulting in orographic cloud which converts to widespread long duration rainfall. Orographic rainfall over the hills covers nearly sixty five percent of time during a year. As a consequence, instability of soil moisture causes landslide affecting badly the habitat around the hills. Over the years, there are so many attempts for the prediction of nonlinear time series [1] using regression approach taking more than one input as a cause of rainfall and single input as a cause of rainfall [2]. For the agricultural dependent economy like India, timely prediction of

P. Verma · S. Chakraborty (✉) · P. Jaiswal
Electronics and Communication Engineering Department, Sikkim Manipal Institute of Technology, Majitar, Rangpo, Sikkim, India
e-mail: swastika.c@smit.smu.edu.in

C. Bhuiyan et al. (eds.), *Water Security and Sustainability*,
Lecture Notes in Civil Engineering 115,
https://doi.org/10.1007/978-981-15-9805-0_25

rainfall is extremely important. Some literatures compare the method of regression, neural network, and clustering of data to get a better result in the prediction [3] of seasonal event like rainfall. Some literature [4] compares the approaches based on auto-regressive integrated moving average (ARIMA), the fuzzy time series (FST) model, and the non-parametric method (Theil's regression). In some work [5, 6], conventional regression model is modified for the prediction of rainfall of different nature by iterating the past values and thereby adding some percentage of error to the input values [7] or taking multiple input like cloud liquid water content, wind gust, humidity, and temperature as a cause of rainfall.

As the rainfall prediction is very important considering agriculture of the country, considering risk [8] due to landslide as a consequent effect of rainfall, this work investigates the best modification of conventional statistical prediction models to predict the rainfall over high rainfall hill region, and the developed model has been validated by the remote sensing data of different time duration.

2 Study Area

See Fig. 1.

Fig. 1 Study area

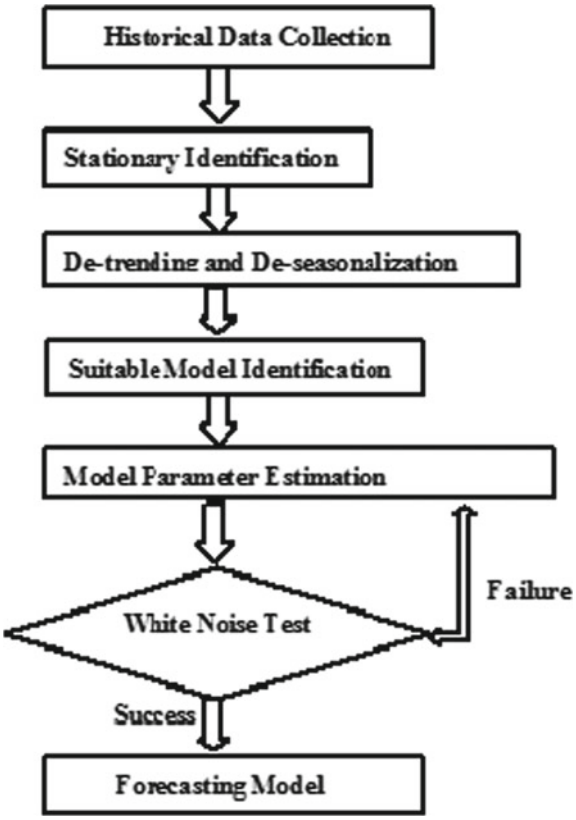

Fig. 2 Methodology of work

2.1 Description of Study Area

The rainfall of the study area taken here, Majitar and Ghum, is orographic in nature which is having sudden rain for long duration for more than fifty percent (March to October) of an average year. For this rainfall, we have collected the time series data of two northeastern Indian stations from the Giovani (NASA). This rainfall is used for the prediction of rainfall with the help of the ARIMA model technique for future use. If it can be done with sufficient time ahead, and habitat may be protected from the immediate devastating effect of rainfall.

Majitar is a small village in Sikkim, and its latitude and longitude are 27.1876° N and 88.4997° E with an altitude of 200 m (660 ft) above sea level. Climate of Majitar is subtropical, lot of rainfall in the month of May, June, July, August, and September. The major cause of rainfall in Majitar is moisture moving across the upslope of hills accompanied by strong wind gust and low cloud cover. So, it is very important to predict the rainfall over the area before it is happening to prevent habitat from the immediate risk of heavy rainfall.

On the other hand, Ghum is a small hill station near Darjeeling Himalayan hill region of West Bengal, India. Its latitude and longitude are 27.0008° N and 88.2437° E, respectively, it lies on 2025 m above sea level, and the climate is warm and temperate. As comparing with winters (November to February), summers (March to October) have much more rainfall with an average temperature 13.9 °C. As it is also the hilly region and due to orographic nature of rainfall, it is very important to study the rainfall feature of this area to prevent the habitat from the adverse effect of landslide.

2.2 Data Source

Giovani is the Web data source for providing user the National Aeronautics and Space Administration (NASA) geophysical gridded data from various satellites and surface observations to analyze or to derive important scientific conclusions. It facilitates researchers with the capability to analyze or examine data on atmospheric parameters. Historical satellite-driven monthly rainfall data of thirty-nine years (1980–2018) having spatial resolution of $1^\circ \times 1^\circ$ for two northeast (NE) Indian hill stations having very slight climatic variation is considered in this study.

3 Methodology

The historical data of thirty-nine years of the two sites viz Majitar (altitude 200 m) and Ghum (altitude 2258 m) are pre-processed involving cleaning part to avoid any spurious value or to fill any missing value. After this step, the data is smoothened to avoid any sudden spike in the data. The data after pre-processing and smoothening is taken as the input of the for the ARIMA model. ARIMA model is preferred here for prediction as it has a fixed structure to suit for the prediction of time series sequential data. The ARIMA model is used for the forecasting monthly precipitation of the two stations Majitar and Ghum with a step of ten step ahead. The model coefficients specifically the model order and model delay are changed to various values, and at each step, the prediction error is calculated. In that way, the model is tuned for lowest prediction error. Then, the error is calculated in terms of MSE, RMSE, SI, R^2 value, and MAE between the dataset used as the input for ten step ahead prediction of rainfall and predicted series of rainfall by the tuned model.

Following equations are used for analysis:

The ARIMA model equations are

$$A(z)y(t) = C(z)e(t)$$

Equation for Majitar:

$$A(z) = 1 - 4.709z^{-}1 + 10.1z^{-}2 - 12.74z^{-}3 + 9.994z^{-}4 - 4.609z^{-}5 + 0.9673z^{-}6C(z) = 1 - 3.365z^{-}1 + 5.374z^{-}2 - 4.935z^{-}3 + 2.521z^{-}4 - 0.3701z^{-}5 - 0.3719z^{-}6 + 0.287z^{-}7 - 0.08603z^{-}8$$

Equation for Ghum:

$$A(z) = 1 - 4.219z^{-}1 + 8.28z^{-}2 - 9.609z^{-}3 + 6.879z^{-}4 - 2.82z^{-}5 + 0.4886z^{-}6C(z) = 1 - 2.699z^{-}1 + 3.652z^{-}2 - 2.659z^{-}3 + 0.9706z^{-}4$$

4 Results

From the thirty-nine years of dataset, we find that comparison of the rainfall intensities forecasted by the two procedures indicates that forecast of the average rainfall intensity is closer to the observed value which is further counter confirmed by the lower error values between the prediction and actual values of the two stations.

Figure 3 shows the rainfall of thirty-nine years (1980–2018) of the two hill stations, Majitar and Ghum having altitude 200 m and 2258 m, respectively. So, this figure shows that at Majitar, the rainfall is quite high compared to other hill Ghum. After that, the predicted value of precipitation ten step ahead is found in Fig. 2. for the two stations, so that an early indication of extreme rainfall can be obtained.

Figure 4 shows the plot of actual rainfall with predicted rainfall. From the figure, it is very clear that the model developed successfully predicted the rainfall over this area. After doing prediction with ten step ahead for thirty-nine years, we have done error estimation with the help of the parameters like R^2 value also F-statistics and P-value for three hill stations. F-statistics or fixation statistics indicate the statistically expected level of attribute of discrepancy in a dataset. It is mathematically calculated as the ratio of two scaled sums of squares of the elements of the dataset. Therefore, it reflects the variability within the dataset.

The p-value signifies the level of marginal significance within a statistical hypothesis test representing the occurrence of a given feature within the dataset.

F-test of Table 1 indicates that the observed R-squared is reliable and is not a random selection for the dataset used. Therefore, the prediction model is statistically reliable and can be useful for complex rainfall like orographic rainfall. Percentile test (P Test) further confirms the result of F-test. Before all the models are experimented, the residual diagnostics test has been done, and best models produce white noise residuals with well-behaved ACF plots that are selected. As per Table 2, the model coefficients that are less than ten show the simplicity of the prediction of complex variable like orographic rainfall. RMSE value of the dependent variable like historical

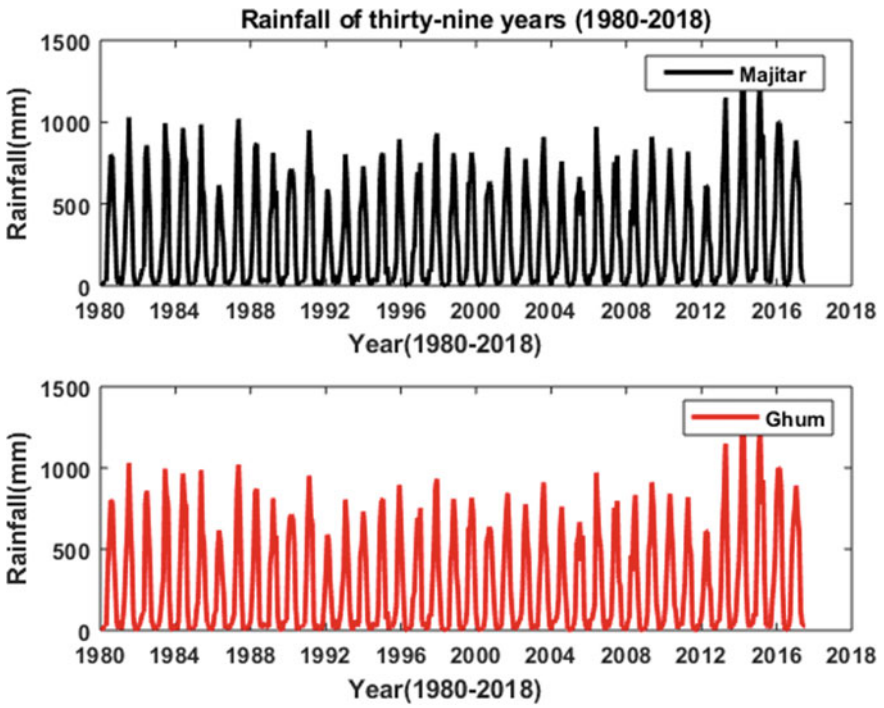

Fig. 3 Rainfall of thirty-nine years (1980–2018) of two hill stations (Majitar and Ghum)

rainfall as indicated in Table 2 shows nearly an expected estimation. For scale-free measures of fit, MAE is calculated. First a couple of "best possible" models are selected, and after that best *n* estimated models based on the lowest RMSE or MAE has been selected for the prediction.

This table shows that the various parameters after prediction of rainfall give the better result with scatter index which is minimum in Majitar, and mean absolute error (MAE) is also minimum in Majitar because of its higher altitude. So, we fix the model na and nc value which is 6 and 4 for Ghum, but for Majitar it is 6 and 8 for the betterment of result, and na and nc are polynomial order and delays of the model, respectively.

5 Summary and Conclusion

Rainfall has got a direct impact on agriculture, and on the other hand, it is also the major cause of the natural disasters like landslide. So, in order to arrange for any mitigation of the above said issues, we need to predict the event at an early stage of it happening. The regression model tuned for this work shows acceptable error

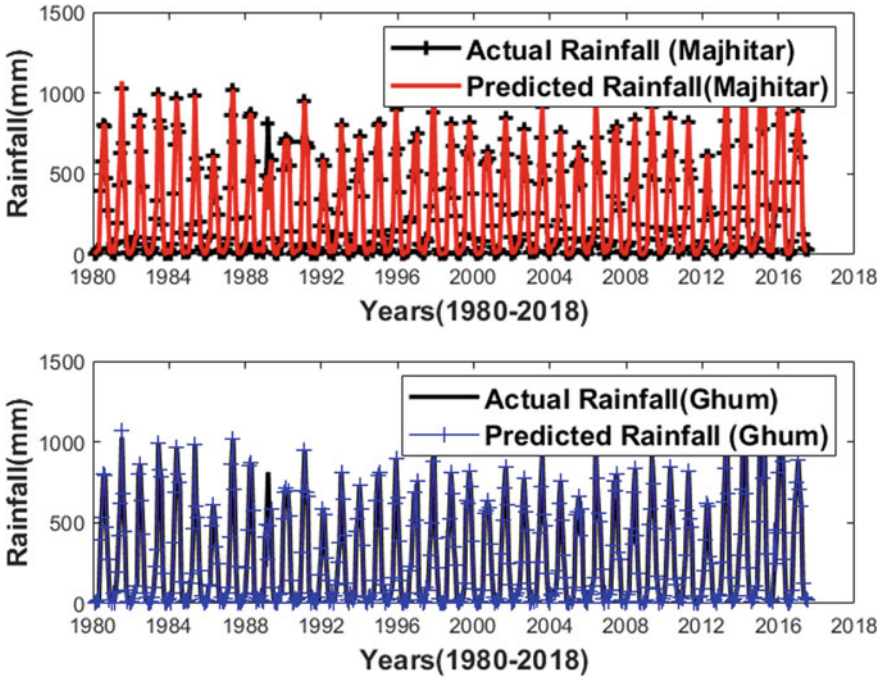

Fig. 4 Ten step ahead for prediction for Majitar and Ghum (1980–2018)

Table 1 Table of parameters of the predicted rainfall of the two hill stations (R^2 value, F-statistics, and P-value)

Stations	$R2$	F-statics		P-value	
		Simulated	Recorded	Simulated	Recorded
Majitar	0.8799	0.898	0.898	0.8767	0.5453
Ghum	0.8666	0.891	0.891	0.8925	0.5503

Table 2 Parameters of the two hill stations (Majitar and Ghum) are SI (Scatter index, mean absolute error, mean square error, and root mean square error)

Stations	SI	MAE	na	nc	MSE	RMSE
Majitar	0.074	0.091	6	8	13.96	20.708
Ghum	0.763	0.1	6	4	9.408	15.043

value indicating better prediction. In future, rainfall data of more stations with higher altitude is necessary to validate the improved orographic rain prediction model.

Acknowledgements Analyses and visualizations used in this study were produced with the Giovanni online data system, developed and maintained by the Goddard Earth Sciences Data and Information Services Center (GES DISC), National Aeronautics and Space Administration (NASA).

References

1. Rehman H (2012) An analysis of past three-decade weather phenomenon in the mid-hills of Sikkim and strategies for mitigating possible impact of climate change on agriculture (http://sikenvis.nic.in/writereaddata/)
2. Guhathhakurta P (2006) Long-range monsoon rainfall prediction of 200 for the districts and sub-division Kerala with artificial neural network. Curr Sci 90(6):773–779
3. Burlando P (1993) Forecasting of short-term rainfall using ARMA models. J Hydrol 144:193–211
4. Wang HR, Wang C, Lin X, Kang J (2014) An improved ARIMA model for precipitation simulations. Nonlinear Process Geophys 21:1159–1168
5. Lucio PS (2007) Spatiotemporal monthly rainfall reconstruction via artificial neural network-case: study: South of Brazil. Adv Geosci 10:67–76
6. Yun-Jian Z (2017) Changes in extreme precipitation events over the Hindu Kush Himalayan region during 1961–2012. Adv Clim Change 8:166–175
7. Makridakis S, Hibon M (1997) ARMA models and the Box-Jenkins methodology. J Forecast 16:147–163
8. Veiga CPD, Veiga CRPD, Catapan A, Tortato U, Silva (2014) Demand forecasting in food retail: a comparison between the holt winters and ARIMA models. WSEAS Trans bus econom 11:608–614